Parameterization of a Next Generation In-Vivo Forward Solution Physiological Model of the Human Lower Limb to Simulate and Predict Demographic and Pathology Specific Knee Mechanics

A Dissertation Presented for the
Doctor of Philosophy
Degree
The University of Tennessee, Knoxville

Ian Michael Zeller
May 2018

Copyright © 2018 by Ian Michael Zeller
All rights reserved.

DEDICATION

To my late father **Daniel Zeller** for teaching me dedication

To my mother **Sandra Zeller** for teaching me perseverance

To my brother **Harrison Zeller** for teaching me patience

To my wife Dr. **Jennifer Green** DVM for believing in me and reminding me to never give up

ACKNOWLEDGEMENTS

I would first like to take this opportunity to thank Dr. Richard Komistek for giving me opportunity to study in the Center for Musculoskeletal Research. Your experience and guidance has been incredible throughout this process. The experiences I have gained and the people that I have met will continue with me throughout my career thanks to the opportunities that I have had at the Center for Musculoskeletal Research. Thank you for taking a chance on me.

I would also like to thank Dr. Adrija Sharma for sharing with me his vast technical knowledge and incredible programming skills. I have learned so much through our interactions and he has been one of the best mentors I could have possibly asked for at CMR.

Thank you, Dr. Mohamed Mahfouz, for sharing with me your pioneering work on ethnicity and bone morphology which serves as the basis for my research.

Thank you, Dr. William Hamel, for teaching me to look at dynamic systems from a completely new robotics perspective

Thank you, Dr. Lee Martin, for teaching me to think like an entrepreneur and always looking at engineering from an entirely new perspective

I also want to thank Rebecca Robertson for all her help over the years, especially coordinating with both subjects and collaborators, making sure that projects get started and maintain all deliverable deadlines. In fact, thank you for all that you do making sure the lab does not fall apart.

I would also like to thank my colleagues, including Dr. John Mueller and Dr. Brad Meccia, who laid the groundwork for my dissertation research. Dr. Sumesh Zingde who's wisdom I still pass on to the newest grad students. I also wanted to thank Dr. Chris Carr, Jake Smith and Thibaut de Bock for all their help as I began in the lab. I also want to thank Dr. Michael La Cour and (almost Dr.) Trevor Grieco for their assistance, advice and comradery throughout my time in the lab. I am going to miss working with you guys. Finally, I also want to thank the newer graduate students for all of their help and eagerness to learn. Manh Duc Ta, Milad Khasian, Jarrod Nachtrab and Garett Dessinger, make sure to take advantage of every opportunity you guys have at CMR; it pays off dividends in the long run.

In addition, I would also like to thank all of the undergraduate research assistants that worked on my projects throughout the years. Thank you "Ace" Ali, Bryan Medina, Morgan Howard, Caroline Burch, Tanya Smith, "Ace" Patel, Madison Kirk, Maggie Frasier, Jessie Barb and Lauren Crothers. Your assistance has made my life much easier, and I certainly appreciate that. I also wanted to give a special thanks to Leyton Adams, Daniel Nalepa, Jan Bruckbauer, and Ben Rouse who all helped to organize data, write code and give feedback for this dissertation.

Lastly, I wanted to thank some of the educators that have made my Ph D possible. This includes my high school chemistry teacher, Elizabeth Golowenski, who peaked my interest in research, my college calculus professor, Dr. Irina Viktorova, who took me to present at my first academic conference and my materials professor, Dr. Marian Kennedy, who both believed in me and convinced me that I could make it through the Ph D process.

ABSTRACT

The human knee from a mechanical perspective is arguably one of the more complex of the joints of the human body and for this very reason there are a number of pathological factors that can adversely affect knee function, leading to pain, stiffness and an overall reduced quality of life. To rectify these disease conditions, a variety of intervention techniques exist, all of which are predicated on a thorough understanding of the forces and motions that occur at the knee.

Various techniques have been developed to further the understanding of how the knee functions; however, many of these strategies involve time and cost consuming processes in order to assess functionality of the knee. Mathematical modeling is a methodology that uses mathematical equations of motion to solve for forces, or in the case of forward modeling, motions given a known set of forces. Such a model is capable of replicating the functionality of the knee in vivo.

One application of such a model is in the context of total knee arthroplasty design. Intended for the restoration of functionality after late stage osteoarthritis, total knee arthroplasty devices are highly dependent on their associated design features and the use of a theoretical model affords the opportunity to test the performance of a device without ever needing to manufacture or implant it.

In addition, there are also surgical applications where a mathematical model can test joints that otherwise cannot be evaluated under conventional means. This includes modeling of the healthy knee, as well as various functionality-limiting pathological conditions. Perhaps more importantly is the ability to evaluate different

intervention techniques to determine the effectiveness in doing so identify which technique most effectively resolves the pathological issues.

Advances to the model have focused on parameterization while contributing to a validated normal knee model, an enhancement on the efficiency of the muscles that drive flexion, facilitated methods to evaluate articular geometries and enhancements providing more realistic physiological motions. The model has also been enhanced to account for demographics, as well as abnormal pathology with additional parameters added to better understand gait mechanics at the knee.

TABLE OF CONTENTS

Chapter One: Introduction 1
1.1 Anatomy of the Knee 1
1.1.1 Anatomic Definitions 1
1.1.2 Bony Architecture 3
1.1.3 Ligamentous Architecture 8
1.1.4 Muscular Architecture 9
1.2 Knee Motions 12
1.3 Osteoarthritis 16
1.4 Total Knee Arthroplasty 19
1.5 TKA Assessment and Analysis 21
1.6 Mathematical Modeling 24
1.7 Forward Solution Modeling 26
Chapter Two: Background 29
2.1 Goals of Total Knee Arthroplasty 29
2.2 The Normal Knee 30
2.3 Existing TKA Designs 32
2.2.1 Posterior Cruciate Retaining vs Posterior Stabilized 33
2.2.2 Mobile vs Fixed Bearing 37
2.2.3 Condyle Asymmetry 38
2.2.4 Single Femoral Radius 40
2.2.5 Gradually Reducing Femoral Radius 40
2.2.6 Personalized TKA Implants 43
2.4 Limitations of Modern TKA 46
2.5 TKA Design Process 48
2.6 TKA Assessment Techniques 50
2.6.1 Implant Retrieval 50
2.6.2 Wear Simulators 53
2.6.3 Cadaver Testing 54
2.6.4 Telemetry 55
2.6.5 Fluoroscopy 58
2.7 Mathematical Modeling 60
2.7.1 Forward and Inverse Modeling 60
2.7.2 Optimization and Reduction models 63
2.7.3 Commercial Modeling Techniques 66
2.8 The University of Tennessee Model 73
2.8.1 Geometric Setup 75
2.8.2 Kane’s Dynamics 80
2.8.3 Autolev 81
2.8.4 Muscle Control 82
2.8.5 Contact Detection 84
2.8.6 Initial Conditions 89
2.8.7 User Interface 91

Chapter Three: Objectives and Contributions 93
3.1 Objectives 93
3.2 Contributions 94
Chapter Four: Parameterizing the Native Knee 96
4.1 Purpose 96
4.2 Introduction 98
4.3 Methods 100
4.3.1 Patient Demographics 100
4.3.2 Fluoroscopic Analysis 101
4.3.3 Kinematic Analysis (Mathematical Model) 104
4.3.4 Comparing Results 107
4.4 Results 108
4.5 Analysis and Discussion 111
4.6 Summary and Conclusion 120
Chapter Five: Parameterizing the Extensor Mechanism 123
5.1 Purpose 123
5.2 Introduction 124
5.3 Methods 128
5.3.1 Improving Velocity Functions 131
5.3.2 Improving Wrapping Points 133
5.3.3 Muscle Force Distribution 133
5.3.4 Pelvic Tilt 136
5.3.5 Device Sensitivity 140
5.4 Results 141
5.5 Analysis and Discussion 149
5.6 Conclusion 151
Chapter Six: Parameterizing Flexion Activities 153
6.1 Purpose 153
6.2 Introduction 153
6.3 Methods 155
6.4 Results 159
6.4.1 Adding the Foot 159
6.4.2 Adding Tibia Rotations 165
6.5 Analysis and Discussion 171
6.6 Conclusion 175
Chapter Seven: Parameterizing Articulating Geometry 176
7.1 Purpose 176
7.2 Introduction 178
7.3 Methods 182
7.3.1 Contact Detection 182
7.3.2 CAD Model Creation 192
7.3.3 Defining Geometries 194
7.3.4 Creating Parametric Surfaces 194
7.4 Conformity Results 201
7.5 Post Placement Results 207

7.6 Summary and Conclusion 209
Chapter Eight: Parameterizing Demographics 212
8.1 Purpose 212
8.2 Introduction 214
8.3 Methods 217
8.3.1 Testing Ligament Attachment Sites 217
8.3.2 Testing Articulating Geometries 219
8.4 Articular Morphology Results 222
8.4.1 Male Theoretical Patients 223
8.4.2 Female Theoretical Patients 223
8.4.3 Caucasian Theoretical Patients 227
8.4.4 African Theoretical Patients 227
8.4.5 East Asian Theoretical Patients 231
8.4.6 Comparing Theoretical Patients 231
8.5 Soft Tissue Attachment Results 238
8.6 Conclusion 246
Chapter Nine: Parameterizing Pathological Conditions 251
9.1 Purpose 251
9.2 Introduction 252
9.3 Methods 256
9.4 Results 257
9.4.1 Arthritic Results 257
9.4.2 ACL Deficient Results 260
9.4.3 Varus Valgus Deformity Results 263
9.5 Conclusion 267
Chapter Ten: Parameterizing of Gait 268
10.1 Purpose 268
10.2 Introduction 268
10.3 Methods 269
10.4 Results 270
10.5 Conclusion 278
Chapter Eleven: Validation 281
11.1 Validation Using Fluoroscopy 281
11.2 Validating with Telemetry 282
11.3 Validating with Other Models 284
Chapter Twelve: Assumptions Limitations and Future Direction 287
12.1 Assumptions 287
12.2 Limitations 288
12.3 Future Direction 289
Chapter Thirteen: Conclusion 291
List of References 293
Vita 307

LIST OF TABLES

Table 1: Although the knee is constrained by many different soft tissue elements, there are eight primary structures that provide the majority of mechanical stability each with a unique role. 11
Table 2: The Food and Drug Administration (FDA) give guidelines for various medical devices. These classifications and associated controls vary based on device risk. 49
Table 3: There are a number of structures and forces that act on the knee and although the complexity is reduced from the true anatomical knee, the motel strives to retain as many of these structures as possible. There are also several assumptions made by the model. (Used with permission from [119]). 79
Table 4: This analysis included ten healthy patients in total with a roughly even gender split and demographics representative of patient populations. 102
Table 5: The average kinematic results for the ten subjects were compared. .. 110
Table 6: The spline directions and associated variables are dependent on the surface being approximated. Each spline consists of a constant, a height function, and a time function. 199

LIST OF FIGURES

Figure 1: The spatial definitions of the human body are divided into three separate planes that intersect to form three respective axes. While the anterior/posterior axis, superior/inferior axis, distal axis and lateral axis are defined away from their respective planes, proximal and medial axis are defined toward their respective planes. (Figure modified from [1]) 2
Figure 2: On the distal end of the femur anatomy diverges into two well defined condyles represented pictographically (A) and in surgery (B). Image derived from [2].....4
Figure 3: The knee joint (center) itself contains the tibiofemoral joint (left) between the tibia and femur, as well as the patellofemoral joint (right) between the patella and femur.....6
Figure 4: In addition to the tibia, femur and patella, there are additional bones that provide mechanical force transmission, bounding conditions, and mechanical reinforcement, including the pelvic bones, the foot bones and the fibula. 7
Figure 5: There are several many ligaments and other soft tissue that provide mechanical stability to the femur as it rests on the tibia. Figure modified from [2].....10
Figure 6: The anterior view of the quadriceps muscle group (left) and the posterior view of the hamstring muscle group (right). 13
Figure 7: There are three primary quantifiable motions of the knee which are flexion/extension (left), internal/external femoral rotation (center) and anterior/posterior translation of the medial and lateral femoral condyles (right). 15
Figure 8: There are five primary categories that constitute activities of daily living. From a biomechanics perspective, the most important is ambulatory function which can be further assessed through activities modified from flexion/extension and gait activities.....17
Figure 9: The healthy knee (left) consists of smooth articulating surfaces and normal joint space, whereas the arthritic joint (right) shows discontinuous cartilage, osteophyte formation and a compressed joint space (Figure modified from American Academy of Orthopedic Surgeons [16]). 18
Figure 10: A total knee arthroplasty device replaces damaged articulating surfaces of the knee joint with metallic and plastic components (Figure modified from Mayo Clinic). 20
Figure 11: A traditional total knee arthroplasty device consists of two metal components mounted into the femur and tibia, along with a bearing to facilitate smooth motion. In some cases, the patella is resurfaced with bearing material as well. 20
Figure 12: Cadaver rigs, mechanical wear simulators and fluoroscopy are all methods used to assess knee implant device performance.....23

Figure 13: Kinematic parameters are assessed for TKA components much like the kinematics for the native knee. These values are flexion, medial and lateral condyle translation in the AP direction and axial rotation of the femoral component about the proximal/distal axis. 25
Figure 14: Mathematical modeling can be used to simulate implant device performance under certain in vivo condition for various activities. 27
Figure 15: Inverse modeling determines forces from a given set of motions through dynamic equations of motion, and forward modeling determines motions given a particular set of forces through dynamic equations of motion. 27
Figure 16: Leszko, et. al. proposed the six motions that can be experienced by the knee using circular disks as analogs for femoral condyles. 31
Figure 17: The motions of the normal "healthy" knee typically incorporate both medial and lateral posterior motion with a rotation in the external direction [25]. 31
Figure 18: There are many types of TKA devices, each with their own unique design features. Some implants are personalized (left column), while others feature a rotary arc coupled with a single radius (left center). Some include purely symmetric designs (right center) while others feature asymmetric condyles to promote certain motions (right column). 34
Figure 19: The posterior stabilized (PS) TKA features a cam and post mechanism that provides mechanical support for the resected PCL (left). Cruciate retaining devices (PCR) have no such mechanism but retain the native PCL from the patient. 36
Figure 20: Asymmetric TKA devices use the different medial and lateral femoral radii to drive axial rotation. Since the lateral condyle has a larger radius, it travels further than the medial condyle during flexion, thus promoting axial rotation. 39
Figure 21: The single radius knee features a constant femoral radius throughout flexion. In doing so, the TKA promotes mid-flexion stability by fostering smooth motions and consistent collateral ligament forces. Figure modified from Stryker, Inc. 41
Figure 22: The gradually reducing radius design features a transition region between early and late flexion where the condyle radius gradually becomes smaller as a function of flexion. 42
Figure 23: Personalized TKA implants are created to fit patient femoral and tibial anatomy based on CT scan geometries (top). The main factors that are evaluated are the medial and lateral femoral radii as well as the trochlear groove geometry. Both the femur and the tibia components are designed to fit their respective bones and incorporate the geometry of these determined radii. Figure modified from Conformis, Inc. 45
Figure 24: The TKA design process in general contains four steps. From initial conceptualization, a device must be evaluated to ensure it meets both safety and efficacy standards. This process also tests various design features to ensure and demonstrate that they work as intended. Once this evaluation

had been completed, the design enters a looping process where revisions occur until the design has been proven to work successfully and adequately. Upon completion, the device moves on to additional processes such as manufacturing integration and commercialization, as well as the early phases of post market surveillance to ensure continued compliance with regulatory measures. 51
Figure 25: There are three main techniques for the mechanical assessment of TKA devices, including: cadaver testing which uses mechanical actuators to simulate muscle control while measuring motions (left), wear simulators which use prescribed motion patterns to perform long wear analysis over large quantities of cycles (center), and fluoroscopy which determines device motion in vivo through video x-rays and a component registration process (right). 52
Figure 26: Telemetric knee implants are specially designed devices equipped with force transducers that are able to measure and transmit contact force data for analysis. 56
Figure 27: During fluoroscopic evaluation, subjects perform various activities with surveillance by a video x-ray machine. The video is then cut into frames of interest (top) assigned components and transformations through a registration process (middle) and from these transformations, measurements can be taken to assess device performance. 59
Figure 28: Forward solution modeling begins with a mechanical system and uses the equations of motion to solve for motions from forces. Inverse modeling does just the opposite and uses the equations of motion to solve for forces when known motions are applied to the system. 62
Figure 29: Finite element modeling can be used to demonstrate interaction between mechanical interfaces which are represented as discrete elements. Such is the case in models of the Kansas knee simulator (figure modified from [94]). 68
Figure 30: One of the primary advantages of finite element analysis is the ability to model deformable bodies, this makes such methods ideal for analyzing soft tissue deformation under loading conditions (Figure modified from [131]) 68
Figure 31: In 2008, Dr. Sharma successfully built a model capable of calculating forces that closely match those of telemetric evaluation (Image from [127]). 69
Figure 32: Opensim provides the basic framework and setup for mechanical systems representing much of the body, including the knee. This is an open source program that allows for the validated configurations for various analysis (Image modified from [134]). 71
Figure 33: ADAMS provides the capability to assess biomechanics systems under a variety of conditions. These setups are primarily inverse models and afford the opportunity to assess internal stresses and associated deformations (Figure modified from MSC Software). 74

Figure 34: The modeling process consists of several distinct processes that develop and solve dynamic equations of motions under varying conditions with specific sets of inputs and outputs at each process.....76
Figure 35: The free body diagram of the knee shows the overall system setup including associated bones, muscles and ligaments with their respective frames of reference. (Used with permission from [119]) 78
Figure 36: The model incorporates two muscle controllers that are used to set knee adjust the quad forces to match profiles set by the user. In the case of flexion, all four quads are activated to achieve flexion to match a specific profile using a PID controller (left). In addition, there is a PD controller stabilizing the patella about the SI axis that affects the force in the vastus medialis and lateralis (right) (Used with permission from [118]).....83
Figure 37: The contact detection algorithm is defined through two complimentary surfaces, one of which is a point cloud and the other is a surface polynomial. The surface polynomial is also built to contain a convex hull which essentially acts as the bounding parameters for the contacting surface (Used with permission from [118]).....85
Figure 38: Many TKA contact models incorporate the low point assumption that contact occurs on the lowest point of the femur. While true on a flat surface, the concave bearing surface can invalidate this assumption (Used with permission from [118]). 85
Figure 39: Using the cross products, the convex hull algorithm can be used to determine if a point lies within the convex hull. To do this the cross product is taken between the vectors connecting each test point to two points of the convex hull. In the top row the third case has a negative cross product meaning the point lies outside the convex hull. In the bottom row all cross products are positive therefore the point being tested lies within the convex hull (Used with permission from [118]).....87
Figure 40: In order for the contact detection algorithm to denote contact, two conditions must be met. First, the point cloud on the femoral component must be less than the polynomial surface for the bearing (left) and second, this contact must occur within the projection of the convex hull (right). 87
Figure 41: Should penetration be detected, equations are used to calculate the contact forces where X and Z are anteroposterior and mediolateral directions respectively and Y is the proximal/distal direction. The normal force equations are based on the normalized partial velocities factored with penetration distance (Pen), Penetration stiffness value (K) and rate of penetration change and B is a factor on the penetration velocity applied exclusively in the vertical direction. These normal forces are also used to calculate frictional forces which are factored as contributions to the kinematics of the system (Used with permission from [118]). 88
Figure 42: To setup a simulation a visualization is used to both place components relative to bones as well as place bones relative to each other to achieve realistic initial conditions. 90

Figure 43: The model has been built to include an intuitive and efficient user interface which allows for a user to place components and ensure that desired spatial changes are being made. 92
Figure 44: Accurate bone models were generated for each subject using CT scans and a segmentation process. These models were made to include the six inches of the epiphysis of the femur. 102
Figure 45: From top to bottom: beginning with the fluoroscopic sequence, the fluoroscopic images are isolated to include the frames of interest. The 3D scene is then recreated using a registration process. This leaves the digitized bone models in a recreation of the fluoroscopic scene. Using the transformations and rotations of these components, the kinematics are calculated. 103
Figure 46: AP points for a right knee as measured by 3D-to-2D image registration process. The midline of the normal knee is defined through the best fit circles of the medial and lateral sides of the tibia plateau. Points A and C are defined as positive AP positions, while B and D are defined as negative AP positions. A translation from a positive point to a negative point is denoted as a negative translation. If an MAP point is more anterior than the LAP point, such as points A and D, the angular orientation is positive. A pivot from point C to D about point A is an example of positive axial rotation. This method of motion definition was originally used by Grieco, et al [65]. 104
Figure 47: Beginning with the segmented bones from the CT scan (left), the bone models to be used as mathematical inputs are altered to only reflect articulating geometry (center). The model is then smoothed using a meshing algorithm and the results are used as mathematical inputs. 106
Figure 48: The meniscus geometry was originally obtained from a segmented MRI scan and used to build a continuous, solid body meniscus. 106
Figure 49: Results are shown for the medial (blue) and lateral (red) condyle translations between the fluoroscopic analysis (dashed) and mathematical simulations (solid) during 120 degrees of flexion. 109
Figure 50: Results are shown for the axial rotation measurement between the fluoroscopic analysis (yellow) and mathematical simulations (green) during 120 degrees of flexion 109
Figure 51: Medial and lateral condyle position depictions for an arbitrary simulation of the normal knee with low conformity (left) and higher conformity (right). 112
Figure 52: Using the pertinent articulating geometries, simulations can be performed to replicate in vivo conditions across a variety of activities. 114
Figure 53: Proximal view of the average kinematics through 120 degrees of flexion measured through mathematical simulation (left) fluoroscopic analysis (right). 117
Figure 54: Force loading profiles for both ACL and PCL fibers during a simulated deep knee bend. 119
Figure 55: Summary of fluoroscopic results for normal knees (Komistek 2003). 119

Figure 56: Separate modeling results for an initial case (left) and a case with increased medial conformity (right). 121
Figure 57: The quadriceps muscle group consists of four muscles. The vastus medialis, lateralis and intermedius all originate on the proximal femur and insert on the proximal patella. The rectus femoris also inserts onto the patella; however, it originates on the pelvis. The quadriceps tendon anchors the distal side of the patella, and all of these muscles collectively control knee extension. 126
Figure 58: The flexion of the knee in the model is controlled by a PID controller that applied quadriceps force to match a target function that is input by the user. While the flexion is input by the user, the forces are determined to match, and this efficiency of the mechanism is an important factor. 127
Figure 59: The quadriceps mechanism is directly related to the constraining forces applied by the muscle and ligament soft tissue structures. 129
Figure 60: During flexion the wrapping of the extensor mechanism on the femur bone can contribute to changes in the force vectors administered through the quadriceps muscle definitions. 129
Figure 61: Previous iterations of the model have achieved extensor mechanism forces of roughly 5.7 times BW. Literature suggests these forces should be approximately 2.5 times BW. 130
Figure 62: During deep flexion, the quadriceps muscles experience wrapping about the trochlear groove of the femur. The offset of this point from the femoral bone may affect the forces of the quad muscles. 134
Figure 63: At full extension the multiple quad muscle fibers apply similar forces, however in deeper flexion some of these fibers have advantageous lines of action and for that reason the force definitions have been altered to allow for some of these fibers to be favored over others. In one instance the two fibers of the rectus femoris maintain equivalent contributions (top right) and another where the proximal fiber contributes three times the force of the distal fiber (bottom right). 137
Figure 64: Prior iterations of the model assumed a stationary pelvic bone. To enhance physiological accuracy, this bone was given a specified rotation as a function of flexion. 138
Figure 65: Adding the rotation onto the pelvic bone facilitates a compliance that diminishes the need for direct quad force contributions. For the stationary pelvis, the quads are the only force contribution (blue), whereas the rotated pelvis contributes an additional force that helps facilitate flexion (green and blue). 139
Figure 66: To evaluate the effect of each geometric factor, a PCR device was taken and one by one the features were substituted to match an anatomically based geometry. 142
Figure 67: Updating the velocity functions in the model improves muscle efficiency and drops quad forces for 5.7 times BW to 4.3 times BW. 142

Figure 68:Moving femoral muscle wrapping points anteriorly or posteriorly provides minimal differences in quad forces compared to a controlled simulation defined with the wrapping point positions. 144
Figure 69: Re-distributing muscle forces between various fibers appear to increase quad forces compared to a control ratio for force distribution. While this does not necessarily mean that there is not an effective distribution of forces that would contribute to improved efficiency, the tested configurations demonstrated marginal force increases. 145
Figure 70 Pelvic tilt during the simulation is central to extensor mechanism efficiency compared to a stationary control simulation.....146
Figure 71: In order to better assess the role of articulating geometry and functionality of the extensor mechanism, two different articulating geometries were compared. The original is a PCR device and it was compared to a modified normal knee. Each feature was added individually and then collectively and these features included changing to a symmetric patella, adding an ACL, defining the trochlea, defining femoral condyles and defining the bearing surface. 148
Figure 72: Earlier iterations of the model have achieved quadriceps mechanism forces of about 6 times BW (left). Using several strategies, the forces were able to be mitigated to 2.5 times BW (right) which is a value that has been reported empirically in literature. 152
Figure 73: Using fluoroscopy, two measurements were taken in vivo at various time steps. The rotation of the femur in the tibia reference frame (yellow) and the rotation of the tibia in the global reference frame. 157
Figure 74: An analogue goniometer was used to measure various angles between the ground, foot and tibia. These samples were captured computationally at 100hz. 158
Figure 75: The foot consists of a variety of bones that were assumed to be rigidly attached for this particular analysis. 160
Figure 76: The previous iterations of the model (left) facilitated tibia rotation at a specified angle (θ) relative to the ground in which the Newtonian frame was established (blue dot). The improved version of the model includes the foot, as well as a second angle (ϕ) about the point where the foot contacts the ground where the Newtonian frame is established. version of the model includes the foot as well as a second angle (ϕ) about the point where the foot contacts the ground where the Newtonian frame is established. 160
Figure 77: Using an analogue goniometer attached between the foot and the ground, flexion and extension angles were collected (orange), as well as eversion and inversion of the foot (blue). These measurements are effectively the pitch and roll of the foot, respectively. 161
Figure 78: Using the goniometer, the ankle flexion between the foot and the tibia was collected. 161
Figure 79: The simulations where the foot flexes tend to demonstrate greater femoral posterior translation. 163

Figure 80: The simulations where the foot flexes tend to demonstrate similar femoral anterior translation patterns with slightly greater translational velocities. 163
Figure 81: The simulations where the foot flexes tend to demonstrate greater axial rotation compared to simulations with a stationary foot. 164
Figure 82: The simulations where the foot flexes tend to demonstrate greater quad mechanism forces compared to simulations with a stationary foot. 164
Figure 83: Evaluated fluoroscopically, normal knees on average appear to experience the greatest magnitude of femorotibial rotation, while PS and PCR devices not only experience significantly less rotation but also differing rotation values between each other. 166
Figure 84: Evaluated fluoroscopically, normal knees on average appear to experience the greatest magnitude of tibial rotation in the global reference frame, while PS and PCR devices not only experience significantly less rotation but also differing rotation values between each other. 168
Figure 85: When both positive and negative rotations determined fluoroscopically are applied to the tibia of the model, external tibia rotation tends to increase lateral femoral posterior translation while external tibia rotation tends to decrease lateral femoral translation. 169
Figure 86: When both positive and negative rotations determined fluoroscopically are applied to the tibia of the model, external tibia rotation tends to increase medial femoral anterior translation while external tibia rotation tends to decrease medial anterior femoral translation. 170
Figure 87: When both positive and negative rotations determined fluoroscopically are applied to the tibia of the model, external tibia rotation tends to increase femoral external rotation while external tibia rotation tends to decrease femoral external rotation. 172
Figure 88: Computer models of all TKA components can be imported through software. These components are purely for visualization purposes as mathematical representations need to be derived. 183
Figure 89: Using an iterative calculation algorithm, regions of points are selected that have the potential for contact. This is done for the femoral condyle surfaces (top left), patella surface (top right) and any anterior or posterior CAM mechanisms (bottom). 185
Figure 90: Using a regression algorithm, polynomial surfaces are fit to each articulating surface. These surfaces each correspond to one of the point clouds from Figure 89, including the bearing surfaces (top left), trochlear groove (top right) and any bearing posts (bottom). 186
Figure 91: The convex hull (shown in blue) represents the outer bounds of the contacting surfaces for the lateral side of the bearing. This same process is also applied to the medial side, posts, and trochlear groove. 189
Figure 92: In order for the contact detection algorithm to denote contact, two conditions must be met. First, the point cloud on the femoral component must be less than the polynomial surface for the bearing (left) and second, this contact must occur within the projection of the convex hull (right). 191

Figure 93: If the two conditions are met for contact detection to occur, then a force will be calculated as a function of point acceleration, penetration and material stiffness and fed back into the mechanical system. 191
Figure 94: As all polynomial surfaces are generated, the interface affords the opportunity to make changes with respect conformity, height and tilt. Possible the most relevant of these changes is the ability to change sagittal conformity which can be decreased (left) or increased (right).....193
Figure 95: The user is given the option by the interface to select a destination for the output of the stl files and any associated parametric equations. 195
Figure 96: All surfaces on the bearing component can be exported as mesh surfaces for medial and lateral bearing surfaces as well as bearing post surfaces. 195
Figure 97: The parametric equations are exported in the form of an excel sheet which can be easily imported into NX or any other prevalent CAD Software. These equation sets are normalized between 0 and 1 for values of t and corresponds to a parametric curve that matches the exported surface meshes. This is done to offer the capability to edit and knit surfaces as needed.....198
Figure 98: The surface will be created from six total splines (three in each direction). The splines that align with drawing planes are labeled with numbers 1 and 2 (the constant expression is zero) and the additional splines are labeled with letters A,B,C,D. 199
Figure 99: The surfaces with associated component splines can be combined to demonstrate all elements of the parametric surface spline creation. 200
Figure 100: The homogenous equations (those that rest on the anatomic planes) are determined through two spline expressions.....202
Figure 101: The remaining four expressions for the parametric splines are output in terms of their spline components. 203
Figure 102: The medial and lateral conformity can be adjusted in the model. In this case, the increased conformity is exaggerated to show the conformity differences. Note that this analysis also included a cam and post mechanism (not shown). 205
Figure 103: Decreasing bearing conformity appears to increase medial translation magnitudes.....205
Figure 104: Decreasing bearing conformity appears to increase lateral translation magnitudes. 206
Figure 105: Decreasing bearing conformity appears to facilitate axial rotation magnitudes. 206
Figure 106: To test conformity without interaction from post mechanisms, a similar study was setup using a PCR device which varied medial and lateral bearing conformity independently and concurrently.....208
Figure 107: To test post placement using the model, several simulations were set where the position of the post mechanism was moved either anteriorly or posteriorly. 210

Figure 108: The model showed that moving the cam and post mechanism posteriorly both lead to earlier engagement and higher forces overall when engagement occurred. 210
Figure 109: Distinct morphological differences exist on the distal femur between genders, ethnicities and individual subjects. 213
Figure 110: Mahfouz, et al demonstrated significant femoral morphological differences between anteroposterior and mediolateral bone dimensions [70]. 216
Figure 111: Mahfouz, et al. demonstrated significant tibial morphological differences also between anteroposterior and mediolateral bone dimensions [70]. 216
Figure 112: In order to assess the role of soft tissue location regarding kinematics, a sensitivity analysis will be performed both where only origins are shifted and where both origins and insertions are translated. 218
Figure 113: For all African (blue), Asian (orange) and Caucasian (grey) demographics tested, there are unique anatomical features that may contribute to kinematic aberrations. 220
Figure 114: In order to control for bone size, all geometries under evaluation were isotopically scaled to a uniform mediolateral dimension. 221
Figure 115: Theoretical subject 2 experienced greater femorotibial axial rotation. 224
Figure 116: Theoretical subject 2 experienced greater lateral femoral condyle translation. 224
Figure 117: Theoretical subject 2 experienced greater medial femoral condyle translation. 225
Figure 118: Female femoral tibial rotation for both theoretical subjects. 225
Figure 119: Female lateral femoral condyle translation for both theoretical subjects 226
Figure 120: Female medial femoral condyle translation for both theoretical subjects 226
Figure 121: Caucasian femoral tibial rotation for both theoretical subjects. 228
Figure 122: Caucasian lateral femoral condyle translation for both theoretical subjects 228
Figure 123: Caucasian medial femoral condyle translation for both theoretical subjects 229
Figure 124: African femoral tibial rotation for both theoretical subjects. 229
Figure 125: African lateral femoral condyle translation for both theoretical subjects 230
Figure 126: African medial femoral condyle translation for both theoretical subjects 230
Figure 127: Asian femoral tibial rotation for both theoretical subjects. 232
Figure 128: Asian lateral femoral condyle translation for both theoretical subjects. 232
Figure 129: Asian medial femoral condyle translation for both theoretical subjects 233

Figure 130: Femoral tibial rotation is compared for a subject from all theoretical groups. 234
Figure 131: Lateral condyle translation is compared for a subject from all theoretical groups. 236
Figure 132: Medial condyle translation is compared for a subject from all theoretical groups. 237
Figure 133: Each soft tissue attachment is defined relative to bony landmarks on the bone architecture. For this reason, it is a reasonable expectation that morphology will shift these bony landmarks and thus shift the attachment sites. Figure modified from [2]. 239
Figure 134: The only LCL origin shift that demonstrated sensitivity to anteroposterior directional translation was a shift in the proximal direction. 241
Figure 135: Although a proximal origin shift contributed to a slight deviation from the other analysis, there was not a substantive influence on medial condyle translation. 241
Figure 136: Because of the shift in the lateral condyle translation, the axial rotation also demonstrated a sensitivity to a proximal origin shift. 242
Figure 137: Femoral rotation demonstrated minimal sensitivity to MCL origin shifts. 242
Figure 138: The only analysis to demonstrate sensitivity to MCL origin shifts was the medial compartmental force. 243
Figure 139: Translating the LCL origin and insertion in various directions does not demonstrate kinematic sensetivity in the model. 243
Figure 140: Translation of the MCL contributes to minimal deviations in kinematics except for an increase in posterior femoral translation when shifted proximally. 244
Figure 141: Similarly, compared to the lateral side of the knee, the medial femoral condyle also experienced a posterior shift in medial condyle translation. 244
Figure 142: The medial and lateral differences in femoral translation offset to a net consistency when the MCL is shifted, regardless of direction. 245
Figure 143: The only factor to be sensitive to MCL translation across all increments is the contact force of the medial femoral condyle. 247
Figure 144: Anterior and posterior shifts to the insertion of the patella tendon tend to contribute to equivalent phase shifts in the translation of the lateral femoral condyle. 247
Figure 145: Anterior and posterior shifts to the insertion of the patella tendon also tend to contribute to equivalent phase shifts in the translation of the medial femoral condyle. 248
Figure 146: The medial and lateral condyle translational shifts tend to offset constituting to minimal variations in axial rotation. 248
Figure 147: Varus and valgus deformities result from the articulating surface of the femur rotating either internally (varus) or externally (valgus) about the anteroposterior axis compared to the neutral orientation of the femur. While

small deformations on an individual basis are common, greater than five degrees of rotation denotes a deformity.....253
Figure 148: Posterior cruciate retaining total knee devices retain the posterior cruciate ligament (center). While sometimes considered advantageous, if the PCL ligament is compromised, it becomes unable to keep the knee posterior (left) leading to extensor mechanism impingement. A proper PCL maintains the device posteriorly facilitating proper kinematics (right).....255
Figure 149: To replicate varus and valgus conditions, the femoral surface was rotated five degrees internally for varus (red) and five degrees externally for valgus (blue). 258
Figure 150: Between the healthy and arthritic subjects, there was minimal kinematic difference outside of early flexion. 259
Figure 151: Increased friction in the model produced a need for greater quadriceps force. 261
Figure 152: Greater coefficients of friction also contributed to increased PCL forces. 261
Figure 153: Putting the ACL in tension or in slack directly contributes to the ACL force applied within the model. 262
Figure 154: When the ACL is in slack, the initial position of the lateral condyle begins posteriorly compared to a properly tensioned ACL. This initial position contributes to mitigated rotation and adverse kinematics. 264
Figure 155: Partially due to the difference in lateral translation, a PCL with half the tension begins four degrees externally rotated. The motion patterns become similar around 25 degrees of flexion. 264
Figure 156: Between healthy and varus or valgus aligned knees, there is not a substantial effect on kinematics due to the deformity. 265
Figure 157: The theoretical subject with the valgus deformity demonstrated lateral contact forces greater than the healthy knee while the varus subject demonstrated lesser medial contact forces.....265
Figure 158: The theoretical subject with the varus deformity demonstrated medial contact forces greater than the healthy knee while the valgus subjects demonstrated lesser medial contact forces.....266
Figure 159: Throughout the development of the model, the ankle definition has gradually added elements from the ankle, to the foot and finally the toes, which are necessary for gait. 271
Figure 160: The addition of the toes adds another set of specified angle rotations to the model. The θ angle represents the rotation of the toes with respect to the Newtonian reference frame, the angle ϕ represents the angle between the foot and the toes, and φ represents the angle between the foot and ankle. 271
Figure 161: Throughout the gait cycle, the flexion of the foot increases with respect to the Newtonian frame. In addition, the contact point where the forces connect to the Newtonian frame shifts anteriorly to replicate the motion and contact pattern of the foot. 272

Figure 162: To make the transition from stance phase (left) to swing phase (right) the model must be inverted and center the rotation on the pelvis instead of the foot. 273
Figure 163: During stance phase the foot maintains constant ground contact while the knee enters a cycle of flexion followed by extension. 274
Figure 164: The knee flexion increments have slight differences between stationary flexion and gait where the gait pattern experiences a narrower parabolic pattern with greater flexion. 274
Figure 165: During gait the simulation predicted less tibiofemoral axial rotation compared to stationary flexion. 276
Figure 166: Compared to stationary flexion, the gait pattern produced a similar pattern with smaller magnitudes of medial anteroposterior translation. 276
Figure 167: Compared to stationary flexion, the gait model produced a smaller overall magnitude of lateral condyle translation with the posterior to anterior transition occurring prior to the flexion extension transition in the model. .. 277
Figure 168: Swing phase occurs immediately following stance phase as the foot leaves the ground. The activity then becomes passive until the foot reestablishes contact with the ground. 277
Figure 169: Aside from a slight phase shift in the positive time direction, the two flexion patterns between swing and stance phase are similar. 279
Figure 170: Between swing and stance phase, the femoral rotation patterns are similar. 279
Figure 171: The swing and stance phase motion patterns are similar with the notable exception of the posterior motion occurring as swing phase ends. 280
Figure 172: The medial condyle translations are similar between both swing and stance phase. 280
Figure 173: Average kinematic results for ten normal, healthy subjects evaluated both through the model and through fluoroscopy. 283
Figure 174: The telemetric device is a modified total knee arthroplasty where the tibia component is equipped with a force sensor that transmits force measurements externally to a data acquisition system. 283
Figure 175: The mathematical model was able to predict contact forces to within 15% of the telemetrically measured values. 285

CHAPTER ONE: INTRODUCTION

Throughout the course of this dissertation, various aspects of the human knee will be investigated through physical and computational methods. In order to sufficiently understand both geometry and physiology of the knee as a mechanical system, it first becomes necessary to have a functional understanding of knee anatomy. Such a knowledge base will be necessary to fully comprehend the development of the mathematical model and significance of subsequent discussion.

1.1 Anatomy of the Knee

1.1.1 Anatomic Definitions

Familiarity with medical spatial terminology is a crucial aspect of describing the human body. There are three separate planes that are used to describe the anatomical structures. The sagittal plane bisects the body into left and right sides; the coronal plane divides the body between front and back; and the transverse plane divided the body between top and bottom.

Within these planes exists an anatomical system of axes that is useful for describing the positions and motions of the body. The superior/inferior (SI) axis is defined by the intersection of the sagittal and coronal planes. The anterior posterior (AP) axis is defined by the intersection of the transverse and sagittal planes, and the medial/lateral (ML) axis is defined by the intersection of the transverse and coronal planes (Figure 1).

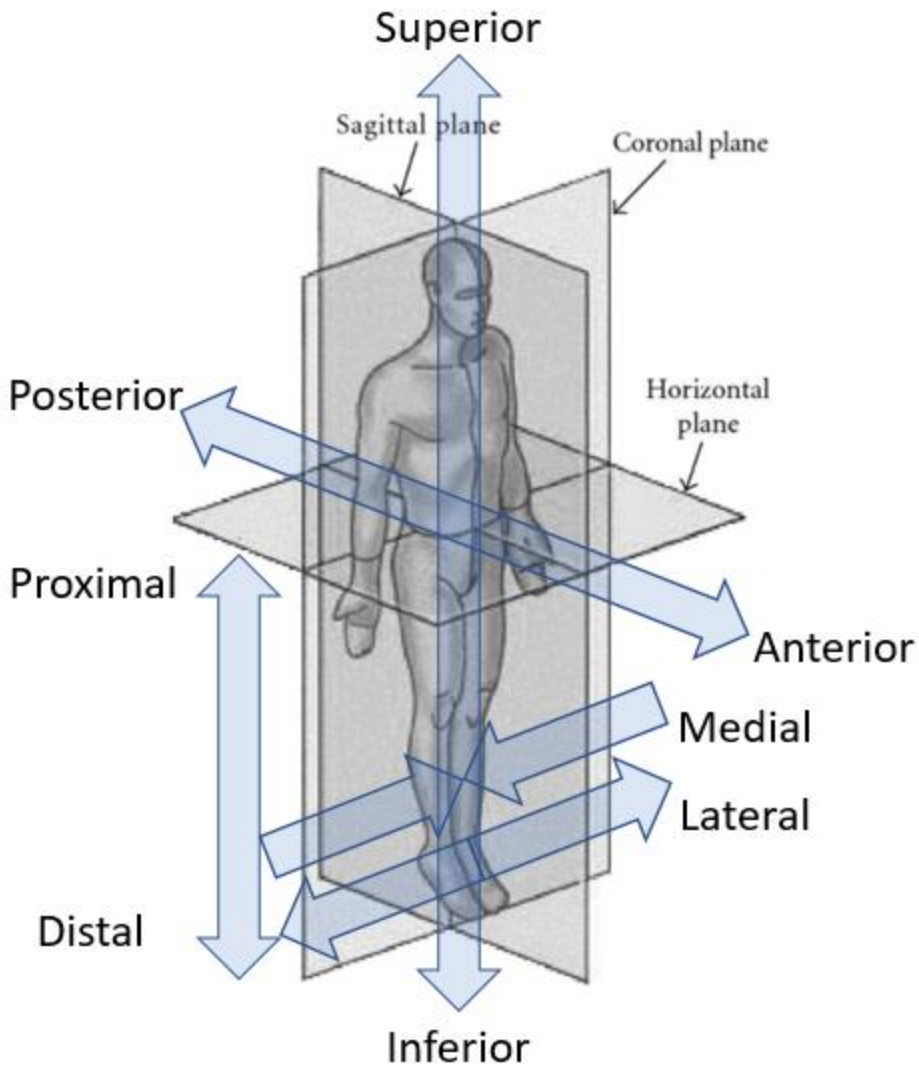


Figure 1: The spatial definitions of the human body are divided into three separate planes that intersect to form three respective axes. While the anterior/posterior axis, superior/inferior axis, distal axis and lateral axis are defined away from their respective planes, proximal and medial axis are defined toward their respective planes. (Figure modified from [1])

The medial/lateral and proximal/distal axes are unique compared to the others. The medial axis is defined toward the sagittal plane, whereas the lateral axis is defined away and the proximal axis is defined toward the transverse plane and the distal axis is defined away. These definitions are necessary because they maintain common axis system regardless of bone orientation and configuration. For example, the anteroposterior axis at full knee flexion is the same as it is during full flexion. There are additional axes, such as plantar/dorsal and cranial/caudal; however, these have limited application to the knee.

1.1.2 Bony Architecture

The knee is an excellent example of a diarthrodial joint, meaning that it represents the attachment between several bones with the interfaces insulated by a capsule of synovial fluid [2]. While the knee is colloquially referred to as a single joint, in actuality it is a complex system of two joints between three interfaces bridging three bones [2].

The first and most prevalent of these joints is the tibiofemoral joint, connecting the femoral and tibial bones which are the two longest bones in the human body [2]. The femur is a long bone with the femoral head protruding on the proximal epiphysis (end near the torso) which connects to the acetabulum of the pelvis at the hip. The distal epiphysis (end away from the torso) of the femur branches into two convex femoral condyles, with one being medial (toward the centerline of the body) and the other being lateral (away from the centerline of the body) (Figure 2).

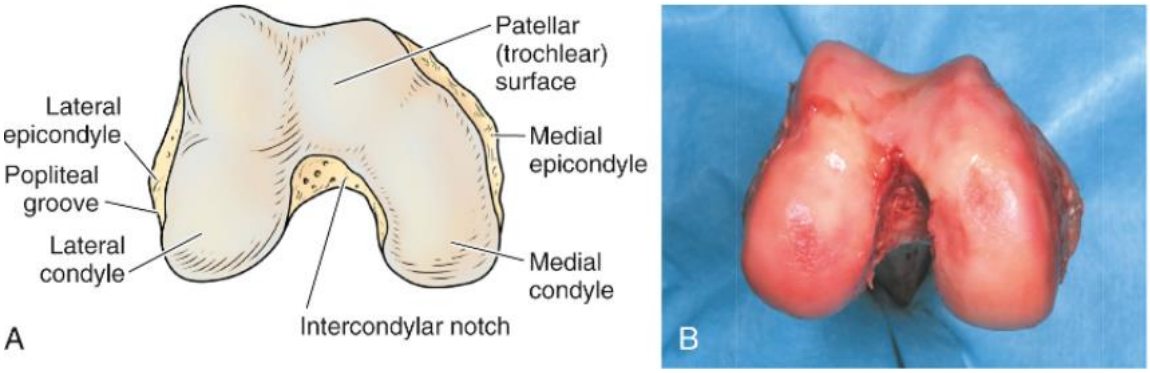


Figure 2: On the distal end of the femur anatomy diverges into two well defined condyles represented pictographically (A) and in surgery (B). Image derived from [2].

The tibial bone lies distal of the femoral bone and is capped with two concave indentations on its proximal epiphysis which complement the medial and lateral epicondylar geometry of the femur. These create two interfaces between the femur and tibia with one being medial and the other being lateral [2]. The tibia then extends distally through its diaphysis, connecting to the talus of the ankle (Figure 3).

The second joint that makes up the knee is the patellofemoral joint which consists of the disk-shaped patellar bone and the femoral trochlea, which is the anterior (front) side indentation of the vertical femur connected through a single interface (Figure 3). The tibiofemoral and patellofemoral joints work in synchrony, where the tibiofemoral joint bears most of the weight from the body. The patella facilitates the transfer of forces from the extensor mechanism during flexion and extension.

In addition to the bones that make up the knee joint, there are also additional bones that are relevant through proximity and are fundamental in defining the knee as a mechanical system [3]. These include the pelvic bones and foot bones which compose the proximal and distal ends of the leg, respectively. The tibia has a smaller bone running parallel called the fibula which provides torsional stability about the proximal/ distal and medial/lateral axis [4] (Figure 4).

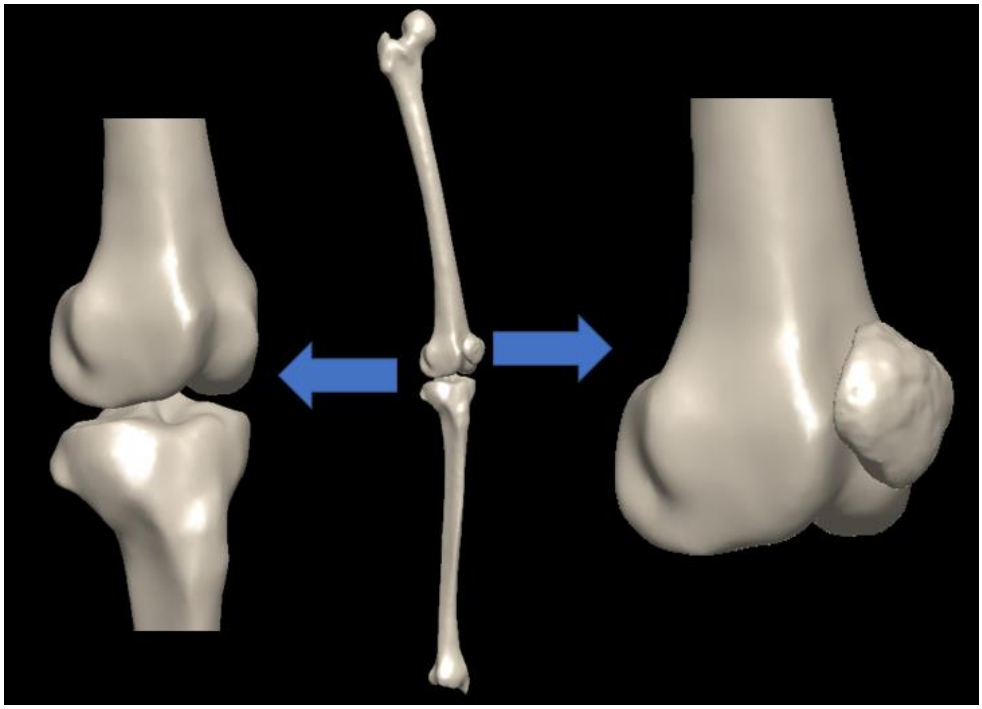


Figure 3: The knee joint (center) itself contains the tibiofemoral joint (left) between the tibia and femur, as well as the patellofemoral joint (right) between the patella and femur.



Figure 4: In addition to the tibia, femur and patella, there are additional bones that provide mechanical force transmission, bounding conditions, and mechanical reinforcement, including the pelvic bones, the foot bones and the fibula.

1.1.3 Ligamentous Architecture

The primary role of bone structures is to support normal, compressive and torsional loads generated through static and dynamic motions of the body. Ligaments, on the other hand, provide mechanical constraint through tension and stability to hold bones together at joint interfaces by constraining certain degrees of freedom. Ligaments by definition connect two bones across an interface. In the case of the knee, there are several ligament structures, including the anterolateral ligament that was discovered in 2013 [5]. Though there are many ligaments, there are five that mainly provide tensile constraint at the knee joint [2].

The anterior and posterior cruciate ligaments are critical stabilizers that cross between the femoral condyles with their main function being to prevent anteroposterior motion of the femur with respect to the tibia. The two collateral ligaments run parallel to each other on the medial and lateral sides of the knee, and their primary role is to resist varus/valgus rotation of the femur with respect to the tibia[2]. The fifth and final ligament is the patellofemoral ligament which has a medial and lateral side connecting the patella to the medial and lateral sides of the femur [2].

There is also soft tissue that constrains the patella in the proximal distal direction. However, these structures attach to the muscles of the quadriceps mechanism, making them technically tendons instead of ligaments, as tendons connect bone to muscle. The patella tendon not only serves as the activation for the extensor mechanics but also acts as a stabilizer for the patella in the groove of the femoral trochlea. In addition, there is a cushion of cartilage that separates the

tibia and femur, providing both a cushion for mechanical impact and stabilization for the femoral condyles on the tibia plateau [2]. Collectively, all of these structures can be seen throughout Figure 5 and Table 1.

From a materials perspective, most biological soft tissue structures are composed primarily of elastin and collagen. This is significant because these materials exhibit viscoelastic behavior where elastin behaves elastically and collagen behaves viscously [3]. Since these structures exhibit viscoelastic behavior, they are heavily susceptible to fatigue creep, especially over long periods of time [4]. For this reason, it is of note that the mechanical performance of ligaments will theoretically dissipate over time, eventually leading to compromised constraint forces, thereby less predictable femoral motion.

1.1.4 Muscular Architecture

The primary muscle groups across the knee are the quadriceps and hamstrings, whereas the quadricep muscles are the main mechanism producing knee motion. As the name implies, the quadriceps consist of four muscle groups. The vastus intermedious, vastus lateralis, and vastus medialis all originate on the distal femur and insert on the proximal patella through the patella tendon [2]. The fourth muscle, the rectus femoris, also inserts on the patella; however, the origin site is on the pelvis. The quadriceps are located on the anterior side of the femur and the posterior side has three counteracting muscles which are the semimembranosus, semitendinosus and biceps femoris.

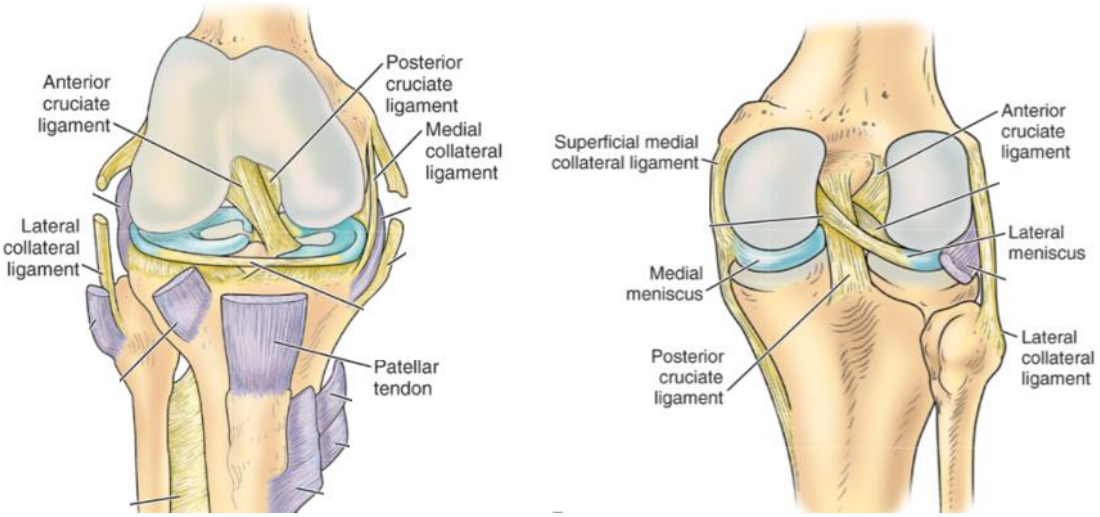


Figure 5: There are several many ligaments and other soft tissue that provide mechanical stability to the femur as it rests on the tibia. Figure modified from [2].

Table 1: Although the knee is constrained by many different soft tissue elements, there are eight primary structures that provide the majority of mechanical stability each with a unique role.

Tissue Structure	Origin	Insertion	Function
Anterior Cruciate Ligament (ACL)	Medial Anterior Tibia	Lateral Femoral Condyle	Resist anterior motion of tibia on femur
Posterior Cruciate Ligament (PCL)	Anterior Medial Femur	Posterior Tibia	Resist posterior motion of tibia on femur
Medial Collateral Ligament (MCL)	Medial Femur	Medial Tibia	Resist valgus rotation of the femur
Lateral Collateral ligament (LCL)	Lateral Femur	Lateral Tibia	Resist varus rotation of the femur
Medial Patellofemoral ligament (MPFL)	Medial Patella	Medial Femoral Condyle	Resist patella spin and medial translation
Lateral Patellofemoral ligament (MPFL)	Lateral Patella	Lateral Femoral Condyle	Resist patella spin and lateral translation
Patella Ligament	Distal Patella	Anterior Tibia	Resist proximal patella motion and anchor the quad muscles
Meniscus	-	-	Provide a low friction cushion between the femur and tibia and provide lateral stability of the femur on the tibia.

These muscles are collectively referred to as the “hamstrings” [2]. The semimembranosus and semitendinosus both originate on the pelvis and insert on the tibia, while the biceps femoris consists of two muscle heads. Both of these muscles insert at the interface between the tibia and fibula, where the short head originates on the femur and the long head originates on the pelvis [2], as seen in Figure 6.

While the quadriceps and hamstrings are antagonistic muscle groups, it is of note that the although the quadriceps muscles control eccentric knee movement (extension) and the hamstrings control concentric movement (flexion), the nature of knee flexion resists the pull of gravity to slow the descent into flexion. For this reason, the quads tend to play a much more active role in active knee flexion, relegating the hamstrings to the roll of a stabilizing muscle group, despite being the primary muscle group for concentric movement. This makes the hamstring muscles most useful under two conditions, passive flexion and stopping during a gait cycle. This is why hamstring injuries are so common in sports, such as football, soccer and tennis, as these are sports that require hard stops, substantially increasing the chances of overloading the hamstrings [6].

1.2 Knee Motions

With a solid understanding of knee anatomy, the next objective is to understand how these anatomical features interact with each other. The biomechanics of generalized musculoskeletal systems is relatively straightforward. Bones provide structural support, resisting compression; ligaments provide

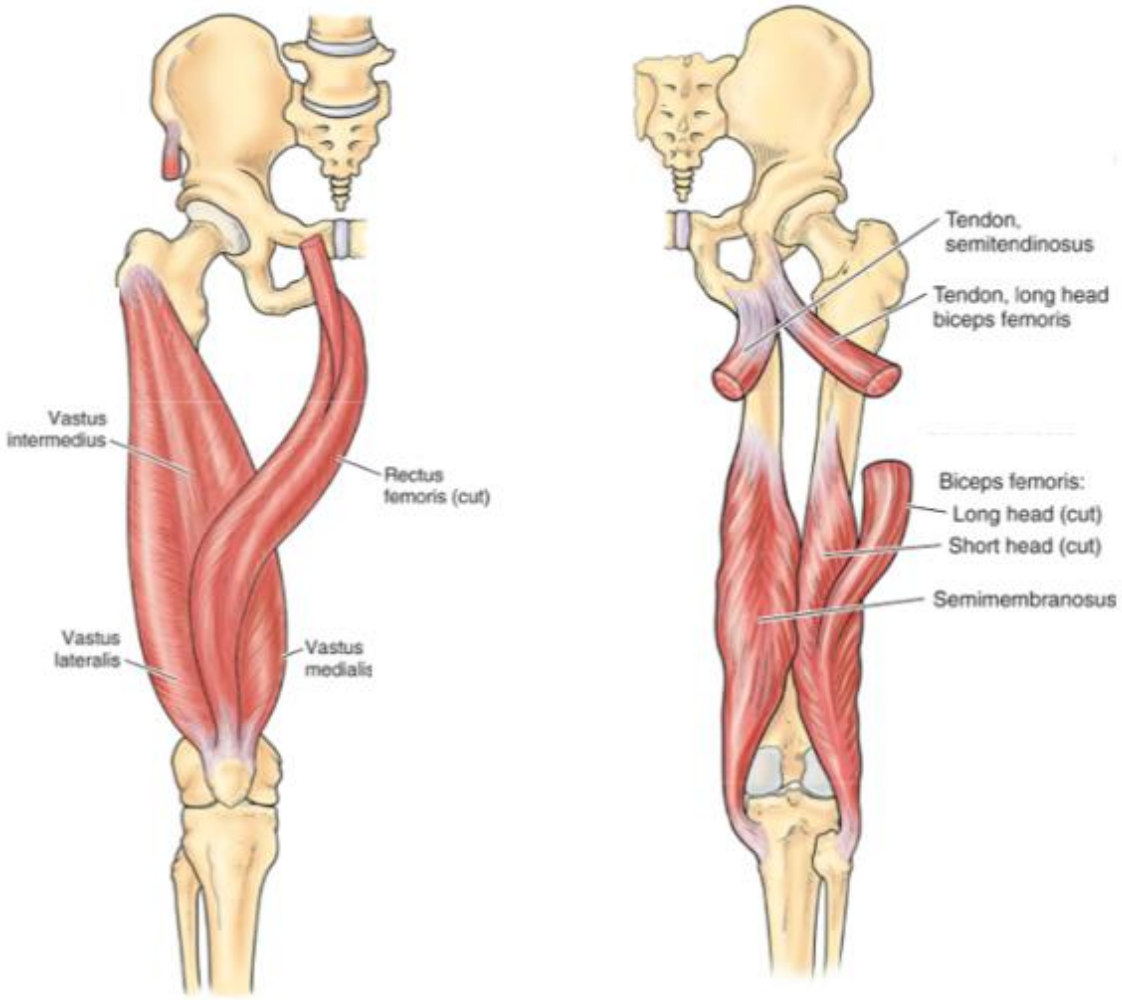


Figure 6: The anterior view of the quadriceps muscle group (left) and the posterior view of the hamstring muscle group (right).

constraint forces that resist when in tension; and muscles are the active force that drive the motions. Sufficive to say, the knee is built on these principles as well.

A properly constrained knee can have three independent degrees of freedom, two of which are rotational (about the medial/lateral axis and the proximal/distal axis) and one is translational (anterior/posterior direction). Under certain conditions, it is possible for the femur to rotate in the proximal/distal axis, demonstrating a phenomenon of condyle liftoff [7, 8]. Due to the constraints within the knee joint, it could also be assumed that the normal knee is actually a one degree-of-freedom joint (knee flexion), while other motions are produced by the constraints at the knee in combination with knee geometry. Intuitively, most of the rotation of the femur is going to be about the medial-lateral axis, which is also considered tibiofemoral knee flexion. In addition to flexion, the medial and lateral femoral condyles translate in the posterior direction during flexion and the anterior direction during extension[9]. This translation is achieved through some combination of rolling and sliding[10]. During this translation the medial and lateral femoral condyles translate differing magnitudes inducing a rotation about the proximal distal axis [9]. If this rotation of the femur is toward the lateral axis of the tibia, then the rotation is considered external, and if it is toward the medial axis, then the rotation is considered internal [11] (Figure 7). Although in this case, the rotation is noted as femoral rotation, it is more accurate to say that rotation occurs between the femur and the tibia.

Flexion and extension are two of several other knee motions which contribute to activities of proper function throughout daily life. Activities of daily

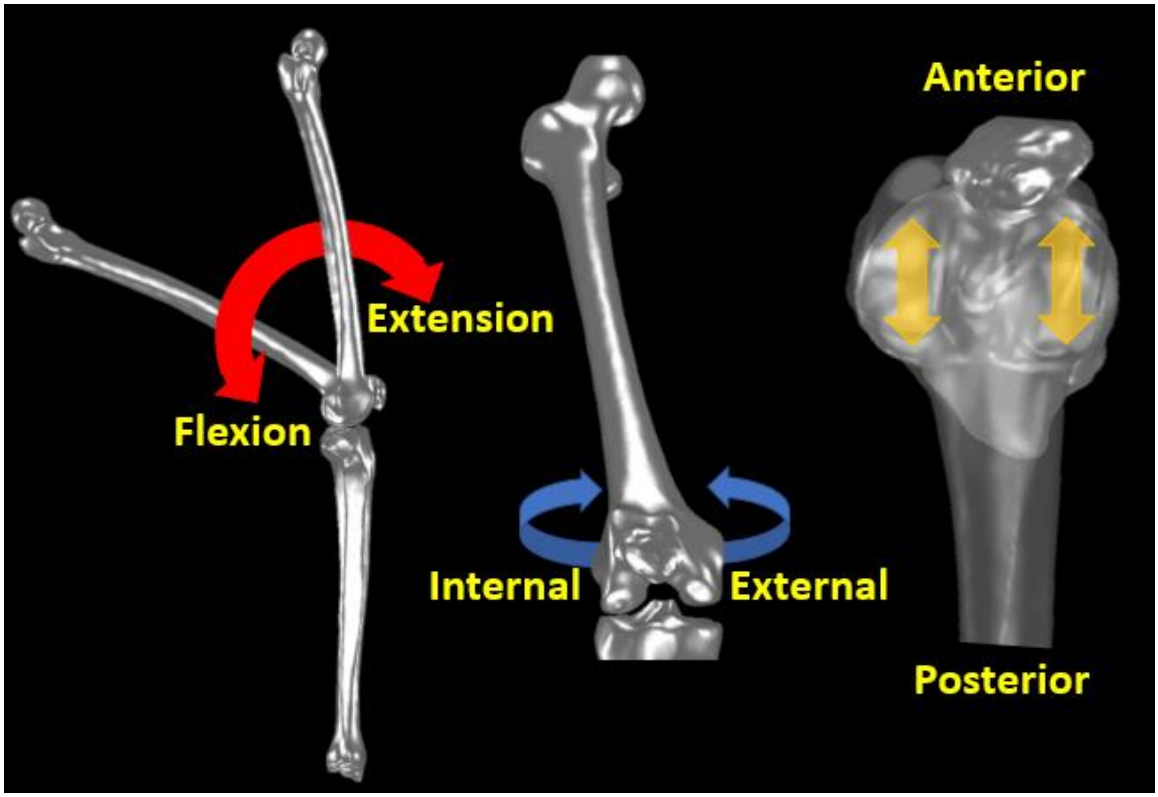


Figure 7: There are three primary quantifiable motions of the knee which are flexion/extension (left), internal/external femoral rotation (center) and anterior/posterior translation of the medial and lateral femoral condyles (right).

living (ADLs) are set activities that are used to objectively assess a patient's quality of life based on the management of a particular illness or injury [12]. In the context of the knee, the ADL that is of the most interest is ambulation or walking (i.e., is a patient successfully able to self-move from place to place successfully and with minimal assistance?). From a biomechanics perspective, the core motions that make up ambulatory activities are squatting, rising from a chair, walking on a level ground, walking up/down stairs and walking up/down on an inclined surface as seen in Figure 8 .

1.3 Osteoarthritis

Smooth, pain free knee motion is predicated on a smooth interface between the tibial and femoral bone interfaces which are insulated through articulating cartilage. Over time and repeated motions, this cartilage gradually breaks down leading to localized stress concentrations and eventually bone on bone contact at the knee. Due to cellular mechanotransduction, these increased stress concentrations will stimulate bone growth (Wolff's law) creating osteophytes on the articulating surface which exacerbate pain and expedite cartilage loss [13-15].

The combination of induced bone osteophytes and degenerated cartilage are collectively referred to as degenerative joint disease or osteoarthritis [16]. Figure 9 shows a side by side comparison between a healthy knee and an arthritic knee. Ostensibly, the damage caused to the joint through both pathological mechanisms contributes to substantially decreased range of motion, increased pain and a progressively worsening hindrance to quality of life for afflicted patients.

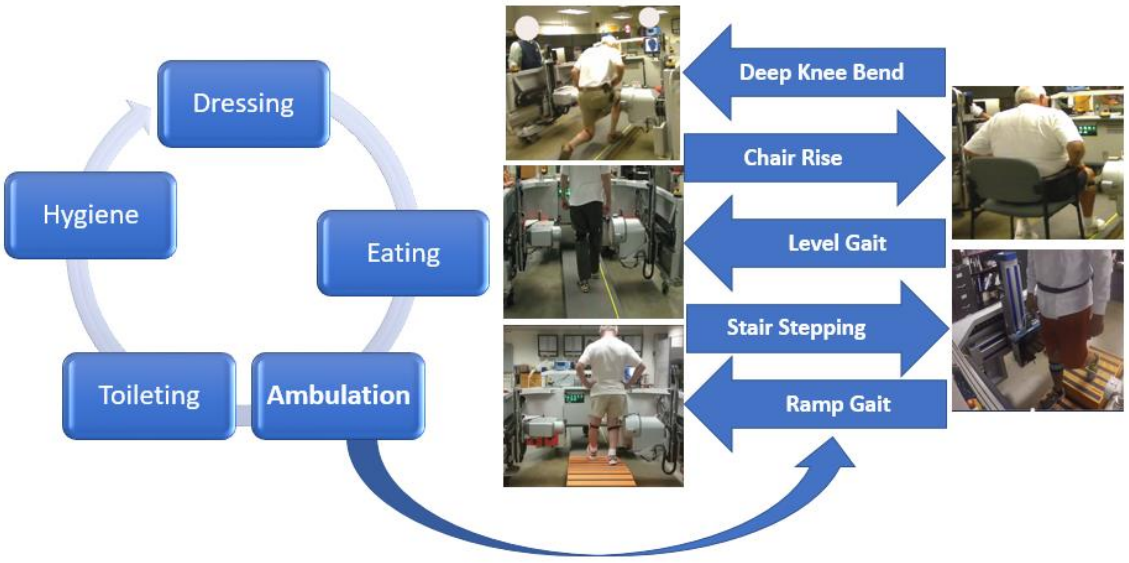


Figure 8: There are five primary categories that constitute activities of daily living. From a biomechanics perspective, the most important is ambulatory function which can be further assessed through activities modified from flexion/extension and gait activities.

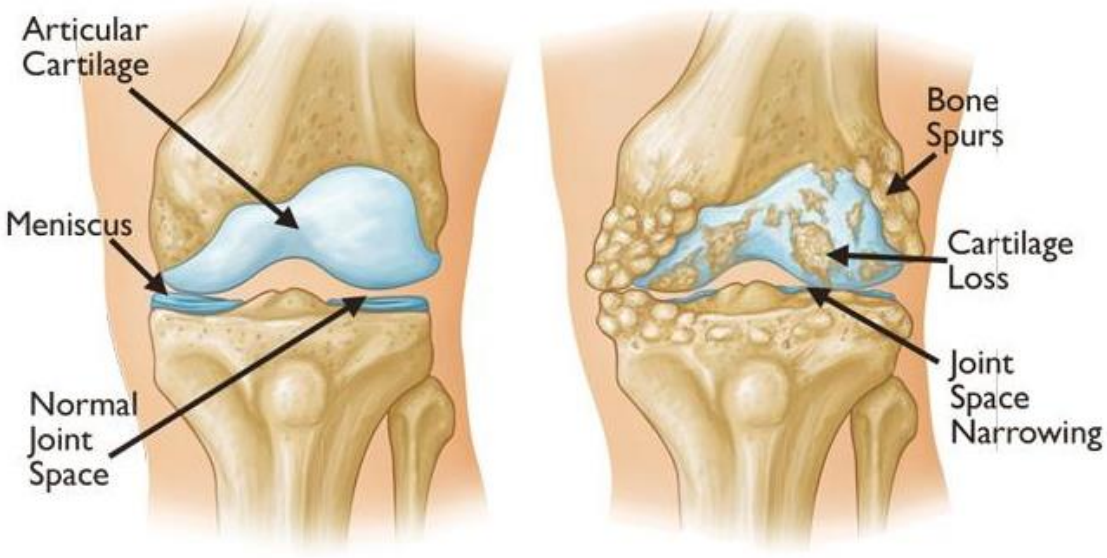


Figure 9: The healthy knee (left) consists of smooth articulating surfaces and normal joint space, whereas the arthritic joint (right) shows discontinuous cartilage, osteophyte formation and a compressed joint space (Figure modified from American Academy of Orthopedic Surgeons [16]).

Although there is currently no cure for osteoarthritis, there are short term treatments that can satiate the symptoms that it causes. The first of these is through lifestyle modification which includes both minimizing activities that aggravate the injury and losing weight to help mitigate knee stresses [16]. Analgesics such non-steroidal anti-inflammatory drugs (NSAIDs) can be used to help manage symptoms. Other medications such as viscosupplementation can be used to attempt to utilize natural processes in the body to restore the properties of joint fluid [16].

While many of these treatments are effective at managing symptoms, the effects will generally diminish over time whether through worsening joint conditions or increased tolerance to medical treatments. Eventually, surgical intervention will be required to restore quality of life.

1.4 Total Knee Arthroplasty

There are many surgical techniques that can be used to treat late stage osteoarthritis, however, the most common and most efficient of these is a total knee arthroplasty (TKA). Arthroplasty is derived from Latin meaning “re-formed joint” which is an appropriate name as a total knee arthroplasty is an artificial joint that replaces damaged bone and cartilage as seen in Figure 10. The typical TKA device is composed of three components. Two of these are metallic and affixed to the femoral and tibial bones and the third is a polymer bearing that provides a smooth articulating surface between the two metallic components (Figure 11). The metal of choice for these devices is typically either titanium or cobalt chrome, as

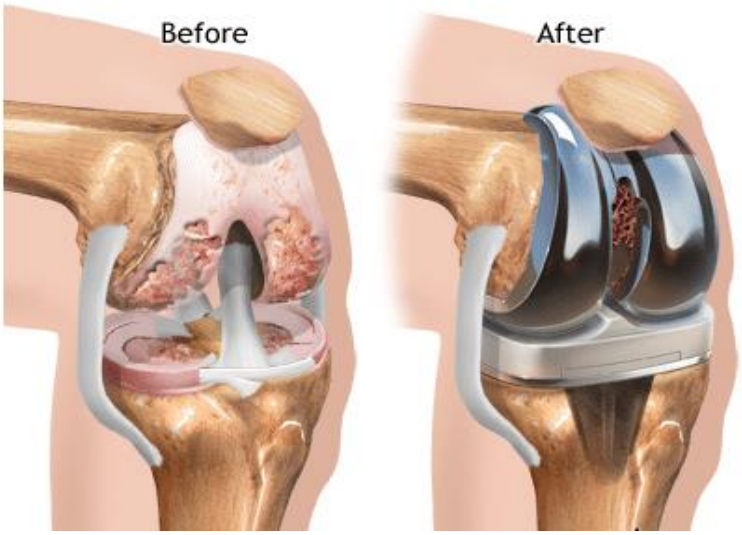


Figure 10: A total knee arthroplasty device replaces damaged articulating surfaces of the knee joint with metallic and plastic components (Figure modified from Mayo Clinic).



Figure 11: A traditional total knee arthroplasty device consists of two metal components mounted into the femur and tibia, along with a bearing to facilitate smooth motion. In some cases, the patella is resurfaced with bearing material as well.

both are biocompatible and possess excellent surface finishing and fatigue properties. While the bearing surface separating the femoral and tibial device components is smooth, the coefficient of friction is still substantially greater than a healthy knee. Because of the susceptibility to friction wear, an ultra-high molecular weight polyethylene is used, as the long chain polymers tend to be more resistant to wear over the life of the device.

Despite most TKA designs aiming to achieve the same process of replacing articulating cartilage, the designs themselves can be quite different, Some TKA devices retain soft tissue structures while others provide artificial stabilization to replace ligament structures. Some focus on simple condyle geometry while others use parametric expressions to define these geometries. There are a variety of design features in various TKA designs each with its own proposed benefit.

1.5 TKA Assessment and Analysis

With such a variety of devices available, the inevitable question becomes not only which performs the best, but also how can they be even be evaluated quantitatively? Understanding joint mechanics is a key aspect of successful total knee arthroplasty design, and there are many commonly used techniques to assess knee joint mechanics both with and without arthroplasty devices. These techniques include cadaver testing, mechanical simulators and fluoroscopic analyses. Each of these methods have their own inherent assumptions, advantages and limitations.

Cadaver testing, also known as ex vivo testing, takes a prospective device and implants it into a post life specimen (knee of a deceased patient). The setup

then performs any number of activities and measurements are taken. Mechanical wear simulators follow a similar setup with the notable exception that the device is placed onto a manipulator with various programmable motions. This technique is typically used to evaluate long term device wear and involves on the order of millions of cycles. Fluoroscopy is an imaging technique where video x-rays are used to register and measure the transformations of device components from which measurements can be assessed.

Cadaver tests, wear simulators and the use of fluoroscopy are examples of ex vivo (after life), in vitro (in glass) and in vivo (in life) testing, respectively (Figure 12). Each technique has both its own advantageous and limitations. Cadaver testing is anatomically accurate and easy to control, but also difficult to facilitate in large numbers and may not be accurately representative of living tissue. Wear simulators are great for high volume in highly controlled environments.

Unfortunately, wear simulators are both time consuming and do not account for variability in patient cycles, as cycles are not controlled by muscles and are therefore more or less the same. Fluoroscopy is the most accurate technique; however, it is also completely dependent on the device being implanted. As an imaging technique fluoroscopy, exposes patients to small amounts of radiation.

From an assessment perspective, there are two main quantifiable factors that TKA assessment seeks to evaluate. The first of these are kinetics which are



Figure 12: Cadaver rigs, mechanical wear simulators and fluoroscopy are all methods used to assess knee implant device performance.

the forces associated with the system containing a device. The second factor is kinematics which are the motions of a system containing the device. The forces of the TKA device tend to focus on bearing surface contact forces between components, as these forces correlate with various wear mechanisms. The motions of the TKA devices are also of interest as these are the general indicators of device performance. Some kinematic factors include flexion, axial rotation and femoral condyle translation as seen in Figure 13. In general, outside of in vivo design, kinetics and kinematics are mutually exclusive. Either forces need to be defined and motions evaluated or motions defined and forces evaluated. In vivo testing somewhat circumnavigates this issue. However, the tradeoff is that the body determines how muscle forces are allocated. The system becomes individualized and difficult to control across groups.

1.6 Mathematical Modeling

While there are many methods that can be used to evaluate the forces and motions of total knee arthroplasty, the vast majority of these techniques are predicated on the physical creation and in most cases, implantation of devices in cadavers or simulators. While this is not necessarily an issue in later stage designs, such methods represent a substantial time investment when evaluating early stage prospective designs that have not yet been validated. Such time-consuming methods not only limit the scope of the device and subsequent analysis but also adds significant time to the design process.

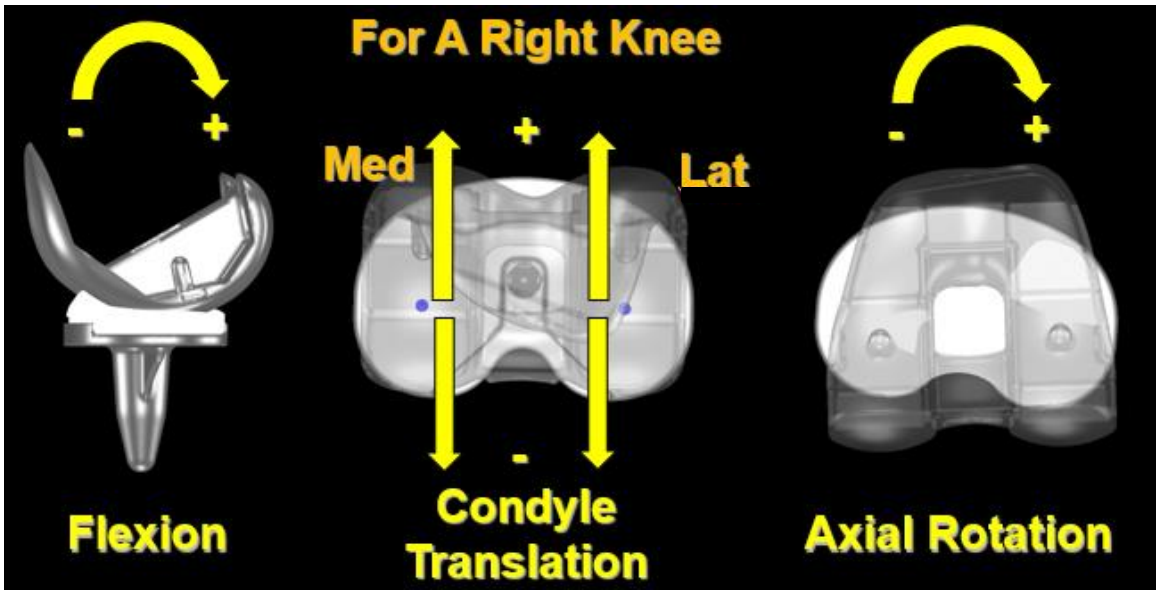


Figure 13: Kinematic parameters are assessed for TKA components much like the kinematics for the native knee. These values are flexion, medial and lateral condyle translation in the AP direction and axial rotation of the femoral component about the proximal/distal axis.

Mathematical modeling techniques utilize theoretical representations of bones, muscles, and ligaments to computationally simulate performance during activities of daily living without the need to manufacture or implant a device. In doing so, such modeling facilitates an efficient and effective design process where devices can be designed, evaluated and revised without the need to manufacture or implant the components (Figure 14).

1.7 Forward Solution Modeling

There are two main types of mathematical models. Inverse modeling uses motions as an input and outputs forces and forward modeling does the opposite by inputting force profiles and outputting motions. From a design perspective, the forward model is the most valuable as the muscle forces in the body are more or less optimized and thus cannot be changed (Figure 15).

The nature of a forward model as a design tool revolves around designers being able to virtually implant devices, determine a muscular force profile and assess the prospective device for the motions that occur during a theoretical simulation. Effectively, such a process simulates how a device would perform if it were to be implanted into a subject. Since the process is computational and can be done quickly, designs can be evaluated and revised faster, leading to more design iterations and better devices compared to physical testing alone. While not intended to be a replacement for physical testing, the goal of mathematical modeling is to improve the understanding of how the knee functions and provide

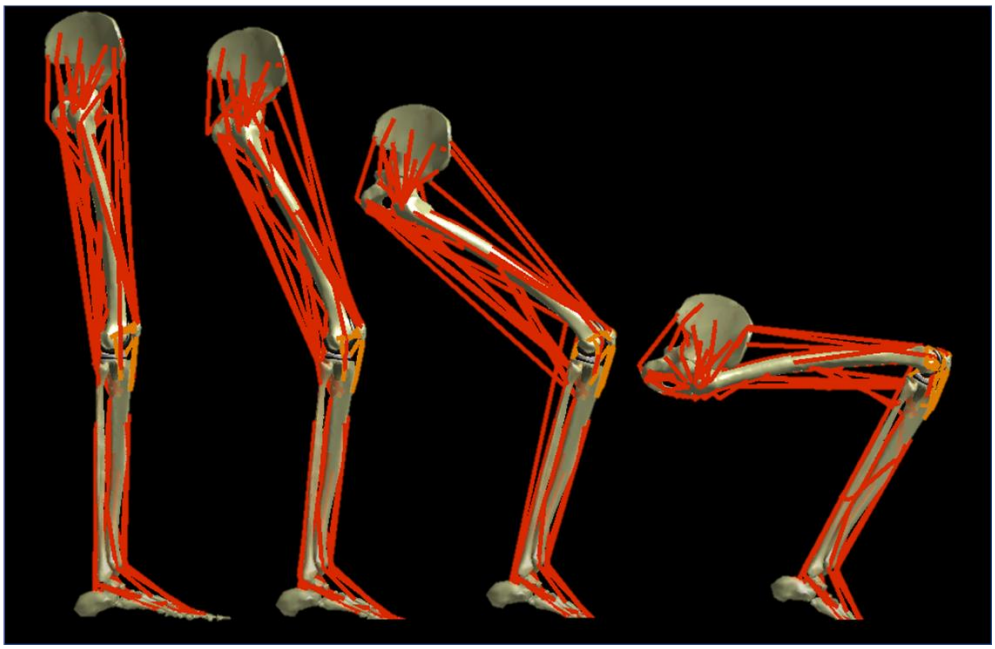


Figure 14: Mathematical modeling can be used to simulate implant device performance under certain in vivo condition for various activities.

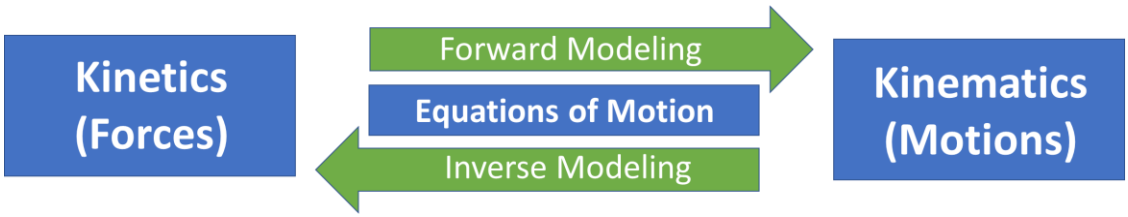


Figure 15: Inverse modeling determines forces from a given set of motions through dynamic equations of motion, and forward modeling determines motions given a particular set of forces through dynamic equations of motion.

both a degree of validation prior to a prospective device ever needing to be manufactured and assessment to improve solutions to complex cases. The fundamental goal of this dissertation will be to take one such existing mathematical model and expand the parameterization therein to explore further applications and gain insight into mechanics of the knee and their dependence on anatomical and physiological input conditions.

‘

CHAPTER TWO: BACKGROUND

2.1 Goals of Total Knee Arthroplasty

The overall goal of total knee arthroplasty devices is to restore joint function as close as possible to that of a healthy individual [17]. The idea of the “Forgotten Knee” is the pinnacle of arthroplasty design, meaning that the device is effective enough at restoring function that the patient completely forgets that they have the device [17, 18].

While pursuit of the forgotten knee is indeed a noble one, there is still a need to objectively quantify procedure success. One popular means of assessing device success is through survey self-reporting [19-22]. These surveys utilize a scoring system that provides a numerical assessment of knee device success. While there are several different surveys, the majority of them focus on self-reported pain levels, limitations to daily activity because of the knee, and overall satisfaction with the device. Unfortunately, these values are self-reported and for this reason they are by nature subjective. Although test administrators seek to remain consistent and unbiased, many questions not only need to consider the perception of the patient but also require the context of preoperative condition.

In an effort to objectively quantify joint performance, a heavy reliance has been placed on analyzing joint mechanics. This is done under the pretext of “If components are moving correctly, then the device must be performing well.” Joint mechanics encompasses both the kinematics and kinetics of the joints and while both are important, kinematics tend to be easier to measure through imaging methods such as fluoroscopy. However, such techniques question what sort of

kinematics are required for a knee implant to be deemed successful, and the general consensus is that the motions of a knee following a TKA procedure should closely mimic that of the normal, healthy knee [9].

2.2 The Normal Knee

The motions of the knee are inherently more complex than its outward appearance may imply and an understanding that how the knee moves is key to facilitating optimal joint function. While many outside orthopedics think of the knee as a hinge joint, there are subtle intricacies to the motion that make replication with artificial components much more complex than it appears. Leszko, et al. proposed the various motions that can experienced by the knee joint [10](Figure 16)

In general, with respect to knee motions, rolling is superior to sliding and the idea is that both condyles of the knee roll posteriorly during flexion and anteriorly during extension. The knee itself is most commonly viewed as a rolling hinge where the geometry of the femoral condyles, coupled with the constraint of soft tissue, forces the lateral condyle of the knee to move up to 20 additional millimeters posterior during flexion, creating a rotation about the medial condyle with 10-20 degrees of rotation [9, 10, 23, 24] (Figure 17). The medial condyle typically remains relatively constant in position and may move anteriorly or posteriorly on a case by case basis.

The kinematics of the normal knee has been quantitatively studied in minute detail, and it has widely been shown that replicating the kinematics of the normal

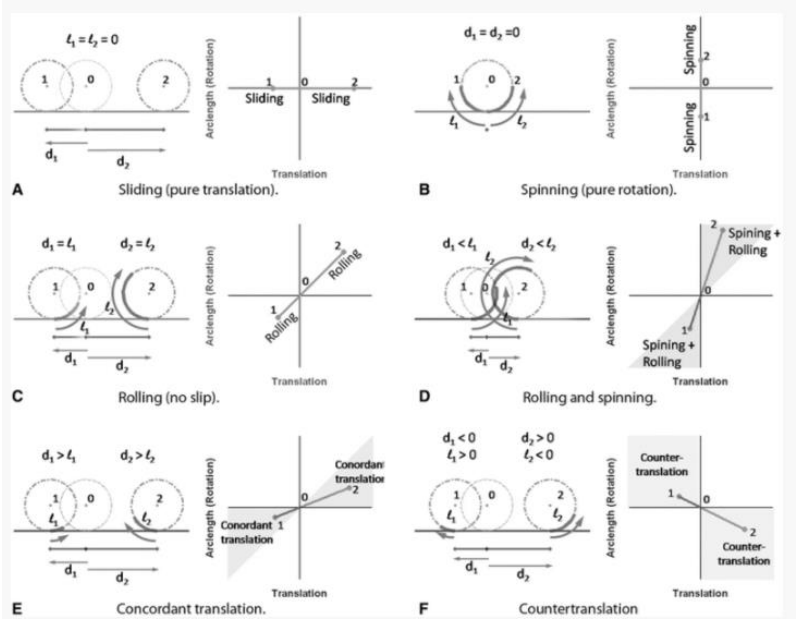


Figure 16: Leszko, et. al. proposed the six motions that can be experienced by the knee using circular disks as analogs for femoral condyles.

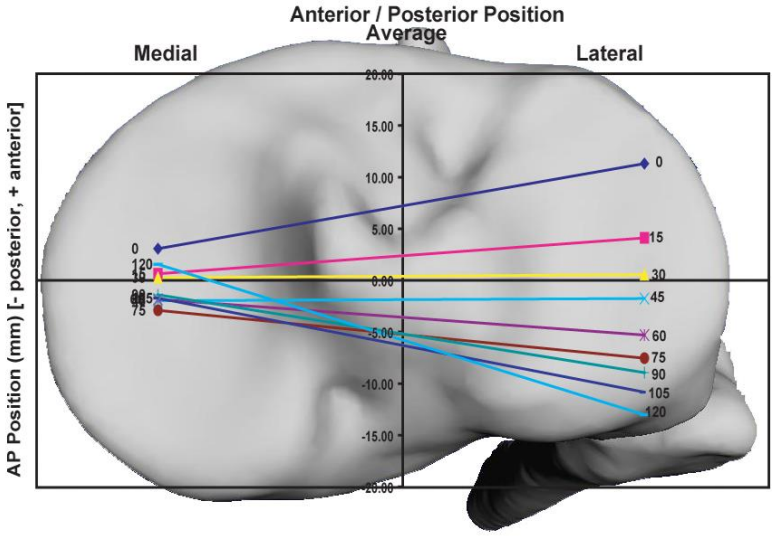


Figure 17: The motions of the normal "healthy" knee typically incorporate both medial and lateral posterior motion with a rotation in the external direction [25].

knee within the context of arthroplasty design will facilitate maximum flexion, improve the functionality of the extensor mechanism and optimize wear patterns at the tibiofemoral interface [9]. For these reasons, it is often the objective of TKA designs to replicate kinematics of the normal, healthy knee in order to improve function and ideally improve patient satisfaction [26-32]. In the normal knee, the lateral femoral condyles have been reported to exhibit an average of -14.1 mm of posterior translation and the medial condyle exhibiting an average of -1.5 mm of posterior femoral translation from full extension to 90 degrees of knee flexion in vivo [9]. This motion is accompanied by approximately 20 degrees of femoral external rotation with respect to the tibia at maximum knee flexion [22] which is facilitated by the asymmetry of the normal knee condyles [9, 25] .

TKA kinematics are typically compared to the healthy knee as a gold standard because such motions facilitate maximum flexion, limit bone impingement and promote proper functioning of the extensor mechanism [9]. Since the primary mechanism of a TKA procedure is to replace the articulating geometries, many devices strive to keep the soft tissue as intact as possible.

2.3 Existing TKA Designs

The goal of any TKA prosthesis is to restore normal, healthy joint function and while there is scientific consensus that this is the goal, the means of achieving that goal are much less agreed upon. Numerous techniques have, however, reported that kinematics of the knee joint after a TKA procedure are highly dependent on implant design [33-38]. In vivo fluoroscopic studies of the normal knee have determined that knee kinematic patterns are primarily determined by

the condylar geometry of the articulating surfaces (Figure 18). Additionally, those studies have revealed what is referred to as the screw-home mechanism, where the lateral condyles experience substantially more posterior motion than the medial condyle throughout flexion [39-41].

2.2.1 Posterior Cruciate Retaining vs Posterior Stabilized

Despite a new emergence of bi-cruciate retaining TKA devices, the majority of prosthesis on the market resect the anterior cruciate ligament (ACL). Posterior cruciate retaining (CR) designs specifically advocate retention of the posterior cruciate ligament (PCL) in order to improve knee kinematics and facilitate more normal performance of activities of daily living [33, 42, 43]. However, these CR implants often led to paradoxical motions with anterior sliding of the femur with respect to the tibia. This phenomenon is believed to be partially due to incorrect balancing of the PCL in CR TKA due to the absence of constraining force from the resected anterior cruciate ligament (ACL). The PCL also is forced to act as the main anteroposterior stabilizer in the natural healthy knee, especially when the knee is in flexion [36] [37].

Since paradoxical motions occur with TKA, and in some cases influenced by degenerated PCL structures, some physicians prefer to use a posterior stabilized (PS) TKA which introduces the presence of the post-cam mechanism to mechanically replace the PCL (Figure 19). Literature has reported that the physical

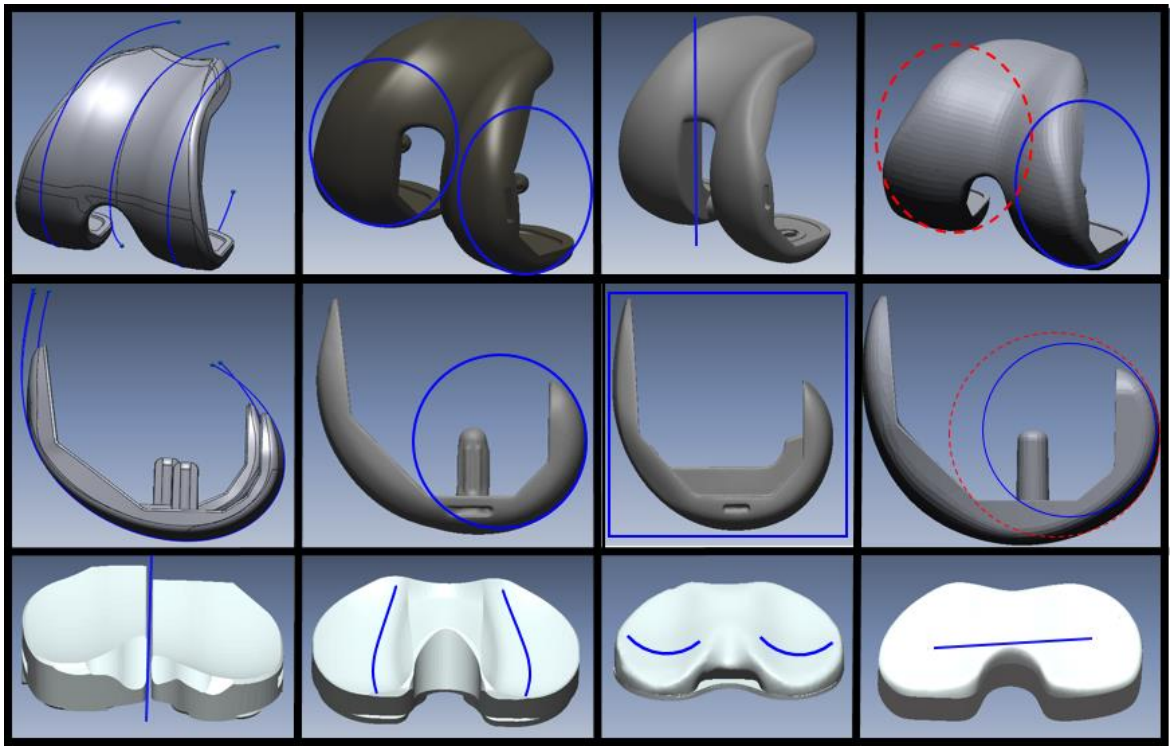


Figure 18: There are many types of TKA devices, each with their own unique design features. Some implants are personalized (left column), while others feature a rotary arc coupled with a single radius (left center). Some include purely symmetric designs (right center) while others feature asymmetric condyles to promote certain motions (right column).

stabilization in PS TKA designs prevents anterior sliding and facilitates greater magnitudes of femoral rollback compared to CR designs [25, 34, 44, 45].Femoral rollback during flexion is a behavior observed in the normal healthy knee [9, 36]. In addition, PS TKA demonstrates several advantages over PCR TKA, one of which is the improved exposure of the tibia simplifying ligament balancing to a degree not possible with PCL retention procedures. Furthermore, abnormal and degenerated PCL morphology is often encountered, creating challenging conditions for reliable gap balancing. By eliminating the reliance on abnormal PCL morphology, ligament balancing becomes more predictable and explained to be an easier surgery to perform [46].

Fluoroscopic studies have also revealed that PS TKA experiences kinematics closer to the normal, healthy knee as the cam post mechanism replacing the PCL prohibits paradoxical anterior sliding, especially during deep flexion. These studies also showed promising results with minimized differences between PS TKA and normal knee kinematics, especially regarding spatiotemporal gait parameters, range of motion during stair climbing [47]. Moreover, PS TKA designs show promise in reducing polyethylene wear through the use of conforming polyethylene bearings that minimize contact stress by increasing contact area [48].

Determination of optimal implant configuration necessary to provide the best patient outcomes remains a primary obstacle for the orthopedics community and often compromises need to be made to choose the device that best fits the needs of the patient [34].

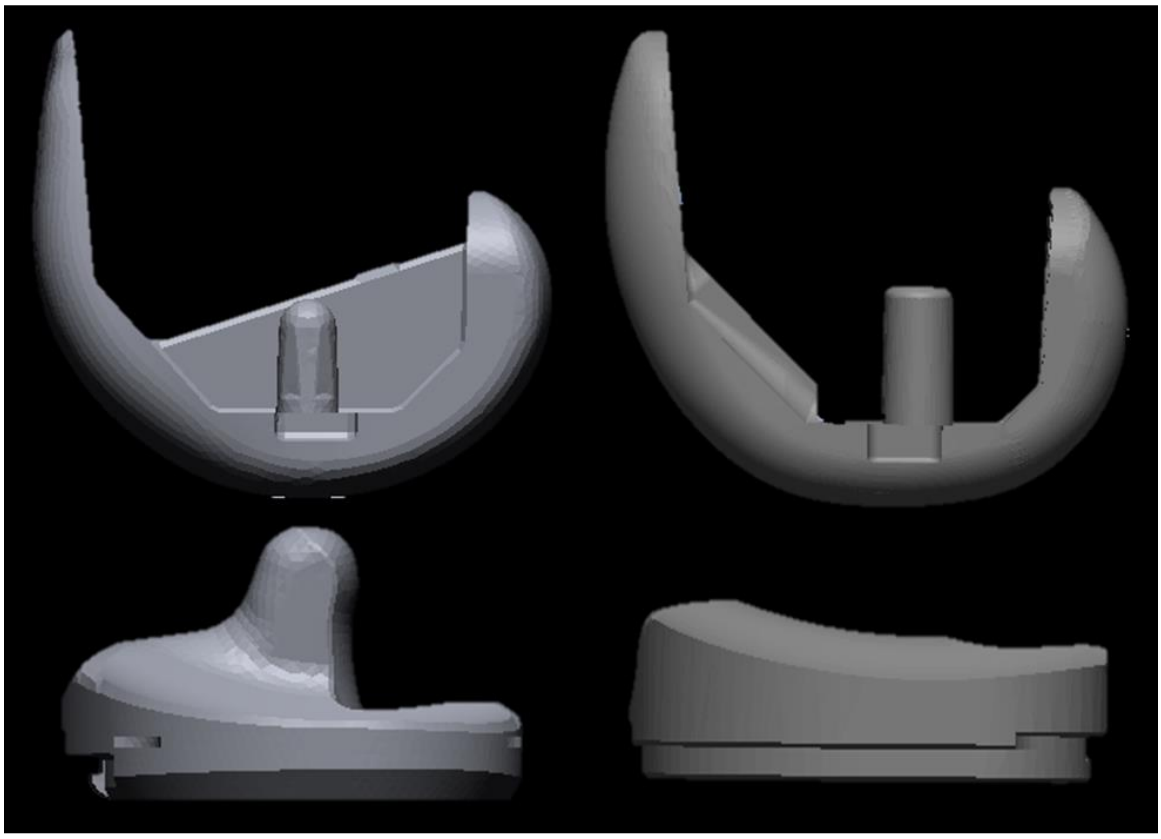


Figure 19: The posterior stabilized (PS) TKA features a cam and post mechanism that provides mechanical support for the resected PCL (left). Cruciate retaining devices (PCR) have no such mechanism but retain the native PCL from the patient.

2.2.2 Mobile vs Fixed Bearing

Much like the debate between PCR and PS devices, there is also an active debate between mobile and fixed bearing devices. In a fixed bearing TKA device, the bearing is rigidly attached to the tibial component of the TKA. As the name implies, in a mobile bearing device, the polyethylene component is still fixed about the mediolateral axis and the anteroposterior axis, but the bearing component is freely able to rotate about the internal/external axis. The mobile-bearing total knee was specifically designed to employ a rotational compliance to reduce contact stresses and ultimately wear. Theoretically, such an idea should create mechanics more similar to healthy knees. While in vitro studies have shown reduced wear with the use of a mobile-bearing implant, in vivo metrics including survivorship, outcomes and kinematics do not appear to produce significantly different results [49, 50]. Post, et al. reported that there is no quantifiable basis to justifying one design over the other [51]. Clinical success was found to be predominantly dependent on the accuracy of component placement, and Post concluded that the best result is achieved when the surgeon is comfortable with a design and can implant that design consistently. Studies have compared the performance of the mobile and fixed configurations in a single patient, concluding that the patient does not demonstrate any difference in terms of range of motion, knee scores, and survivorship [48, 52-54]. Pagnano, et al. studied 240 mobile-bearing TKAs determining that there was not an improvement in patella tracking [55]. An additional multicenter study conducted by Wasielewski, et al. incorporating 527 mobile-bearing TKAs determined that axial rotation greater than ten degrees

during a deep knee bend was achieved in 12% of the tested subjects with almost half experiencing less than 3 degrees of axial rotation [56]. Dennis, et al. in addition reported that kinematics experienced were comparable to that of a fixed bearing TKA [57]. In an effort to assess long term survivorship, LaCour, et al. conducted a ten year follow up determining that the overall rotations of the bearing are retained over long term follow ups [58].

2.2.3 Condyle Asymmetry

Outside of bearing type and retained verses resected ligaments, femoral geometry is an additional factor that has been shown to influence TKA mechanics. One such design feature is the inclusion of asymmetric femoral condyles. Such a design feature includes a lateral femoral condyle with a greater sagittal radius than the medial femoral condyle, which mechanically facilitates a longer path for the lateral condyle during flexion compared to the medial. This differential facilitates a medial pivot while driving axial rotation [59] (Figure 20).

It is of note that the company that manufactures this type of TKA design also makes a gender-specific variant specifically designed to fit female femur geometry, citing geometric differences such as a narrower trochlear grove and a smaller aspect ratio between AP and ML directions compared to male patients [10, 60-63]. This is significant as this is one of the first instances where companies have designed a knee device around a particular demographic.

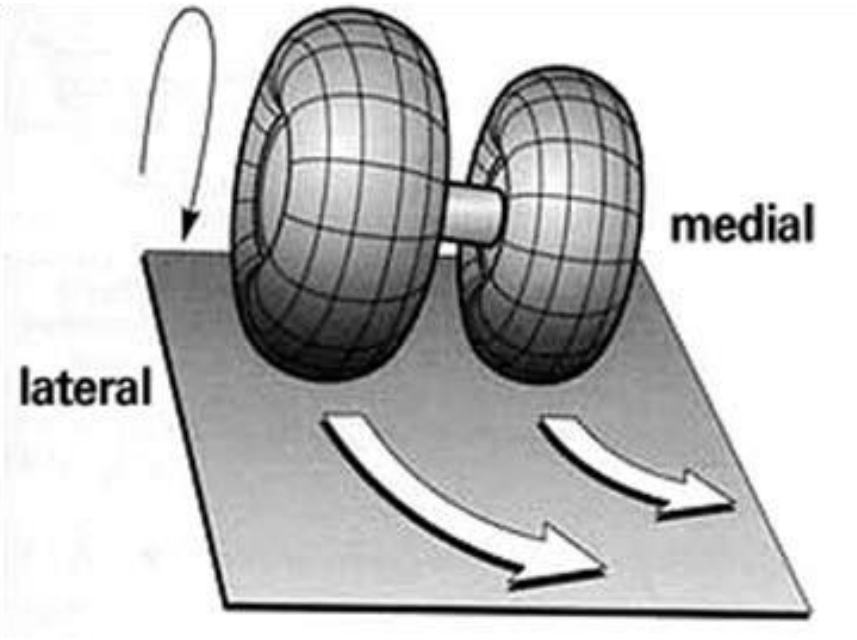


Figure 20: Asymmetric TKA devices use the different medial and lateral femoral radii to drive axial rotation. Since the lateral condyle has a larger radius, it travels further than the medial condyle during flexion, thus promoting axial rotation.

2.2.4 Single Femoral Radius

Whereas most TKA devices feature a femoral radius that varies throughout the course of flexion, the single radius knee features a femoral radius about the center of rotation that does not change during flexion (Figure 21). Most designs that feature a varying radius exhibit a larger radius closer to extension and a smaller, more circular radius closer to full flexion. The design rationale behind this is that a tighter radius will drive greater motion in deeper flexion as is seen with the healthy knee [64].

The single radius type knee incorporates a different principle and utilizes its chief design feature to promote stability throughout flexion. Since the femoral radius is consistent throughout flexion, the collateral ligaments experience roughly the same mechanical deformation, as the length of the collateral ligaments is no longer a function of flexion [18]. In theory, this contributes to smoother motions and stable kinematics throughout mid-flexion, which is especially relevant during gait [64, 65].

2.2.5 Gradually Reducing Femoral Radius

The gradually reducing radius, which is known by its trade name Gradious®, combines the ideas of single and multi-femoral radius TKA designs. Unlike a traditional multi-radius design which features a distinct transition between early and late flexion radii, the gradually reducing radius incorporates a transition region between mid and late flexion where the change in femoral radius is defined through a geometric equation [66] (Figure 22). Much like the other designs, the goal of this



Figure 21: The single radius knee features a constant femoral radius throughout flexion. In doing so, the TKA promotes mid-flexion stability by fostering smooth motions and consistent collateral ligament forces. Figure modified from Stryker, Inc.

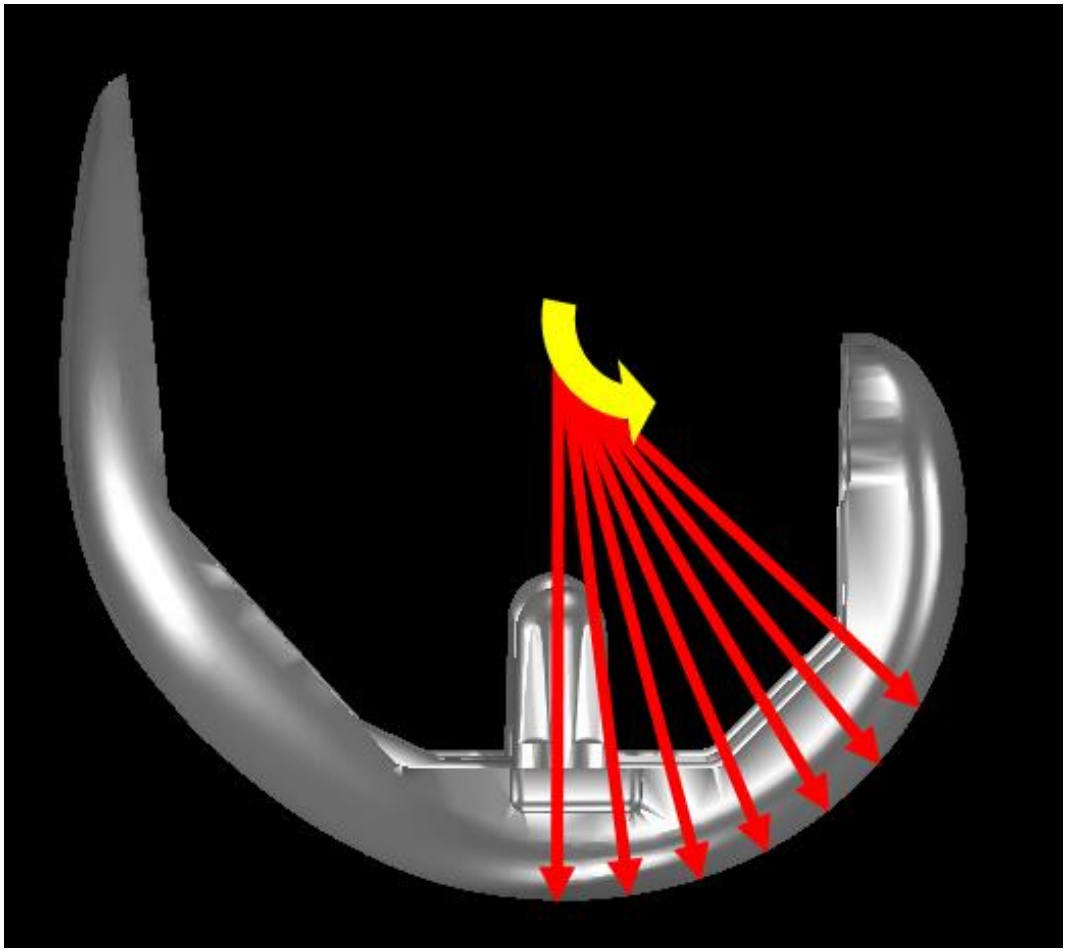


Figure 22: The gradually reducing radius design features a transition region between early and late flexion where the condyle radius gradually becomes smaller as a function of flexion.

TKA type is to facilitate mid flexion stability by eliminating any discontinuities during the flexion process through a continuous transition between early and late flexion. In TKA design, mid-flexion stability is an important metric as a surgeon is able to test stability in full flexion and full extension. It is, however, neither feasible nor practical to check every increment throughout flexion to assess stability [67, 68].

Mid flexion stability is important for a number of reasons and possibly one of the most important reasons is the limiting of the phenomena of condylar liftoff [7]. This occurs when either the medial or lateral femoral condyles lift off of the articulating surface during flexion, which is problematic for three main reasons. The first reason is simply that this is a behavior atypical of the healthy knee. Secondly, it leads to anomalous fatigue behavior of the constraining ligaments. Lastly, it creates higher impact stresses on the polyethylene bearing which may expedite wear and implant loosening, leading to less overall contact area occurring between the condyles and the polyethylene insert, possibly leading to higher contact stresses.

2.2.6 Personalized TKA Implants

Current total knee designs have been largely created based on static models of knee anatomy where the best fitting components are selected from a range of standard fixed sizes, and the surgeon makes the necessary adjustments to fit the implant to the patient during the procedure. In other words, TKA inadvertently alters the bony and soft tissues geometries and constraints built into a human knee to fit a generalized component. As a result, component orientations

and kinematic patterns experienced after TKA can vary substantially from the motions of the native knee to which the patient was accustomed.

One possible reason for these abnormalities could be that these universally fitting implants do not account for patient-specific anatomic factors which intrinsically affect TKA outcomes potentially including patient satisfaction. These factors include patient age, gender, Body Mass Index (BMI) and severity of arthritis [69].

It has been demonstrated that patients will have significant morphological differences and these anatomical differences may need to be accounted for in the design of a successful prosthesis device [70]. This intuitively contributes to a theoretical advantage of gender- and ethnic-specific prosthetic devices. While population-specific devices are a logical next step in device design, they still fail to account for individual variability between patients within ethnic and gender subsets. This implies that patient-specific implants would be advantageous over demographic specific device components [71].

Personalized TKA devices use preoperative CT scans to assess patient geometry and create an implant using both femoral radii and trochlear groove geometries as collected through the CT scans (Figure 23). These components are aligned using mechanical alignment while compensating for any malformed anatomy to create the optimal alignment along the mechanical axis. Zeller, et al. demonstrated that the personalization of the bearing and femoral components of a PCR TKA can contribute to increased femoral rolling during flexion and extension, along with increased magnitudes of internal and external rotation for

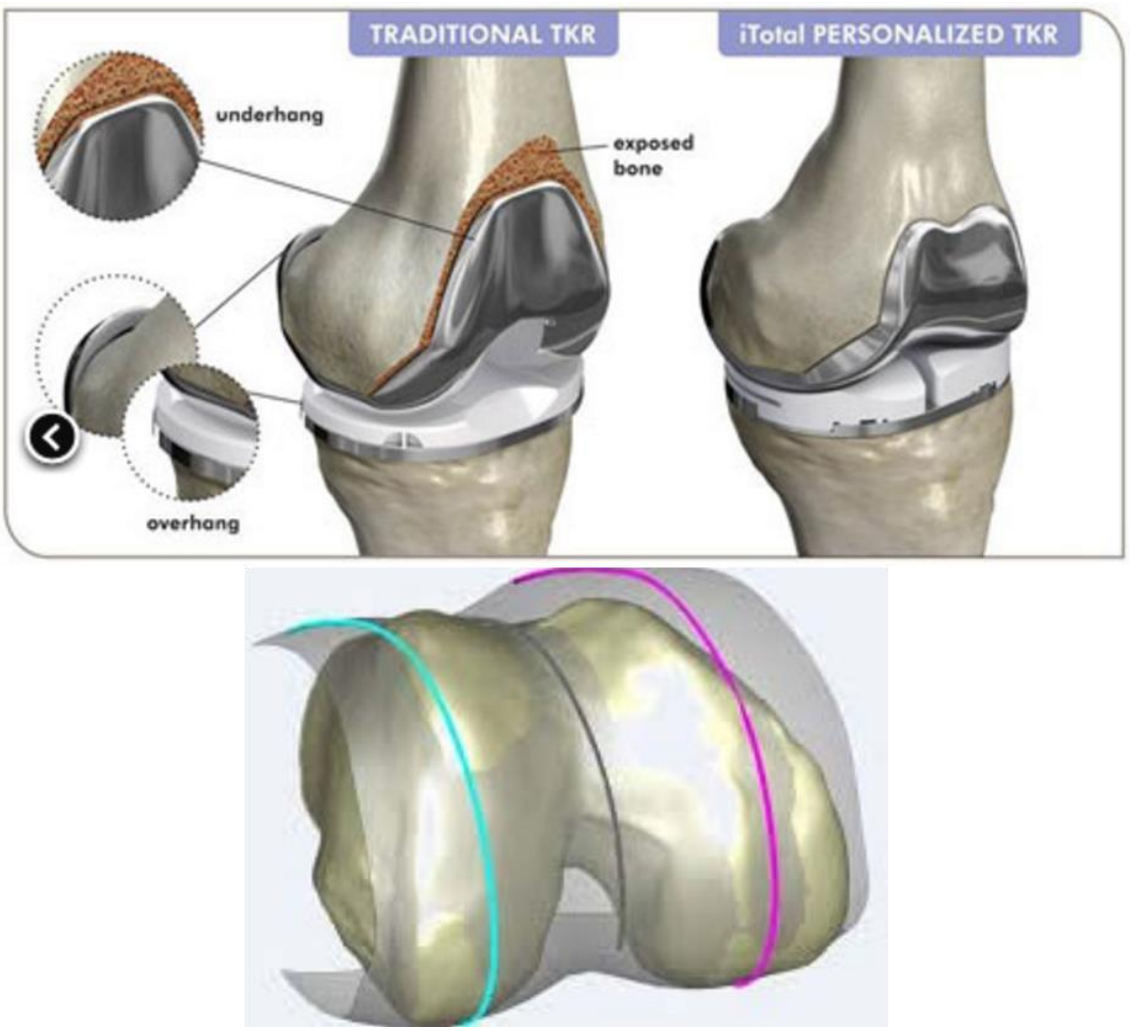


Figure 23: Personalized TKA implants are created to fit patient femoral and tibial anatomy based on CT scan geometries (top). The main factors that are evaluated are the medial and lateral femoral radii as well as the trochlear groove geometry. Both the femur and the tibia components are designed to fit their respective bones and incorporate the geometry of these determined radii. Figure modified from Conformis, Inc.

extension, along with increased magnitudes of internal and external rotation for extension and flexion, respectively.

That study also revealed that personalized arthroplasty components contribute to reduced frequencies of paradoxical motion generally leading to more normal kinematics with attenuated magnitudes. This study used the asymmetric multi-radius TKA, although in its PCR variant, and while these results seemed promising, further study was deemed necessary to evaluate these same devices in their PS forms and to further evaluate the effect of prosthesis fit to a specific patient's effect on mechanical function [72].

2.4 Limitations of Modern TKA

Although nearly all TKA designs aim to replicate the motions of the normal knee, most traditional PCR TKAs generally exhibit consistent instances of paradoxical anterior slide and reverse rotation of the femoral component with increasing flexion [36, 73-75]. This motion pattern is widely believed to be due to the absence of the anterior cruciate ligament (ACL) [9, 25, 76], which counterbalances the PCL to hold the medial and lateral contact points anteriorly on the tibia plateau facilitating posterior rolling during flexion [77-79]. PS TKA designs seek to rectify these paradoxical motions through the introduction of a cam and post mechanism which prevents anterior motion during mid to late flexion by providing a constraint similar to, yet more effective than the PCL. These designs are typically very effective at reducing paradoxical motions, and for this reason, the kinematics tend to more closely mirror that of the normal knee. Thus, they tend to be more mechanically successful, as they do not rely on the intrinsic variability

of the native PCL, often degenerated from years of fatigue loading. While PS TKA designs are generally more successful in the restoration of knee functionality compared to PCR TKA, the kinematic magnitudes remain to be substantially less that comparable motions in the normal knee [9, 10, 25]

Another less intuitive limitation of TKA devices is that over time, advances in joint prosthesis design, surgical technique and manufacturing processes have produced devices that have been continuously improving in performance from generation to generation. Although devices are continuously improving, it is important to note that patient expectations over time are also becoming more demanding [27]. Legacy orthopedic devices previously intended to restore basic ambulatory function, whereas modern devices are expected to facilitate a much more active lifestyle while providing unhindered “normal like” function. Although implant survivorship is upwards of 95% [80-82], approximately one in five patients still report being unsatisfied with their outcomes [27, 29]. For this reason, it is evident that novel designs and methods are necessary to consistently achieve patient satisfaction with the TKA procedure.

Because knee replacement devices are not consistently achieving patient function and satisfaction, there is still a need to develop novel devices that better meet the needs of patients and facilitate the surgical procedure for physicians.

2.5 TKA Design Process

Despite the multivariate nature of the TKA process, from an engineering perspective, the aspect above which most control is exhibited would be the device design. The orthopedics industry is a unique field as there is a substantial regulatory protocol. The governing body in the United States is the Food and Drug Administration (FDA) which mandates classification of medical devices based on inherent risk where each classification requires more stringent controls than the previous (Table 2) [83].

Most implantable medical devices are by nature category III meaning they are both high risk and subject to the most stringent guidelines. Because of this classification, TKA devices require pre-market approval. Pre-market approval (PMA) is a process that assures that a given device will be both safe and effective for its denoted indications,[83-85]. There is a less stringent standard that can be used as long as a device meets substantial equivalency to an already approved device known as pre-market notification (510(k))[85].

Within the confines of the design process, there is a special case that allows for a device to be used sufficiently to assess efficacy and safety. This is called an “investigational device exemption” (IDE) and it requires both a 510(k) and an application for the PMA process. It is during this time the data assessing the device can be gathered and design features can be evaluated.

In order to fulfill the requirements of the PMA, there needs to be sufficient evidence of device performance. The design process precedes the approval

Table 2: The Food and Drug Administration (FDA) give guidelines for various medical devices. These classifications and associated controls vary based on device risk.

Classification	Description	Controls	Examples
Class I	Low Risk	General • Registration • Quality Control • Labeling • 510(k)	• Bandages • I.V. Stand • Sunglasses
Class II	Moderate Risk	Special • Special Labeling • Performance Standard • Guidelines	• Syringe • Surgical Mask • Wheelchair
Class III	High Risk	Require Pre-Market Approval	• Heart Valve • Pacemaker • TKA

process and is meant to create a device that both satisfies both the performance and safety needs of the patient. The design process itself is iterative by nature and it involves a design loop consisting of design, analysis, and revision. The idea is that a device is designed, it is evaluated quantitatively for performance. The Information is then used as insight to revise the design. Depending on evaluation techniques, this can be a time-consuming process which is then repeated until sufficient performance is achieved by one of the design iterations and the process can move forward for approval and manufacturing integration (Figure 24).

2.6 TKA Assessment Techniques

Of the all the phases of the design process, the most important is the analysis phase. This is where the validity of design features is assessed along with other performance aspects for a prospective device. Not only is the assessment process aimed to provide information to prove how effectively a device rectifies a shortcoming in existing TKA designs, but it will also provide critical information for the device approval process. There are many different techniques that can be used each with varying degrees of involvement, time and feasibility (Figure 25).

2.6.1 Implant Retrieval

Implant retrieval provides possibly the most accurate assessment of implant wear over long periods of time. This process features devices primarily either removed during revision surgery or recovered on necropsy. Studies have claimed to correlate patient activity and repetitive motion wear patterns[86, 87] allowing for a reasonable assessment of device damage sustained over its working life.

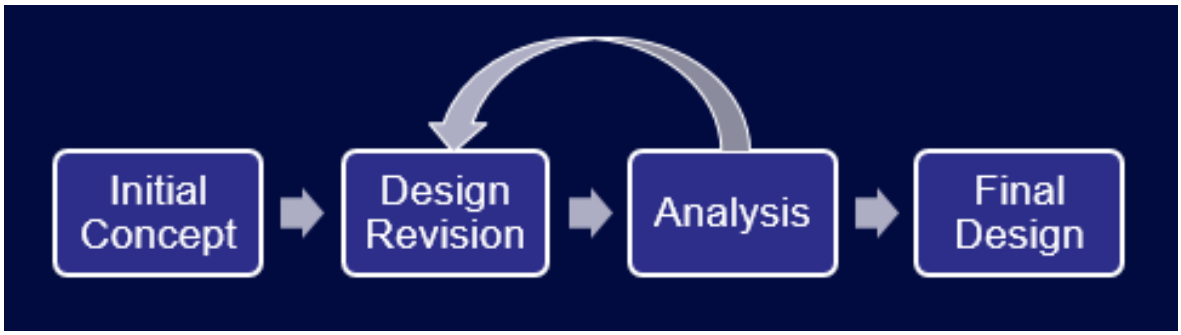


Figure 24: The TKA design process in general contains four steps. From initial conceptualization, a device must be evaluated to ensure it meets both safety and efficacy standards. This process also tests various design features to ensure and demonstrate that they work as intended. Once this evaluation had been completed, the design enters a looping process where revisions occur until the design has been proven to work successfully and adequately. Upon completion, the device moves on to additional processes such as manufacturing integration and commercialization, as well as the early phases of post market surveillance to ensure continued compliance with regulatory measures.



Figure 25: There are three main techniques for the mechanical assessment of TKA devices, including: cadaver testing which uses mechanical actuators to simulate muscle control while measuring motions (left), wear simulators which use prescribed motion patterns to perform long wear analysis over large quantities of cycles (center), and fluoroscopy which determines device motion in vivo through video x-rays and a component registration process (right).

Despite being one of the most accurate assessments of implant performance, there are two issues that limit feasibility during the implant design process. The first of these is that the process in not well controlled as necropsies are performed with minimal information regarding lifestyle, activity levels and general patient history. Even considering known patient history would be difficult as it would be expected to vary on a case by case basis. The second issue with implant retrieval is that it requires a device to not only be manufactured and implanted, but also requires the device to run the course of its life which is some cases can be as high as 20 years [88]. These studies are still critical to the overall assessment of TKA devices, nonetheless, they are prohibitively time consuming for use in the design process, especially early in the process.

2.6.2 Wear Simulators

Simulating TKA performance over its functional life can become incredibly time consuming and for this reason, wear simulators seek to replicate an equivalent number of cycles, expediting the process over a shorter timeframe. Wear simulators affix the TKA components within a mechanical device that repeatedly executes force and motion profiles that attempt to replicate in-vivo conditions over millions of cycles, thereby simulating years of device performance [89]. These studies have come to various conclusions that correlate wear patterns to both length of implant life and patient activities [86, 87]. Unfortunately, these studies utilize motions that are too well controlled, often categorized as “ideal motions” and thus, fail to corroborate wear patterns and the interpatient variability seen through implant retrievals [90-92]. While eventually simulator testing will be

required in the design process for approval, the process as a whole is better suited to refinement of a nearly complete design. The limitations in number of implants tested, and most importantly time are factors that make this process less effective during early stages of TKA development.

2.6.3 Cadaver Testing

Cadaveric rigs such as the Kansas and Purdue Knee Simulators, implant the TKA device into a cadaver leg which is then manipulated along the extensor mechanism using hydraulic actuators [93, 94]. These methods provide more in-vivo “like” conditions compared to more traditional testing rigs because they both incorporate knee kinematics under the soft tissue constraints and provide physiological constraint forces to produce a closed chain system. While these rigs are able to replicate certain physiological kinematics such as the “screw home” mechanism and femoral rollback, the findings can be inconsistent outside of early flexion (30 degrees)[95]. Unfortunately, the muscles are not truly driving the motions because profiles are used to create tension within the soft-tissue structures. The mechanics of the knee are also heavily influenced by the forces that are introduced by artificial physiological activators, thus the kinematic outcomes of may not necessarily match in vivo conditions. Furthermore, it is difficult to test large volumes of devices and high cycle counts because of both the difficulty of obtaining and nature of cadaveric samples respectively.

Beyond the rig itself, a pressing debate in the testing of biological tissue is the effect of living verses non-living tissue mechanics. A particular study by Stemper, et. al reported there is not a statistical difference between the biological

mechanics of fresh tissue and previously frozen tissue. Refrigeration of specimens, however, over the short term can adversely affect tissue mechanics [96]. This means that external factors are capable of affecting performance mechanics.

For these several reasons, there is considerable debate as to how representative a cadaver test actually is of in vivo conditions. Furthermore, much like wear simulators, these techniques additionally require physical manufacturing of implants and take a substantial amount of time for preparation and analysis. Even beyond these limitations, cadaver testing still does not easily facilitate repetitive motion analysis over large numbers of testing cycles.

2.6.4 Telemetry

Telemetry has the ability to report very accurate, real-time measurement of resultant forces in six degrees of freedom, and has gained wide scale credibility and approval in the research community for the reporting of in vivo kinetics [97]. Telemetric implants are more or less traditional TKA implants that are equipped with force sensors that are able to read transcutaneously (Figure 26). The first reported instance of measuring tibiofemoral forces via an instrumented implant in a TKA patient was done in 2006 by D'Lima. Patients in this study experienced increased contact forces during a lunge activity ranging from 1.7 to 2.77 times body weight (BW), with peak forces occurring between 27% and 82% of the cycle [98].



Figure 26: Telemetric knee implants are specially designed devices equipped with force transducers that are able to measure and transmit contact force data for analysis.

For chair rising and sitting, all patients demonstrated two independent regions, exemplifying net force peaks [98-100]. The first of these (average, 1.83 times BW) was found at the early portion of chair rising (between 11% and 20% of the cycle), compared to the second (average, 1.61 times BW) which was found at a later portion of the cycle (78% to 83%) [98]. Patient-specific force distribution on both medial and lateral condyles was nearly equivalent for the lunge activity. During a chair-rising activity, it was observed that the lateral condyle experiences increased force ratios (from 61.7% to 74.2% of total force) compared to the medial condyle. An additional study that was conducted by the same authors assessed tibiofemoral forces within a single patient group during activities of daily living such as walking and cycling [98]. This group found that during level walking, the knee experiences forces from 1.8 to 2.5 times BW. These forces are very similar to those experienced by a subject walking comfortably on a treadmill. During the bicycling, forces peaked at 1.03 times BW[98-100]. Patients experienced increased forces while exercising on an elliptical trainer, with a mean peak tibial force of 2.24 times BW [98, 101].

Despite being the gold standard for kinetic measurements in vivo, there are three significant limitations to telemetric implants. First, they require a device to be implanted in a single patient, thus not allowing for multi-subject analyses. Secondly, they are very expensive and can be time consuming to develop. They also fall under scrutiny of regulatory agencies, adding additional cost and safety regulations. Thirdly, the device itself must be standardized in order to properly

incorporate measurement components. These are all factors that limit the use of telemetry in early stage implant design.

2.6.5 Fluoroscopy

Whereas telemetry is the gold standard of determining device kinetics, fluoroscopy is the gold standard of assessing joint kinematics. During fluoroscopy, a patient performs various activities within a fluoroscope which provides an x-ray video sequence. Frames of interest are then selected from the video sequence and the videos are corrected for any distortion that may occur from the image intensifier of the x-ray machine. CAD models can then be either obtained or created and used in a registration process, where the components are superimposed over the silhouettes on the x-ray images in order to recreate the fluoroscopic scene with the device components. The positioned components can then have their transformations extracted and kinematic measurements can be taken in any desired reference frame [102-104](Figure 27).

This process has been validated using cadavers to an accuracy of 0.5 degrees and 0.5mm [102] and has been used over the course of a large number of kinematic studies, evaluating various TKA design features ranging from condyle geometry, ligament structures and normal healthy knees [9, 65, 72, 103, 105-107]. Fluoroscopy has also been shown to be advantageous over skin mounted markers, as there are limited artifacts in the analysis due to skin movement [108-110].

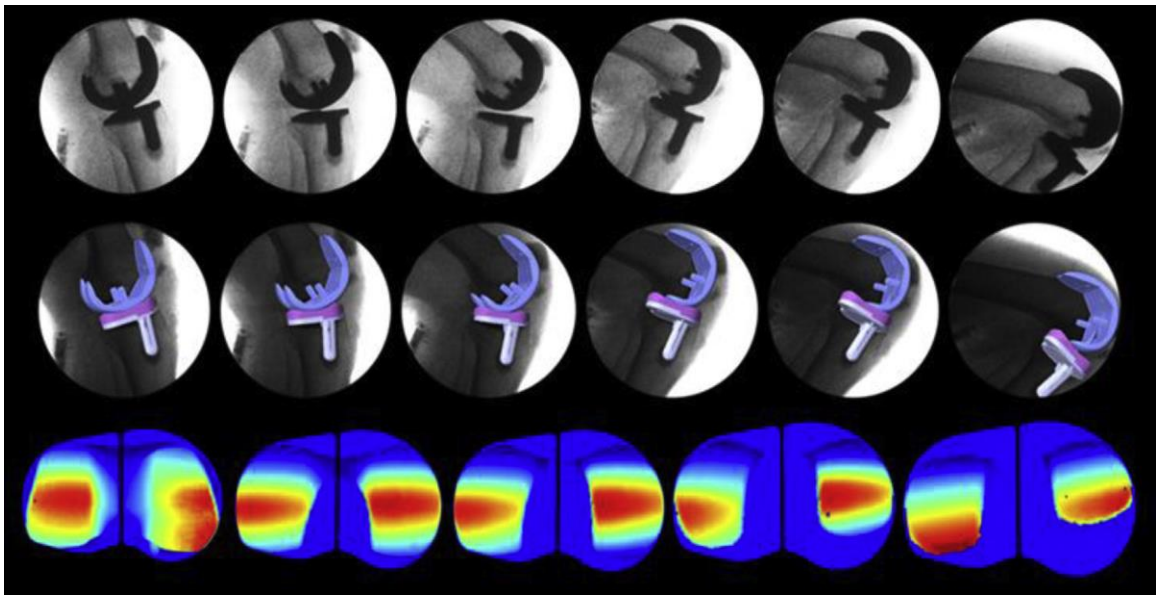


Figure 27: During fluoroscopic evaluation, subjects perform various activities with surveillance by a video x-ray machine. The video is then cut into frames of interest (top) assigned components and transformations through a registration process (middle) and from these transformations, measurements can be taken to assess device performance.

While fluoroscopy is one of the best measurements for in vivo kinematics, it succumbs unfortunately to the same limitations as other assessment techniques in the design process. That is that it requires a device to be both manufactured and implanted leading to substantial cost and time investments. Thus, it is not necessarily an effective evaluation technique for early stage designs where a device simply is not yet ready for in vivo implantation.

2.7 Mathematical Modeling

The two most common limitations across all the physical testing techniques are time and cost, specifically with regard to manufacturing, implanting and evaluating a device. These limitations are further compounded by the iterative nature of the design process where these devices will need to be created and tested to both validate and improve existing design features.

Mathematical modeling is different because instead of building a physical system to evaluate a given device, the mechanical performance is derived computationally. Since this entire process is done computationally, it not only expedites the process by eliminating physical devices but also limits costs purely to those of a computational nature. This is makes computational modeling especially useful in the early stages of development when the design is in its inchoate phases because of the ability to circumvent the need to manufacture or implant a device.

2.7.1 Forward and Inverse Modeling

Mathematical modeling can be fundamentally subdivided into two basic categories. Inverse modeling is the calculation of kinetics from kinematics

(determines forces given known motions) and forward modeling which is the calculation of kinematics from kinetics (motions given known forces) (Figure 28). Either of these modeling strategies are computational representations of physical systems and the resulting information can be used to provide design feedback for new TKA devices.

In the past, inverse models have been used that have been supplemented with fluoroscopy to determine the forces experienced by a device through a specific set of motions. This can be particularly useful when attempting to determine soft ligament forces [111] and muscle forces [112]. For example, Lundberg [113] had developed a parametric inverse model to determine tibiofemoral contact forces for TKA patients during level walking. This group found that peak force experienced was 3.3 times BW, ranging to a maximum of ±0.5 times BW (at 67% stance) for normal forces and ±0.82 times BW (at 76% of stance) for resultant forces [99, 100]. These results were very similar to published data acquired through simulation using optimization techniques to determine knee joint forces. Although the mediolateral force distribution was also found to correlate with that of other studies [114-117], calculated forces were markedly increased compared with those reported for similar activities measured using telemetry.

While determining muscle forces is useful, from a device design perspective it is much more useful to determine motions from forces as the human body is very

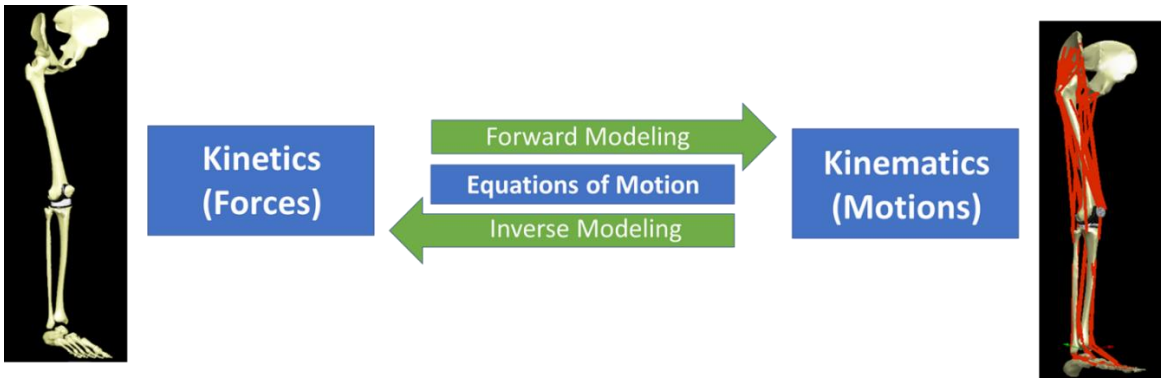


Figure 28: Forward solution modeling begins with a mechanical system and uses the equations of motion to solve for motions from forces. Inverse modeling does just the opposite and uses the equations of motion to solve for forces when known motions are applied to the system.

well optimized, and the eccentric and concentric muscle forces are both set and consistent regardless of the shape of the articulating geometry. What does change, however, is the manner in which forces are transmitted, as well as the forces required to drive motion [118, 119]. This is important because if a knee does not transfer forces correctly, then the muscles may need to apply additional force to drive simple motions. At best, such a case would contribute to stiffness and at worst the muscles may not be strong enough to drive motion. Such a rationale has been used by researchers to explain why forces in TKA can be up to a full times bodyweight greater than in the normal knee[120].

Although these models can be thought of as independent methods, they are very inter-related. They can often be used to validate each other as it would be expected that the forces and motions would be heavily interrelated. For this reason, some models may incorporate both forward and inverse components. For example, the knee joint may be treated as a forward model where the motions are solved for and the hip and ankle may be inverse, where the components are specified to move along a pre-determined force profile [118].

2.7.2 Optimization and Reduction models

Forward and inverse modeling techniques typically determine what parameters are being solved. They do not however determine how those components are solved. The human body is a complex system and one such modeling obstacle is the resolution of muscle redundancy. The human body is unique in that many muscles act in unison to achieve motion. Although each joint may have up to six degrees of freedom, there are any number of muscles that can

activate to achieve these motions and the solution to the redundancy problem is one that allows all muscle forces to be accounted for. One complication is that the system must be mathematically determinant (i.e., the number of equations of motions does not exceed the number of unknown variables) in order to be solvable. There are two such methods to determining such a system.

The first is through an optimization technique to solve an indeterminate muscle force system [121-123]. Optimization employs some form of a cost function. The most famous example is the Crowninshield and Brand function which uses a scaler function produced by the sum of muscle forces accounting for cross sectional area [124, 125]. Using this function, it is possible to solve for muscle forces, although the process is computationally intensive. Years later Yamaguchi et al. would develop an improved method using the pseudoinverse of the acceleration matrix to solve for a multiplier matrix which can ultimately be transposed to give the optimal muscle stresses and their associate magnitudes [126]. While this can be an accurate method, like most optimization techniques there are assumptions that are made in the process that may or may not necessarily be representative of the system.

The premise for the reduction technique is the assumption that all of the forces and torques that a group of muscles provide will be reduced to a single force, or torque specific to that degree of freedom. This means that from a mathematical perspective, the individual muscles are summed together creating a determinant system. [48, 127, 128]. It is possible to estimate muscle forces based on this method however it is of note that these muscle forces are simple allocations

of various forces coupled with attachment site geometries. Much like optimization methods assumptions need to be made to keep the system determinant, the advantage to reduction is that these assumptions occur post hoc. Therefore, they are less influential on the overall equations of motion for the system.

Using a reduction technique, Komistek, et al. developed a fluoroscopy driven inverse model fundamentally based upon Kane's System of dynamics [129]. This model demonstrated that the maximum force acting between the femur and tibia for a healthy subject is 1.7 to 2.3 times BW [129], although such forces were found to be heavily influenced by walking velocity. This approach also lead, Sharma, et al. to assess tibiofemoral forces for subject with PS and CR high-flexion knees during deep flexion, finding that forces increase with increasing flexion and the medial condyle force was always higher than the lateral condyle force independent of TKA design [48]. For validation purposes, the model was compared with telemetrically acquired, fixed-bearing data demonstrating that for the telemetric implant, maximum medial forces were 1.9 times BW at 90 degrees of flexion and maximum lateral forces were 2.2 times BW at 105 degrees [48]. This same model predicted peak forces of 1.89 times BW at 90 degrees and 2.05 times BW at 101 degrees, respectively, for the medial and lateral condyles[99, 100]. In addition, these same researchers evaluated two groups of five patients each with wither a fixed or mobile bearing TKA during a flexion activity. They found that tibiofemoral force for both device types is similar in both pattern and magnitude [129]. Confirming previous studies these researchers found an uneven force distribution between the two femoral condyles where the medial condyle

consistently experiences higher forces compared to the lateral condyle. During this case, the average medial tibiofemoral force ranged from 0.5 times BW at full extension to 2.72 times BW at full flexion for mobile-bearing subjects, compared to fixed-bearing subjects which experienced a range of medial forces, between 1.04 times BW at full extension and 2.73 times BW at full flexion [129]. The lateral medial force ranged from 0.34 to 0.91 times BW for mobile-bearing subjects compared to a range of 0.43 to 0.92 times BW for fixed-bearing subjects [129]. These results are comparable to telemetric studies[100].

2.7.3 Commercial Modeling Techniques

In order to better facilitate these modeling techniques, various software programs have been developed to improve and streamline user interaction. Although the math and the underlying methodologies are similar, these programs each have unique roles with respect to forward and inverse modeling, as well as reduction and optimization methodologies. The primary role of each software relates how the systems are developed, which factors are considered and how the equations of motion are developed.

2.7.3.1 Finite Element Method

While there are many programs that can operate finite element analysis, Abaqus Is one of the most prevalent software programs used in industry. Finite element models take a continuous total geometry and breaks it into discreet segments. The size and quantity of these elements varies on a case by case basis, although more elements generally lead to more accurate results. The tradeoff is that more elements also substantially increase computational time.

The main advantage of finite element analysis is its ability to model deformable bodies. This is done by incorporating spring elements that are affected by contacting forces between adjacent elements on contacting surfaces (Figure 29 &Figure 30). Studies have used this method for kinematic analysis and with certain property configurations, the model can approximate a ridged body. Under the assumption of rigidity, deformative properties can be used to determine contact forces which can thereby be used to constrain or move the model components. Finite element models have been validated against fluoroscopic and telemetric data; however, it is not uncommon for articulating surfaces to be reduced to account for model stability and solution time [130].

Dr. Sharma developed an improvement to this methodology by incorporating discreet spring elements mechanically based on the properties of high molecular weight polyethylene. By controlling kinematics, the calculated bearing forces were achieved to within 1% of BW (Figure 31). Of greater note is the computational efficiency of this method, as the simulation ran on the order of minutes compared the equivalent finite element system which took hours [127].

2.7.3.2 Opensim

Open sim is a software that was developed in an attempt to standardize modeling techniques and facilitate collaboration between researchers in biomechanics. Based on the principles of forward modeling, Opensim uses various known muscular force profiles to drive kinematics and calculates the forces that

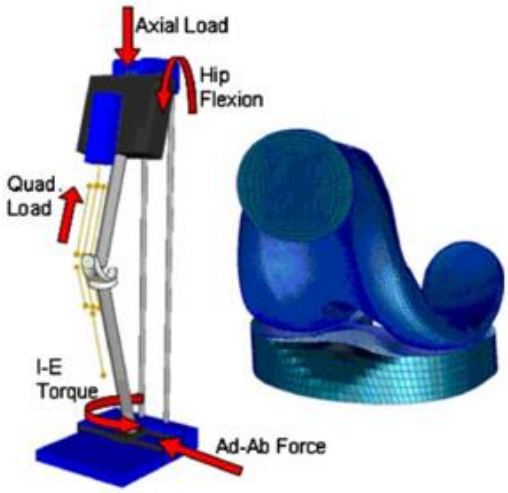


Figure 29: Finite element modeling can be used to demonstrate interaction between mechanical interfaces which are represented as discrete elements. Such is the case in models of the Kansas knee simulator (figure modified from [94]).

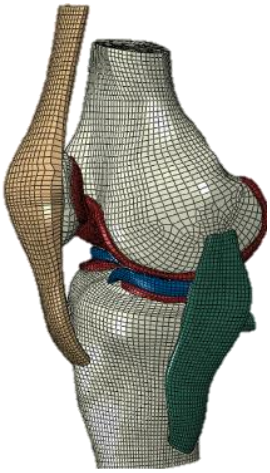


Figure 30: One of the primary advantages of finite element analysis is the ability to model deformable bodies, this makes such methods ideal for analyzing soft tissue deformation under loading conditions (Figure modified from [131]).

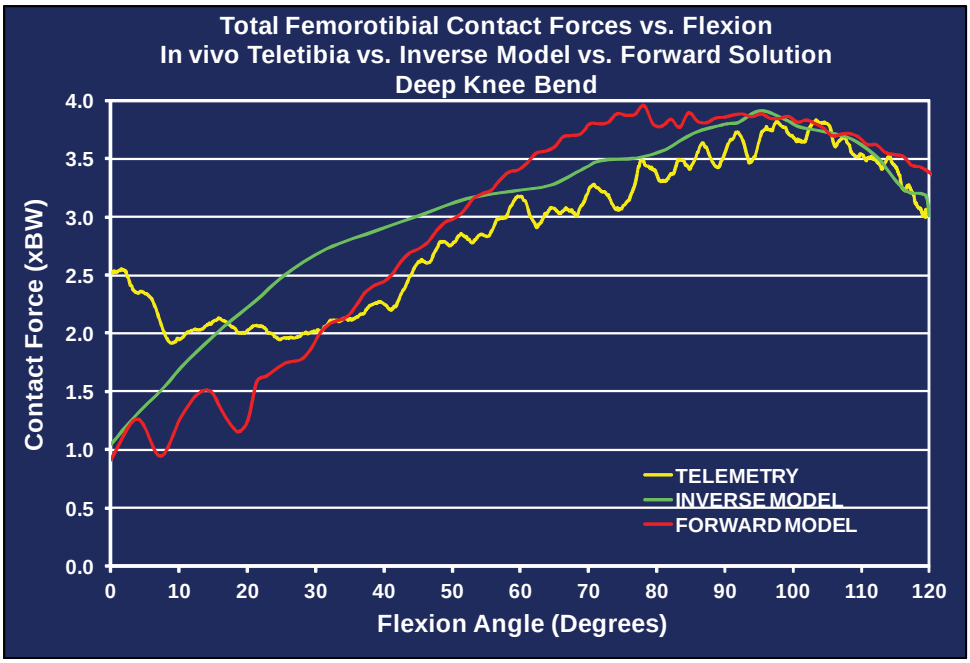


Figure 31: In 2008, Dr. Sharma successfully built a model capable of calculating forces that closely match those of telemetric evaluation (Image from [127]).

are required to do so [132] (Figure 32). The muscle forces are determined through an optimization based inverse model and can be altered by the user to determine muscle sensitivities with respect to motions. Opensim also offers the ability to set up subject-specific models built up by parameter and then allows other users to use these configurations for further analysis.

Opensim has been used in the past to model systems up to 21 degree-of-freedom model with 92 actuating muscles simulating gait [133]. In addition, to using identifying irregular muscle patterns in patients afflicted with gait disorders [132] and produced lower limb models to better understand passive joint movements [134].

2.7.3.3 AnyBody

AnyBody Modeling System is an inverse dynamic software that utilizes optimization strategies to model a wide variety of fields ranging from biomechanics and ergonomics to aerospace and defense [135]. Even in biological applications, the program has the ability to model individual muscle forces, soft issue elastic energy and even metabolism. Using telemetric and motion capture data, this software was recently used to build an individualized model to better understand TKA mechanics [136].

2.7.3.4 LifeModeler

LifeModeler is a modeling software that allows for integration with CAD programs to import model geometries of anatomical structures including muscles, ligaments, and contact surfaces and from which wrapping and contact algorithms can be factored into analysis.

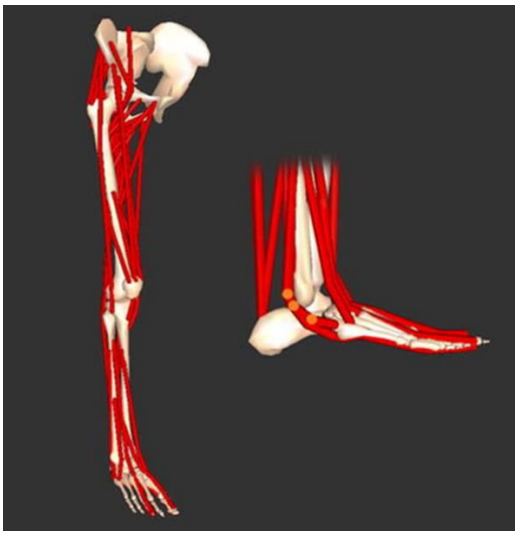


Figure 32: Opensim provides the basic framework and setup for mechanical systems representing much of the body, including the knee. This is an open source program that allows for the validated configurations for various analysis (Image modified from [134]).

One particular study considered mobile and fixed-bearing PS, a high flex, fixed-bearing design and a simple hinged design, evaluating the positioning of the patella with a sensitivity analysis. In this case, it was possible to simulate these conditions where the patella was located too far proximal or too far distal in otherwise identical patients [137], a case that is not possible to evaluate without the power of mathematical modeling to simulate these theoretical cases. This model demonstrated that patella forces are highly sensitive to patella positioning, particularly in the proximal distal direction which is an important consideration for design engineers as it improves the understanding of the role of the patella in the forces of the knee [137]. Unlike other modeling software, Lifemodeler is specifically aimed toward modeling in orthopedics as the software is owned by Smith & Nephew, Inc. who are predominantly an orthopedics company.

2.7.3.5 ADAMS

Short for Automated Dynamic Analysis of Mechanical systems, ADAMS is a multibody dynamic system that is used primarily for inverse modeling of closed chain dynamic systems. What is unique about ADAMS is the inclusion of material property-based (elastic modulus and Poisson's Ratio) deformation similar to what would be demonstrated by a low node finite element software. Much like Lifemodeler, this software has a litany of applications in aerospace and automotive applications along with use in orthopedic studies [138]. The inverse nature has made it particularly useful in studies to determine ligament responses under mechanical loading [111, 139], as well as contact mechanics and determining stiffness and compliance matrices on a device specific basis [140](Figure 33). While an excellent inverse modeling tool, the forward capabilities for this software

are limited which keeps its primary usefulness to assessment of mechanical response as opposed to dynamic forward motion assessment.

2.8 The University of Tennessee Model

This dissertation project is a continuation of the model originally created by Dr. John Mueller and then further advanced by Dr. Brad Meccia developed at the University of Tennessee. The purpose of this model has been to evaluate existing knee implants and to function as a design tool that can be used to assist implant designers in the assessment of future TKA concepts. As with math modeling in general, this process is advantageous over other assessment techniques given its ability to quickly and accurately predict in vivo kinematics. The alternative to such a model would be the time intensive process of manufacturing and implanting a device which is not always feasible, especially in the early stages of development.

The development of these models first began with Dr. Richard Komistek's work with Dr. Thomas Kane, the inventor of Kane's Dynamics [129], and then further advanced by Dr. Adrija Sharma who developed an inverse model for TKA assessment using modified principles or finite element analysis. Such a technique was substantially more computationally efficient than existing finite element methods while producing comparable force profiles [127]. Dr. Mueller then developed a forward solution model capable of predicting in vivo kinematics and loads for normal knees, and TKA validated with fluoroscopy [119]. Dr. Meccia then

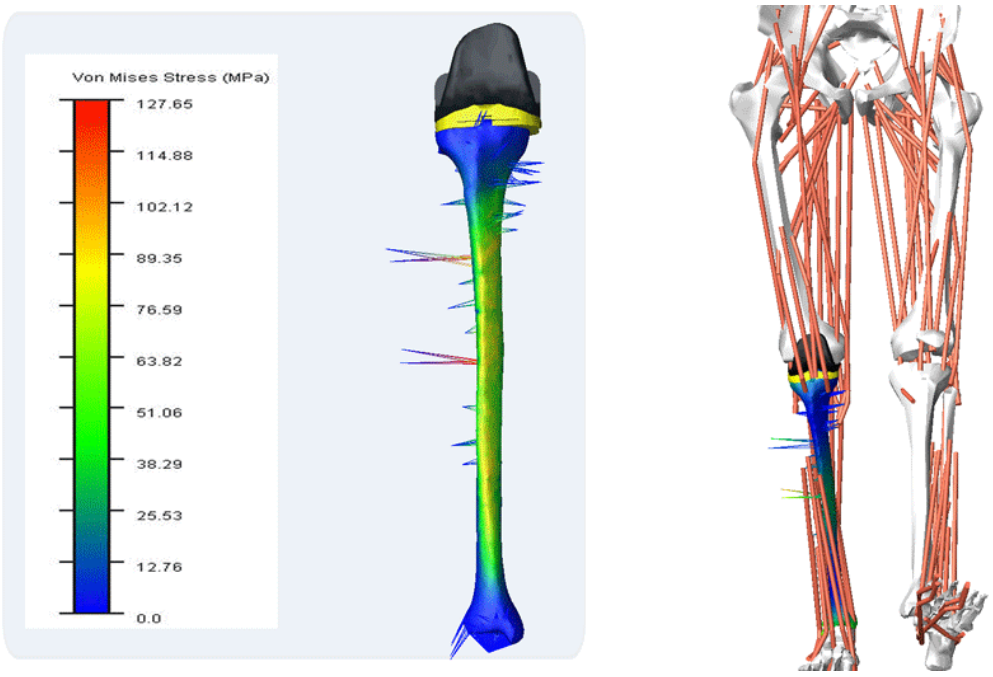


Figure 33: ADAMS provides the capability to assess biomechanics systems under a variety of conditions. These setups are primarily inverse models and afford the opportunity to assess internal stresses and associated deformations (Figure modified from MSC Software).

expanded on this model by broadening the capabilities to assess varying types of total knee replacement devices [118]. The next logical progression is to expand this work to encompass varying types of patients which is the advancement proposed in this dissertation.

The model setup begins with an anatomically defined system of rigid bodies using Autolev, a program that serves as a symbolic manipulator or “equation calculator.” The equations of motion relating the forces and motions of the system are set up using Kane’s multi-body system of dynamics. These equations are built to accommodate implant device geometries and using a contact detection algorithm and a controller applied on the active muscles, the equations of motion are solved dynamically for the variables that are of interest to the user. The end result is an assortment of kinetic and kinematic data for which transformation matrices can be obtained and animated. In other words, the model defines a mechanical system, populates it with constraints as defined by a user and outputs quantitative and animation results (Figure 34).

2.8.1 Geometric Setup

This model that has been developed is specifically focused on the evaluation of the knee. The system is represented by four bones which are all assumed to be rigid in that the amount of deformation experienced under mechanical loading is negligible. These bones are the tibia, patella, femur and pelvis. These bones by default all have three rotational and three translational degrees of freedom for a total of six degrees of freedom. The inclusion of soft

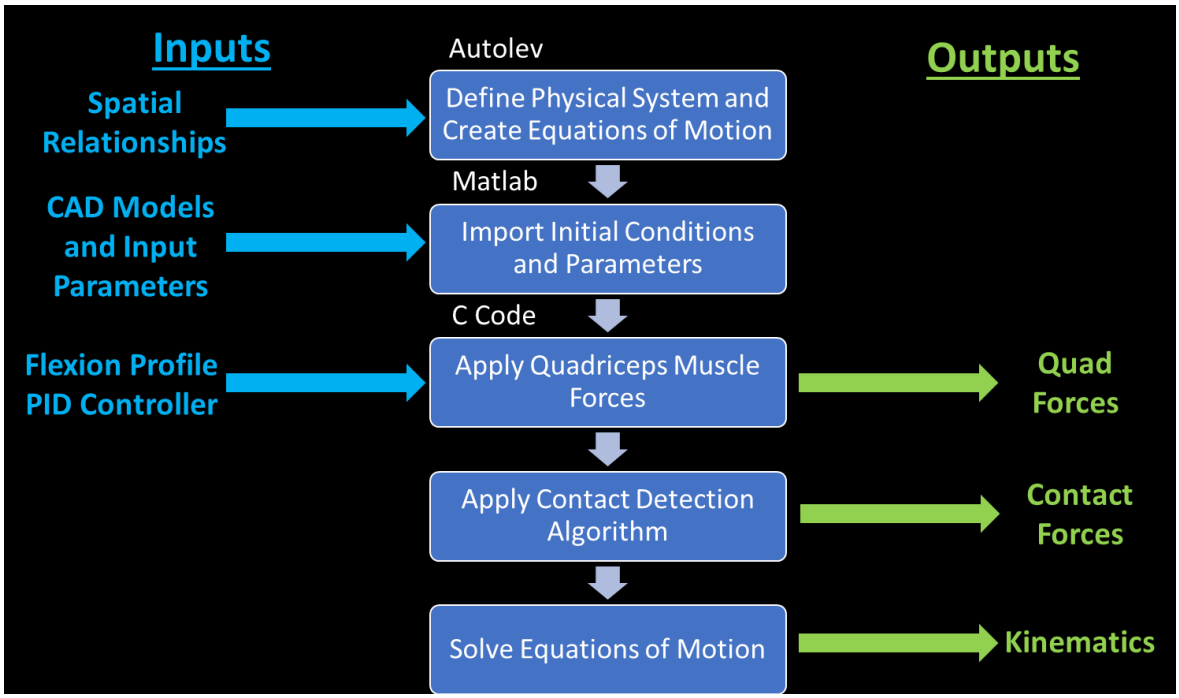


Figure 34: The modeling process consists of several distinct processes that develop and solve dynamic equations of motions under varying conditions with specific sets of inputs and outputs at each process.

tissue ligaments constrain certain degrees of freedom, facilitating the motions that the knee demonstrates.

Soft tissue in general can be a collective term and in this case, it is representative of the muscles, tendons and ligaments that function together and actuate the mechanical system. The model incorporates the anterior and posterior cruciate ligaments, the medial and lateral collateral ligaments, the patella tendon and the medial and lateral patella femoral ligaments. In addition to the tendons and ligaments, the system contains two main muscle groups. The quadriceps and the hamstrings. The quadriceps originate partly on the anteroproximal femur and partly on the anterior pelvis and all of the fibers insert on the proximal patella. The hamstrings originate on the posterioproximal side of the femur and insert on the posterior proximal epiphysis of the tibia. Despite the antagonistic nature of the quadriceps and hamstring muscles, gravitational resistance drives the quadriceps muscles to play a much bigger role than the hamstrings. They need to counteract gravity to control a fall during flexion and drive motion during extension. The hamstring muscles act more as a stabilizer during these motions [119].

While the anatomical knee contains far more complexity with numerous elements, the idea behind the model representation is to simplify the mechanical model exclusively to the key elements that contribute to knee mechanics (Figure 35 & Table 3).

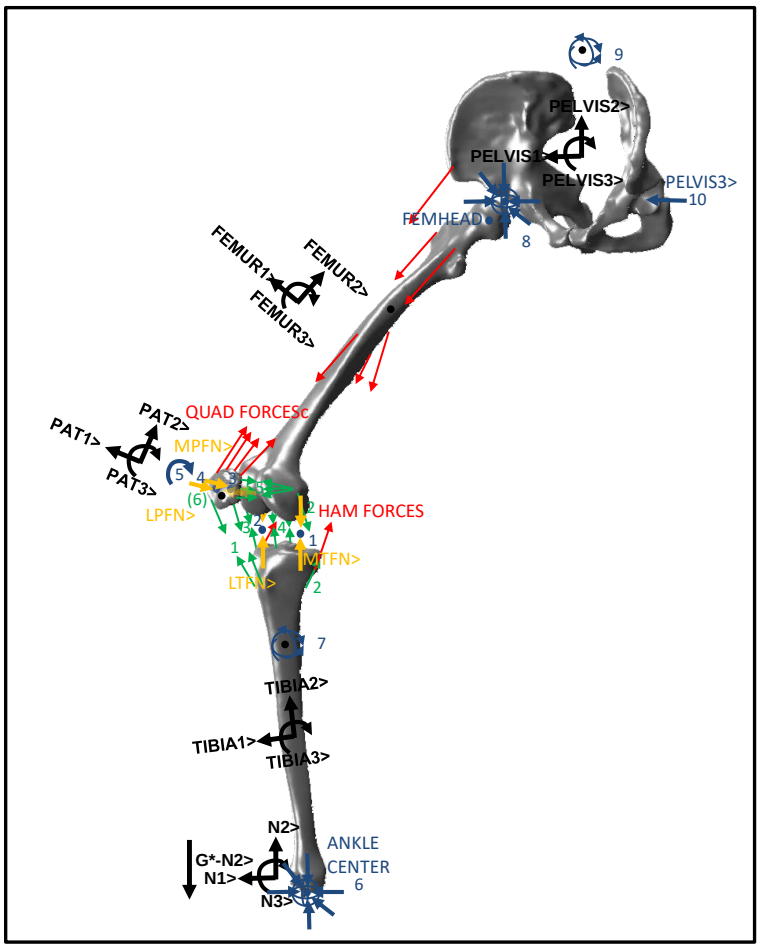


Figure 35: The free body diagram of the knee shows the overall system setup including associated bones, muscles and ligaments with their respective frames of reference. (Used with permission from [119])

Table 3: There are a number of structures and forces that act on the knee and although the complexity is reduced from the true anatomical knee, the motel strives to retain as many of these structures as possible. There are also several assumptions made by the model. (Used with permission from [119]).

SUMMARY OF WEIGHT BEARING DEEP KNEE BEND MODEL OF A RIGHT LEG	
GRAVITY	Gravity acts in the –1*N2> direction
BODIES	-PELVIS (3 rotations specified, fixed to femoral head), FEMUR (3 DOF), PATELLA (3 DOF), TIBIA (3 rotations specified, fixed to N (ground) at the ANKLE CENTER) -Mass and inertial properties calculated from literature -Orthogonal system of unit vectors established for each body 1> points anterior 2> points superior 3> points lateral
CONSTRAINT FORCES (BLUE NUMBERS AND BLUE AND YELLOW ARROWS ON FIGURE 35)	1. Medial TF Geometric Constraint force acting between FEMUR and TIBIA in the MTFN> direction 2. Lateral TF Geometric Constraint force acting between FEMUR and TIBIA in the LTFN> direction 3. Medial PF Geometric Constraint force acting between FEMUR and TIBIA in the MPFN> direction 4. Lateral PF Geometric Constraint force acting between FEMUR and TIBIA in the LPFN> direction 5. Constrain Rotation of PAT in PAT3> with Knee Flexion 6.TIBIA translation constrained to N (ground) at ANLE CENTER 7. 3 TIBIA rotations specified as function of knee flexion 8. PELVIS translation is constrained to the femoral head on FEMUR (FEMHEAD) 9. 3 PELVIS rotations in N are specified as a function of knee flexion 10. Mediolateral translation of the point on FEMUR, FEMHEAD, in the PELVIS3> direction is specified as a function of flexion
LIGAMENT FORCES (GREEN NUMBERS AND ARROWS ON FIGURE 35)	1. Patella Ligament Medial and lateral, Two Bundles Each 2. Medial Collateral Ligament Three Bundles includes wrapping 3. Lateral Collateral Ligament One Bundle 4. Posterior Cruciate Ligament and Anterior Cruciate Ligament Two Bundles Each 5-6. Lateral and Medial Patellofemoral Ligaments Three Bundles for Each
ACTIVE MUSCLE FORCES (IN RED ON FIGURE 35)	-QUAD FORCES are applied to PAT at the insertion points and FEMUR at the muscle origin points. Controlled using a PID controller with an additional flexion acceleration feedback element and a PD controller which stabilizes PAT tilt -HAM FORCES may be applied to the insertion point on the tibia and origin point on the femur and are a function of knee flexion
IMPORTANT ASSUMPTIONS	-Rigid body model does not allow for condylar lift-off. As long as the TF constraint forces (1,2 above) are in compression this is a reasonable assumption -PAT flexion is prescribed as a function of knee flexion -The mediolateral constraint at FEMHEAD acts as the stabilization provided by the contralateral leg -Contact point on FEMUR and on PAT are prescribed as a function of flexion -Geometry represented by constraining the velocity of contact points in the direction of the tibial or trochlear groove surface normals (LTFN>, MTFN>, LPFN>, MPFN>) to 0. -Ligaments are modeled as non-linear springs with damping

2.8.2 Kane's Dynamics

Although all dynamic systems can produce equations of motion, Kane's Dynamics was used because it is the most computationally efficiency technique. Newtonian dynamics is thorough but requires forces in a system to be balanced. You can only model one rigid body at a time, meaning that every force needs to be calculated, regardless of role in the mechanical system. LaGrange dynamics is energy based and for that reason it can eliminate the need to calculate forces that contribute no work on the system. Despite only calculating active forces, the limitation to LaGrange dynamics is that differentiating energy functions can become computationally time consuming, especially across multibody systems [141].

Kane's method is different as it hybridizes Newtonian and LaGrange dynamics through a concept of partial velocities which are vectors multiplied with generalized speeds. Due to the nature of these mathematical entities, velocities and accelerations can be differentiated using various vector products [141]. Once the vectors are differentiated, the overall forces in the system can be determined element by element with the equation

$$F_r + F_r * = 0$$

where F_r represents the generalized active forces on the system and F_r* represents the generalized interim forces. Active forces are those which are applied to the system and inertial forces are the reactive forces of the elements of the mechanical system [142]. This methodology makes Kane's system off

dynamics far superior in computational efficiency which is why it is used in this model.

2.8.3 Autolev

Autolev is a programming language that acts as a symbolic manipulator for dynamic systems. It relies heavily on Kane's dynamics which makes it highly computationally efficient. It features the ability to create forward and inverse models from defined geometries, properties and constraints. Autolev allows for the creation of dynamic equations by defining bodies, inertial properties, positions, constraint functions and specified functions.

Through these definitions Autolev uses Kane's system of dynamics to determine the equations of motion for the system. While this is a straightforward process in inverse modeling, forward modeling is slightly more complicated as some of the components are represented by place holder values which can be solved later as they are built into the equations of motion.

One of the most advantageous features of Autolev is the parametric nature of the equations of motion. Each value in the equations is specified as a variable or constant and the resulting outputs are the following:

- A Matlab, C or Fortran file containing the equations of motion and the necessary algorithms to solve them.
- A directory file containing a list of all of the output values for each timestep of the code.
- An input file that contains all of the values needed for the code to execute.

These outputs help to facilitate robust parametric functionality where values can be easily changed and tested to better suit the analysis. This also comes without the need to edit or recompile the solution code.

2.8.4 Muscle Control

Despite the universal functionality of Autolev, there are limitations to the functions it is capable of performing. One such operation that cannot be performed due to lack of sophistication is the introduction of muscle controllers. In order to integrate a controller algorithm into Autolev, a placeholder variable must be used in the Autolev code for the variable which will be controlled. This variable will later be used as a controller to dictate the forces of the model.

For this specific model, there are two controllers which are involved. The first of these is a proportional integral derivative (PID) controller on the quadriceps mechanism which adjusts the quadriceps forces to fit a specified profile using a function to minimize error [143]. This controller is placed on velocity making it technically a PIDA controller (Proportional Integral Derivative Acceleration). This controller minimizes the quad force error function to achieve a target profile function. This force is distributed roughly evenly among the quadriceps muscles. In addition to the main PID controller, there is a secondary PD (proportional derivative) controller which acts as a stabilizer for the patella spin about the proximal distal axis (Figure 36). While at one point this controller was critical, updates in contact detection have lead t to become antiquated in later versions of the model.

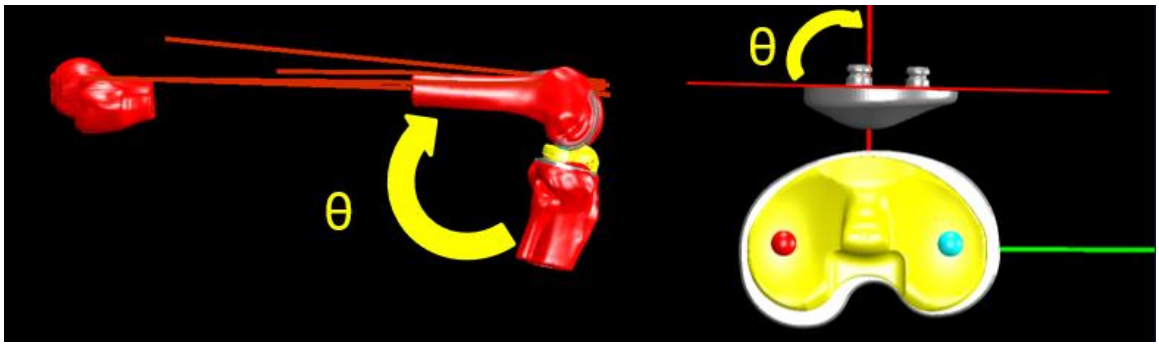


Figure 36: The model incorporates two muscle controllers that are used to set knee adjust the quad forces to match profiles set by the user. In the case of flexion, all four quads are activated to achieve flexion to match a specific profile using a PID controller (left). In addition, there is a PD controller stabilizing the patella about the SI axis that affects the force in the vastus medialis and lateralis (right) (Used with permission from [118]).

The model equations of motion are solved dynamically using the Runge Kutta function at each timestep and the controllers adjust to drive motion to the next timestep based on the overall desired motion profiles.

2.8.5 Contact Detection

In addition, the muscle controllers a second element is added to the model which is needed for proper functionality and this is a contact detection algorithm to simulate the interactions between the articulating components. The contact detection for the model is based upon a simple yet elegant mathematical interpretation. For each surface that can potentially be articulating, the complimentary surfaces are represented as either a point cloud or a polynomial surface in 3D space. When the model solves the differential equations of motion iteratively and at each timestep, each point in the cloud is checked to see where it lies relative to its complimentary contacting surface (Figure 37).

As an example, if the height coordinate of a particular point is equal to the height function, then the two bodies are exactly in contact. If the height for the point is greater than the height function, there is no contact. If the height for the point is less than the height function of the surface, then the model two bodies are not only in contact but in penetration. Many models base their contact detection on a low point assumption, where the lowest point in vertical space is assumed to be in contact. While this is true on a flat surface, the concave bearing surface can create conditions where such an assumption is no longer valid. This method was proposed and developed by Dr. Meccia to account for contact [118] (Figure 38).

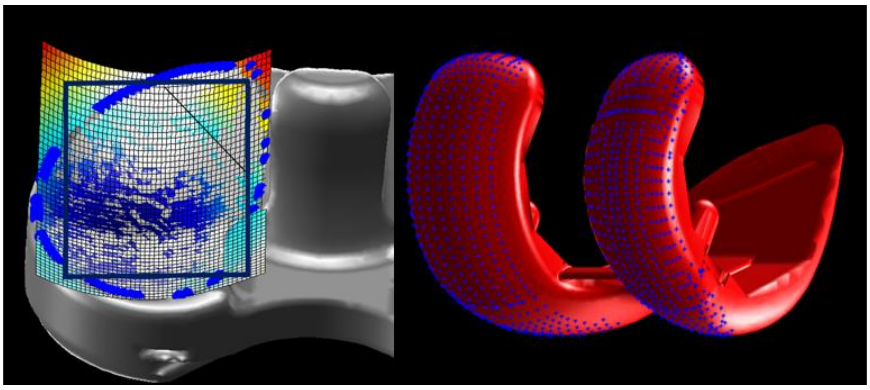


Figure 37: The contact detection algorithm is defined through two complimentary surfaces, one of which is a point cloud and the other is a surface polynomial. The surface polynomial is also built to contain a convex hull which essentially acts as the bounding parameters for the contacting surface (Used with permission from [118]).

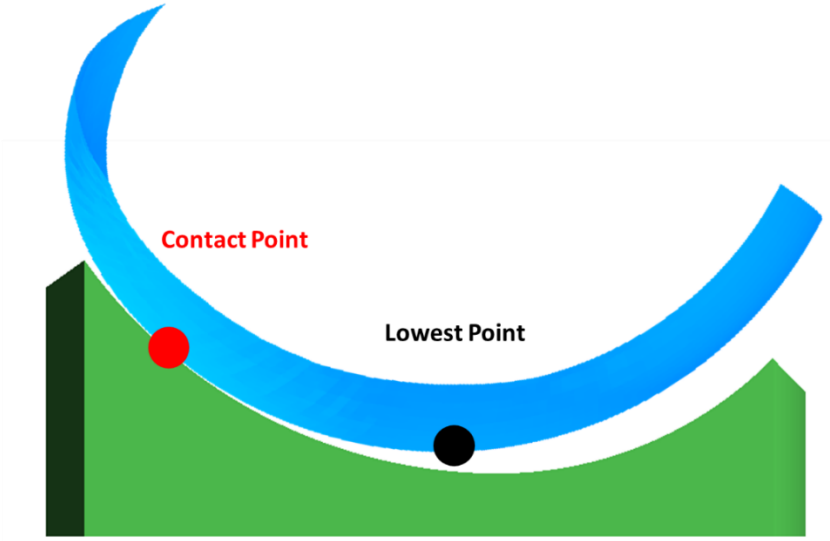


Figure 38: Many TKA contact models incorporate the low point assumption that contact occurs on the lowest point of the femur. While true on a flat surface, the concave bearing surface can invalidate this assumption (Used with permission from [118]).

There is also a secondary element to the contact detection algorithm which is the idea of the convex hall. This was introduced to the model by Dr. Meccia who revised the contact detection algorithm [118]. The convex hull is a two-dimensional set of points projected into a plane that composes the perimeter of the contacting surface. For contact to mathematically occur, the contact points need to be within this region which is determined by the sign of sequential cross products between the testing point and every point of the convex hull (Figure 39) [118].

To summarize, for a point on a body to be considered “in contact” it must meet two specific conditions. It must be both below surface function for which contact is occurring and be contained within the projected region of the convex hull (Figure 40). For each point determined to be in contact a force is determined using the penetration distance (Figure 41). The correlating force is mathematically based on the stiffness of a nonlinear spring. The resultant contact force will then be the sum of these points and contributed back into the force profiles of the model. This methodology is the same regardless of which surface is being assessed for contact the model possessed the ability to evaluate medial and lateral bearing surfaces, anterior and posterior posts and in some cases tri-condylar center bearing surfaces.

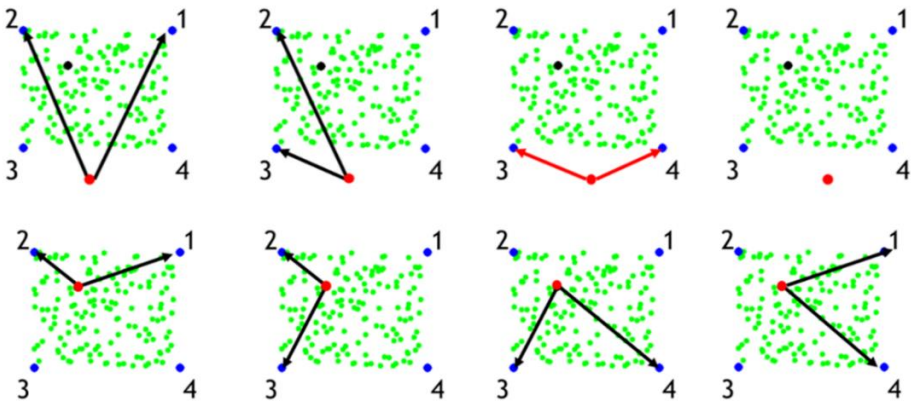


Figure 39: Using the cross products, the convex hull algorithm can be used to determine if a point lies within the convex hull. To do this the cross product is taken between the vectors connecting each test point to two points of the convex hull. In the top row the third case has a negative cross product meaning the point lies outside the convex hull. In the bottom row all cross products are positive therefore the point being tested lies within the convex hull (Used with permission from [118]).

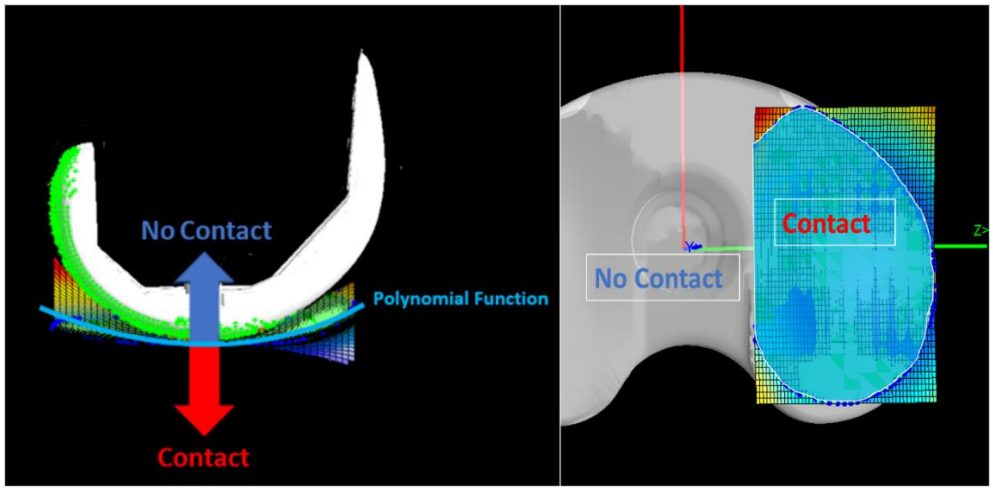


Figure 40: In order for the contact detection algorithm to denote contact, two conditions must be met. First, the point cloud on the femoral component must be less than the polynomial surface for the bearing (left) and second, this contact must occur within the projection of the convex hull (right).

$$\overline{Normal\ Force_{x}} = \frac{-\frac{\partial y}{\partial x} * K * Pen}{\sqrt{\left(\frac{\partial y}{\partial x}\right)^2 + \left(\frac{\partial y}{\partial z}\right)^2 + 1}}$$

$$\overline{Normal\ Force_{y}} = \frac{K * Pen + B * \frac{dPen}{dt}}{\sqrt{\left(\frac{\partial y}{\partial x}\right)^2 + \left(\frac{\partial y}{\partial z}\right)^2 + 1}}$$

$$\overline{Normal\ Force_{z}} = \frac{-\frac{\partial y}{\partial z} * K * Pen}{\sqrt{\left(\frac{\partial y}{\partial x}\right)^2 + \left(\frac{\partial y}{\partial z}\right)^2 + 1}}$$

$$\overline{Friction\ Force_{x}} = -\mu * \frac{V_x}{V_{Tot}} * \left|\overline{Normal\ Force}\right|$$

$$\overline{Friction\ Force_{y}} = -\mu * \frac{V_y}{V_{Tot}} * \left|\overline{Normal\ Force}\right|$$

$$\overline{Friction\ Force_{z}} = -\mu * \frac{V_z}{V_{Tot}} * \left|\overline{Normal\ Force}\right|$$

Figure 41: Should penetration be detected, equations are used to calculate the contact forces where X and Z are anteroposterior and mediolateral directions respectively and Y is the proximal/distal direction. The normal force equations are based on the normalized partial velocities factored with penetration distance (Pen), Penetration stiffness value (K) and rate of penetration change and B is a factor on the penetration velocity applied exclusively in the vertical direction. These normal forces are also used to calculate frictional forces which are factored as contributions to the kinematics of the system (Used with permission from [118]).

2.8.6 Initial Conditions

The final component that is necessary to set up the model is the placement of the device components and the initial bounds of the model. This includes the placement of implanted components, the properties of soft tissue, the controller gains and parameters and essentially any other values that need to be set or updated prior to run time.

Component placement is possibly one of the most important aspects of the initial modeling setup. Throughout this process, each TKA component is placed relative to its corresponding bone, where it is assumed to be rigidly attached once it is placed. This includes the tibia, femur and patella components. The bones are then placed relative to each other in such a way that the tibia and femur are aligned, as are the patella and femur (Figure 42). It is of note that the force algorithm is based on differential equations and for this reason the surfaces cannot be in initial contact as the numerical methods rely on preceding and proceeding values which intuitively do not exist for the first timestep in the simulation.

In addition to initial positions it is also possible to set mechanical ligament properties and initial strain values for each fiber of each ligament. There are also a number of simulation control variables which can also be adjusted and are the parameters that directly affect the simulation. These include controller gains, controller switches, and integration parameters.

The ability to edit these simulation parameters quickly and easily represents a significant strength of the model. Changing these values gives the user the ability to change the simulation conditions and perform thorough sensitivities to better

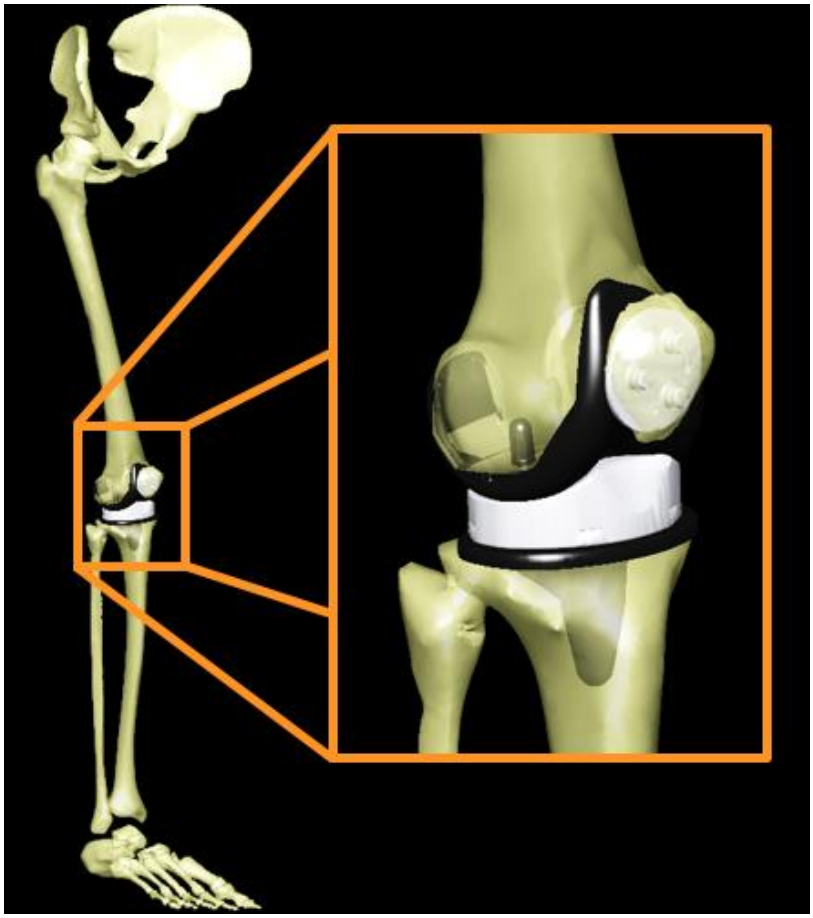


Figure 42: To setup a simulation a visualization is used to both place components relative to bones as well as place bones relative to each other to achieve realistic initial conditions.

understand how and why a TKA device performs as it does. Furthermore, elaborate testing is advantageous evaluating device features and determining what changed need to be made to future iterations.

2.8.7 User Interface

While there are a substantial number of parameters that can be changed within the model, understanding the model well enough to make these changes without using only scripts or any sort of visualization requires months of training and years of practice. To better facilitate user friendliness and expedite the learning curve, Dr. Meccia developed a user interface that allows for substantially easier component placement and model visualization (Figure 43). Not only does such an interface facilitate ease of use but also allows for fast and frequent evaluation to ensure the model is running as intended. In addition, the visualization allows for simplified trouble shooting and provides more insight for the behavior of a prospective device.

Another asset of the simplified interface and improved visualization is the ability to quickly train new model users. In doing so analysis can be performed quickly and consistently by multiple users. This facilitates large scale sensitivity studies and further enhances the power of the model analysis.

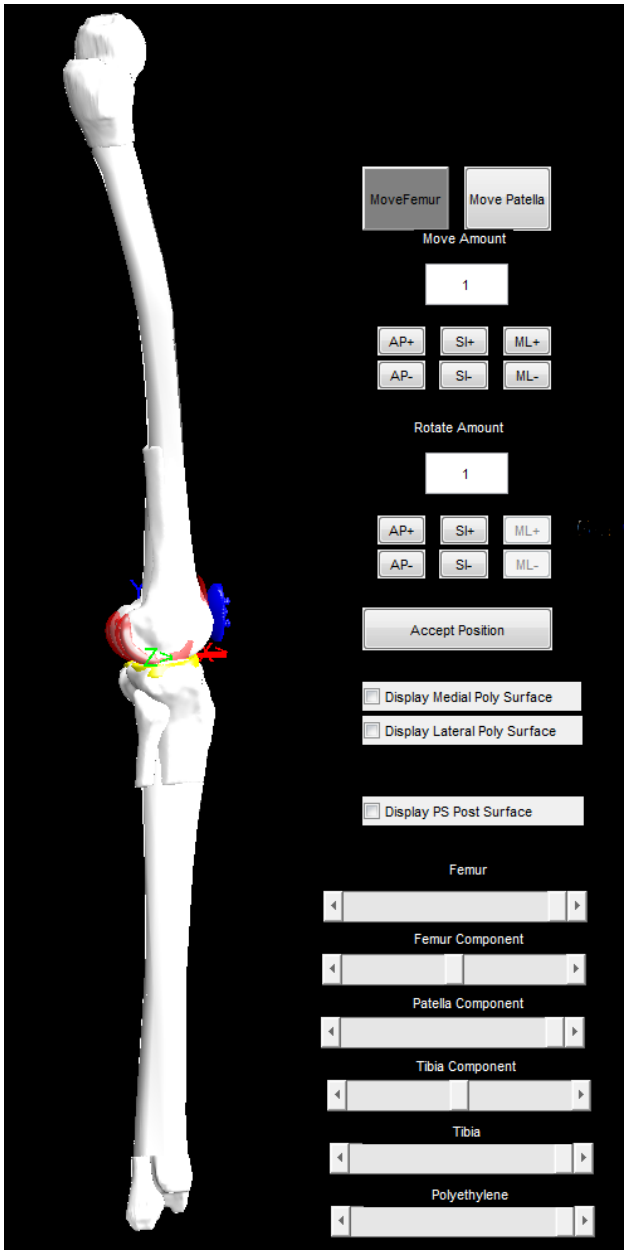


Figure 43: The model has been built to include an intuitive and efficient user interface which allows for a user to place components and ensure that desired spatial changes are being made.

CHAPTER THREE: OBJECTIVES AND CONTRIBUTIONS

3.1 Objectives

Despite the vast capabilities of this new version of the model in comparison to the previous two iterations, it remains to be device centric model in that most of the capabilities are meant to be applied to the TKA design process. While this is certainly an effective application of modeling technology, there are additional patient centric applications to which the capability of altering and evaluating joint performance in a theoretical space can be of substantial consequence. Not only does this include enhancing the design assessment process through patient variations and enhanced geometric capabilities, but also has a clinical aspect where complex cases can be assessed using the model. Such applications could allow surgeons to gather more information and decide on the best course of action to restore ambulatory quality of life to orthopedics patients with knee pathology and complications.

The objective of this dissertation will be to expand the parameterization of this version of the model, advancing the previous mathematical models in order to create and augment a tool capable of evaluating knee motions and forces with both design and clinical context. Such a model will seek to accomplish the following:

- The model will enhance features as a design tool capable of assessing and altering implant geometries while interfacing with design engineers through computer aided design tools and principles.

- The model will strive to expand its library of demonstration activities, adding more degrees of complexity to existing activities to improve physiological realism.
- The model will be enhanced for clinical relevance by modeling the native, healthy knee and in doing so allow for geometric and mechanical alterations capable of simulating various knee pathologies.
- The model will expand its number and types of patients for which simulations can be run. This allows for subjects to be tested under various conditions and devices to be evaluated in different patient populations.

3.2 Contributions

There are a variety of models that exist throughout both commercial and private settings that can be used to analyze total knee replicant devices. While many of these models produce excellent results, they are often limited by both scope and application to clinical settings. The previous iterations of this model were seeking to avoid many of these pitfalls while aiming to be as robust and accurate as possible. Earlier versions of this model have done well to increase the factors of consideration and incorporate accurate anatomical architecture. They have also facilitated a parametric nature that has improved ease of use and allowed for accurate in vivo testing of prospective devices. This model can produce hundreds of results and can be tweaked to better fit clinical needs.

While previous versions of this model have been excellent, there are still improvements for the model to promote clinical relevance. One of the greatest examples is the analysis revolving around a single patient created around roughly average data. One of the primary contributions of this dissertation is to produce a model that is robust enough to assess a variety of patient types, under a variety of

conditions. The model also strives to evaluate additional activities while improving motion patterns and anatomical configurations to better represent in vivo conditions. Neither an equivalent model nor mechanics results exist in biomechanics literature; thus, this is a novel contribution which advances the field of knee research. This dissertation contributes the following:

1) Parameterization the normal, healthy knee and development of a forward solution model capable of assessing knee kinematics under various circumstances.
2) Parameterization of the extensor mechanism and ensure that optimal quadriceps force transmissibility is achieved.
3) Parameterization of articulating surfaces and introduction of a parametric technique that can be utilized by CAD designers.
4) Parameterization of flexion activities, including ankle and hip updates to create better representations of physiological motions.
5) Parameterize demographics and create a model that is able to assess a multiple patient demographics including variations in gender, race, and pathological joint condition.
6) Parameterize gait and provide simulated kinematic and kinetic data.

CHAPTER FOUR: PARAMETERIZING THE NATIVE KNEE

4.1 Purpose

The generalized goal of total knee arthroplasty (TKA) is to facilitate the restoration of native joint function following late stage osteoarthritis. And for this reason, it is important to develop a thorough understanding of the mechanics of a normal healthy knee, including motions, forces and the interplay between bone and soft tissue. While there are variety of methods for the assessment of TKA mechanics, many of these methods have both cost and reliability limitations making them prohibitive to large scale experimentation. These limitations can range from an ineffective replication of physiological systems to the inability to accurately and reliably measure forces within a system, especially in the context of a normal, non-implanted, healthy knee.

One such means of overcoming these analysis limitations is through the development of mathematical models that use anatomical, physiological and empirical inputs to computationally simulate joint mechanics. This can be done in an inverse or forward manner to solve for either joint forces or motions, respectively. While mathematical modeling provides a useful and efficient method of device assessment, to provide meaningful analysis, the model must be verified with existing data to ensure accuracy and repeatability.

The purpose of this contribution is to further the development of a mathematical forward solution model to assess the mechanics of the normal knee and determine the accuracy of the predicted motions using data from fluoroscopic

studies. This analysis will not only give additional insights into the accuracy of the model, but also a refinement of the soft tissue properties that constrain the system. These soft tissue properties can then be applied to TKA designs to give a more accurate assessment of TKA device performance. This validation was done by retrospectively analyzing in vivo kinematics for ten normal, healthy subjects from full extension to 120 degrees using fluoroscopy and a 3D-to-2D registration method. All ten subjects had previously undergone CT scans, allowing for the digital reconstruction of native femur and tibia geometries for the registration process. These same geometries were then input into a ridged body forward model based upon Kane's system of dynamics. The resulting kinematics were compared between fluoroscopy mathematical simulations for each subject.

In comparing the simulation kinematics using the mathematical model to the results from a fluoroscopic study, the goal is to demonstrate that results of a forward model can be a viable assessment of knee mechanics. While the accuracy is acceptable, minor changes to soft tissue can be applied to further improve consistency across distinct patients. By validating mathematical simulation as a feasible means of mechanical assessment, it becomes possible to evaluate mechanics using inputs to reflect extraordinary and theoretical instances, such as trauma patients and congenital deformities unable to be assessed by other methods. The nature of the model also allows for a seamless transition to assess TKA mechanics, creating a more efficient means of evaluating both device design and surgical technique.

4.2 Introduction

Total knee arthroplasty has historically been a highly successful procedure indicated for the restoration of mechanical function and quality of life following late stage osteoarthritis. Although modern implants have been developed using sophisticated design features, the universal ambition of most designs is still to achieve motions and forces comparable to a native, healthy knee [25]. It is widely believed that restoring these motions will alleviate pain, stiffness and functional limitations [26, 28, 29, 144-146], ultimately improving patient satisfaction and consistently producing positive outcomes overall [147]. For this reason, a successful TKA design is predicated on a thorough understanding of kinematics, kinetics, soft tissue properties, and anatomic geometries of the normal knee.

Measuring in vivo joint mechanics is inherently difficult as it is necessary to find an accurate technique minimizing measurement interference. The most accurate method of assessing contact forces within a TKA is an implanted telemetric device that is able to measure and transmit loads through an external conduit [148, 149]. This technique is prohibitively expensive and is also invasive as a TKA device needs to be implanted. The most accurate method of assessing in vivo joint kinematics is through fluoroscopy which determines arthroplasty component positioning and orientation using x-ray images. Therefore, in the use of these two measurement techniques, telemetry is limited to measuring kinetics, and fluoroscopy is limited to measuring kinematics, while neither is particularly successful measuring soft tissue forces directly. Mathematical modeling is one means of overcoming these limitations using computer simulations to replicate these physical systems and calculate results in silico [118, 119, 127, 150, 151]. In

the context of TKA, mathematical models have thus far been used to analyze implant geometry, joint reaction forces, and in vivo kinematics for an entirely theoretical patient. The input parameters for the model can then easily be modified and the resulting measurements are derived and reviewed, creating a highly effective device design tool. There are two primary subcategories of mathematical modeling: inverse models which derive forces for a system given the subsequent motions and forward mathematical models which derive motions from a given system of forces.

While mathematical modeling is an extremely powerful tool, it is necessary to assess how accurately the theoretical model can predict the functionality of physical systems. This is particularly difficult within the human body as physical systems are incredibly complex and need to be described precisely to give reasonable results. A model that reasonable replicates a physiological system can be validated, meaning it can be reliably used for analysis and further improve utility as a tool for design and assessment.

This study is a continued enhancement of a previously developed rigid body, forward solution reduction model of the tibiofemoral and patellofemoral joints [118, 119]. While this model has been used in the past to assess TKA designs, the most recent work has allowed for the assessment of normal knees for a variety of cases. Measuring the normal knee is important because, although TKA designs tend to have relatively consistent anatomic shapes, discretized over several scaling factors to account for size variations, normal, healthy knees can maintain localized variations between and even within subjects. While the hard tissue

anatomy can vary substantially between subjects, the ligament anatomy and physiology factors contribute even more into effective implant designs, as this soft tissue provides a substantial portion of the mechanical constraint across the anatomic bodies of the joint. Therefore, mathematical modeling of the normal knee allows for not only assessment of implant shapes but also interactions with soft tissue. By validating the resulting normal model with the mechanics observed during an activity, the soft tissue properties can be evaluated to achieve a match of these motions. The resulting properties can be applied to simulations evaluating TKA, creating a much more accurate and consistent simulation method for assessment.

As previously stated, this contribution aims to simulate 120 degrees of flexion using anatomical inputs for ten subjects and then compare the simulation results to fluoroscopic results (retrospectively) for those same ten subjects to determine similarities and differences, ultimately assessing the validity of the theoretical knee model tailored toward normal knees.

4.3 Methods

4.3.1 Patient Demographics

This study evaluated ten subjects initially analyzed fluoroscopically, then theoretically using the mathematical model. There were four males, and six females evaluated and the average age was 57.4 years, average height was 1.7 meters, with a mass of 79.5 kg and an average BMI of 28.7 (Table 4).

All subjects were healthy volunteers with no reported history of musculoskeletal problems. To determine their anatomical geometry, each subject

underwent a CT scan from the ankle to the hip, and the resulting maps were segmented to create a 3D geometric representation of the femur, tibia and patella. Institutional Review Board (IRB) approval had been previously obtained from each collection site involved and informed consent for all participating study participants was acquired (Figure 44).

4.3.2 Fluoroscopic Analysis

Using the gathered CT scans, computer aided design (CAD) were derived, representing subject geometry. Using a mobile fluoroscopy system capturing video images at 60 Hz, a deep knee bend was performed and captured demonstrating movement from full extension to maximum flexion [65, 72]. Kinematics were then evaluated from full extension to 120° of flexion at increments of 30° using a 3D-to-2D registration technique [152]. Through this technique, CAD models of segmented bones superimposed over x-ray images and the resulting transformations were obtained using these matches (Figure 45).

In order to establish a quantifiable axis system through which movement can be tracked, an axis was established at the midline of the tibial plateau, connecting the centers of the circular representations of the medial and lateral plateaus approximated using circles. Using the angle connecting the contact points of the medial and lateral knee sides, axial rotation was calculated (Figure 46).

Table 4: This analysis included ten healthy patients in total with a roughly even gender split and demographics representative of patient populations.

Gender	
Gender (male/female)	4/6
Average ± Standard Deviation	
Age (years)	57.44 ± 7.15
Height (meters)	1.66 ± 0.10
Mass (kg)	79.46 ± 15.24
BMI (kg/m^2)	28.71 ± 5.07

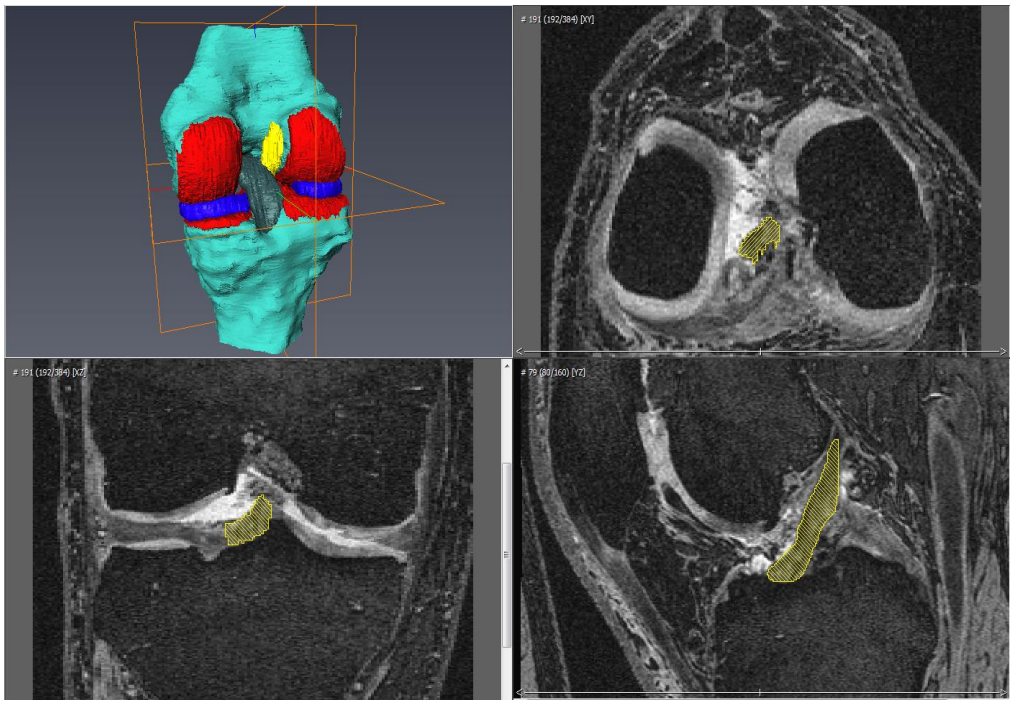


Figure 44: Accurate bone models were generated for each subject using CT scans and a segmentation process. These models were made to include the six inches of the epiphysis of the femur.

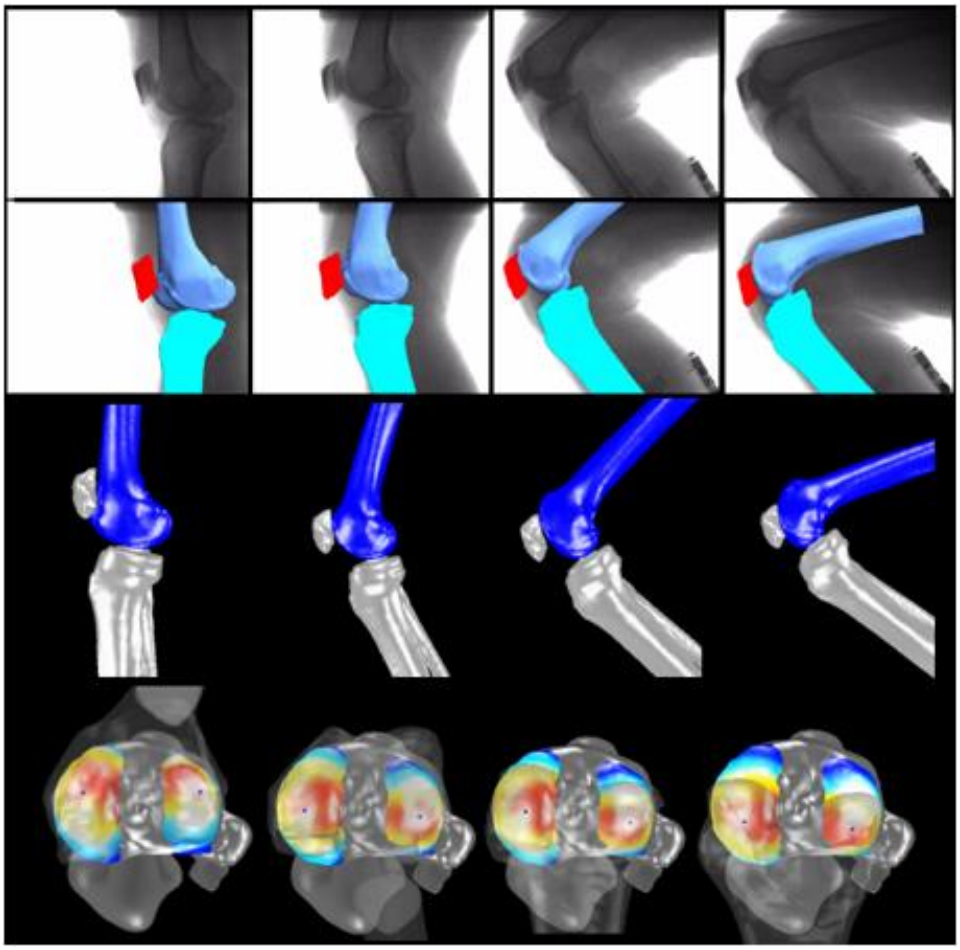


Figure 45: From top to bottom: beginning with the fluoroscopic sequence, the fluoroscopic images are isolated to include the frames of interest. The 3D scene is then recreated using a registration process. This leaves the digitized bone models in a recreation of the fluoroscopic scene. Using the transformations and rotations of these components, the kinematics are calculated.

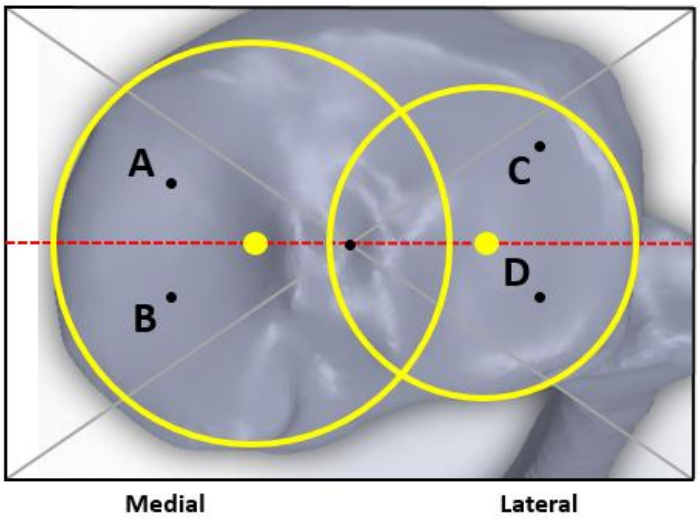


Figure 46: AP points for a right knee as measured by 3D-to-2D image registration process. The midline of the normal knee is defined through the best fit circles of the medial and lateral sides of the tibia plateau. Points A and C are defined as positive AP positions, while B and D are defined as negative AP positions. A translation from a positive point to a negative point is denoted as a negative translation. If an MAP point is more anterior than the LAP point, such as points A and D, the angular orientation is positive. A pivot from point C to D about point A is an example of positive axial rotation. This method of motion definition was originally used by Grieco, et al [65].

4.3.3 Kinematic Analysis (Mathematical Model)

The mathematical model evaluation of these subjects also utilized the same CT scan derived CAD models as the fluoroscopic method; however, the models are smoothed using several global remeshing algorithms. This smoothing allows for the geometries to be more easily converted to inputs, and this minimally affects the global shape of the bones. The models are then reduced to remove artifacts not pertinent to articulating surfaces (Figure 47).

Considerable research was also conducted to recreate a meniscus surface to incorporate into the model to better represent the anatomy of the normal knee. The surface is representative of the bearing being added into TKA models. This was done by creating an anatomic bearing based on the geometries observed in a segmented meniscus (Figure 48). Unlike the polyethylene bearing which has a reasonable assumption of rigidity, the meniscus has deformable mechanical properties, meaning that the assumption of rigidity is no longer valid. For this reason, the meniscus is left out of the analysis and the articulating surfaces are adjusted accordingly to account for this if needed. While the meniscus is not included in this analysis, it is something that can easily be either added or accounted for mathematically with the already defined surfaces. The mathematical model itself includes the tibia bone along with the femur, patella and pelvis. It also includes the quadriceps muscles, hamstring, both cruciate and collateral ligaments, patella ligament, lateral and medial patella femoral ligament.

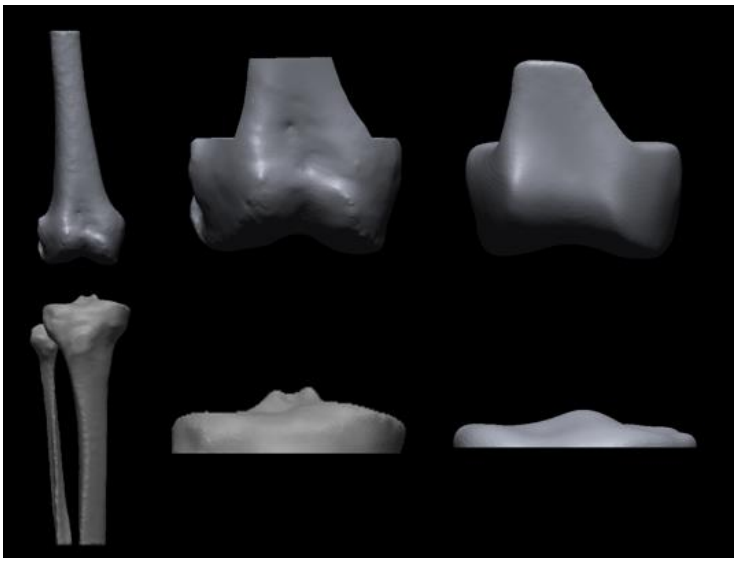


Figure 47: Beginning with the segmented bones from the CT scan (left), the bone models to be used as mathematical inputs are altered to only reflect articulating geometry (center). The model is then smoothed using a meshing algorithm and the results are used as mathematical inputs.

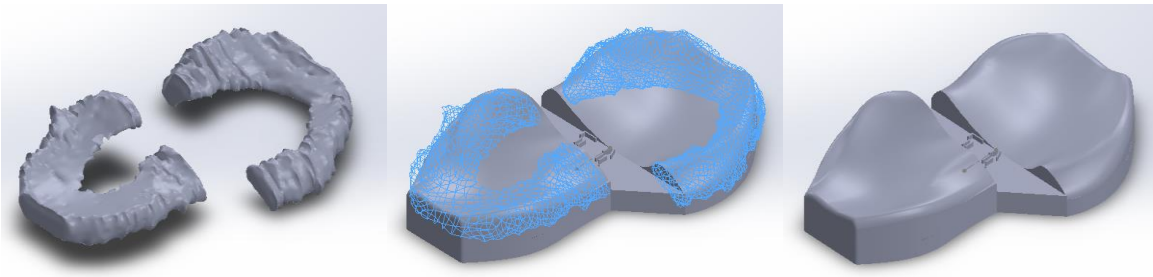


Figure 48: The meniscus geometry was originally obtained from a segmented MRI scan and used to build a continuous, solid body meniscus.

Using the symbolic manipulator Autolev (OnLine Dynamics, Inc., Sunnyvale, CA), the equations of motion are derived for the system using Kane's system of dynamics [118, 119, 127]. Unlike Newtonian dynamics, which solves for force as the product of mass and acceleration, Kane's dynamics uses generalized coordinated, partial velocities, and partial angular velocities to formulate a set of differential equations [153]. These equations are than solved iteratively using the Runge-Kutta method for given force inputs from a controller set to adjust the quadriceps force based on flexion between the femur and tibia [118, 119]. There is also a secondary controller employed to stabilize the patella [118]. At each iteration, the new transformations of each component are determined through a contact detection algorithm coupled with the constraints created by adjacent soft tissue. The controller is set to begin the simulation at 5° of tibiofemoral flexion and continue to use the quadriceps force to slowly decent to 120°, falling with gravity while moving the hip toward a fixed ankle point.

At each iteration, the transformations of all components were obtained. This is effectively the same result as the fluoroscopic method and the resulting MAP, LAP translations and femorotibial rotations are calculated in the same manner as the fluoroscopic analysis.

4.3.4 Comparing Results

Both the measured and simulated methods will have resultant kinematics at 30° increments for each of the ten patients. By comparing the MAP, LAP, and axial rotation values at these flexion increments, the differences between the two methods can be observed. If these results are similar, then it can be concluded

that the model successfully predicts normal knee kinematics for these ten subjects and may be a reliable means of future analysis.

4.4 Results

At full extension, the fluoroscopic analysis of all ten subjects demonstrated an average medial condyle position of 2.6 mm, a lateral condyle position of 0.3 mm and an axial orientation of 1.2° of internal rotation from the neutral axis. At 120° of flexion, all ten subjects demonstrated an average medial condyle position of -1.0 mm, a lateral condyle position of -15.7 mm and an axial orientation of 14.4° of external rotation. From full extension to 120° of flexion, fluoroscopy determined a medial condyle translation of -3.6mm, a lateral condyle translation of -16.0mm and an axial rotation if 15.7 (Figure 49 & Figure 50). For these values, a negative translation denotes posterior femoral rollback and a positive axial rotation denotes external rotation during flexion (Table 5).

At full extension, the mathematical model for all ten subjects determined an average medial condyle position of -2.5 mm, a lateral condyle position of -2.4 mm and an axial orientation of -10.2° of internal rotation. At 120° of flexion, all ten subjects were determined to have an average medial condyle position of -4.7 mm, a lateral condyle position of -16.5 mm and an axial orientation of 9.9° of external rotation. From full extension to 120° of flexion, the model determined a medial condyle translation of -2.2mm, a lateral condyle translation of -14.0mm and an axial rotation if 20.1. Again, for these values a negative translation denotes posterior femoral rollback and a positive axial rotation denotes external rotation during flexion.

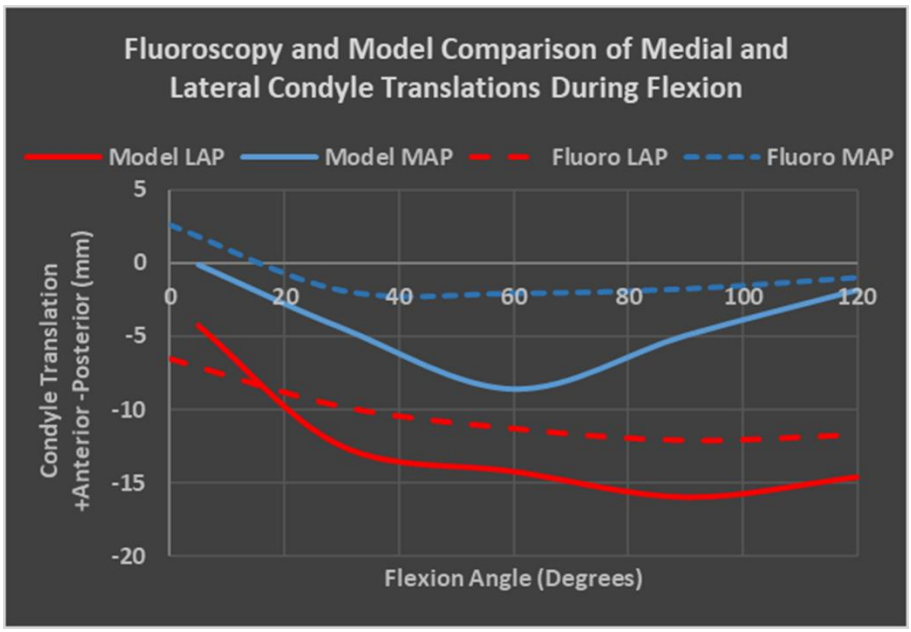


Figure 49: Results are shown for the medial (blue) and lateral (red) condyle translations between the fluoroscopic analysis (dashed) and mathematical simulations (solid) during 120 degrees of flexion.

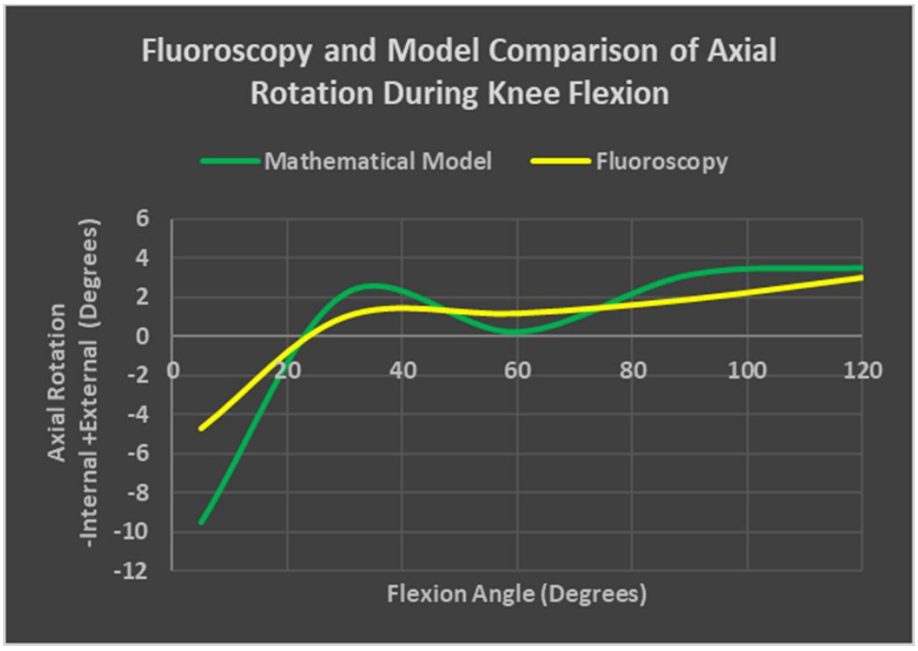


Figure 50: Results are shown for the axial rotation measurement between the fluoroscopic analysis (yellow) and mathematical simulations (green) during 120 degrees of flexion.

Table 5: The average kinematic results for the ten subjects were compared.

	Fluoroscopy	**Mathematical Model**
Medial Condyle Position (Full Extension)	2.64 ± 3.08	-2.55 ± 3.81
Lateral Condyle Position (Full Extension)	0.31 ± 6.18	2.43 ± 2.62
Axial Orientation (Full Extension)	1.27 ± 3.48	-10.17 ± 1.93
Medial Condyle Position (Max Flexion)	-0.99 ± 2.41	-4.71 ± 3.62
Lateral Condyle Position (Max Flexion)	-15.71 ± 4.94	-16.47 ± 3.38
Axial Orientation (Max Flexion)	14.38 ± 7.85	9.93 ± 3.33
Medial Condyle Translation (0°-120°)	-3.63 ± 3.61	-2.16 ± 4.70
Lateral Condyle Translation (0°-120°)	-16.02 ± 9.60	-14.04 ± 5.20
Axial Rotation (0°-120°)	15.66 ± 6.38	20.10 ± 4.20

Fluoroscopic evaluations only allow for the assessment of kinematics, but more advantageously, the model does have the capability to output several kinetic values such as contact, muscle and ligament forces. While there is not a direct measurement derived from fluoroscopy that can be used to assess forces, the effect of the forces on kinematics evaluated can determine the interrelationship between kinematics and forces. Figure 51 shows one such example of how constraining forces can be varied to affect kinematics by altering the medial and lateral conformity of the bearing. Increasing conformity leads to more guided motion and effectively a more constrained joint with more predictable kinematic patterns.

4.5 Analysis and Discussion

This study compares kinematic results for subjects obtained through fluoroscopic analysis and the forward solution model. In general, the model demonstrated results in agreement with fluoroscopic analysis. Medial condyle positioning was on average 3-5 mm more posterior and lateral condyle positioning was 1-3 mm posterior compared to fluoroscopic results. This is mainly due to the initial conditions that were utilized since they were not similar to the initial position of the subjects at full extension assessed during the fluoroscopic evaluations. The model also calculated an additional 5-9 degrees of internal rotation compared to fluoroscopic results. Perhaps most importantly, the model on average predicted fluoroscopic results to within 1.5 mm of medial translation, 2 mm of lateral translation and 4.5° of axial rotation. While there are published results regarding rigid body forward modeling, this model is one of the few sophisticated enough to

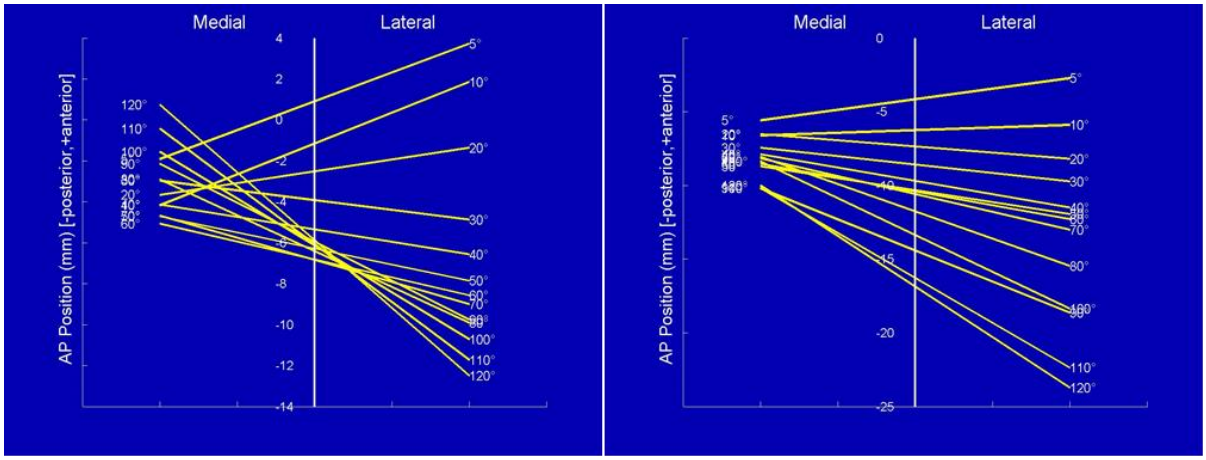


Figure 51: Medial and lateral condyle position depictions for an arbitrary simulation of the normal knee with low conformity (left) and higher conformity (right).

simulate in vivo conditions[118, 119, 127] (Figure 52). Furthermore, results are promising and show an excellent potential to predict fluoroscopic results for the normal knee.

While these results are in good agreement, there are still continued developments that are currently being added to the model. Although every method of mathematical modeling is inherently based on assumptions, we are actively trying to limit these in the definition of the system. One of the most prominent assumptions is that, as a deformable body, there is minimal interaction due to the meniscus geometry. Ligament properties are also based on literature and often acquired through in vitro analysis which, while close, may not depict the exact properties that would otherwise be observed in vivo. We are also making strides to attempt to account for individual variability, which is much more prevalent in the normal knee compared to TKA.

Evaluating for individual variation would ensure that devices are designed to function properly in a wide variety of patients, contributing to consistent achievement of successful patient outcomes. The muscle patterns and flexion profiles across joints are also factors that can vary, although the model accounts for this through an average flexion profile at each joint derived from empirical data. Since every subject has a unique geometry, it becomes more difficult to determine the true starting positions for each individual. The simulation algorithm includes a settling period that seeks to establish stable initial conditions. Initial conditions are still very important and the initial positions may be slightly different due to additional soft tissue. For this analysis, it was also assumed that the initial positioning of the

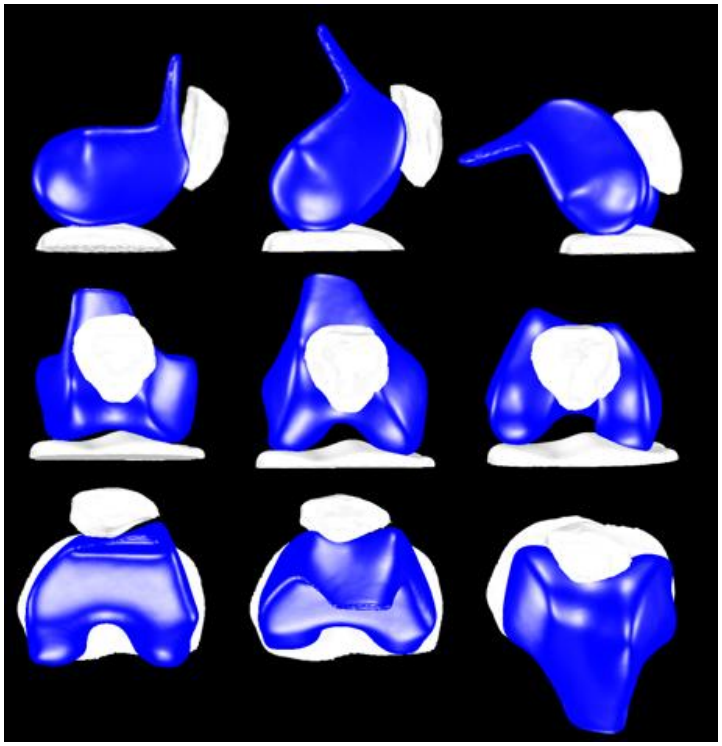


Figure 52: Using the pertinent articulating geometries, simulations can be performed to replicate in vivo conditions across a variety of activities.

femur and patella components were nearly identical between all ten patients, which were scaled to be of similar size. Lastly, while ten subjects are a reasonable start to validating this model, more subjects are needed for a more definitive conclusion. While these assumptions and limitations exist, they can easily be accounted for within the model and the results of the study are still very promising regarding prediction of normal kinematics computationally.

Normal knees have been well studied fluoroscopically, and it has been reported that the lateral femoral condyle exhibits an average of -14.1 mm of posterior translation and the medial condyle exhibits an average of -1.5 mm of posterior femoral translation from full extension to 90 degrees of knee flexion in vivo [9]. This motion is accompanied by more than 20 degrees of femoral external rotation with respect to the tibia at maximum knee flexion [9]. The asymmetry of the normal knee condyles contributes to this rotation [9, 25] and these kinematics overall facilitate the extensor mechanism to promote maximum flexion [25].

The fluoroscopic results from this study are comparable to published results, and the calculations from the model are nearly identical to within 1 mm and 1° for both translation and rotation parameters versus published results [9]. While average data is excellent, the individual geometric differences still create variability between each normal knee for all three measured parameters, which precipitated the use of averages for this study over comparison of individual subjects, both fluoroscopically and mathematically. Additionally, human subjects inherently possess individual variations while performing activities, coupled with regional

differences. This may help to support the subtle differences between the three sources of data.

The average overall motions between the fluoroscopic and simulated data using the mathematical model are in agreement (Figure 53). Interestingly, these differences in initial position resulted in minimal overall translation and rotation magnitudes since these results are within 2 mm and 4.5 ° degrees between the fluoroscopic and simulated results. The main concern is having correct initial conditions so that the model could replicate early flexion more similar to the fluoroscopic data. The model generally predicted components shifted posteriorly and rotated internally. The author postulates that a potential cause of these differences is the exclusion of the meniscus, as the femoral condyle settles into a dwell point contingent upon on the tibial plateau geometries, instead of meniscal geometries. Given the position of the meniscus, it is to be expected that inclusion would result in an anteriorized dwell point at full flexion, thus, effectively changing the axial orientation. Finally, while muscles are adequately represented in the model, to maintain a mathematically determinant system, the muscles interactions must be simplified. While these variations exist, the model can easily be adjusted to better replicate soft tissue and produce more accurate predictions. The model can even solve for contacting forces contributing to kinematics, creating an adaptive system to explore, simulate, and understand more complex iterations of the knee.

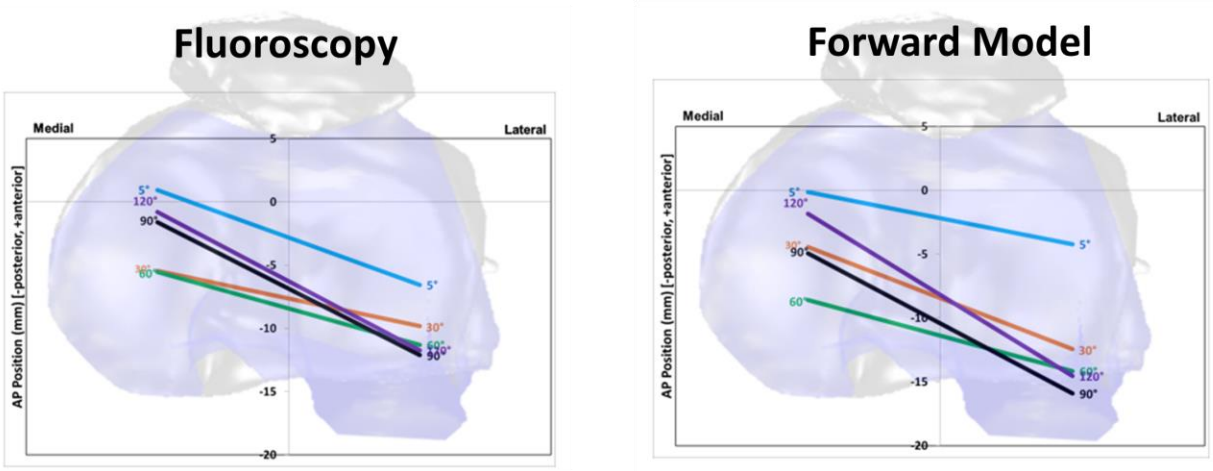


Figure 53**:** Proximal view of the average kinematics through 120 degrees of flexion measured through mathematical simulation (left) fluoroscopic analysis (right).

While the primary objective for this study was to successfully predict normal knee kinematics based on fluoroscopic results, a secondary objective was to use that information to better apply ligament properties to the model. There are three main factors that affect ligament forces through these mathematical definitions. The first is the origin and insertion of the ligaments on the bones. The second is the geometry of the ligament, including the number and size of the fibers, and third is the mechanical properties of the ligament themselves. The anatomic definitions of the ligament attachments are well defined in literature, so for this reason, the bulk of this analysis focuses on the mechanical properties of the ligaments. There are two properties that are of interest: the initial length of the ligament (if it were unloaded), and the stiffness, representing how effectively forces resist a change in length. The property that we have chosen to adjust is the slack length (length of the ligament with no tension), and this was selected because it is a factor that tends to vary from person to person. By changing this value in the model, an optimal set of properties was determined for a general case and these properties can now be applied to the PCL (posterior cruciate ligament) in a TKA in addition to the ACL (anterior cruciate ligament) forces (Figure 54).

Another consistent observation in nearly all the simulations, although not previously reported in fluoroscopic analysis, is the occurrence of anterior motion of the medial condyle. Studies have shown that while the lateral condyle tends to move posteriorly, the medial condyle tends to remain relatively stationary allowing for smaller magnitudes of motion in either the anterior or posterior direction. Such an observation can be seen in late flexion from Komistek 2003 (Figure 55).

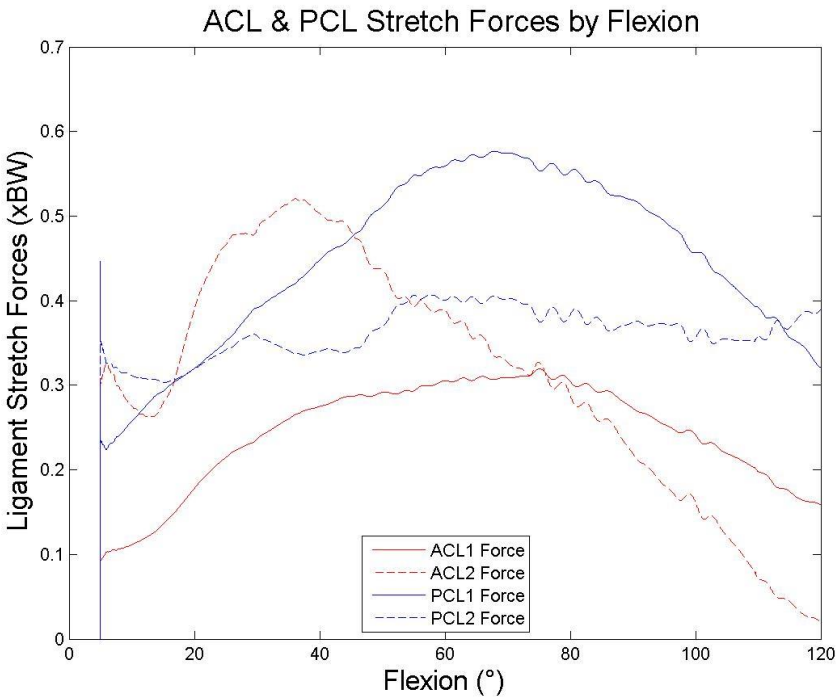


Figure 54: Force loading profiles for both ACL and PCL fibers during a simulated deep knee bend.

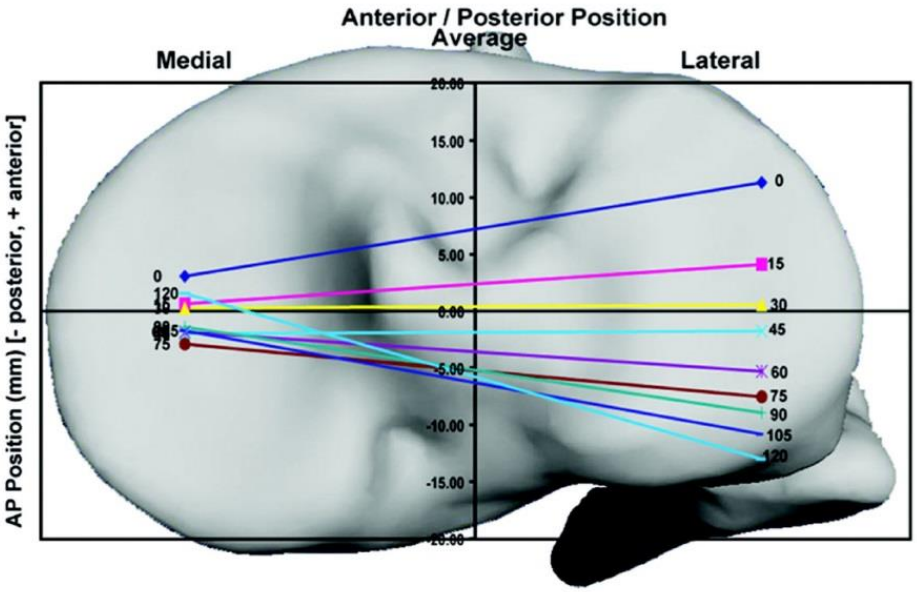


Figure 55: Summary of fluoroscopic results for normal knees (Komistek 2003).

Fluoroscopic analysis demonstrated a similar trend to published results, moving posteriorly, except for the last flexion increment during which the medial condyle experienced anterior motion. There are many potential reasons for this and under closest observation is the conformity of the medial bearing analogous surface. Initial positioning and soft tissue interaction are also potential factors for consideration, but given the constructs of the model, conformity is the easiest factor to change and observe. Increasing the medial bearing conformity facilitates a stationary condyle, and conversely, reducing conformity promotes motion. By altering these conformities, a pseudo constraint force is added inhibiting undesired motion. Revisiting Figure 51 (Figure 56), the original simulation (left) experiences anterior medial motion, while increasing the medial conformity contributes to a more stationary medial condyle.

This creates a motion pattern more consistent with fluoroscopic studies from this and other studies. It is of note, however, that such a change also contributes to higher forces, which are needed to maintain the kinematic patterns, therefore optimization between these changes is important.

4.6 Summary and Conclusion

The results from this study revealed that the mathematical model was successful in the ability to predict normal knee kinematics that were previously determined using fluoroscopy within 2 mm and 4.5°. Furthermore, the simulation results were within 1 mm and 1° of previously published average normal knee results. While translation and rotation results were similar, there were differences

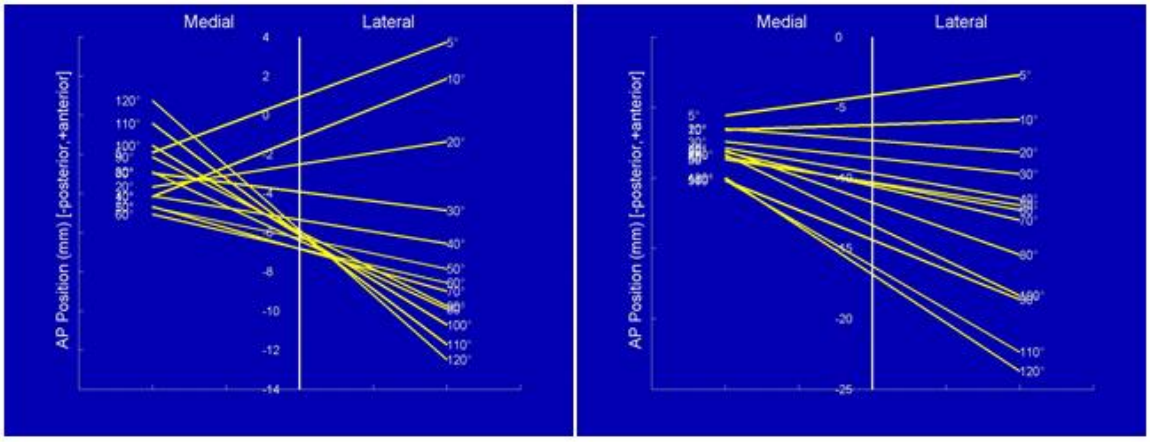


Figure 56: Separate modeling results for an initial case (left) and a case with increased medial conformity (right).

in initial position likely due to assumptions made regarding soft tissue. These results have important implications as the kinematics of the normal knee can be efficiently assessed computationally. These results can also be used to determines oft tissue properties to better assess TKA designs. There is also potential allowing for the kinematic assessment of knees with trauma injuries and congenital defects to better understand pathological mechanics and evaluate treatments to correct these mechanics and restore both functionality and quality of life. This ambition is particularly relevant, as the model can provide a simple transition for the assessment of TKA to be used as a tool to assess both device design and evaluate surgical techniques.

CHAPTER FIVE: PARAMETERIZING THE EXTENSOR MECHANISM

5.1 Purpose

The quadriceps mechanism drives the flexion of the model, and as such, the forces that are introduced are significant to both the kinetic and kinematic results. While such measurements are very difficult to measure in vivo, theoretical simulation offers the potential to assess and design around the transmission of force through the extensor mechanism. The effectiveness of the quadriceps mechanism transmission force through the quadriceps muscle groups is referred to as the quadriceps efficiency. In other words, quadriceps efficiency is a measure of how much force is produced by the muscle as a ratio of how much of that force effectively contributes to muscle movement.

In a system analogous to the control scheme of the human body, the model controls are activated through a PID controller which minimizes deviation from a specified flexion profile [118, 119]. The nature of such a system dictates that only the amount of force needed to drive flexion will be applied to the system, and inefficient transfer of forces leads to increased muscle activation to achieve similar results compared to an efficiently operating muscular system.

Quadriceps efficiency is important because a poorly functioning mechanism will require substantially more activation to achieve similar flexion results contributing to greater muscle stiffness [154] and clinical outcomes ranging from poor range of motion [25] to dissatisfied patients [29]. For this reason, it is

advantageous to ensure that the quadriceps muscles are operating as efficiently as anatomically possible.

In order to more accurately contribute quadriceps forces to the model, the purpose of this contribution will be to evaluate different simulation parameterization strategies. This will increase extensor mechanism efficiency and in doing so, decrease the quadriceps forces required to drive motion during active simulations.

5.2 Introduction

While the model itself is specifically aimed to be a forward model in that kinematics are determined from kinetics, there are specific elements where the forces are obtained through other means. This primarily includes both the quadriceps forces, which are provided to the model in the form of a controller algorithm, and the contact forces, which are determined through a contact detection algorithm.

The initial quad forces predicted by earlier iterations of the model tend to be high compared to the magnitude of force determined to occur in vivo [155]. The total quadriceps force tends to be about three times BW compared to about 5-6 times BW predicted by the model [118, 119]. This disparity is a factor that emphasizes a lack of efficient force transmission, as greater force is required to recreate an equivalent in vivo motion, and in the case of the controller, minimize deviation from a desired flexion profile.

A properly functioning extensor mechanism is interrelated to the kinematic performance of both a normal knee and a TKA device. It is believed that TKA devices tend to have reduced quadriceps efficiency compared to normal knees [25]. There are also clinical implications as poorly functioning muscle control can create lasting clinical issues including muscle stiffness [154, 156], discomfort and dissatisfaction [27, 28, 157, 158]. Such analysis is also important because excessive muscle forces contribute to higher forces elsewhere in the knee, which may contribute to clinical complications, such as device fatigue and implant loosening.

Prior to the mathematical assessment of the quads mechanism, confidence must first be established in the accurate and constant measurement of force transmission between the model and existing validation sources. It is for this reason that the force of the extensor mechanism must be rectified and reduced to better match values in literature.

The quadriceps mechanism contains four main muscles that originate on either the proximal femur or the anterior pelvis [2] (Figure 57). These muscles insert on the distal patella and follow a direct path in early flexion, which gradually transitions to a muscle wrap about the distal femur in deep flexion [118, 119]. There are also four additional attachments on the distal side of the patella that compose the patella ligament (technically a tendon), which acts as the anchor for the quadriceps mechanism on the tibia [2]. The activation of these muscles is dictated through a PID controller that determines the necessary forces to meet a specified profile [118, 119] (Figure 58).

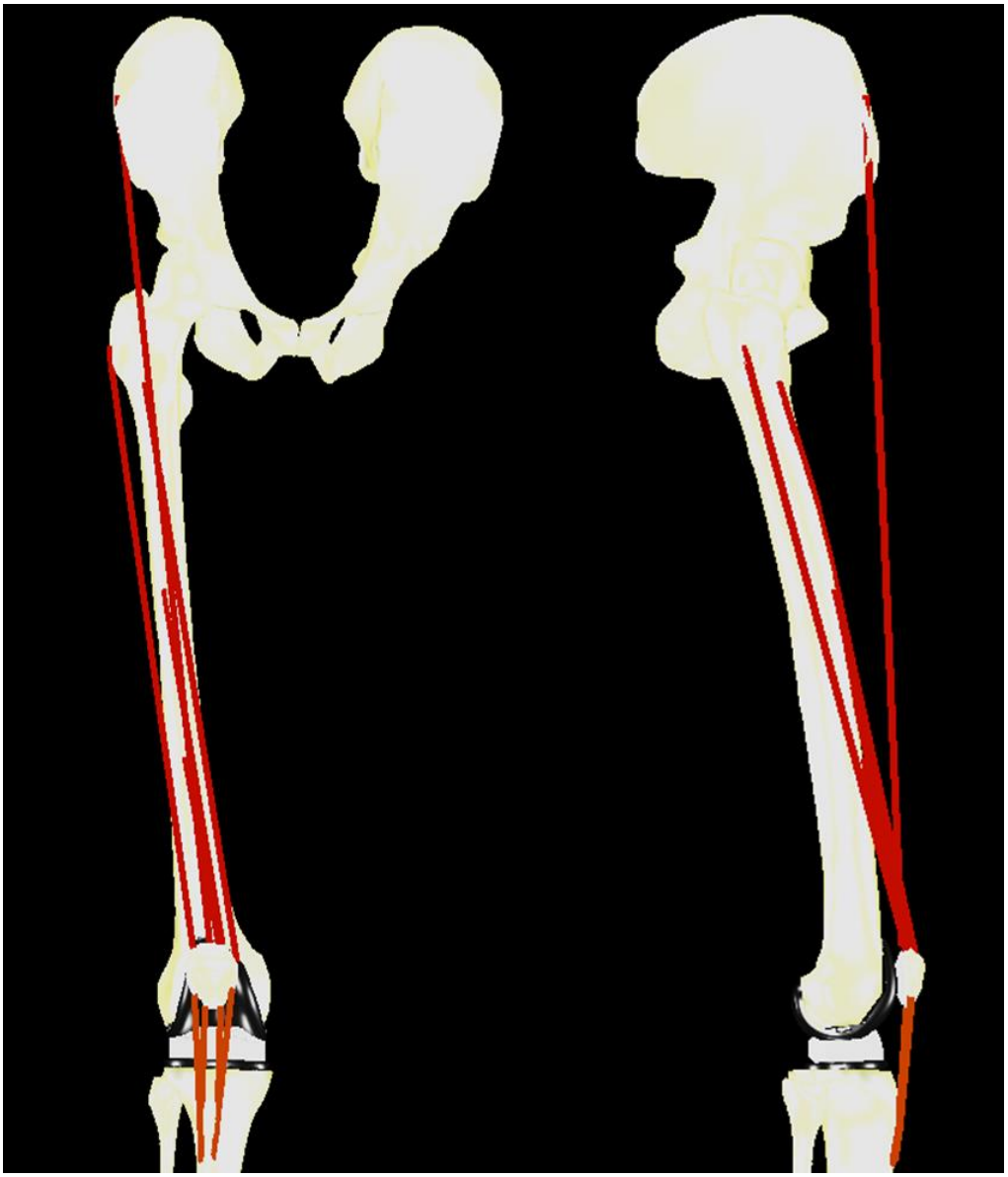


Figure 57: The quadriceps muscle group consists of four muscles. The vastus medialis, lateralis and intermedius all originate on the proximal femur and insert on the proximal patella. The rectus femoris also inserts onto the patella; however, it originates on the pelvis. The quadriceps tendon anchors the distal side of the patella, and all of these muscles collectively control knee extension.

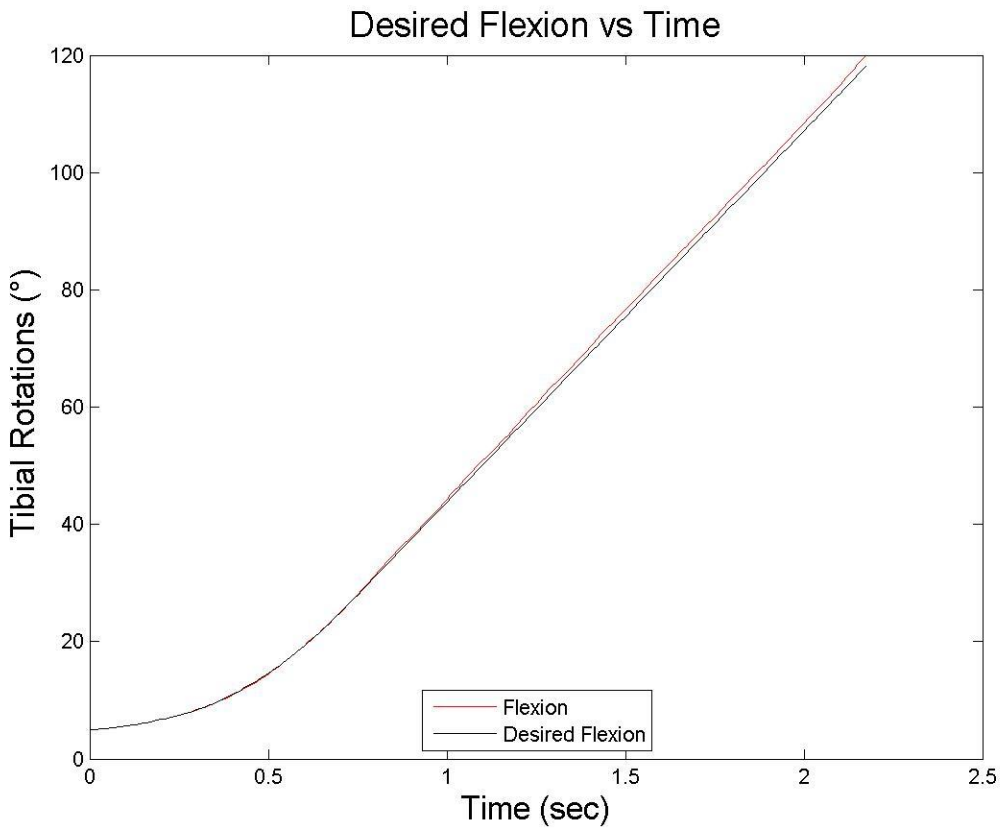


Figure 58: The flexion of the knee in the model is controlled by a PID controller that applied quadriceps force to match a target function that is input by the user. While the flexion is input by the user, the forces are determined to match, and this efficiency of the mechanism is an important factor.

In an effort to reduce the force required, various methods must be evaluated to improve the transmission of these activating forces. There are a variety of means by which this can be done, and these methods range from simple code changes to additional specified motions to adjusted wrapping points (Figure 59Figure 60). A successful improvement of efficiency will more than likely hinge on some combination thereof.

The ability to accurately predict quad forces is not a trivial task. In doing so, results can determine how a device affects muscle structures and what design features contribute to the most effective joint motion. While muscle plasticity in the musculoskeletal system can contribute to optimization over time through atrophy and hypertrophy, this process can be limited in its magnitude and duration, making extensor mechanism efficiency an important design consideration. This not only fosters adequate physical therapy but also mitigates muscle weaknesses as a result of surgery [159, 160].

5.3 Methods

To maximize efficiency of the quadriceps muscle groups and reduce quadriceps muscle forces in the order similar to in vivo conditions, in the range near 2.5 times BW (Figure 61), there are several strategies that can be employed. The first and most intuitive method is to adjust the attachment and wrapping points to better represent physiological configurations. The forces exerted by the quad mechanism are heavily influenced by moment arms. Along those lines, another means of improving the quads efficiency would be to improve wrapping. This

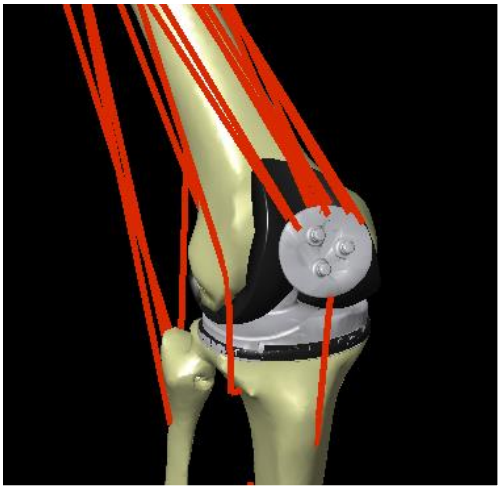


Figure 59: The quadriceps mechanism is directly related to the constraining forces applied by the muscle and ligament soft tissue structures.

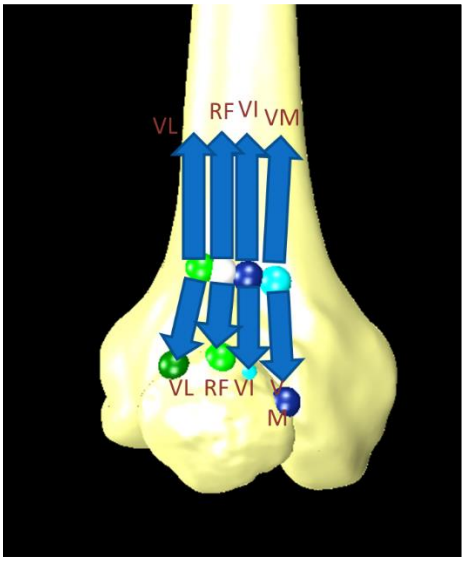


Figure 60: During flexion the wrapping of the extensor mechanism on the femur bone can contribute to changes in the force vectors administered through the quadriceps muscle definitions.

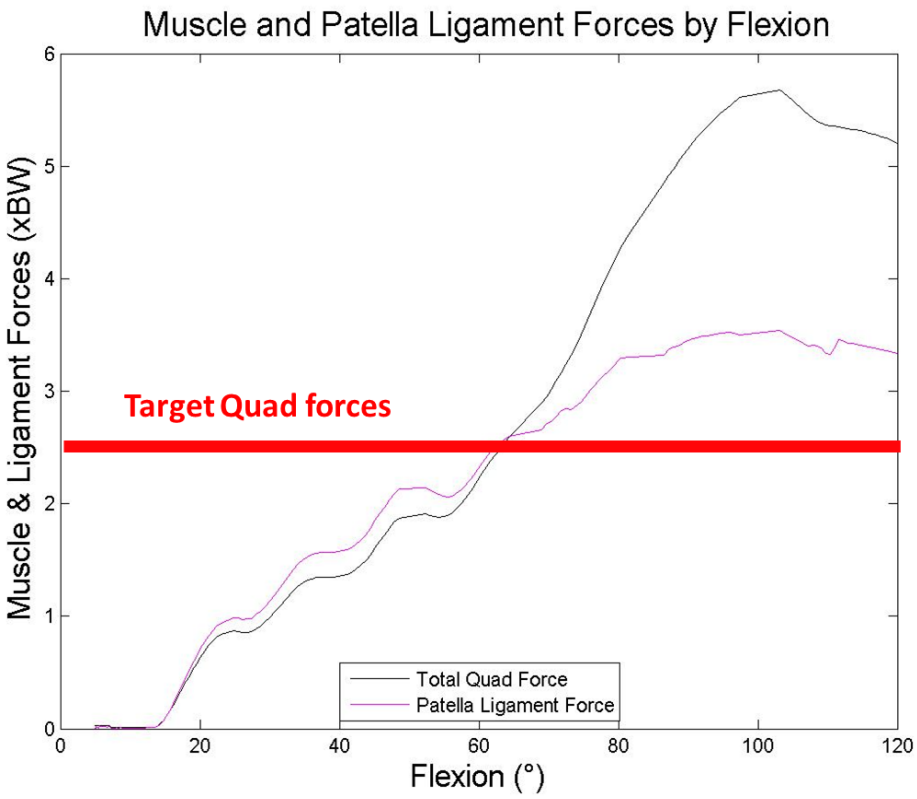


Figure 61: Previous iterations of the model have achieved extensor mechanism forces of roughly 5.7 times BW. Literature suggests these forces should be approximately 2.5 times BW.

includes both adjusting wrapping points and redefining how the wrapping points function.

One other less intuitive method for improving efficiency is the adjustment of specified functions on other bodies such as the pelvis. As with the other methods, this will affect the joint rotation about both the knee and the ankle, contributing to changes in the moment arms and quadriceps efficiency. This allows more complex motions, which can lead to reduced origin and insertion distances.

Another possible strategy is to redistribute the forces differently between the muscle fibers. Many optimization techniques would utilize such a strategy between the four muscles of the extensor mechanism. However, in order to maintain the reduction nature of the model, it may be possible to utilize different fiber attachments to better transmit quadriceps force. There is one final strategy: simply checking how these forces are calculated. This includes the velocity functions and ensuring that no muscles are antagonistic to each other or exerting force in the wrong direction.

Collectively, these strategies should allow for an improved understanding of the extensor mechanism function and allow for the improvement of the quadriceps interaction.

5.3.1 Improving Velocity Functions

The existing model uses Autolev to generate the equations of motion for the knee using Kane's system of dynamics. While the program is very accurate at building these equations, it is sometimes subject to error with respect to how

various parameters are defined. This mode has been built through an iterative process, so as advancements occur, in some cases, it becomes necessary to change definitions to better fit the system.

One manifesting application for such a technique relates to the manner in which velocities are defined. There are two possible syntax variations for the calculation of velocities, and these are through either traditional velocity calculations or a V two points (V2pts) command, which determines a point to point velocity. Traditional velocity calculations are simple in that they take the velocity of a given point in a reference frame and add that component velocity to the velocity of a previous reference frame. Alternatively, the latter of these two methods uses the V2pts command in the symbolic manipulator which states:

> *"V2Pts finds the velocity, in a first reference frame, of a first point fixed in a second reference frame, given the velocity, in the first reference frame, of a second point fixed in the second reference frame, the angular velocity of the second reference frame in the first reference frame, and the position vector from the second point to the first point"* [161].

While it may not be readily apparent, there is a fundamental difference between the two methods where traditional velocity functions are meant to calculate velocities between bodies and point to point velocities need to be used exclusively for calculating relative bodies in the same frame on the same body. While initially such a distinction may seem trivial, the equations of motion are heavily dependent on these velocities, and for that reason, ambiguously defined velocity calculations could contribute to antagonizing muscle forces greatly hindering muscle efficiency. In order to improve velocity functions, these muscles will be verified to confirm that

they are correctly defined. This will ensure only non-negative muscle forces expansion is a physiological impossibility.

5.3.2 Improving Wrapping Points

Early iterations of the model were predicated on the assumption that many of the attachment sites are set directly on the bone architecture of the knee. While this is a valid assumption under many cases of tendon and ligament attachment, muscle wrapping points potentially exist with a spatial offset from the bone interface. This is important because an offset wrapping point creates a greater moment arm, allowing for amplified administration of torque about the center of rotation of the knee (Figure 62).

To test this theory, the anteroposterior position of the wrapping points will be varied by ±5 mm in the anteroposterior direction and evaluated for its effect on quadriceps mechanism forces. Only the sensitivity in the AP direction will be tested as it is the most valid proof of concept for offsetting muscle attachments. In addition, variations on the mediolateral direction are expected to be less consequential to quad mechanism forces, and proximal distal sensitivity is physiologically trivial as there is a defined wrapping point of contact.

5.3.3 Muscle Force Distribution

The model contributes muscle forces as vectors, which by definition have an infinitely small thickness, and while this assumption is perfectly valid from a mathematical perspective, noted additions must be made to the vector definitions to account for anatomical thickness in the model. This is done through two main

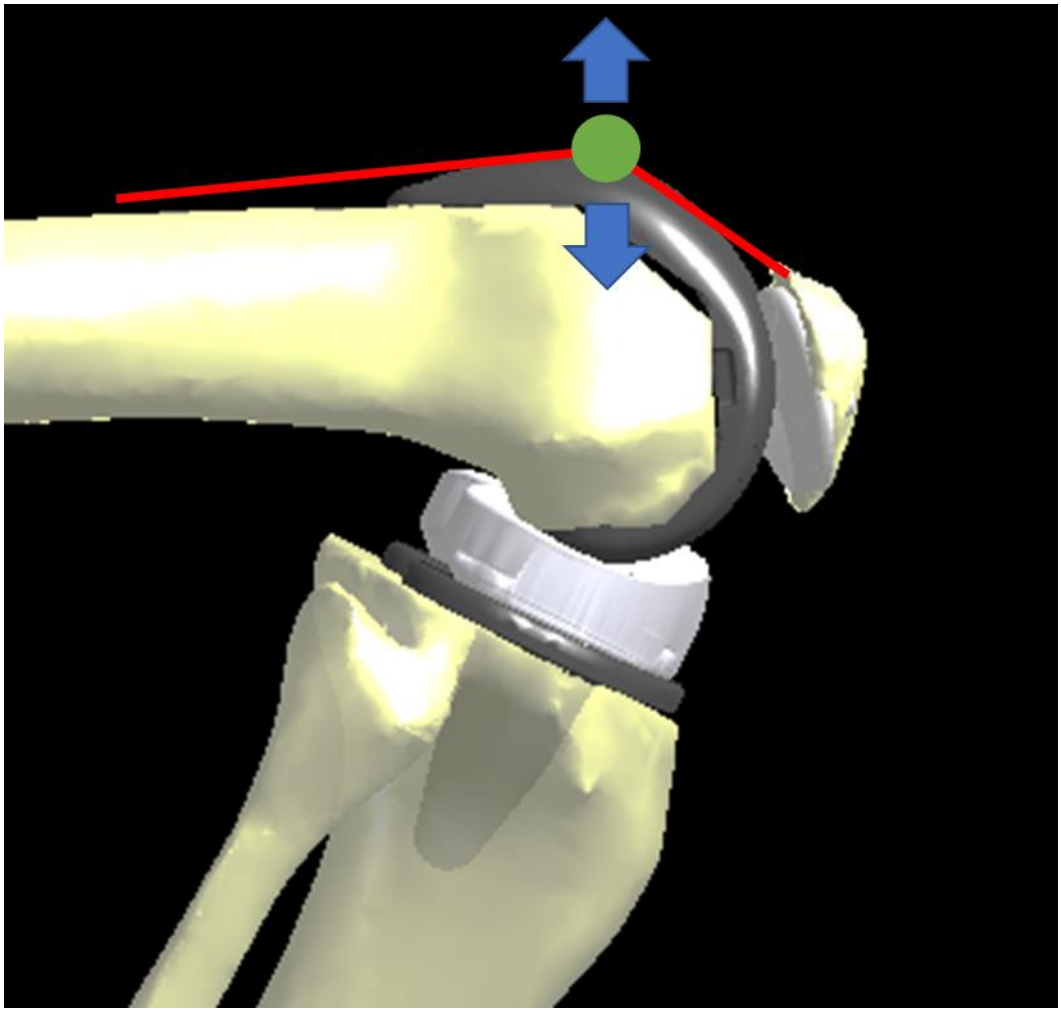


Figure 62: During deep flexion, the quadriceps muscles experience wrapping about the trochlear groove of the femur. The offset of this point from the femoral bone may affect the forces of the quad muscles.

practices which are attachment site distribution, where attachments are set through a region composed of multiple vectors at the origin and insertion, and inclusion of multiple fibers to roughly account for muscle thickness with several distinct origin and insertion sites. The latter may be a promising strategy to improve extensor mechanism efficiency. The rectus femoris is an excellent example, as the muscle essentially has two origins, one on the femur and the second on the pelvis. Despite having both attachment sites on the femur, the same principle applies to the vastus lateralis, intermedius and medialis in that one muscle vector attaches on the epiphysis and the other attaches on the diaphysis of the femur.

It is not expected that these two attachment sites would vary during early flexion; however, once wrapping occurs, there is a distinct possibility that the moment arms would vary drastically as one vector will be offset more than the other from the bone surface. In addition to the moment arm, offsetting a muscle attachment site will create a different inclination angle. These two factors combined may influence the ability of the quadriceps mechanism to administer the force of the controller, thus leading to decreased quad activation.

To test this idea, an element has been added to the code that distributes the activation between the mid and end attachment sites of the muscle. This is done in such a way that early flexion is a roughly even distribution between the forces from the two vector fibers. As wrapping occurs deeper into flexion, the activating muscle favors the more proximal attachment site. To do this, a multiplicative factor (x) is included to the force calculation where $x \epsilon [0,1]$ and the force is distributed such that the distal fiber applies a force of x and the proximal

fiber applies a force of 1-x (Figure 63). This means that a factor of 0.25 would generate 25% of force applied at the distal attachment site and 75% at the proximal attachment site. A value of 0.5 negates the difference and distributes the force evenly between the two attachment sites. It is hypothesized that concentrating this force on the proximal attachment site will lead to improved quadriceps efficiency.

5.3.4 Pelvic Tilt

Another assumption made by earlier iterations of the model is that the pelvis remains stationary during flexion (Figure 64). While this is initially a reasonable assumption for the sake of simplicity, the pelvis in reality encompasses a more complex motion that may contribute to quadriceps efficiency. The bones of the pelvis flex concentrically during knee flexion and there is a dual faceted purpose behind this (Figure 65). The first of which is that the motion of the pelvis shortens the muscle length between the origin and insertion of the rectus femoris. The second is that shifting the pelvis forward moves the center of mass of the torso closer to the line of action. Moving the center of mass for the torso is important because the torso is the conduit through which the force of BW is introduced into the model. Moving this force closer to the knee will mitigate the moments applied to the femur and thus less resistance is applied to the quadriceps mechanism.

By rotating the pelvis as a function of flexion, a mechanism of compliance is applied to the quadriceps mechanism, which it is hypothesized will mitigate the force applied to an equivalent stationary pelvis (Figure 65). To test this hypothesis,

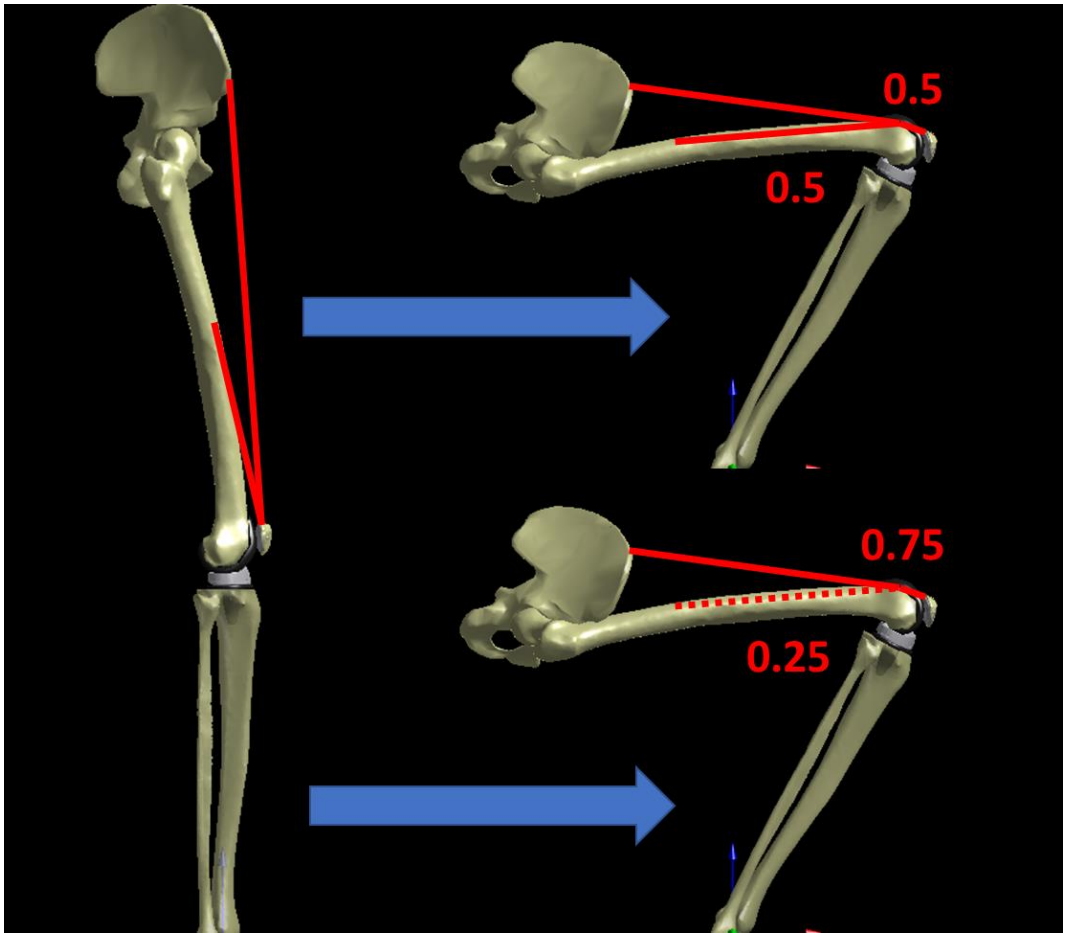


Figure 63: At full extension the multiple quad muscle fibers apply similar forces, however in deeper flexion some of these fibers have advantageous lines of action and for that reason the force definitions have been altered to allow for some of these fibers to be favored over others. In one instance the two fibers of the rectus femoris maintain equivalent contributions (top right) and another where the proximal fiber contributes three times the force of the distal fiber (bottom right).

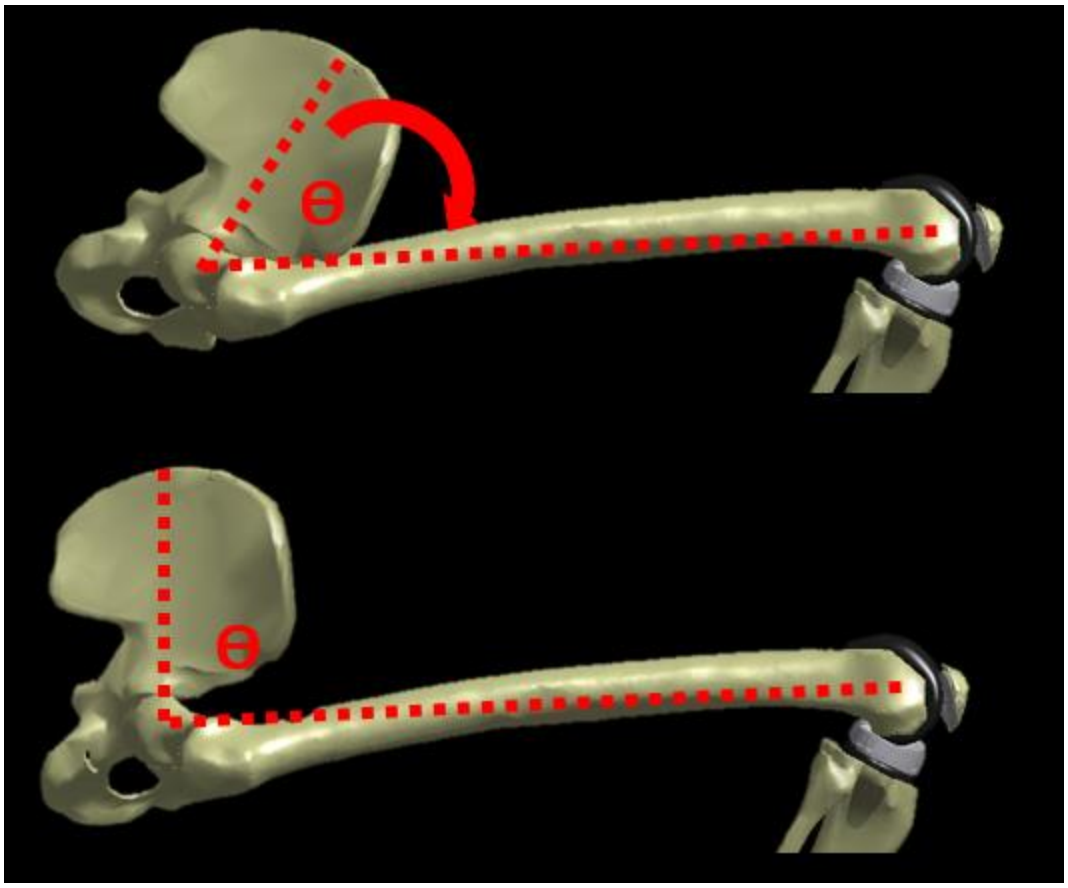


Figure 64: Prior iterations of the model assumed a stationary pelvic bone. To enhance physiological accuracy, this bone was given a specified rotation as a function of flexion.

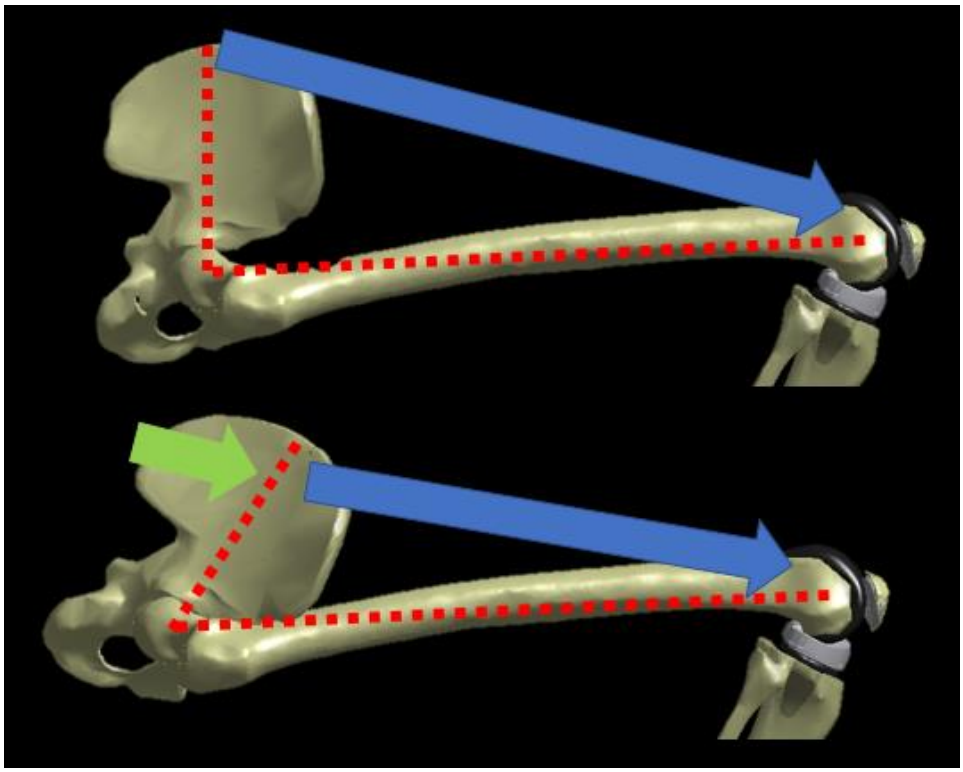


Figure 65: Adding the rotation onto the pelvic bone facilitates a compliance that diminishes the need for direct quad force contributions. For the stationary pelvis, the quads are the only force contribution (blue), whereas the rotated pelvis contributes an additional force that helps facilitate flexion (green and blue).

the pelvis was redefined as an inverse element with a specified rotation and an interactive torque in the direction of the quads activation mechanism.

5.3.5 Device Sensitivity

While there is clinical significance to the effectiveness of the quadriceps extensor mechanism, the relationship between this mechanism and device design is much less understood. To maintain clinical relevance, there needs to be a controlled comparison between two articulating geometries to assess the sensitivity. This also serves as a proof of concept that articulating surface architecture can be an influence on the forces required to drive flexion.

One of the pressing questions with respect to articulating geometry is the effect that geometry plays on the muscle forces. Therefore, testing articulating surface architecture seems to be an intuitive means of assessing such a strategy. To do this a geometric sensitivity is performed using two separate geometries. The first of these is a traditional PCR device and the second is a modified healthy knee.

The goal in this investigation is to assess which factors contribute most to quadriceps forces. Therefore, a systematic swap of components was performed. Specifically, a simulation was set up containing a PCR device, then one by one elements of the normal, healthy knee were added until eventually the model setup was exclusively that of the normal knee. At each interval, a simulation was carried out and the resulting quadriceps forces were determined. Based on the differences in force profiles, the effect of each feature can be isolated.

Overall, five factors were evaluated, and these were patella shape (symmetric vs asymmetric dome), ACL constraint, trochlear groove geometry, femoral condyle geometry, and overall bearing geometry (Figure 66). Such a design of experiment emphasized the effect each element has on the quad forces.

5.4 Results

The wrapping points of the quadriceps on the femur are intrinsically complex based on the geometric definitions that are associated with their respective anatomy. This complexity stems from the origin, insertion and wrapping sites all being across different reference frames. The muscles originate in the femur reference frame, insert on the patella and wrap on the femur. To accurately reflect these variations, the anatomical definitions were updated accordingly.

Since there are various ambiguities in the velocity function, the previous iterations of the model produced antagonistic muscle forces contributing to greater forces required by the controller. By rectifying these definitions between reference frames, the contradicting elements are removed using more rudimentary velocity functions and the result is a drop in quad forces from 5.5 times BW to 4.25 times BW (Figure 67).

Improving wrapping definitions is a marginally effective strategy for facilitating extensor mechanism efficiency, especially above 90 degrees of knee flexion. Three instances were tested to arrive at this observation. The first was the

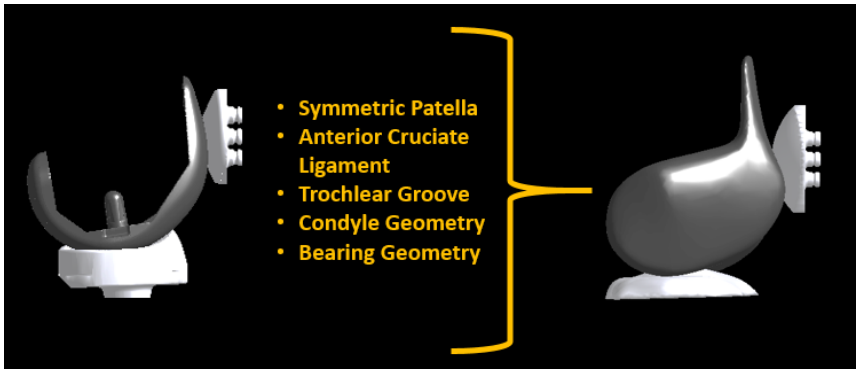


Figure 66: To evaluate the effect of each geometric factor, a PCR device was taken and one by one the features were substituted to match an anatomically based geometry.

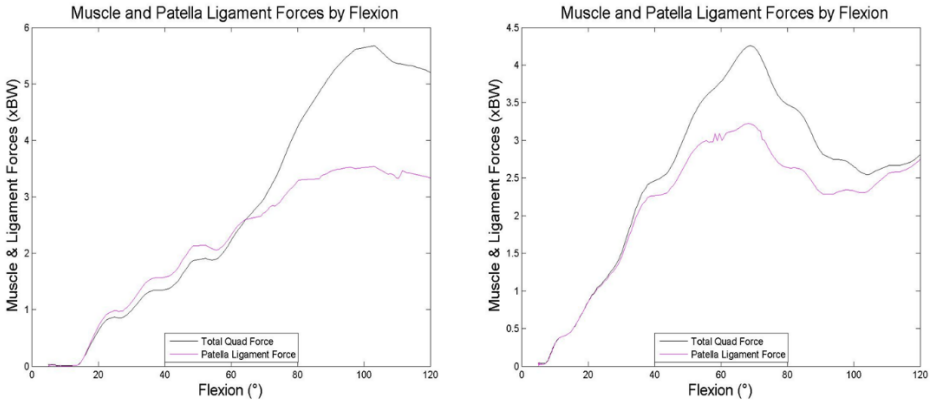


Figure 67: Updating the velocity functions in the model improves muscle efficiency and drops quad forces for 5.7 times BW to 4.3 times BW.

initial setup that had been used previously, and the second and third were identical, except that the wrapping points had been offset by 5mm either anteriorly or initial setup that had been used previously, and the second and third were identical, except that the wrapping points had been offset by 5mm either anteriorly or posteriorly. Increasing this offset in the anterior direction contributed to increased quad forces to drive flexion, and in the posterior direction, the forces decreased compared to the original configuration. While this is a notable difference and provides a sufficient proof of concept, it is interesting that the flexion profiles between all three instances do not vary substantively until upwards of 100 degrees of flexion. At the greatest difference, the variation between the anterior and posterior offsets led to a total of 75% of BW difference with an approximately equivalent change in force in each direction compared to the original configuration in the positive and negative directions (Figure 68).

Quite similarly, variations in muscle contribution ratios have an effect on the overall quadriceps forces; however, this effect is once again limited to late flexion and represents a full difference of approximately half times BW (Figure 69). It is consequential that the original configuration of ratios had the most optimal performance, while variations across the positive and negative spectrum increased extensor mechanism forces. The initial configuration for the muscle contributions focused primarily on the rectus femoris and vastus intermedius with the lateralis and medialis becoming more consequential during muscle wrapping.

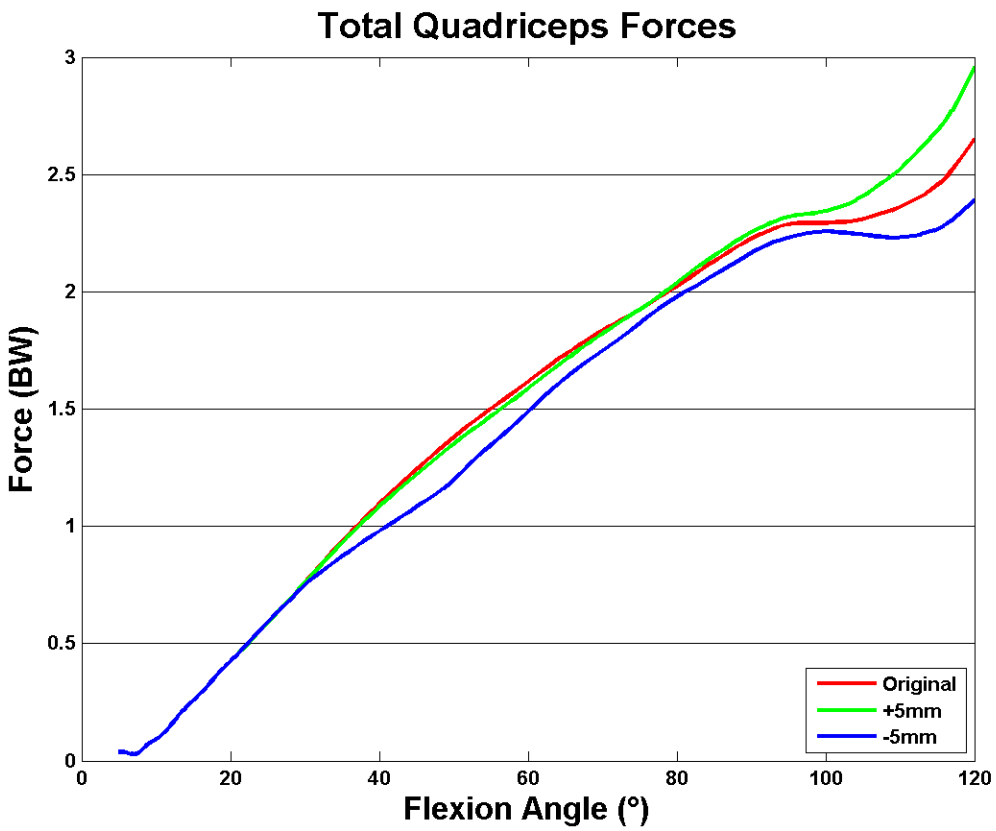


Figure 68:Moving femoral muscle wrapping points anteriorly or posteriorly provides minimal differences in quad forces compared to a controlled simulation defined with the wrapping point positions.

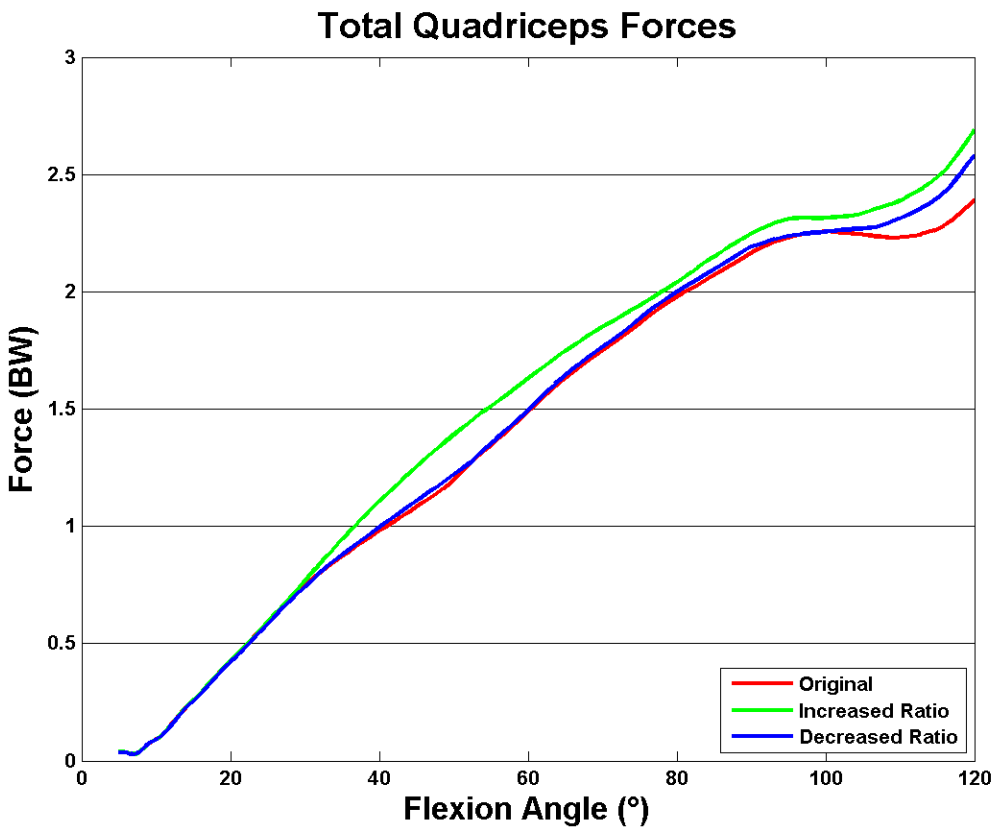


Figure 69: Re-distributing muscle forces between various fibers appear to increase quad forces compared to a control ratio for force distribution. While this does not necessarily mean that there is not an effective distribution of forces that would contribute to improved efficiency, the tested configurations demonstrated marginal force increases.

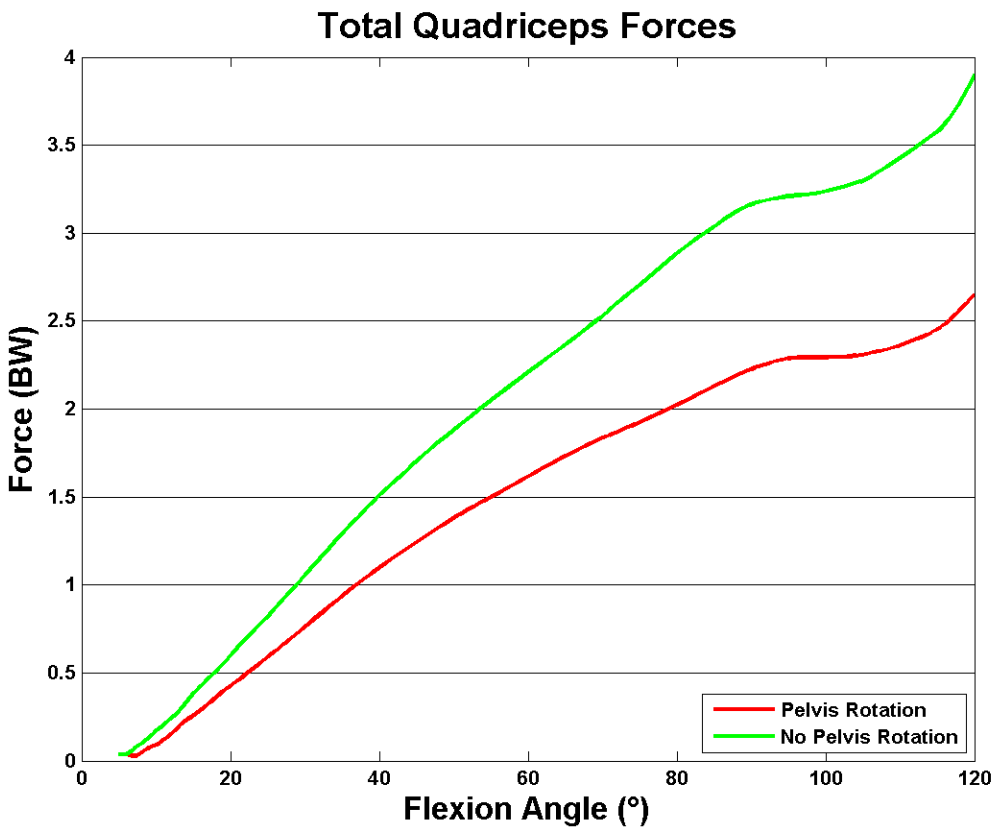


Figure 70 Pelvic tilt during the simulation is central to extensor mechanism efficiency compared to a stationary control simulation.

The most effective technique for the enhancement of the extensor mechanism efficiency was the addition of the pelvis to tilt about the medial and lateral axis. Two scenarios were tested, one in which the pelvis rotated forward linearly and another where the pelvis remained stationary. From initial flexion, the pelvis rotation was demonstrated to be effective in the facilitation of force transfer from the quads mechanism, contributing to a quad force reduction of one and half times BW compared to the stationary pelvis bone (Pelvic tilt during the simulation is central to extensor mechanism efficiency compared to a stationary control simulation.). The quads mechanism, while wrapping position, muscle distribution and bone kinematics are all effective to varying degrees at improving the extensor mechanism efficiency, these are all factors dependent upon the simulation parameters. From a design tool perspective, the articulating surface should play a role in the efficiency of the extensor mechanism, and for this reason, a comparison was carried out to evaluate the effect of each design feature on the overall quad forces.

Comparing a multitude of features between a PCR TKA device and a normal knee geometry, the most influential factors affecting muscle forces were the femoral trochlea geometry and bearing femoral condyle geometry. Factored together, these differences contribute to a difference of 2.5 times BW in the quad forces at maximum flexion (Figure 71).

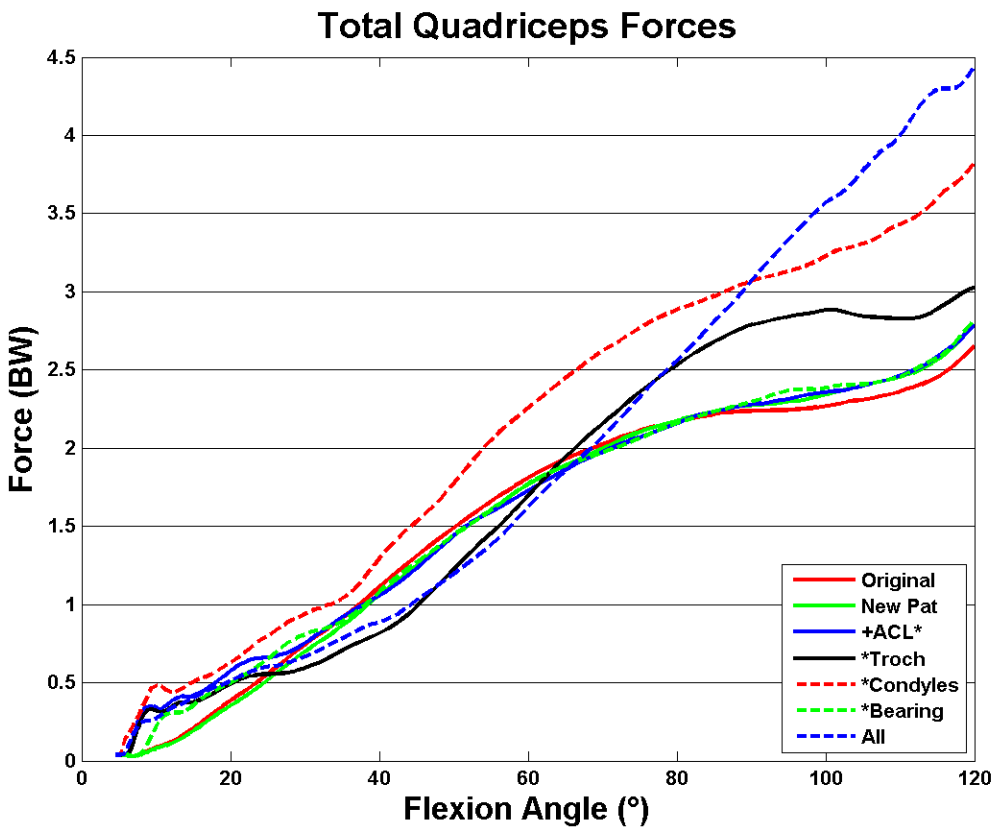


Figure 71: In order to better assess the role of articulating geometry and functionality of the extensor mechanism, two different articulating geometries were compared. The original is a PCR device and it was compared to a modified normal knee. Each feature was added individually and then collectively and these features included changing to a symmetric patella, adding an ACL, defining the trochlea, defining femoral condyles and defining the bearing surface.

5.5 Analysis and Discussion

The utilization of wrapping point optimization and muscle fiber allocation had a minimal effect of minimizing quad forces and facilitating quadriceps efficiency. These conditions were tested and while there may be alternative configurations which would facilitate additional muscle force reductions, the proof of concept simply is not there for the cases tested. Furthermore, the magnitudes needed to produce meaningful changes would be prohibitively difficult to achieve in addition to being hindered by physiological confines of the lower limb as a mechanical system.

Specification of a pelvic tilt on the other hand was highly effective in the reduction of quad forces and similarly enhances the physiological accuracy of the knee. The rotation of the pelvis not only moves the body center of mass closer to the line of action of the knee, but the rotation also provides an interactive torque which creates mechanical compliance adding to the quad forces already present. Since a partial torque exists, the force contributed by the quads mechanism is can be lessened and the same results can be achieved. While this rotation is assumed to be linear, it is possible and simple to add a higher order polynomial indicative of more physiologically accurate motions.

Even though one of these methods was substantially more effective than the others, the recommended course of action across all simulations is to include a combination of all these methods. There may be additional analyses needed to achieve an optimal parameterization, however, the process as shown can be modeled effectively.

Beyond parameterization of model properties, this contribution also seeks to establish an improved understanding of how geometric features affect the functionality of the extensor mechanism -- an analysis well within the capability of the model. Using a step- by-step design of experiment, it was determined that the most influential geometric features were the trochlear groove geometry and femoral condyle geometry. Serving as a proof of concept, these two influential features are intuitive as the quadriceps insert on the patella, which directly contacts the trochlear groove. The femoral geometries facilitate the motion between the femur and tibia surfaces. Furthermore, all of these features collectively make the largest influence on the extensor mechanism and in one form or another, every one of these features carries an influence on quad forces.

It is also of consequence that this evaluation of articulating surfaces is in actuality an assessment of the normal knee verses a TKA. Possibly the most interesting finding is that the forces in the extensor mechanism tend to be lower prior to roughly 70 degrees of flexion for the normal knee and then lower for the TKA above that range. This finding is not a trivial finding as this means that the quadriceps mechanism is less efficient and thus needs to actuate more force for early flexion activities for a TKA compared to the normal knee. While the normal knee does appear to require larger forces in deep flexion, the majority of activities of daily living center around gait types of activities meaning that this particular TKA device does not facilitate flexion and extension as well as the normal knee.

5.6 Conclusion

There are a variety of strategies for improving extensor mechanism efficiency and reducing quadriceps force, and while some of these revolve around minor parameterization of the model, the most effective strategies assess the system as a whole to improve motions and facilitate muscle activation. The pelvis is the primary example of this, however other bones such as the foot may also provide additional kinematic contributions. In addition, articulating geometry can also play a significant role, particularly when pertaining to the femoral condyles and trochlea. Finally, the main objective of this contribution was to try to achieve sufficient efficiency such that flexion could be properly facilitated through a sum of 2.5 times BW worth of muscle force to match existing literature and that objective was successfully achieved (Figure 72).

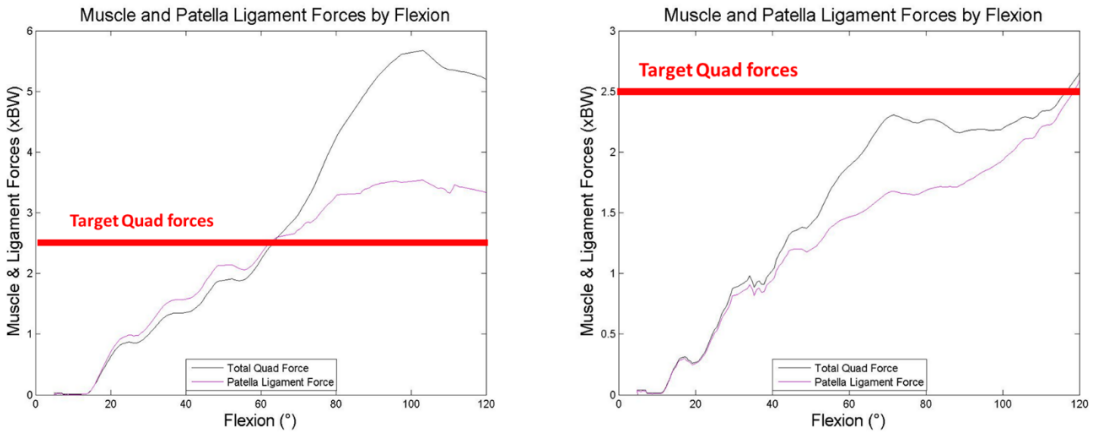


Figure 72: Earlier iterations of the model have achieved quadriceps mechanism forces of about 6 times BW (left). Using several strategies, the forces were able to be mitigated to 2.5 times BW (right) which is a value that has been reported empirically in literature.

CHAPTER SIX: PARAMETERIZING FLEXION ACTIVITIES

6.1 Purpose

One of the most important takeaways from the analysis of the extensor mechanism is the notion that improving physiological accuracy in the model can have positive influences on simulation results. Since this is an iterative process, many of these motions were simplified as analysis processes were developed. As capabilities increased and a more thorough understanding has developed, the ability to restore some of this complexity becomes possible. The purpose of this contribution is to restore some of the complexity previously omitted from the model.

The two physiological improvements that are of the most interest is the addition of the foot as a separate body (talus, heel and metatarsals) and the release of constraints that oversimplify the rotation of the tibia. In making these improvements to the model, the desire is that more accurate simulations can be performed, and the addition of the structures of the foot opens the possibility of additional activities, such as level ground and complex gait activities. The purpose of this contribution is to evaluate the motions of the theoretical knee simulator and look at ways to make them more accurate and more representative, such that they can be more applicable for the sampling of in vivo patient mechanics.

6.2 Introduction

Throughout the development of the mathematical model, various assumptions were made, often to simplify the knee as a system and meet the capabilities of the model. This is a perfectly common practice in the development

of mathematical models and as understanding and capabilities improve, much of the complexity originally omitted can be restored to allow for more representative in vivo activity simulations.

As a forward solution model, one of the most common assumptions is the introduction of specified motions which are used to recreate physiological movement away from the joint of interest. In this case, the forward solution model solves for certain motions at the knee joint; however, there are additional motions that are necessary to drive the mechanics of the knee. There is no reason to solve for the kinematics at other joints and for this reason they are assumed to be calculated using inverse dynamics. Since motions are input into these joints instead of forces, the degrees of freedom can be calculated as a function of either flexion or time, and in doing so, the motions can be prescribed through some form of a polynomial function.

Often in the early development stages of the model, these inverse parameters are relegated to simple movement, if they even move at all. In order to facilitate complex motions, these complex movements are added back and the belief is that they will allow for a better replication of in vivo conditions. Chapter 5 has an excellent example of this where the specified function was added to the pelvic rotation about the mediolateral axis and the motion pattern was used to facilitate the functionality of the extensor mechanism.

The first and most noticeable assumption in the previous iterations of the model is the omission of the foot and all associated bones. It was assumed for the sake of complexity, as well as the ability to replicate knee simulators for validation

purposes, that the model began at the ankle. Therefore, the first task to improve the physiological accuracy of the model will be to replicate the foot in the model.

The second focus with respect to improving model accuracy is the introduction of more complex motions. For instance, the previous iterations of the model specify rotations at the ankle as both unidirectional and linear. This is far from the case, as early and late flexion rarely tend to have very different motion patterns. Furthermore, the addition of the foot allows for alterations to other bone flexion values, such as the tibia about the ankle. This is both more accurate from a motion perspective and should contribute to more realistic kinematics and kinematic patterns at the knee.

6.3 Methods

The addition of the foot allows for a translational component to the tibia to be introduced. One unique challenge to the inclusion of the foot is the determination of functions to be specified. In order to correctly apply these to the model, the motions must first be fit to a polynomial function as input as a function of time or flexion. In this case, such an equation will be fit using data derived from an analog goniometer, which is a device used to measure angles in orthopedic research (Figure 74). Once these motions have been assessed, the average magnitude of foot flexion will be used to determine the motion of the foot in the revised version of the model. Once the new tibia and foot movements are determined and evaluated mathematically, these new parameterizations can be used in the model and the subsequent results can be evaluated to determine the kinematic effects.

Another facet of improving kinematic accuracy is the ability to replicate the motions of the tibia. While it is well understood that the femur rotates axially with respect to the tibia, the movement of the tibia in the Newtonian (global) reference frame is much less understood.

To measure these, a pilot fluoroscopy study was conducted using three distinct patient groups. The first group included ten normal, healthy subjects. The second group included 30 PS TKA subjects while the third group included 24 PCR TKA subjects. These subjects performed a deep knee bend under fluoroscopic surveillance which was then registered to bone and device models using a registration process. From there, two measurements were taken: the first was the rotation of the femur with respect to the tibia, and the second was the rotation of the tibia with respect to the global reference frame (Figure 73). Such values can be extracted from the transformations of the components determined through the registration process. These parameters are important as the rotation of the femur is a kinematic parameter solved for by the model. However, the rotation of the tibia is currently unaccounted for in the model. Once flexion is determined, such an input can be applied to the model and used in future analysis. Additionally, such a study will be useful in assessing the kinematic differences between normal knees, PS knees and PCR knees.

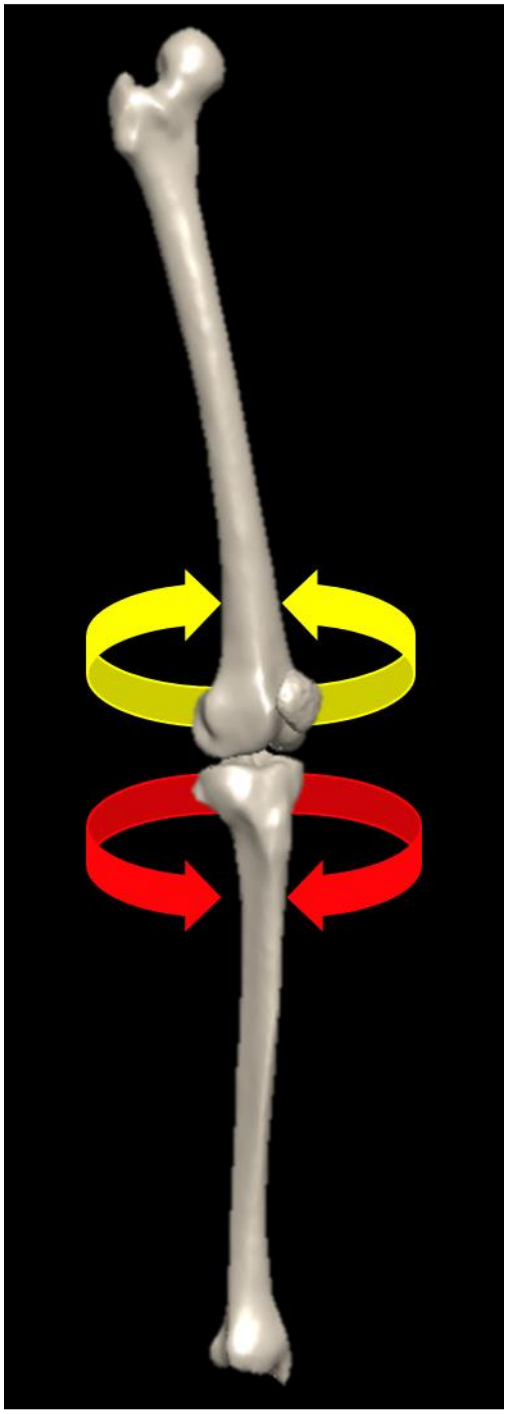


Figure 73: Using fluoroscopy, two measurements were taken in vivo at various time steps. The rotation of the femur in the tibia reference frame (yellow) and the rotation of the tibia in the global reference frame.



Figure 74: An analogue goniometer was used to measure various angles between the ground, foot and tibia. These samples were captured computationally at 100hz.

6.4 Results

6.4.1 Adding the Foot

The foot itself contains more than 20 bones which are assumed to be rigidly attached within a single anatomical structure (Figure 75). From a mechanics perspective, the metatarsals (toes) can have their own degrees of freedom; however, for this case it will be assumed that they are rigidly attached. The toes have an expanded role in gait analysis so this will be expanded in Chapter 10. From previous versions, the model has the ability to dictate tibia motion through a polynomial function, but the addition of the foot is completely new and contains an additional specified function for flexion and extension about the contact point with the ground (Figure 76).

Using an analog goniometer, the flexion profile for the foot can be determined, and this profile can be specified into the model treating the foot as an inverse element (Figure 77). This is exactly how the tibia flexion is built in the model. Despite the inclusion of tibia flexion, one notable improvement is that this process can be done to improve the fitting function representing tibia flexion as well (Figure 78). To include the foot in the model, additional components need to be added, namely the contact point and the connection to the ankle. The rest of the model is fundamentally the same.

Once the function for the correct foot rotation was extracted from goniometer data, it becomes possible to substitute those values into the model to simulate kinematic performance based upon the new physiological parameters.

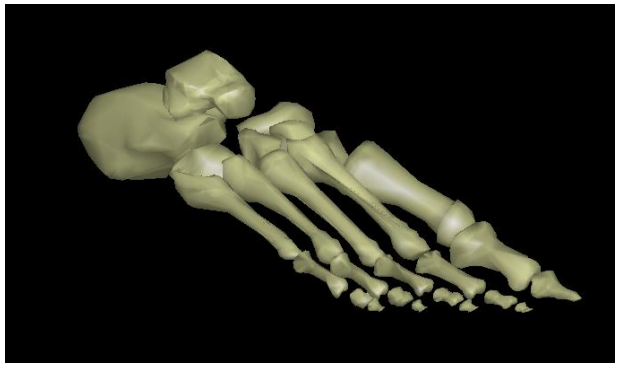


Figure 75: The foot consists of a variety of bones that were assumed to be rigidly attached for this particular analysis.

.

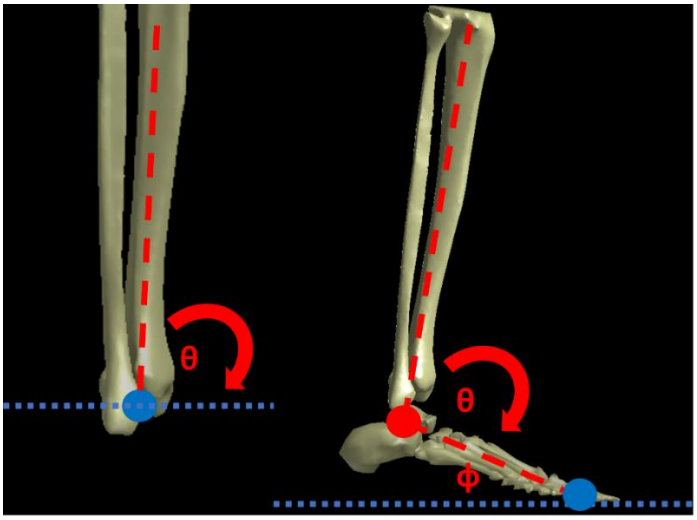


Figure 76: The previous iterations of the model (left) facilitated tibia rotation at a specified angle (θ) relative to the ground in which the Newtonian frame was established (blue dot). The improved version of the model includes the foot, as well as a second angle (ϕ) about the point where the foot contacts the ground where the Newtonian frame is established.

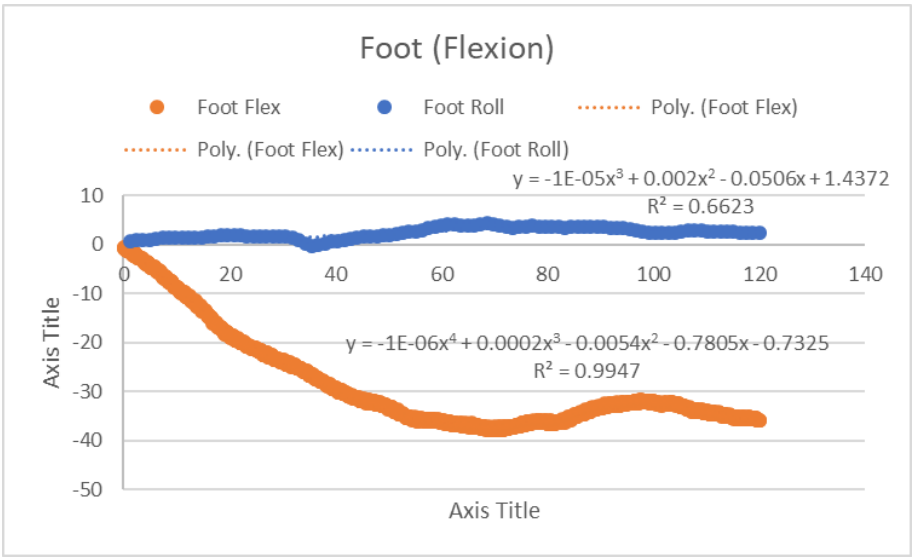


Figure 77: Using an analogue goniometer attached between the foot and the ground, flexion and extension angles were collected (orange), as well as eversion and inversion of the foot (blue). These measurements are effectively the pitch and roll of the foot, respectively.

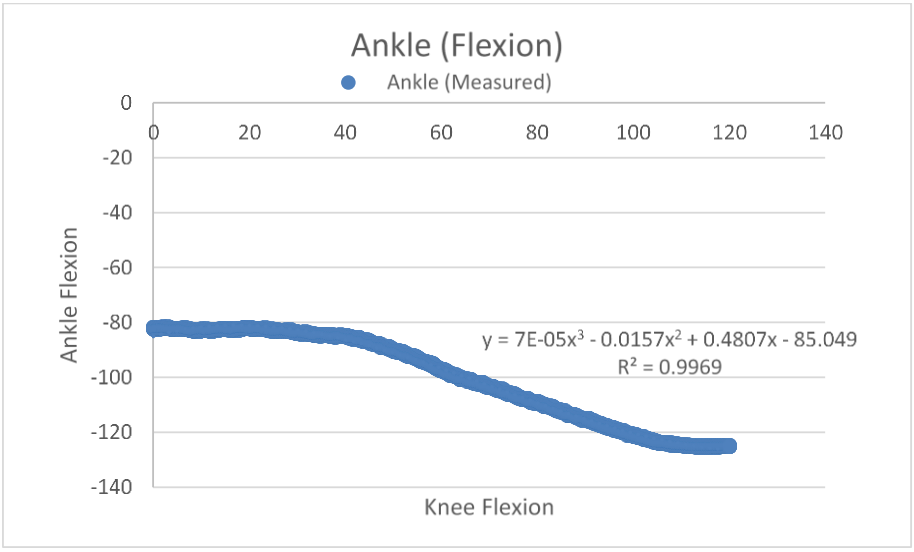


Figure 78: Using the goniometer, the ankle flexion between the foot and the tibia was collected.

The goniometer devices read both foot flexion and extension, as well as eversion and extroversion which was assumed to be negligible.

In order to assess the role of the foot, there were three simulations performed in total. The first of these simulations involved a control which assumes that a foot is not included in the model. The second simulation includes the foot, but it is assumed to be stationary. It is expected that there would be minimal difference between these two simulations. Finally, the third simulation includes a mobile foot, as well as additional complexity to the tibia rotation where the flexion profile is assumed to be parabolic instead of linear. Attempts were made to utilize higher order functions, such as cubic and quartic, however, these specified functions do not achieve neither consistent stability nor reproducible results. There is no discernable difference between simulation without a foot and with a stationary foot. However, simulations where the foot was specified to move presented distinct kinematic and kinetic patterns from the other two. Adding the motions to the foot appears to have contributed to greater lateral femoral condyle translation, slightly greater medial anterior translation and an additional two degrees of axial rotation (Figure 79, Figure 80, Figure 81). These measures are objectively more like the normal knee, demonstrating advantageous PCR mechanics. The foot addition however did increase peak extensor forces by 1.5 times BW (Figure 82).

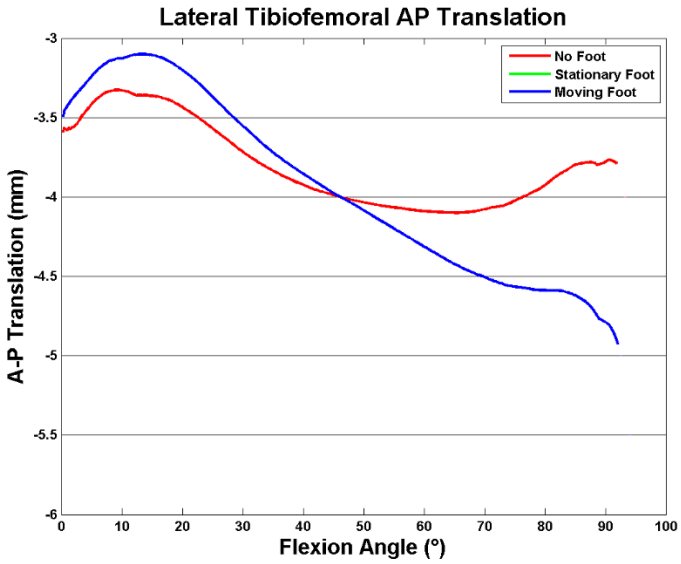


Figure 79: The simulations where the foot flexes tend to demonstrate greater femoral posterior translation.

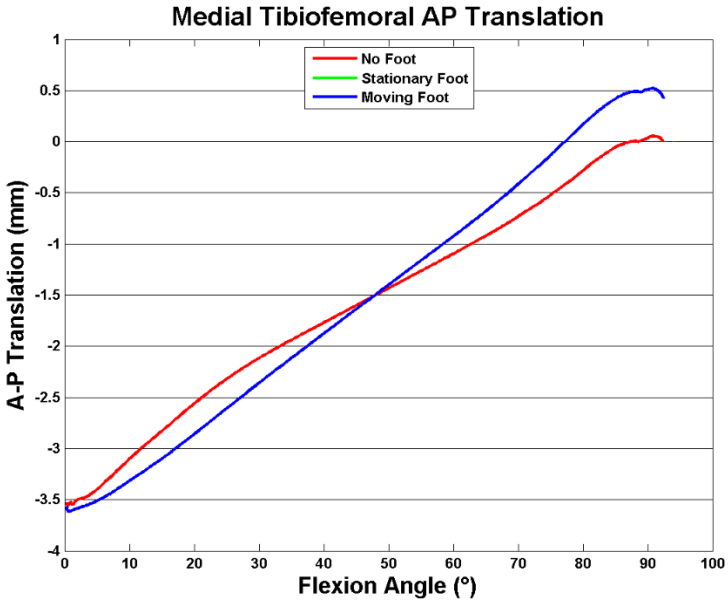


Figure 80: The simulations where the foot flexes tend to demonstrate similar femoral anterior translation patterns with slightly greater translational velocities.

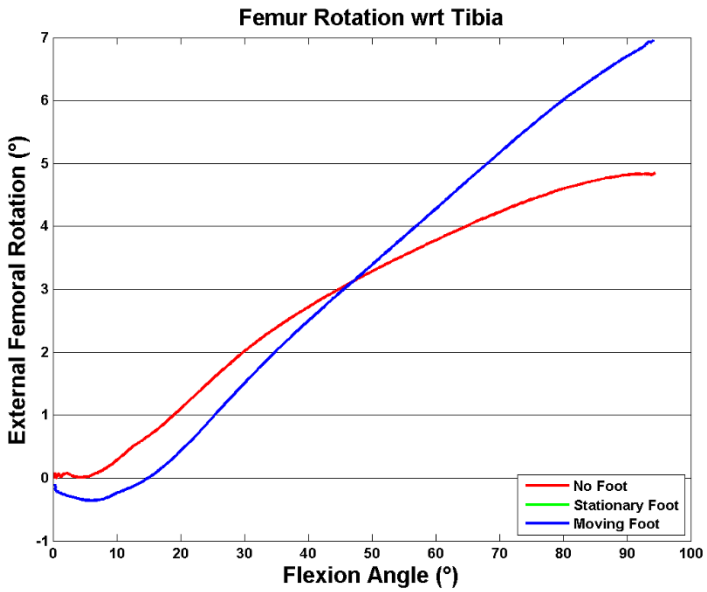


Figure 81: The simulations where the foot flexes tend to demonstrate greater axial rotation compared to simulations with a stationary foot.

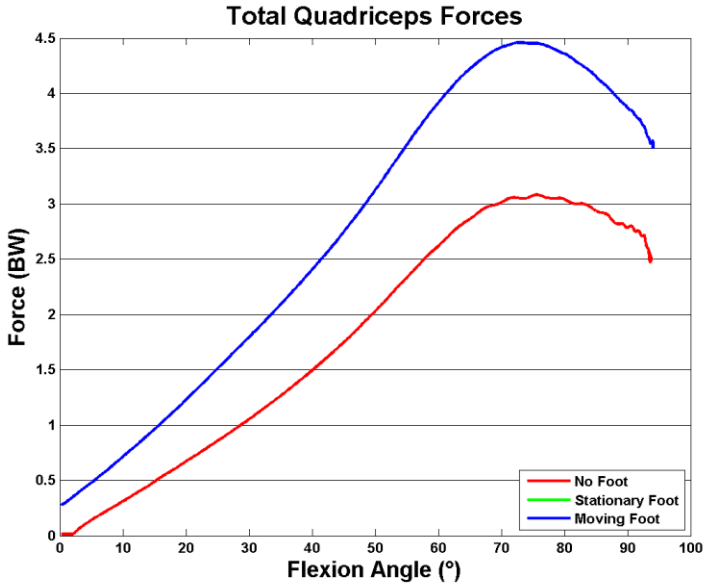


Figure 82: The simulations where the foot flexes tend to demonstrate greater quad mechanism forces compared to simulations with a stationary foot.

6.4.2 Adding Tibia Rotations

In addition to the introduction of the foot, there are other improvements that can be made to the specified components of the simulations to better approximate in vivo motions, and the tibia is one such element. Unlike the ankle, rotations of the tibia are both much more nuanced and subject to skin motion artifacts. For this reason, fluoroscopy was used to determine these motions.

To better understand both the motions of the tibia and femur, a fluoroscopic evaluation and registration process was performed and the resulting transformations were compared in several reference frames. Additionally, this process was done for PS, PCR and normal knees to promulgate an improved understanding of their respective knee mechanics.

During this analysis, it was found that the average normal knee experienced approximately 20 degrees of rotation axially with respect to the tibia compared to five degrees for a PS and two degrees for a PCR (Figure 83). This analysis is similar to other fluoroscopically reported data and methods which confirms that the femur rotates with respect to the tibia bearing surface. Likewise, this data mirrored similar studies demonstrating not only that TKA kinematics vary widely from the native knee to TKA devices but also that the PS mechanics tend to be advantageous over PCR mechanics.

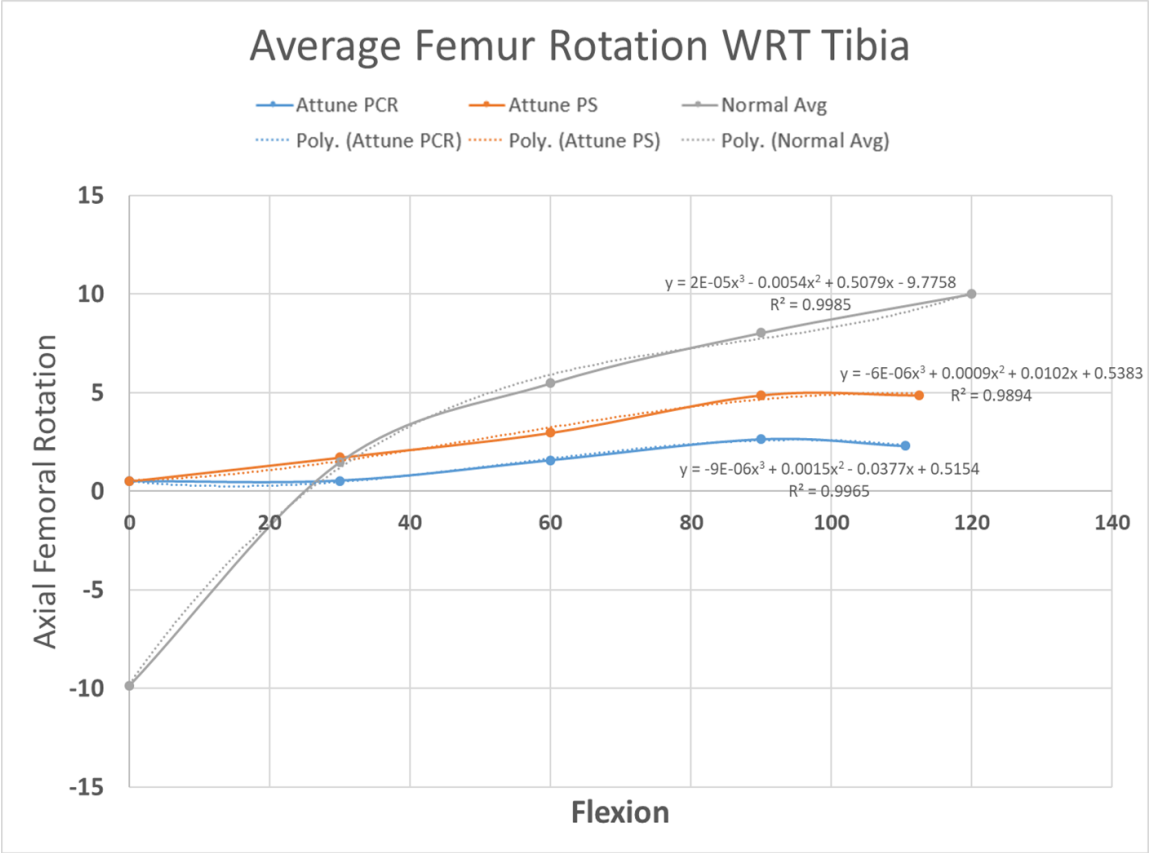


Figure 83: Evaluated fluoroscopically, normal knees on average appear to experience the greatest magnitude of femorotibial rotation, while PS and PCR devices not only experience significantly less rotation but also differing rotation values between each other.

While femoral rotation is often a reported element of kinematic analysis, the rotation of the tibia itself with respect the ground is often overlooked. In this case, it was observed that the normal knee exhibited 14 degrees of tibia rotation with respect to the global reference frame. This is compared to seven degrees for the PS and six for the PCR (Figure 84).

Much like what was done with the foot, the rotation patterns of the tibia were regressed and substituted into the model as inverse specified functions with respect to tibia rotation. In other words, the functions determined fluoroscopically were used to induce these same rotations on the tibia as a function of flexion. Since the motions of the femur are solved for given the forward nature of the model, these regression equations are not input into the model but instead used as validation tools, as it would be expected that these would be the resulting kinematics for the same set of inputs. This analysis was done using a normal knee set of geometries.

The resulting tibia rotation about the proximal distal axis was fit with a cubic function used as an input through the model as a specified tibial rotation about the proximal distal axis. In the interest of understanding the role of this rotation, both a positive (external) and negative (internal) rotation directions were used.

It was observed that rotating the tibia internally as a function of flexion greatly increased the posterior translation of the lateral femoral condyle and increased anterior translation in the medial femoral condyle (Figure 85 & Figure 86). Together these two metrics create a large difference in axial rotation as the

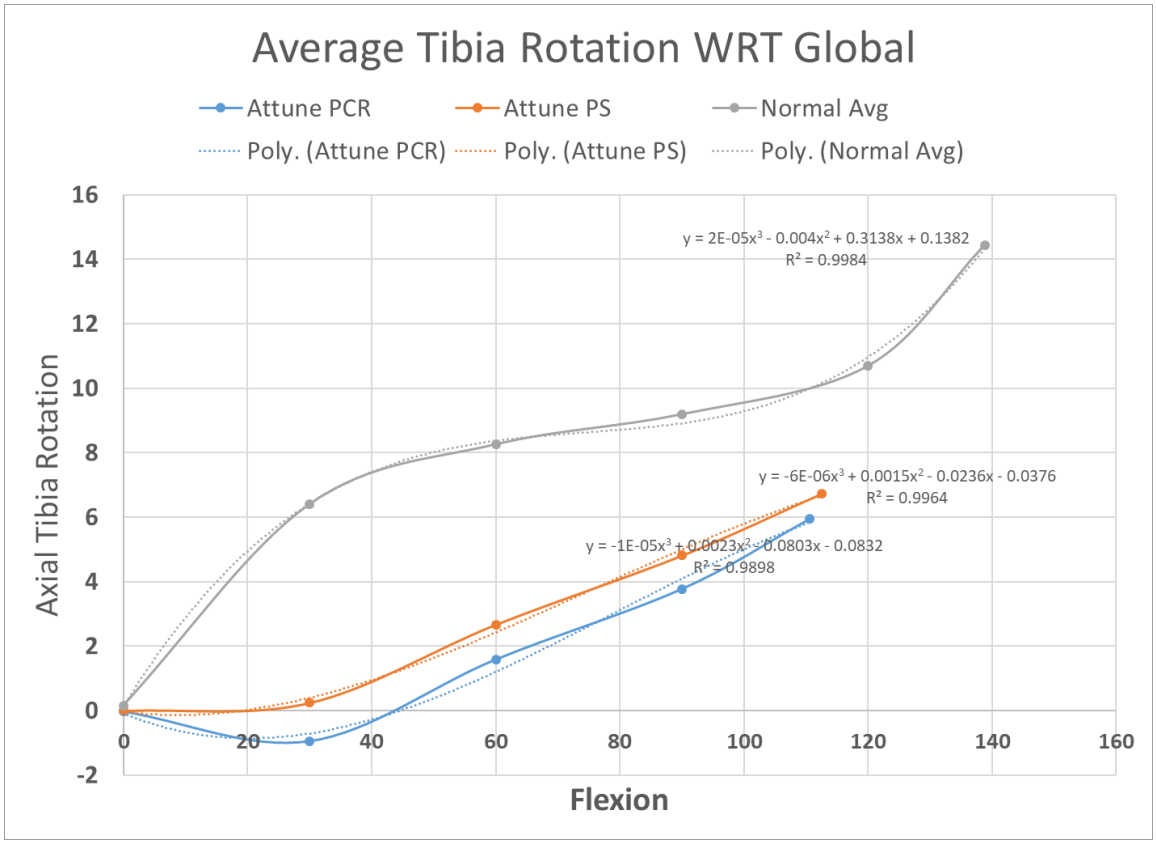


Figure 84: Evaluated fluoroscopically, normal knees on average appear to experience the greatest magnitude of tibial rotation in the global reference frame, while PS and PCR devices not only experience significantly less rotation but also differing rotation values between each other.

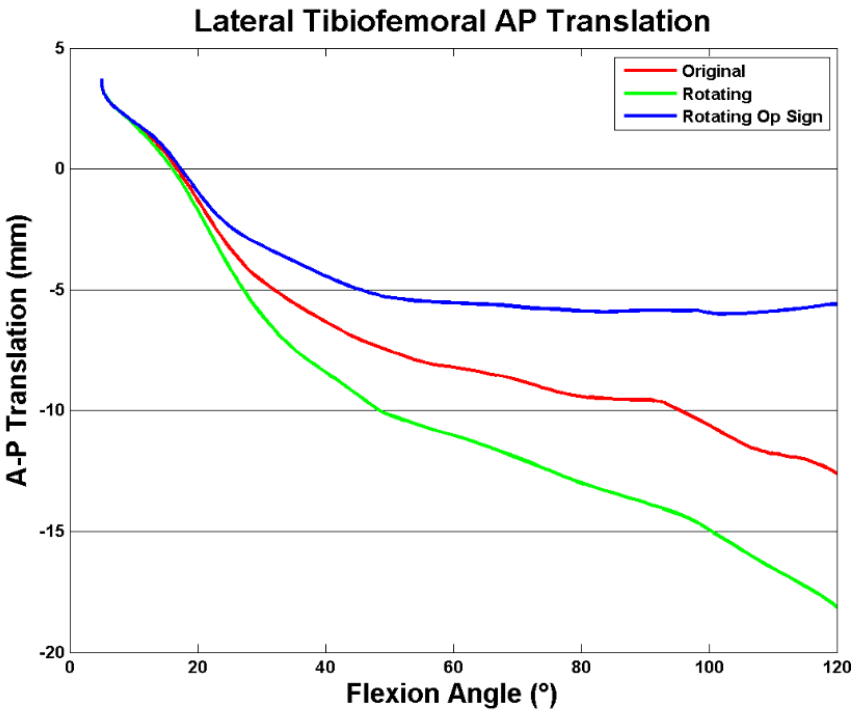


Figure 85: When both positive and negative rotations determined fluoroscopically are applied to the tibia of the model, external tibia rotation tends to increase lateral femoral posterior translation while external tibia rotation tends to decrease lateral femoral translation.

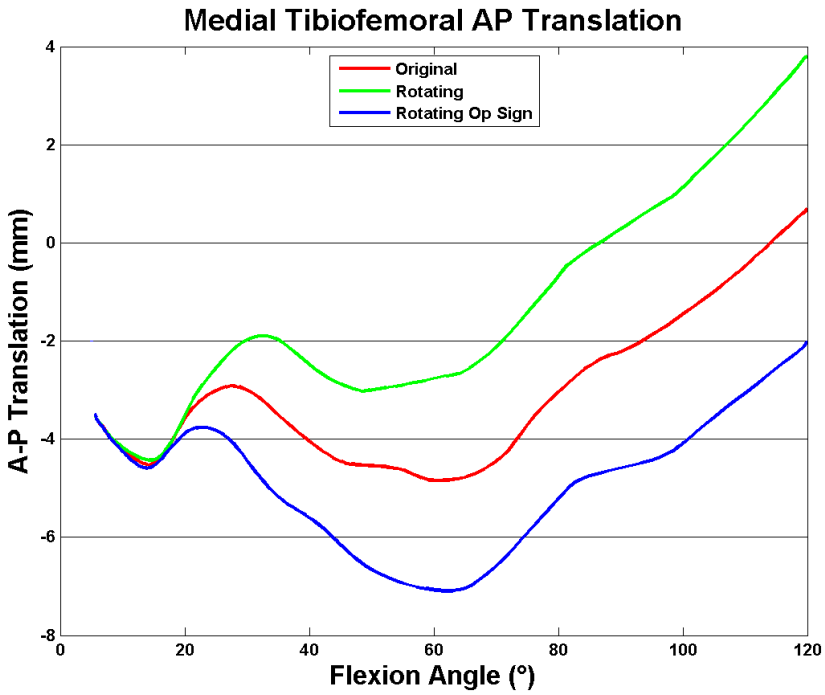


Figure 86: When both positive and negative rotations determined fluoroscopically are applied to the tibia of the model, external tibia rotation tends to increase medial femoral anterior translation while external tibia rotation tends to decrease medial anterior femoral translation.

rotation of the femur relative to the tibia is effectively the sum of the internal rotation of the tibia and external rotation of the femur in their respective frames of reference (Figure 87). Conversely, external tibial rotation mitigates these differences. Axial rotation of the tibia was observed to have a negligible influence on extensor mechanism forces.

6.5 Analysis and Discussion

The addition of the foot into the model is aimed at increasing the physiological accuracy of in vivo simulations. Compared to an otherwise identical simulation where the foot is either held stationary or omitted altogether, the kinematics appear to be closer to the kinematics of the normal knee, resulting in greater translational and rotational magnitudes. Possibly the most important observation from the inclusion of the foot is that the overall tibia flexion about the medial lateral axis is mitigated, since the positioning of the knee is no longer exclusively reliant on the flexion of the tibia, but the sum of the tibia and foot flexion relative to the ground. It is believed that this difference, in conjunction with the addition of a higher order flexion profile on the tibia, contributed to very different positioning of the tibia in global space. For this reason, the kinematics at the knee are affected. This also is a factor that may be useful to evaluate future device designs as the kinematics appear improved over previous iterations. While the kinematics at the knee demonstrated improvement at the knee, the kinetics were not as positively affected. The efficiency of the quadriceps mechanism decreased with the addition of the foot, contributing to an increase in extensor mechanism forces of approximately 1.5 times BW. While there are a number of factors that

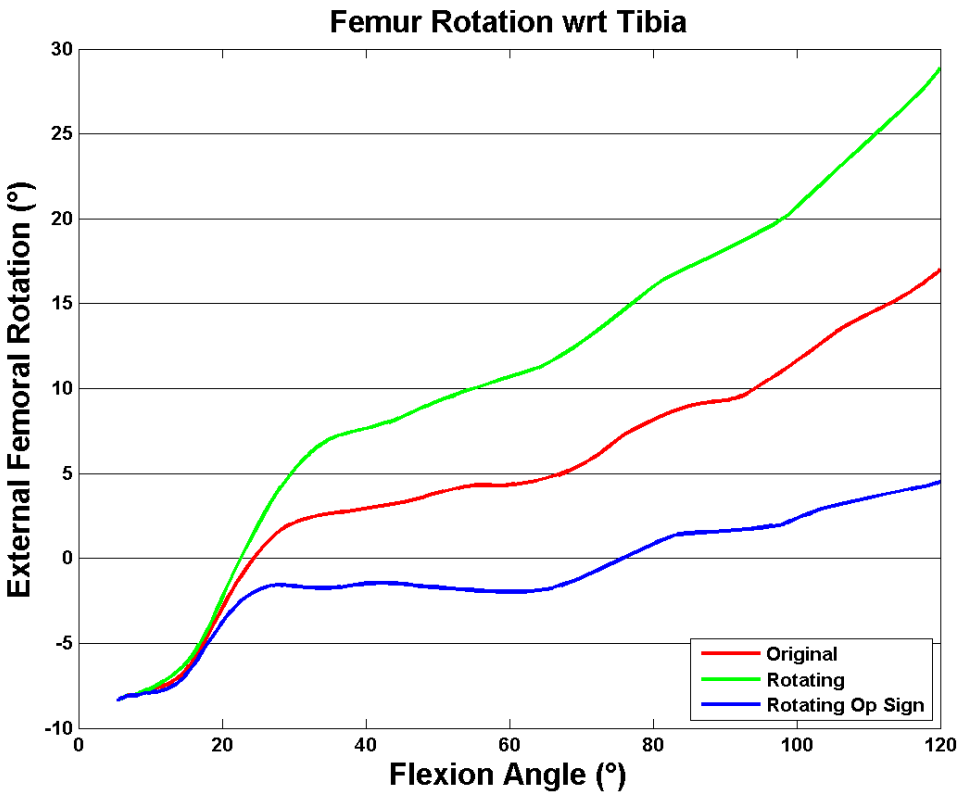


Figure 87: When both positive and negative rotations determined fluoroscopically are applied to the tibia of the model, external tibia rotation tends to increase femoral external rotation while external tibia rotation tends to decrease femoral external rotation.

may contribute to such an increase, the most logical explanation relates to the forward tilt of the tibia. When the ankle was the center of rotation for the tibia, flexion was based on the positions of femur and tibia. By adding the foot, that same system is effectively tilted forward at an angle equivalent to foot flexion. For this reason, the femur needs to achieve a different orientation with respect to the downward pull of gravity and because of this angle, it must provide additional activation to achieve flexion. The only way to resolve this, much like the pelvis, would be to add an interactive torque which can supplement the quadriceps forces during flexion.

The nature of the parameterization also allows for variations on the rotation of the foot relative to the ground (the Newtonian frame) to achieve motion patterns that may be specific to individual subjects. Should such an analysis be desired, the flexion profiles can easily be determining through imaging and direct measurement techniques.

Possibly one of the most consequential findings of this analysis relates to the rotation of the tibia in vivo. It has been widely documented and reported that there is a substantive difference between kinematic values of the femur with respect to the tibia dependent on the device or geometry being used. What is unique about this particular study is that it not only verifies the femoral behavior, but also demonstrates that such a behavior applies to the tibia in the global reference frame as well. There are two scenarios that were evaluated: when the tibia rotates with and counter rotates against the femur. While the setup as demonstrated is intended to be a proof of concept, such rotation in vivo is expected

to be a combination of the two independent rotations. Specifically, it is widely believed that the tibia rotates internally and the femur rotates externally. Such a motion facilitates proper kinematics while maintaining a proper joint line. The significance with this data is that it is a unique distinction between femoral and tibial rotations and furthermore, this difference is distinct between normal knees and varying TKA types.

Since the tibia rotations in the model are driven by inverse specified function, there is not a current capability to evaluate the tibia in a forward manner. Therefore, the analysis of model kinematics is limited to these rotations being specified as inputs, specifically the scope of this contribution focuses on the normal knee, but the implication is that each TKA device and normal geometry may in fact have a unique tibial rotation profile. Such a set of parameters would need to be included on a case by case basis until such time that the tibial rotation mechanism and its role in device geometry is better understood.

When evaluating the normal knee, it becomes apparent that the rotation of the tibia bears a heavy influence on tibiofemoral kinematic results. As would be implied, compared to a control function where the tibia remains stationary about the proximal/distal axis, rotating the tibia internally (against the femur) tends to amplify all kinematic values, and rotating the tibia externally (with the femur) tends to attenuate such kinematics. Not only do these results imply that a successful model can utilize these rotations to simulate in vivo conditions, but also that there may be articulating surface design features that can influence such mechanics.

The rotation of the tibia had a negligible effect on the forces required by the extensor mechanism to drive flexion.

6.6 Conclusion

The addition of the foot facilitated more physiologically accurate motions, and in doing so, the kinematics of TKA devices were improved to be a closer representation of that the normal, healthy knee. Likewise, the addition of tibia rotations about the proximal/distal direction and increased complexity in the medial/lateral direction also facilitated improved kinematics. However, there is a caveat that these tibiofemoral motions are highly dependent on the specified motions of the tibia in the global reference frames. Furthermore, it was shown using fluoroscopy that the design of articulating surfaces and device type can affect tibiofemoral and talotibial motions. This such an influence was built into the model utilizing an inverse strategy.

CHAPTER SEVEN: PARAMETERIZING ARTICULATING GEOMETRY

7.1 Purpose

A substantial focus in the development of the graphic user interface for the forward solution model has thus far been geared toward the visualization of the bones, soft tissue and associated geometries of the knee. While this is certainly useful for analysis purposes, the power of the model is greatly enhanced by the ability to change inputs to better embody, and perhaps even improve, the design rationale. These changes can range from simple (such as changing a property value) to highly complex, (changing an entire geometric surface of a prosthesis component).

Although the ability to change geometric surfaces is intuitive from an analytical perspective, it raises some unique challenges extracting information from the model for the purposes of both validation and manufacturing. In order to accurately represent the physical system in other mathematical models or to manufacture the devices being evaluated, the geometries need to be extracted exactly as they are to preserve the integrity of the simulation results. In other words, the geometries must be recreated exactly, as they are in the simulation to reliably produce the same results.

Many TKA components are highly dependent on mathematical parameterization. For this reason, the extraction of geometries from the model will be two-fold: the creation of a geometric output representative of the articulating surface for each component, and extracting these geometries. These will be used

to create sets of mathematical equations that can be used to recreate these geometries in a parametric manner conducive to manufacturing techniques. These parameters will focus primarily on medial and lateral condyle bearing conformity in addition to post shape that can be applied on both an anterior or posterior post.

Given the ability to not only change, but also extract model geometries allows for an in-depth analysis of bearing conformity. While most of the analysis for this report pertains to the geometry of the bearing surface, as it is the most relevant in the analysis process, this is a process that can be applied to the shape of the femoral trochlea or the bearing post shape as well.

There are a number of conditions under which the sagittal and coronal bearing conformity may need to be changed to better match anatomical constraints. One such case encompasses the medial pivot arthroplasty design, whereas an axial rotation is induced by a difference between the condyle translations of the medial and lateral condyles during flexion. Such conditions can be induced or magnified as needed in existing designs to better facilitate medial pivot kinematics. There are a multitude of methods that may produce this result. However, the most intuitive is the increasing of medial condyle conformity and a decrease in lateral condyle conformity. The end result is a more stationary medial condyle and a more mobile lateral condyle which facilitates axial rotation. Increasing constraining geometry will however lead to increased contact forces. There is a proportional effect to this phenomenon and for that reason the design geometry can be tuned as needed.

The primary factor used in this analysis is sagittal conformity, although other factors can be influenced as well, including coronal conformity, proximal/distal height, and sagittal tilt. These geometric changes can be applied to the trochlea and either cruciate stabilizing post. In light of these results and prospective analysis, work will continue to evaluate and facilitate prosthesis geometries to optimize joint kinetics and kinematics. Interface advances will allow for the accurate representation of these components and all associated changes into 3D modeling software.

7.2 Introduction

Mathematical modeling is an incredibly powerful tool that could be used in design and development of orthopedic devices. Not only does it allow for the evaluation of existing designs but also provides a theoretical framework to build confidence in new designs without the need to invest in building nor implanting the devices. By nature, the device design process is highly iterative consisting of many cycles alternating between design and verification. In other words, what are the design changes that are made? And do these changes induce the effects that are expected? Eliminating the need to build and implant the device expedites each iteration of the process allowing for more design changes and verification, especially early in the design process. While mathematical modeling (in silico testing) is not a substitute for in vitro and in vivo testing, it does allow for more confidence entering the physical testing phase of the design process. This allows for a more efficient design process allowing for more iterations and ultimately improved confidence in a prospective design.

Due to the iterative nature of the design process, the ability to make changes and evaluate subsequent results is paramount. Previous versions of the development of the forward solution model have been highly dependent on the reception of CAD models from which mathematical features can be derived to build a theoretical representation of a physical system. While this process is effective, it requires a substantial time investment to build the CAD models by individuals with CAD modeling experience in addition to an individual with in depth knowledge of the model to allow for seamless integration into the mathematical system.

Such a multifaceted approach to changing design features can be prohibitively cumbersome and for this reason it is of great interest to incorporate the ability to change the component geometries in the model. This allows for both the fast and easy transitions between design features, allowing for more robust sensitivity analysis which can better facilitate understanding the role of design features and how they affect motions and forces. More importantly is that this allows a simple user interface to make these changes, bypassing the need for extensive CAD knowledge required to create mathematically derived surface geometries. Furthermore, simplifying the user interface allows single parameter quantification of design factors, such as conformity, height, etc. Quantification is important in this regard because it allows for well controlled sensitivity analysis and design of experiment to better understand and optimize features.

Improving the ability to change geometries in the model interface also provides a unique challenge as these geometries will need to be replicated in a CAD program to build prototypes and integrate into the manufacturing process.

This is a process commonly referred to as “new product integration” and it ensures that the device can be correctly created using existing manufacturing techniques. While the intuitive result would be to output a full 3D body CAD model, this is both not feasible with the existing software and perhaps more importantly, the ability to edit the resulting geometries would be severely limited. For this reason, the developers have opted to output only the geometries of articulating surfaces and all associated equations. The purpose of this is two-fold as it both limits the model outputs to the geometries that can be changed and allows for seamless integration using a cad program. While this integration does require a prior knowledge of CAD software to create the final device, this process is only required at the completion of the use of the model, therefore, the process need only be completed once compared to at every change prior to this addition. Because of both the proprietary, complex nature of implant components, it is not possible or necessary to export an entire model. Although manufacturing is a primary purpose for exporting these geometries, the exports also allow for the exact transfer of model geometries and associated changes to other models which can be used to compare and ultimately validate between models.

There are a number of articulating surfaces in a TKA device and every articulating surface, by definition, has at least two interfacing surfaces. Through the contact detection algorithm used by the model, each geometry is set up as sets of complementary point clouds and surfaces. The medial and lateral bearings, anterior/posterior posts, and femoral trochlea are set up as polynomial surfaces regressed to fit the original geometry. The femur component, anterior/posterior

cams, and patella are all set up as point clouds, complimenting their respective surfaces. The algorithm at its core is simple, at each iterative timestep every point in each cloud is evaluated for its distance to the surface. If the distance is positive, no contact is occurring, if it is in contact. And if it is negative, then contact is occurring and the contact force can be determined proportionally. These mathematical surfaces are important as the surface changes are applied through variations in the regression coefficients. For this reason, the only factors that will chance are those corresponding to surfaces. In other words, it is assumed that any change in articulating surface can be done through one of the two contacting surfaces and it will also be assumed that any changes in the model are made through changes in the polynomial surface as opposed to the point cloud. This assumption is made as it is more computationally efficient and provides for a more reliable transmission between programs, a similar process could be applied to the point clouds to make any changes via scaling and rotation transformations; however, that is outside of the focus of this contribution.

Finally, there are many applications to which this new process can become useful and the most intuitive of these is the evaluation of medial and lateral bearing conformity. Conformity changes are primarily employed to guide motions, provide surface constraints and facilitate motions and forces. Increasing conformity tends to limit motion while increasing contact forces and the converse is true for decreasing conformity. The updates to the model provide a vehicle for the optimization of conformity to facilitate medial pivot or other kinematics as required by a design. This same logic can be applied to post shape and trochlear groove

geometry. However, conformity has been shown to demonstrate the greatest effect on kinematics and kinetics.

7.3 Methods

7.3.1 Contact Detection

Understanding the nature of the contact detection algorithm in the model is integral to understanding the extraction of geometric features. The model begins with a defined set of bodies and surfaces, all of which are coded in such a way that they allow for robust inputs. These inputs can range from coefficient values, to distances between attachment sites for muscles, and to gains and constants to be used in controllers.

One such input is the geometry for the prosthetic device. The initial step in the process is the introduction of implant geometries. These components must be of a point cloud or mesh file type (.iv, .wrl or .stl) instead of an IGS with non-uniform rational basis spline (NURBS) as the mesh structure is critical to calculations that need to be performed.

While these models are representative of exact components that are imported, the geometries are purely for visualization purposes (Figure 88). In order to perform calculations for the model, two types of geometric features need to be extracted. These two features are point clouds and polynomial contact surfaces. Once such mathematical entities have been derived, they can be adjusted by placing and transforming the components to the desired position.

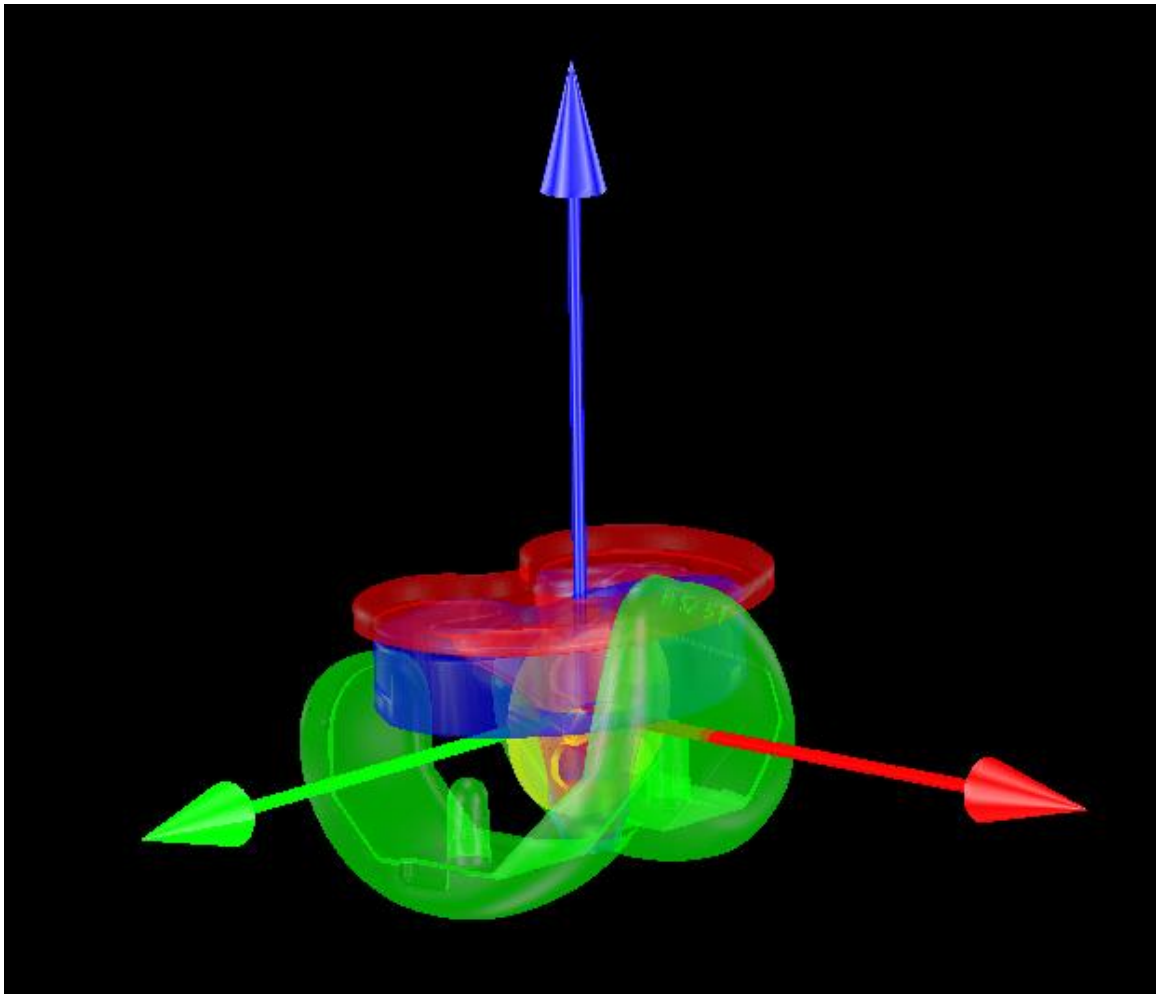


Figure 88: Computer models of all TKA components can be imported through software. These components are purely for visualization purposes as mathematical representations need to be derived.

7.3.1.1 Point Cloud Extraction

The first calculation that needs to be extracted from the geometry is the point cloud that represents the coordinated of the outer bounds of the prosthesis component. This is done by checking the lowest points on the medial and lateral sides of the prosthesis at every possible flexion angle (Figure 89).

These points then undergo a transformation to achieve the initial conditions for the model based on the positioning of the other components. While outside of the scope of this contribution, these point clouds can be transformed to fit curves and distributions creating the ability to edit their geometries by changing the location and density of these points.

7.3.1.2 Polynomial Surface Regression

For reasons that will become evident for the contact detection algorithm, every point cloud must correspond to a complimentary polynomial surface. These surfaces are determined through a 6th order polynomial regression. It was determined that 6th order should be sufficient for replicating articulating geometries while maintaining the majority of the features of the implant component (Figure 90). This may be a higher order than necessary for TKA devices as mathematical definitions tend to be parabolic or cubic order, but the sixth order affords the ability to approximate surfaces with both convex and concave elements simultaneously. The polynomial regression is a sixth order polynomial in terms of either the AP and ML or ML and SI direction. This effectively makes it a height function for independent variables X and Z for the bearing plateaus or Y and Z for the either post. This equation will effectively serve as the one of the two articulating surfaces in the contact detection algorithm and can be generalized by the following:

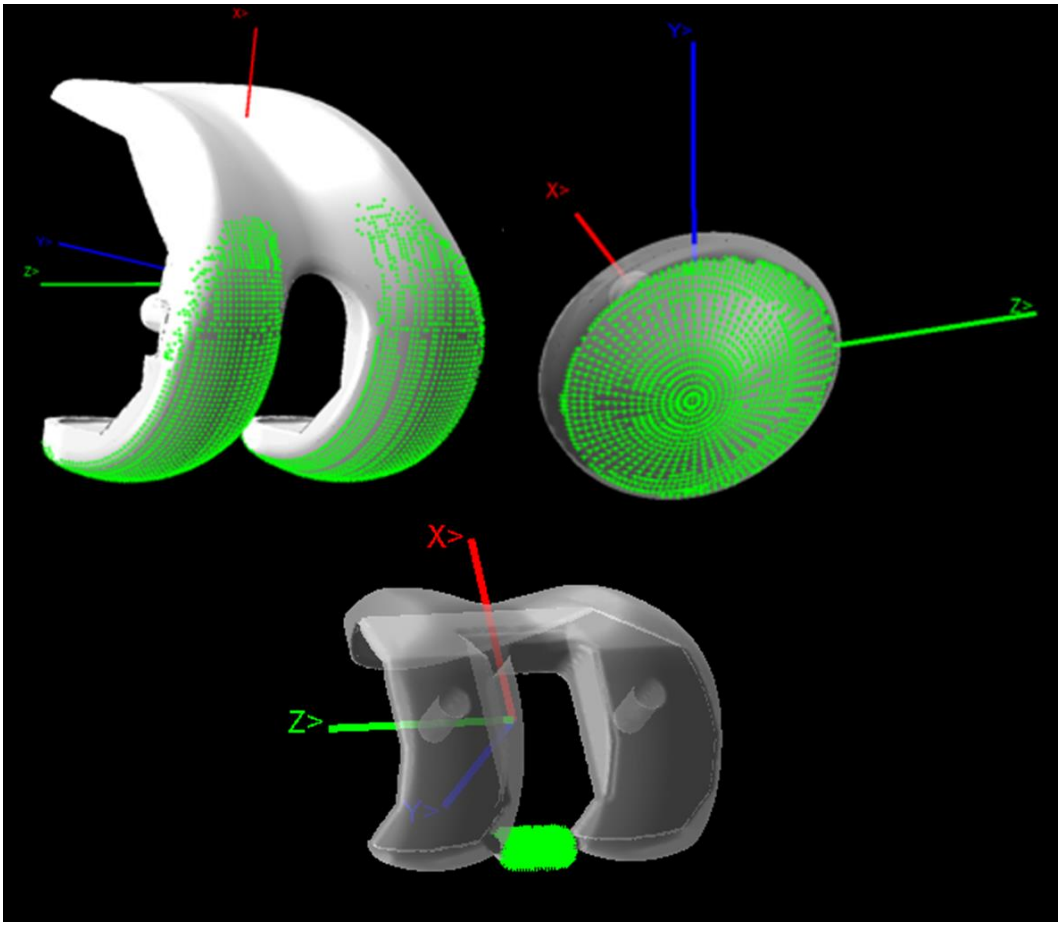


Figure 89: Using an iterative calculation algorithm, regions of points are selected that have the potential for contact. This is done for the femoral condyle surfaces (top left), patella surface (top right) and any anterior or posterior CAM mechanisms (bottom).

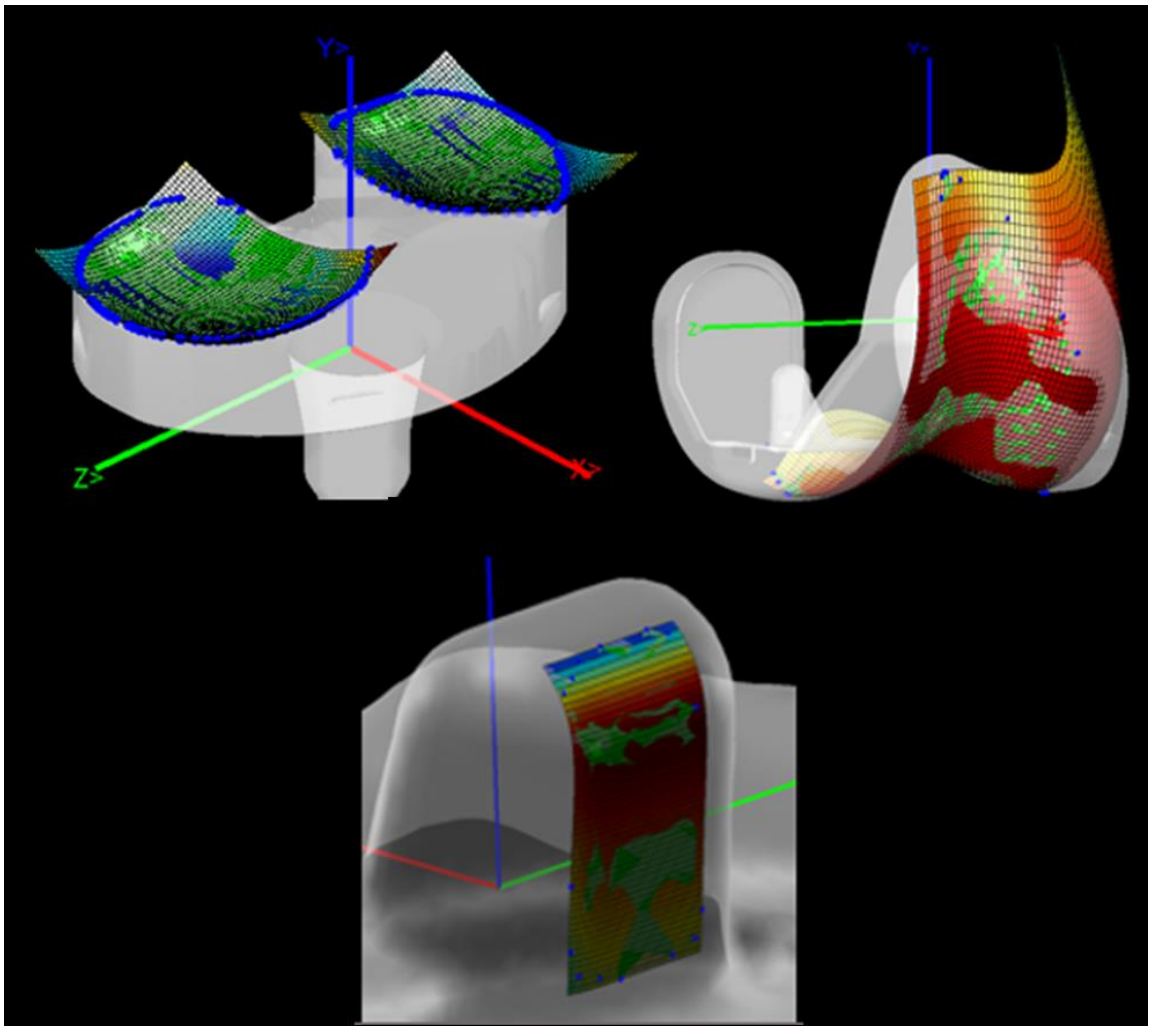


Figure 90: Using a regression algorithm, polynomial surfaces are fit to each articulating surface. These surfaces each correspond to one of the point clouds from Figure 89, including the bearing surfaces (top left), trochlear groove (top right) and any bearing posts (bottom).

$$Height\ Function\ Bearing\ \ (y) = f(x,z) = \Sigma \begin{bmatrix} C & z & z^2 & z^3 & z^4 & z^5 \\ x & xz & xz^2 & xz^3 & xz^4 & xz^5 \\ x^2 & x^2z & x^2z^2 & x^2z^3 & x^2z^4 & x^2z^5 \\ x^3 & x^3z & x^3z^2 & x^3z^3 & x^3z^4 & x^3z^5 \\ x^4 & x^4z & x^4z^2 & x^4z^3 & x^4z^4 & x^4z^5 \\ x^5 & x^5z & x^5z^2 & x^5z^3 & x^5z^4 & x^5z^5 \end{bmatrix}$$

Therefore

$$f(x,z) = C + x + x^2 + x^3 + x^4 + x^5 + z + z^2 + z^3 + z^4 + z^5 + xz + x^2z + x^3z$$
$$+ x^4z + xz^2 + x^2z^2 + x^3z^2 + xz^3 + x^2z^3 + xz^4$$

where

$$x\epsilon[Sagital\ Limits]\ and\ z\epsilon[\ Coronal\ Limits]$$

And for the bearing

$$Height\ Function\ Post\ \ (x) = f(y,z) = \Sigma \begin{bmatrix} C & z & z^2 & z^3 & z^4 & z^5 \\ y & yz & yz^2 & yz^3 & yz^4 & yz^5 \\ y^2 & y^2z & y^2z^2 & y^2z^3 & y^2z^4 & y^2z^5 \\ y^3 & y^3z & y^3z^2 & y^3z^3 & y^3z^4 & y^3z^5 \\ y^4 & y^4z & y^4z^2 & y^4z^3 & y^4z^4 & x^4z^5 \\ y^5 & y^5z & y^5z^2 & y^5z^3 & y^5z^4 & x^5z^5 \end{bmatrix}$$

Therefore

$$f(y,z) = C + y + y^2 + y^3 + y^4 + y^5 + z + z^2 + z^3 + z^4 + z^5 + yz + y^2z + y^3z$$
$$+ y^4z + yz^2 + y^2z^2 + y^3z^2 + yz^3 + y^2z^3 + yz^4$$

where

$$y\epsilon[Transverse\ Limits]\ and\ z\epsilon[\ Coronal\ Limits]$$

These expressions represent the regression function for the component surfaces. These expressions are the same for the medial and lateral bearings as the limits will differ to reflect the position in space. These limits reflect the maximum and minimum values along each axis of the surface being regressed which will fundamentally be different based on the surface being evaluated. The nature of

the regression method alleviates the need for higher order combinations of independent variables creating an inverse symmetry as shown below.

$$\begin{bmatrix} C & z & z^2 & z^3 & z^4 & z^5 \\ x & xz & xz^2 & xz^3 & xz^4 & - \\ x^2 & x^2z & x^2z^2 & x^2z^3 & - & - \\ x^3 & x^3z & x^3z^2 & - & - & - \\ x^4 & x^4z & x^4z^2 & - & - & - \\ x^5 & - & - & - & - & - \end{bmatrix}$$

The absence of these mixed higher order terms is reflected in the regression equation sets which will be used in the contact detection algorithm.

7.3.1.3 Convex Hull

In addition to the polynomial representation of the surface, there is another set of data points that will be needed in the contact detection algorithm, and this is the convex hull. By definition the convex hull is the set of bounding points that encompass a region to be evaluated for contact. The convex hull is automatically calculated to account for the perimeter of the selected surfaces and one such example is shown below with the convex hull demonstrated in blue points (Figure 91).

The convex hull projects the perimeter of the contact region into 2D space and using cross product between a testing point. And any two convex hull points, it can be mathematically determined if a given testing point resides within the bounds of the hull. This is an important consideration as the actual contact surface only exists within this point whereas the surface polynomial extends beyond the bound region. Including such a feature allows for the contact detection algorithm to account for the actual shape of the articulating surface.

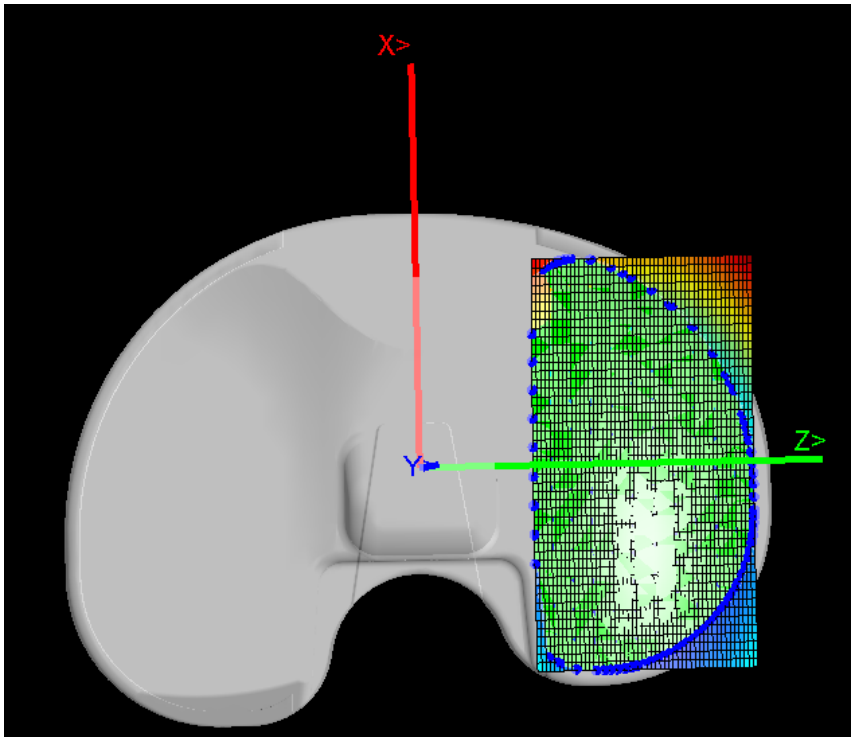


Figure 91: The convex hull (shown in blue) represents the outer bounds of the contacting surfaces for the lateral side of the bearing. This same process is also applied to the medial side, posts, and trochlear groove.

7.3.1.4 Contact Detection

The contact detection algorithm is elegant in its simplicity combining together the point cloud, surface polynomial and convex hull for the condyles, posts, and trochlea to determine which interfaces are in contact at any given time step (Figure 92). This is done mathematically by evaluating the coordinate values of each point cloud point with the polynomial function. If the result is greater than the function, no contact is occurring, if the two are equal contact is just beginning, and if the value is less than that means contact is present and a force is applied.

$$For\ Each\ Femoral\ Cloud\ Point\ of\ Coordinates\ (x,y,z)\begin{cases} y > f(x,z)\ (No\ Contact) \\ y = f(x,z)\ (Contact\ Begins) \\ y < f(x,z)(Contact\ Force\ Present) \end{cases}$$

There is a second check as well that determines if a contact force is to be applied to the model which evaluates whether or not a point lies within the two-dimensional projection of the convex hull. This is important as it is feasible for a point to lie on the contacting surface yet fall outside of the convex hull and under this scenario no contact should occur.

If both the height function and the convex hull function are met, then the normalized force will be calculated as a function of penetration, material stiffness and acceleration. This force is then applied to the system and the results are accounted for as a contact force in the next timestep (Figure 93). It is important to mention that because the contact detection algorithm accounts for proceeding and subsequent points, the model is unable to start in contact as the force cannot be calculated numerically.

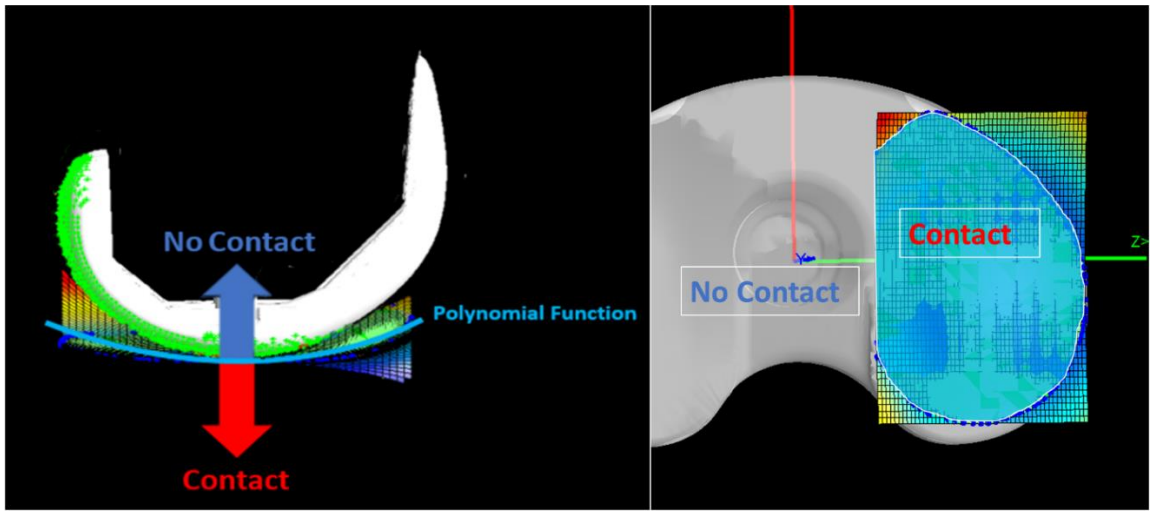


Figure 92: In order for the contact detection algorithm to denote contact, two conditions must be met. First, the point cloud on the femoral component must be less than the polynomial surface for the bearing (left) and second, this contact must occur within the projection of the convex hull (right).

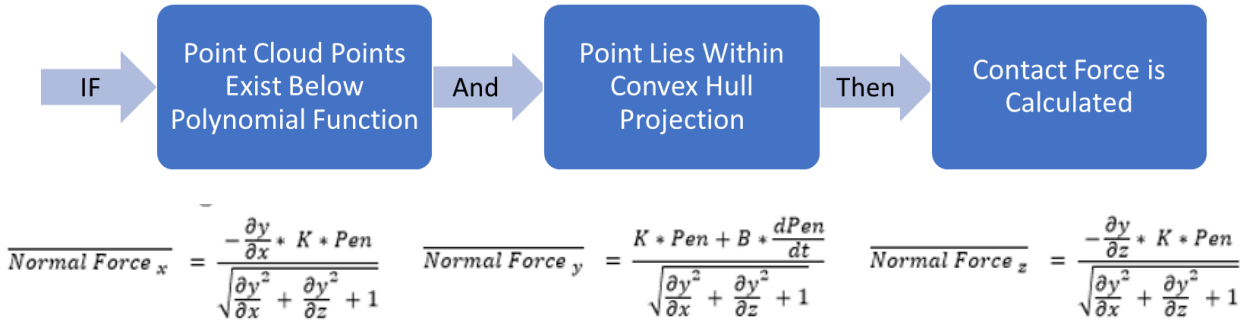


Figure 93: If the two conditions are met for contact detection to occur, then a force will be calculated as a function of point acceleration, penetration and material stiffness and fed back into the mechanical system.

7.3.2 CAD Model Creation

Built into the user interface is the ability to alter the polynomial surface which serves as the bearing surface contact for the model. There are four main factors that can be changed, coronal conformity, sagittal conformity, tilt and height. The height is adjusted by increasing or decreasing the constant term in the polynomial expression, the tilt is affected by changing the linear term in the AP or ML direction. The conformity is altered by changing the x or z squared term for sagittal or coronal respectively (Figure 94).

There are two types of outputs that once extracted may be of use in the reflection of any changes made in the user interface. The first of these is a mesh which is a geometric surface that contains a set of points and associated faces that connect those points. While this appears as a standard CAD surface, it is of note that there is not volume associated with it, nor can the shape be edited in any way. The mesh itself can be used to create mathematical constraints to evaluate the extracted device in a different model (this is exactly what this model does). The other type of output is more for manufacturing and outputs a mathematical surface defined by lines referred to as NURBS (non-rational bias splines) while these appear similar to mesh structures, they are defined mathematically and can be both edited and combined to make a surface in a sweep or loft type of process. Unlike meshes, these component surfaces can be combined with existing geometries in order to create solid parts. Because there are important facets of both of these outputs, both are produced by the model.

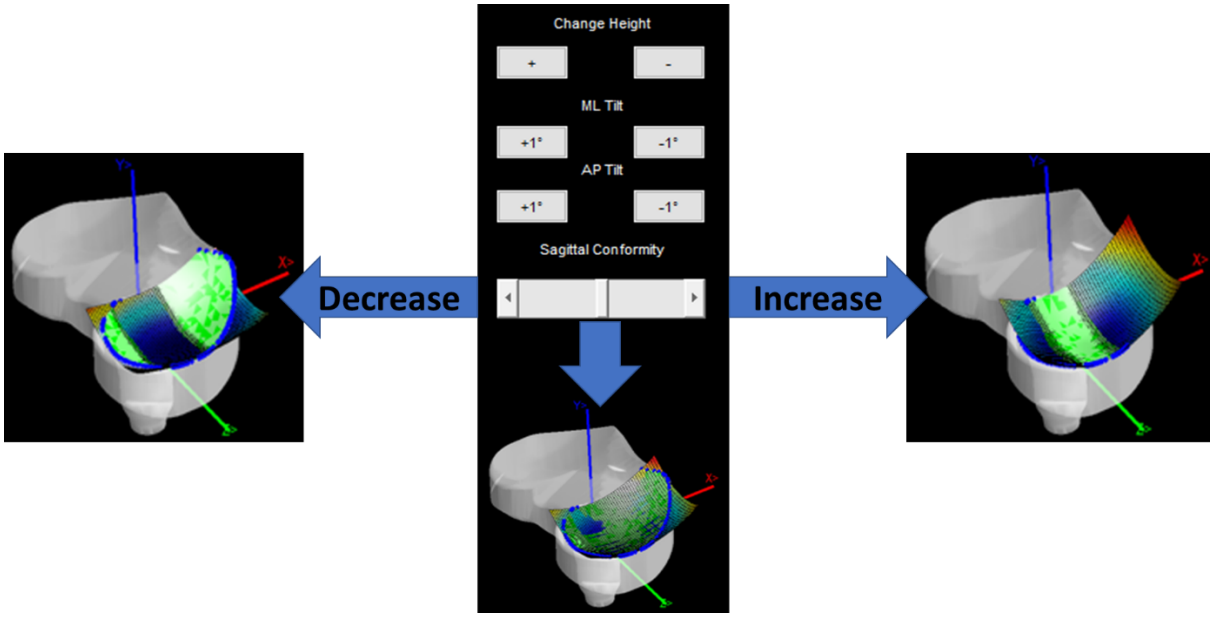


Figure 94: As all polynomial surfaces are generated, the interface affords the opportunity to make changes with respect conformity, height and tilt. Possible the most relevant of these changes is the ability to change sagittal conformity which can be decreased (left) or increased (right).

To export a model, the code has been amended to include a feature that has been added to output any changes made to the polynomial surfaces. The code will then prompt for a save location for an STL file followed by a location for an excel sheet with the parametric equations (Figure 95).

These two outputs encompass both the mesh (stl) and the matching parametric surfaces that make up the newly defined polynomial surface that can then be used in a simulation. Later iterations may export these at runtime, however at the moment the most intuitive time to generate the models is as they are being created in the code.

7.3.3 Defining Geometries

Many models (this one included) operate using mathematically defined meshes to provide the geometric constraints of the implant components. To do this the code takes the mathematically defined surface from the generated polynomial equations and assigns arbitrary graphic points based on the resolution of the surface. These points are then connected through normal faces and output as .stl files. This is done individually by surface (Figure 96) which can then be combined as needed in a cad program.

7.3.4 Creating Parametric Surfaces

Creating an editable surface is much more complicated than simple geometric surfaces. This is in part due to the need to create mathematical vectors (splines) which then can be lofted together to create a mathematically defined surface. In order to create these surfaces, the first determination that must be

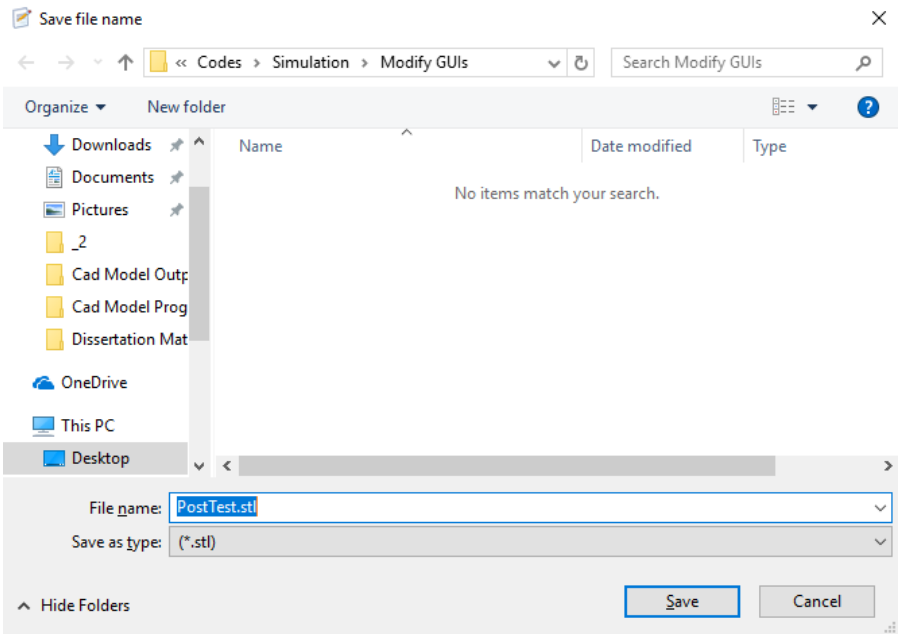


Figure 95: The user is given the option by the interface to select a destination for the output of the stl files and any associated parametric equations.

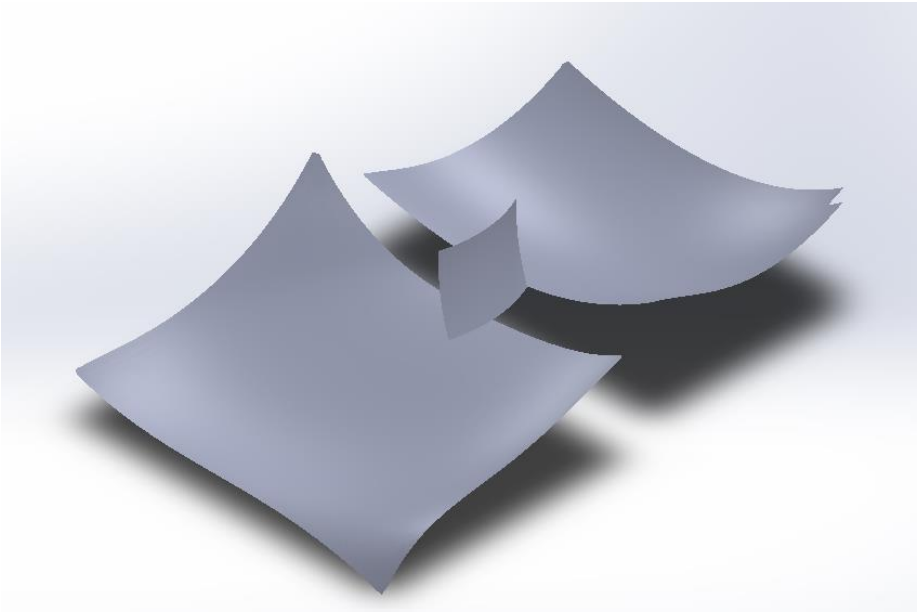


Figure 96: All surfaces on the bearing component can be exported as mesh surfaces for medial and lateral bearing surfaces as well as bearing post surfaces.

made is the number of mathematically defined splines that are needed. While this may vary on a case by case basis, three splines to define each direction.

While the placement of these splines is arbitrary, the most efficient place to start is in the front plane or the right plane. Doing so simplifies the mathematical expression from 21 variables down to 6. This is the case because the cross dimensional term becomes zero. This means that in the front plane z becomes zero and in the right plane x becomes zero. This simplifies the expressions as such that:

$$\begin{bmatrix} C & z & z^2 & z^3 & z^4 & z^5 \\ x & xz & xz^2 & xz^3 & xz^4 & xz^5 \\ x^2 & x^2z & x^2z^2 & x^2z^3 & x^2z^4 & x^2z^5 \\ x^3 & x^3z & x^3z^2 & x^3z^3 & x^3z^4 & x^3z^5 \\ x^4 & x^4z & x^4z^2 & x^4z^3 & x^4z^4 & x^4z^5 \\ x^5 & x^5z & x^5z^2 & x^5z^3 & x^5z^4 & x^5z^5 \end{bmatrix} => \begin{bmatrix} C \\ x \\ x^2 \\ x^3 \\ x^4 \\ x^5 \end{bmatrix} if\ z = 0$$

$$\begin{bmatrix} C & z & z^2 & z^3 & z^4 & z^5 \\ x & xz & xz^2 & xz^3 & xz^4 & xz^5 \\ x^2 & x^2z & x^2z^2 & x^2z^3 & x^2z^4 & x^2z^5 \\ x^3 & x^3z & x^3z^2 & x^3z^3 & x^3z^4 & x^3z^5 \\ x^4 & x^4z & x^4z^2 & x^4z^3 & x^4z^4 & x^4z^5 \\ x^5 & x^5z & x^5z^2 & x^5z^3 & x^5z^4 & x^5z^5 \end{bmatrix} => \begin{bmatrix} C & z & z^2 & z^3 & z^4 & z^5 \end{bmatrix} if\ x = 0$$

In addition to these simplifications the parametric equations need to also be normalized such that the resulting parameters are a function of t where tϵ[0,1]. This can be done by creating x and z functions such that the input t values will be between 0 and 1. This is done for example by multiplying the difference between xmin and xmax by t and adding xmin.

$$f(x) = \Delta x * t + xmin$$
$$f(z) = \Delta z * t + zmin$$

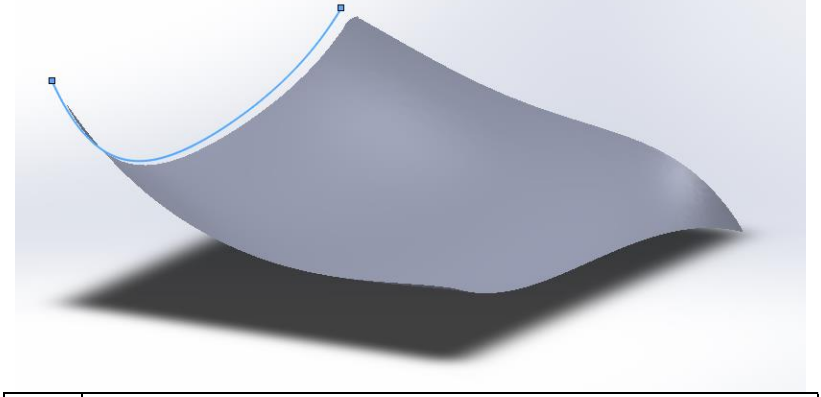
Evaluating these expressions for t gives the parametric curves that need to be created to replicate the new geometry. While this is a broad example, the end result once the values are applied can be seen below in the form of both equations and corresponding surfaces (Figure 97). These are referred to as homogenous equations as they assume to account for a single approximated axis.

Unfortunately, two splines are not sufficient to map the geometry of this surface, attempting to do so would simply sweep the two splines alone each other creating a continuation of the existing splines. In order to account for the intricacies of the surface, two additional splines need to be added in each direction. Because these are no longer on the primary drawing planes, this means that the cross terms are no longer zero and all 21 terms must now be used as each parameter effects a different aspect of the equations (Table 6). These are sometimes referred to as particular or auxiliary equations.

While the complexity is substantially greater the basic principle is still the same. Create expressions using the equations for the polynomial surface (this time a constant will be included in leu of 0) and determine the function of t to normalize the equation between 0 and 1. These constants were chosen to be at one third and two thirds of the total length of the surface (Figure 98).

This same principle can also be applied to the other articulating surfaces in devices such as the Posterior stabilized TKA (Figure 99). These curves are instrumental in the creation of parametric surfaces that can be knitted to existing surfaces to create three dimensional bodies. In this case, SolidWorks was used to assemble the equations. And then the model outputs these equations, and

Name	Lateral Poly Sagital Curve 1					
	XLAW		YLAW		ZLAW	
Formula	SLX1*t+SLXC		SLY5*t^5+SLY4*t^4+SLY3*t^3+SLY2t^2+SLY1*t+SLYC		SLZC	
	SLX1	40.24	SLY1	-55.6869	SLZ1	
	SLX2		SLY2	120.1548	SLZ2	
	SLX3		SLY3	-113.3993	SLZ3	
	SLX4		SLY4	43.3892	SLZ4	
	SLX5		SLY5	1.411	SLZ5	
	SLXC	-20.46	SLYC	7.4089	SLZC	0



Name	Lateral Poly Coronal Curve 1					
	XLAW		YLAW		ZLAW	
Formula	CLXC		CLY5*t^5+CLY4*t^4+CLY3*t^3+CLY2*t^2+CLY1*t+CLYC		CLZ1*t+SLZC	
	CLX1		CLY1	0.9961	CLZ1	-31.47
	CLX2		CLY2	-25.9569	SLZ2	
	CLX3		CLY3	85.5501	SLZ3	
	CLX4		CLY4	-79.7059	SLZ4	
	CLX5		CLY5	22.946	SLZ5	
	CLXC	0	CLYC	-5.6622	SLZC	32.35

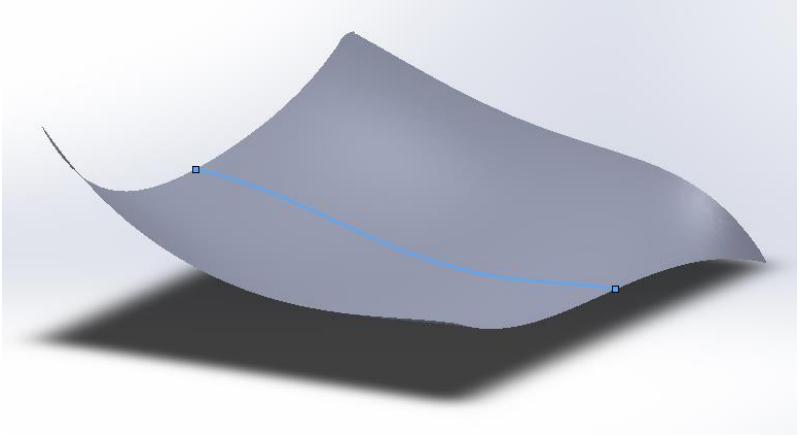


Figure 97: The parametric equations are exported in the form of an excel sheet which can be easily imported into NX or any other prevalent CAD Software. These equation sets are normalized between 0 and 1 for values of t and corresponds to a parametric curve that matches the exported surface meshes. This is done to offer the capability to edit and knit surfaces as needed.

Table 6: The spline directions and associated variables are dependent on the surface being approximated. Each spline consists of a constant, a height function, and a time function.

	For Bearing Surface	For Post Surface
Proximal-Distal Direction	Not Applicable	X= Height Function Y=t Z=Constant
Medial-Lateral Direction	X= Constant Y=Height Function Z=t	X= Height Function Y=Constant Z=t
Anterior-Posterior Direction	X= t Y=Height Function Z= Constant	Not Applicable

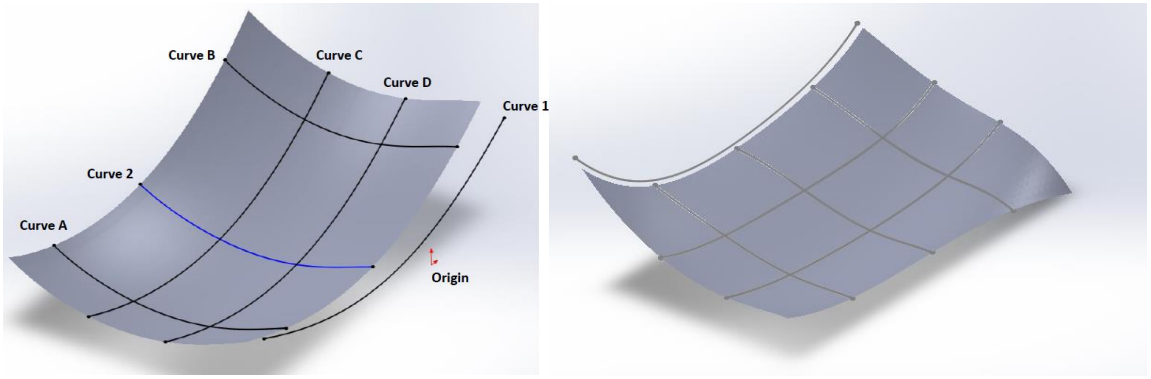


Figure 98: The surface will be created from six total splines (three in each direction). The splines that align with drawing planes are labeled with numbers 1 and 2 (the constant expression is zero) and the additional splines are labeled with letters A,B,C,D.

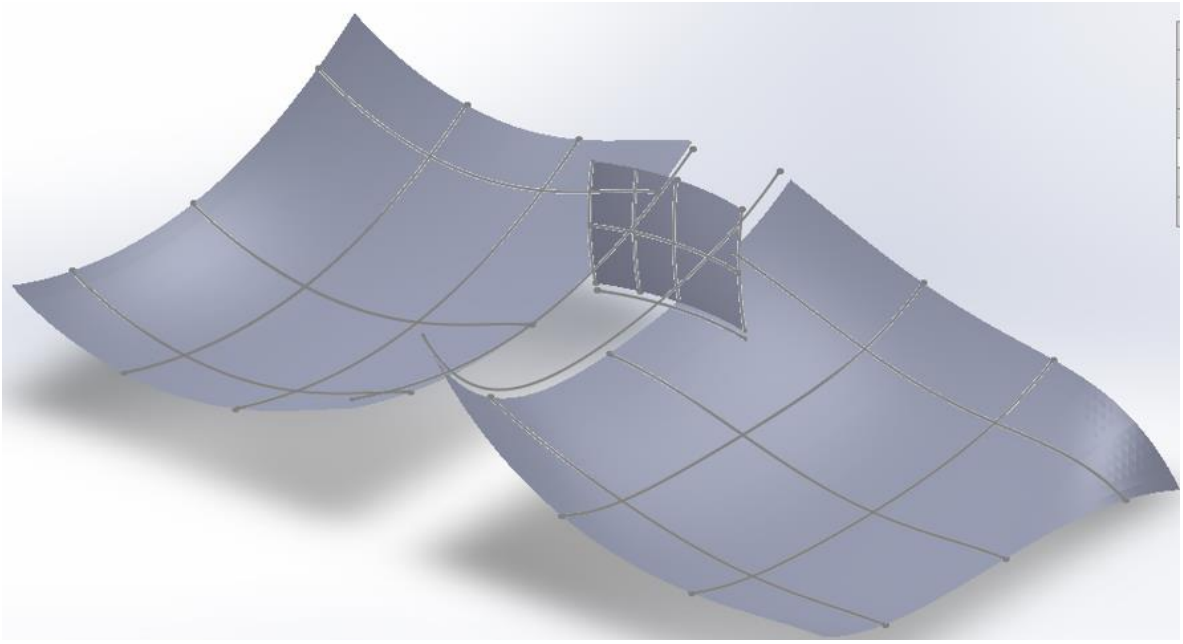


Figure 99: The surfaces with associated component splines can be combined to demonstrate all elements of the parametric surface spline creation.

although SolidWorks was used in this case, any parametric modeler will be able to visualize the parametric equations such as Geomagic or NX. Below is an example of the output from the model (Figure 100 & Figure 101).

7.4 Conformity Results

While there are several factors that can be changed in the user interface, the most valuable of these from a design perspective is the ability to change bearing conformity. In general, the medial pivot TKA design centers around mechanical constraint of the medial condyle during flexion. For this reason, a common design principle is to increase medial conformity which in turn increases constraining contact forces leading to medial pivot style kinematics (Figure 102). While this is the case, it is also important not to over constrain the condyle geometries which leads to the competing philosophy of reducing conformity. In doing so, the knee is permitted to operate more freely, which in a successful design will lead to desired kinematics.

Three analyses were performed using the most recent iteration of the model using a stabilized TKA type. It is of note that the scope of this analysis is to evaluate the effects of medial and lateral conformity. For this reason, the post was deliberately omitted as a 120-degree deep knee bend was performed. The first of the three TKA scenarios was simply a baseline, the second was a decrease in the conformity of the lateral condyle bearing surface, and third was an additional decrease in medial condyle bearing conformity. The conformity is changed by varying the x^2 term in the polynomial equations. This same method can be applied to coronal conformity as well.

Homogenous Curves							Curve #
Name	Medial Poly Sagital Curve 1						
tϵ[0,1]	XLAW		YLAW		ZLAW		
Formula	SLX1*t+SLXC		SLY5*t^5+SLY4*t^4+SLY3*t^3+SLY2t^2+SLY1*t+SLYC		SLZC		
	SLX1	37.7974	SLY1	-5.8484	SLZ1		
	SLX2		SLY2	7.271	SLZ2		1
	SLX3		SLY3	6.132	SLZ3		
	SLX4		SLY4	11.2553	SLZ4		
	SLX5		SLY5	-15.9726	SLZ5		
	SLXC	-20.452	SLYC	1.9077	SLZC	-4	
Name	Medial Poly Coronal Curve 1						
tϵ[0,1]	XLAW		YLAW		ZLAW		
Formula	CLXC		CLY5*t^5+CLY4*t^4+CLY3*t^3+CLY2*t^2+CLY1*t+CLYC		CLZ1*t+SLZC		
	CLX1		CLY1	17.4472	CLZ1	-25.2824	
	CLX2		CLY2	-47.897	SLZ2		2
	CLX3		CLY3	49.4814	SLZ3		
	CLX4		CLY4	-10.634	SLZ4		
	CLX5		CLY5	-8.4959	SLZ5		
	CLXC	0	CLYC	-2.5246	SLZC	-6.5076	

Figure 100: The homogenous equations (those that rest on the anatomic planes) are determined through two spline expressions.

Particular (Auxiliary) Curves							
Name	Medial Poly Coronal Curve A						
tϵ[0,1]	XLAW		YLAW		ZLAW		
Formula	CLXC		CLY5*t^5+CLY4*t^4+CLY3*t^3+CLY2*t^2+CLY1*t+CLYC		CLZ1*t+SLZC		
	CLXA1		CLYA1	17.4472	CLZA1	-25.2824	
	CLXA2		CLYA2	-44.7219	SLZA2		A
	CLXA3		CLYA3	43.2531	SLZA3		
	CLXA4		CLYA4	-6.5239	SLZA4		
	CLXA5		CLYA5	-9.5125	SLZA5		
	CLXAC	-13.4983	CLYAC	-1.6672	SLZAC	-6.5076	
Name	Medial Poly Coronal Curve B						
tϵ[0,1]	XLAW		YLAW		ZLAW		
Formula	CLXC		CLY5*t^5+CLY4*t^4+CLY3*t^3+CLY2*t^2+CLY1*t+CLYC		CLZ1*t+SLZC		
	CLXA1		CLYA1	17.4472	CLZA1	-25.2824	
	CLXA2		CLYA2	-51.0721	SLZA2		B
	CLXA3		CLYA3	58.2175	SLZA3		
	CLXA4		CLYA4	-16.9648	SLZA4		
	CLXA5		CLYA5	-7.272	SLZA5		
	CLXAC	13.4983	CLYAC	2.8876	SLZAC	-6.5076	
Name	Medial Poly Sagital Curve C						
tϵ[0,1]	XLAW		YLAW		ZLAW		
Formula	SLX1*t+SLXC		SLY5*t^5+SLY4*t^4+SLY3*t^3+SLY2t^2+SLY1*t+SLYC		SLZC		
	SLXC1	37.7974	SLYC1	-5.8484	SLZC1		
	SLXC2		SLYC2	14.0585	SLZC2		C
	SLXC3		SLYC3	-4.8567	SLZC3		
	SLXC4		SLYC4	16.828	SLZC4		
	SLXC5		SLYC5	-14.9134	SLZC5		
	SLXCC	-20.452	SLYCC	-2.4636	SLZCC	-23.1941	
Name	Medial Poly Sagital Curve D						
tϵ[0,1]	XLAW		YLAW		ZLAW		
Formula	SLX1*t+SLXC		SLY5*t^5+SLY4*t^4+SLY3*t^3+SLY2t^2+SLY1*t+SLYC		SLZC		
	SLXD1	37.7974	SLYD1	-5.8484	SLZD1		
	SLXD2		SLYD2	11.6169	SLZD2		D
	SLXD3		SLYD3	-0.735	SLZD3		
	SLXD4		SLYD4	14.8405	SLZD4		
	SLXD5		SLYD5	-14.6357	SLZD5		
	SLXDC	-20.452	SLYDC	-2.2417	SLZDC	-14.8509	

Figure 101: The remaining four expressions for the parametric splines are output in terms of their spline components.

Intuition would dictate that increasing medial conformity would inhibit medial condyle motion likewise, reducing bearing conformity would increase motions (Figure 102). Perhaps most importantly, there is a noticeable kinematic difference when only the lateral condyle conformity is changed. This suggests a strong interplay between the properties of both the medial and lateral condyles.

Such a change was also applied to the lateral side produces similar results with respect to increases in condyle motions as conformity is reduced. As with the medial conformity, there is a definite relationship between conformities of medial and lateral sides as individual increases of one likewise influences the other (Figure 103). Through subsequent analysis there appears to be an implicit relationship between the medial and lateral conformities. It is widely believed that axial rotation bears a much more explicit relationship as medial and lateral conformity effect medial and lateral translations which in turn determines axial rotation. In this case, it is evident that conformity changes have led to increases in axial rotation. As stated before, this relationship makes sense as decreasing conformity leads to increased magnitudes of kinematic changes in condyle translation due to limited mechanical constraints. Increasing translation magnitudes likewise contributes to increased rotation magnitudes (Figure 104Figure 105). Therefore, there may be kinematic benefits to increasing and decreasing bearing conformity as it pertains to TKA device design.

While there certainly is validity to these results, the preceding data was acquired from a model that incorporated a cam/post mechanism. This means that there are additional surfaces which may influence kinematics beyond

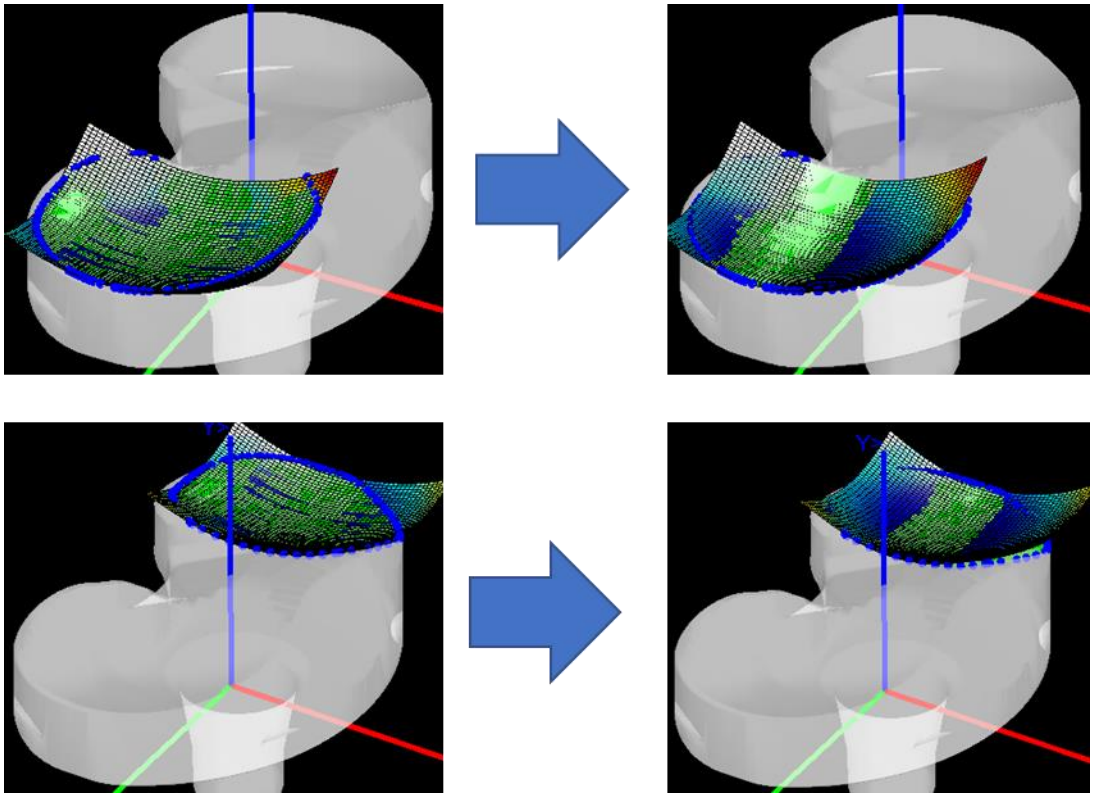


Figure 102: The medial and lateral conformity can be adjusted in the model. In this case, the increased conformity is exaggerated to show the conformity differences. Note that this analysis also included a cam and post mechanism (not shown).

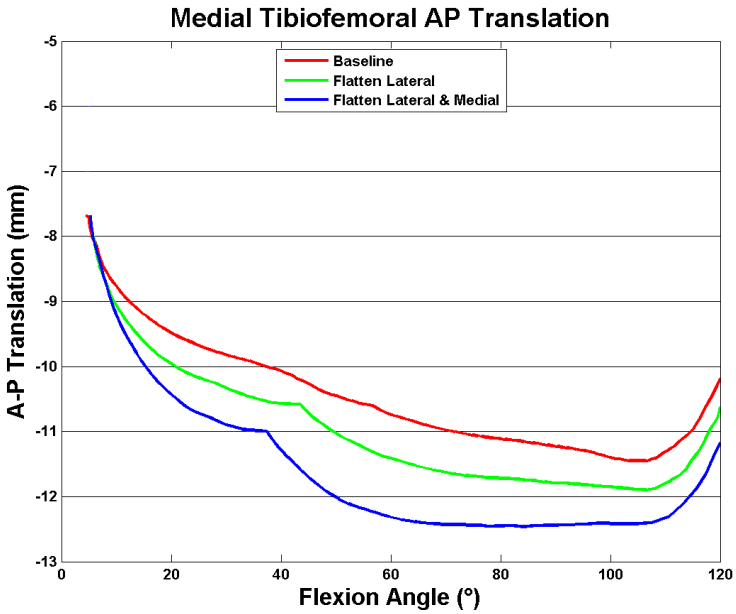


Figure 103: Decreasing bearing conformity appears to increase medial translation magnitudes.

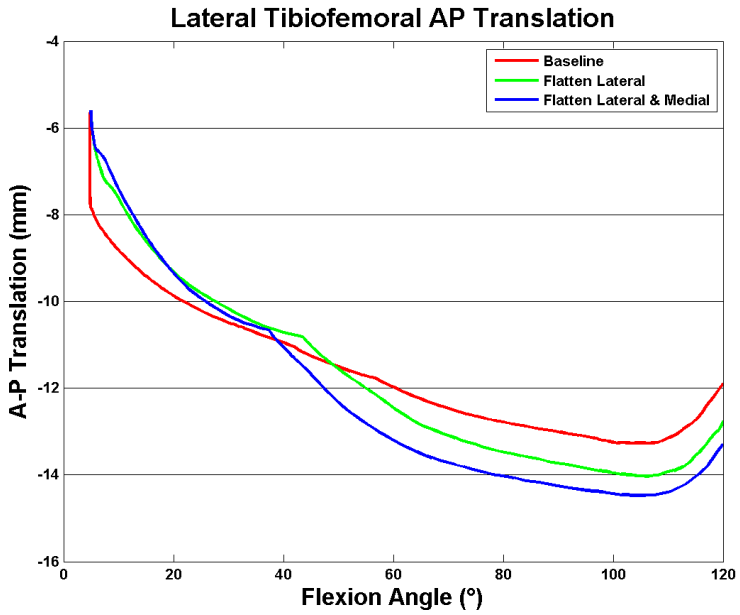


Figure 104: Decreasing bearing conformity appears to increase lateral translation magnitudes.

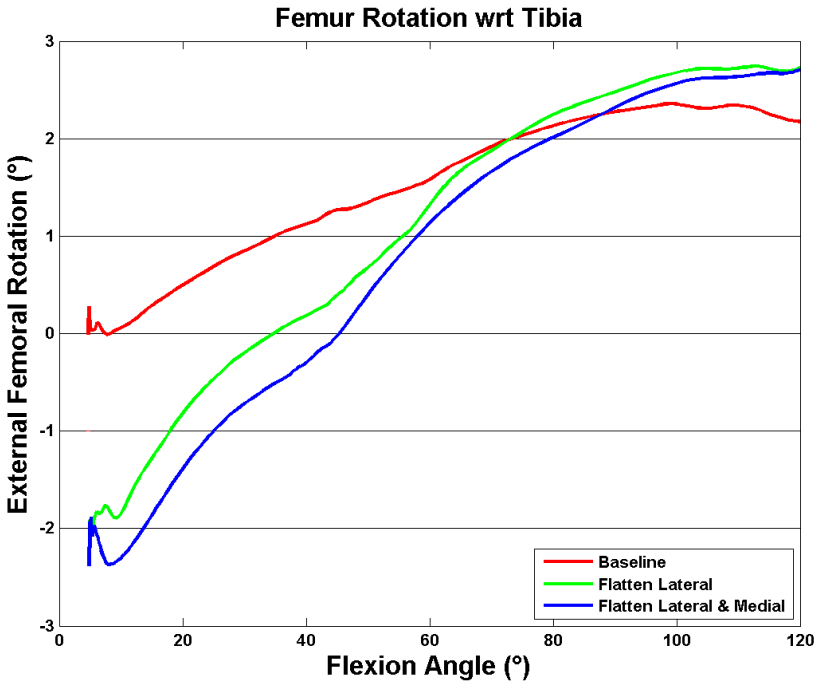


Figure 105: Decreasing bearing conformity appears to facilitate axial rotation magnitudes.

conformational differences in the articulating bearing surface. For this reason, an addition analysis was performed using PCR TKA device to control for any post mechanism influence. This was done by varying medial and lateral conformity both independently and simultaneously.

The results from such analysis were similar to that of the analysis with the post mechanism. Increasing conformity appears to demonstrate that increasing bearing conformity leads to decreased anteroposterior motion over the course of a flexion of the respective condyle, increased anteroposterior motion over the course of a flexion of the opposing condyle, and increased contact forces between femur component and bearing (Figure 106). Material wear tends to increase proportionally with contact forces, thus proper design should caution against too much reliance on conformity to drive motion since wear can be substantially increased.

7.5 Post Placement Results

The model can be used to successfully identify kinematic trends and their relationships between medial and lateral bearing conformity. While this is useful, the model also allows for the assessment of post shape and location to determine how these chances affect TKA kinematics. This contribution focuses primarily on post location, as there are a multitude of cam and post factors that can affect overall kinematics.

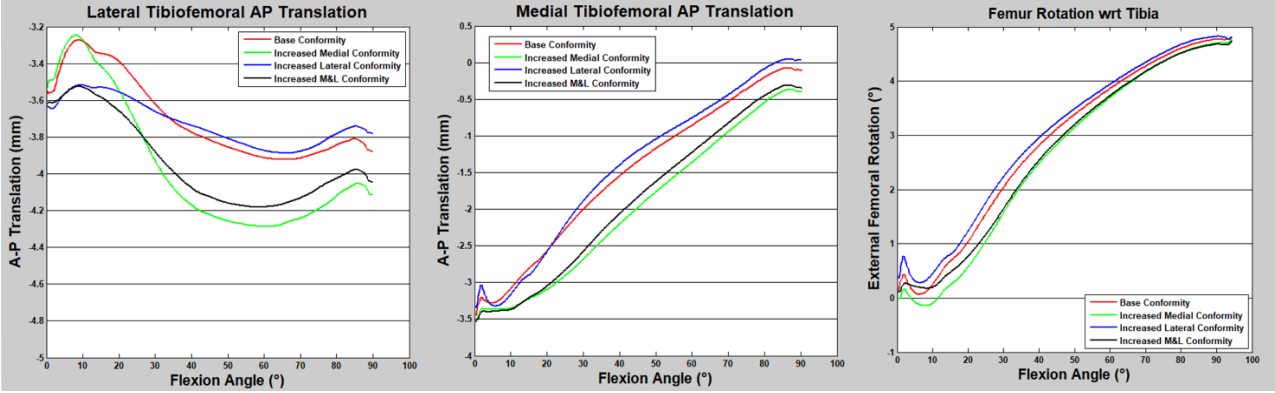


Figure 106: To test conformity without interaction from post mechanisms, a similar study was setup using a PCR device which varied medial and lateral bearing conformity independently and concurrently.

To test this effect, five simulations were run in total and the resulting kinematics were determined using the forward model. These intervals include a baseline, as well as four scenarios where the post is moved in either the anterior or posterior direction (Figure 107). The in vivo kinematics were then simulated under these conditions in an effort to develop a more thorough understanding of the effect that post placement has on the primary kinematic values of interest. It was a PS post used in this analysis as this type of post is common in orthopedic devices.

These simulations showed that only two of the simulations experienced cam post engagement and these two simulations were where the post was moved four and eight millimeters posteriorly (Figure 108).

In PS implant designs, the model shows that post shape and position can dictate device performance, including forces between the PS cam and post which increase linearly during flexion and moving the post anteriorly or posteriorly engages the mechanism later and earlier, respectively. If moved anteriorly enough, engagement may not even occur. When earlier engagement does occur, the forces that are experienced tend to be higher. It is also important to note that kinetic results are also partially dependent on bearing design, as equilibrium dwell points can vary based on bearing geometry so the relationship between bearing and cam and post design is very much interrelated.

7.6 Summary and Conclusion

This report outlines both a recap of recent changes to the contact detection algorithm in the model in addition to the ability to create and edit CAD models.

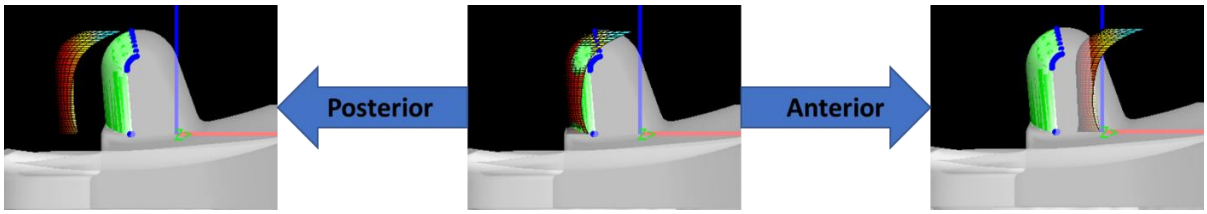


Figure 107: To test post placement using the model, several simulations were set where the position of the post mechanism was moved either anteriorly or posteriorly.

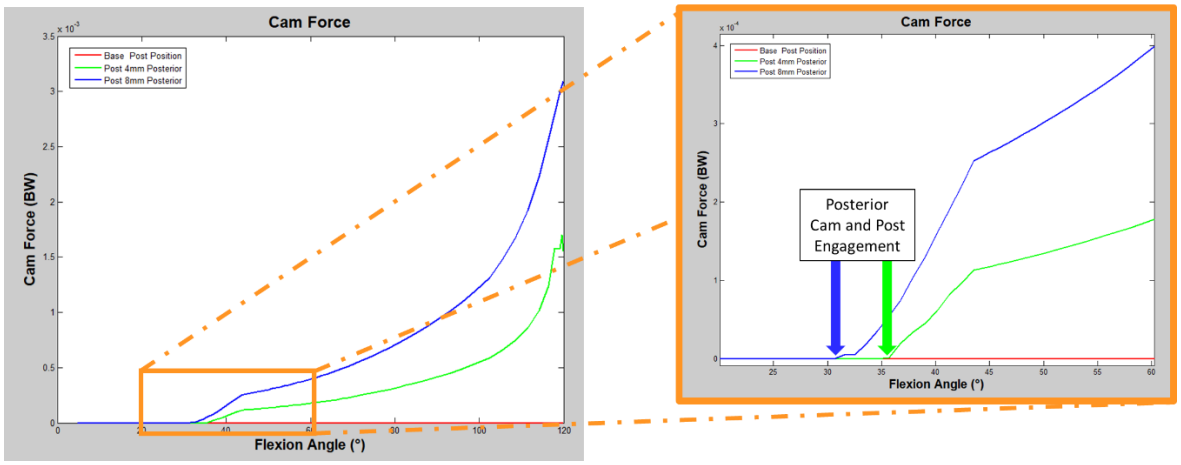


Figure 108: The model showed that moving the cam and post mechanism posteriorly both lead to earlier engagement and higher forces overall when engagement occurred.

These models can then be exported as both mesh and/or parametric surfaces which are useful to research and manufacturing, respectively. Using this new technique, an analysis was carried out evaluating the results of decreasing both medial and lateral conformity, independently and simultaneously. It was observed that both medial and lateral conformities affected overall kinematics with the reduction in conformity manifesting greater magnitudes of motion through a minimization of constraints. These variations directly contributed to changes in axial rotation, emphasizing the importance of medial and lateral conformity collectively in the influence of optimizing joint kinematics. In addition, further analysis is being carried out to improve the user interface and better employ parameterization to create a more robust model useful in more unique aspects of surgical cases and patient groups.

CHAPTER EIGHT: PARAMETERIZING DEMOGRAPHICS

8.1 Purpose

While the model is successful in the simulation of in vivo kinematics, one of the intrinsic limitations lies in that the testing is essentially of a single average patient. In some applications this may be sufficient, but to improve the robustness of the model and apply kinematic assessments to various demographic groups to assess morphology and motion differences (Figure 109). These variations in motion patterns are important because they may be unique to particulate demographic groups. And for this reason, it is possible that designing devices to meet these groups may facilitate more successful patient outcomes.

The goal for this contribution is to parameterize the model between different subject groups, and in doing so, gather data regarding the motion behaviors and contact forces. This will be done evaluating both gender and ethnicity as determining factors. Two subjects are evaluated from each group in an effort to give a cursory evaluation of individual variability within these groups.

Not only does such a contribution enhance the uses of the model as an assessment tool, but the data produced could be useful in determining which devices are ideal for which patients, thus providing surgeons with additional information to make more patient centered surgical decisions

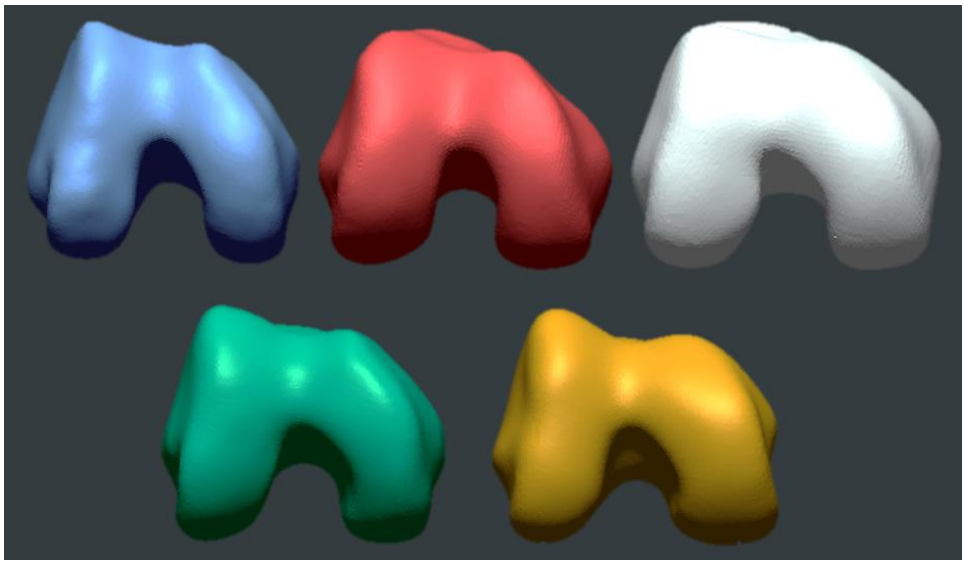


Figure 109: Distinct morphological differences exist on the distal femur between genders, ethnicities and individual subjects.

8.2 Introduction

The model thus far has centered almost exclusively in the analysis a single patient. While it is understood that there is substantial individual variability in the knee, the original inclusion of these geometries attempted to circumvent this issue by incorporating the average geometries over a large number of patients. While this is effective in many cases, there are still many individuals that fall well outside of this average range. Furthermore, the average distribution likely varies more significantly for some groups than others, especially those underrepresented in the average data [162]. There is a need to understand and design devices that are not necessarily gender or race specific, but are evaluated and known to function well in these respective patients. Such a task requires a substantial investment in time and equipment to evaluate devices on such a broad scope, which is where mathematical modeling can be a useful tool to quickly and efficiently evaluate kinematics in multiple patient groups.

There are two main demographic factors that are believed to influence bone morphology and the scope of this contribution will focus on the dynamic modeling of gender and ethnicity [10, 70]. While there are a number of studies that have quantified dynamic differences between these respective groups, this contribution seeks to acknowledge these morphological differences, and in doing so, evaluate the interrelationship between bone morphology and kinematics using a theoretical methodology.

Studies have shown distinct morphological differences between men and women as well as Caucasian, African, and East Asian populations, specifically noting differences in dimensional ratios and curvature [70]. It is of note that

ethnicity and gender are not mutually exclusive; therefore, it is expected that morphological differences will be the summation of both ethnic and gender factors.

Mahfouz, et al. has done extensive work identifying anatomical bone morphologies using a 3D assessment (Figure 110 & Figure 111). This work has determined that six classifications of variations of femur geometries exist based upon dimensional ratios[70]. Leszko, et al. took this idea further and using fluoroscopy, established demographic differences and their associated effects on kinematics. It is important to note that these morphology differences are independent of scaling, so they are size indeterminant, which is why the proceeding analysis normalizes to control for size. Some studies have also attempted to use these anthropomorphic measurements to design knees better suited to certain populations [163]. While understanding the underlying morphology is important, the mechanics of the knee are the ultimate goal to facilitate performance and satisfaction.

Gender and ethnospecific morphology have two roles in the determination of joint mechanics. The most intuitive of the two factors is the geometry of the articulating surface itself. It stands to reason that significant variations in bone morphology will contribute to variations in mechanics, as the bone architecture serves as the constraining geometry for the joint interfaces. Less intuitive are the attachment sites for soft tissue, which are typically attached to bony prominences, and for this reason, distortions from general geometries can contribute to alternate locations for attachment sites. This is significant from a mechanics perspective as

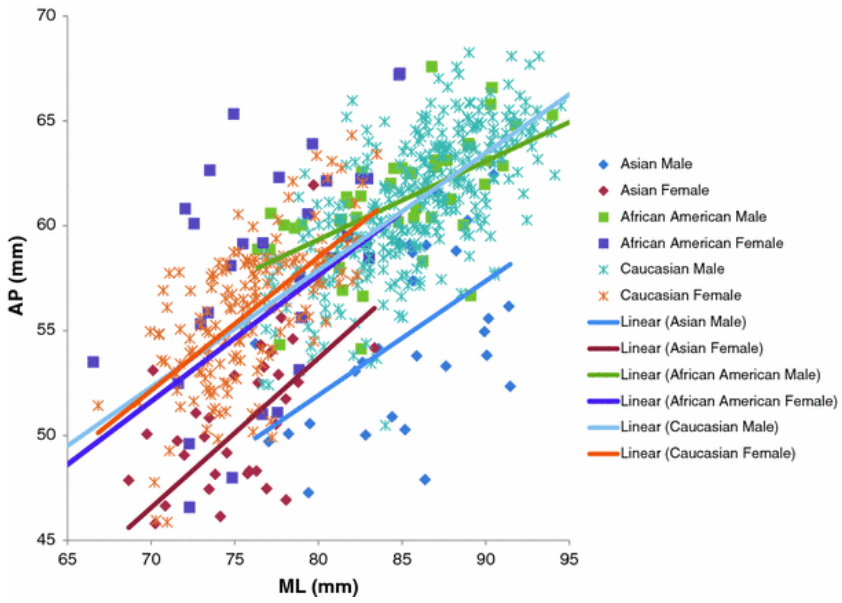


Figure 110: Mahfouz, et al demonstrated significant femoral morphological differences between anteroposterior and mediolateral bone dimensions [70].

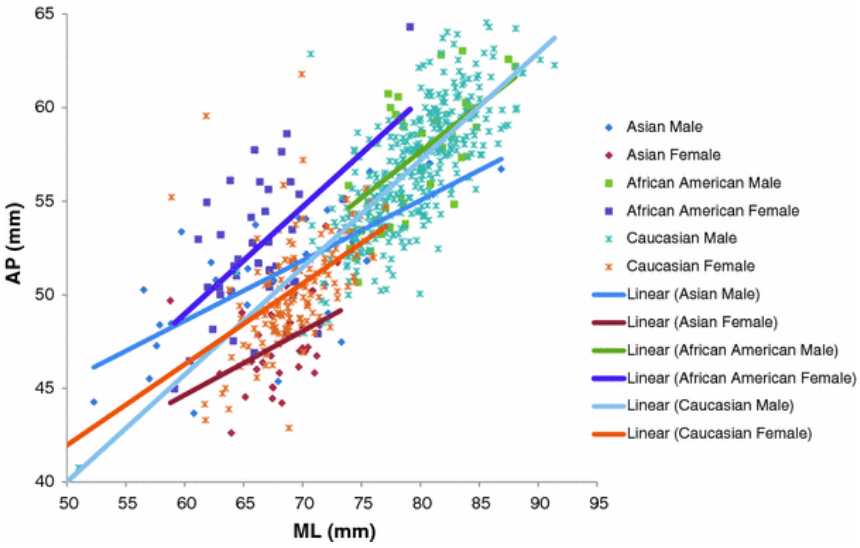


Figure 111: Mahfouz, et al. demonstrated significant tibial morphological differences also between anteroposterior and mediolateral bone dimensions [70].

the attachment sites apply vectors of constraining forces which are determined by both force magnitude and direction.

Due to the nature of soft tissue constraints, the first aspect to be evaluated using the model will be a sensitivity of the positions of the collateral and patellar ligaments. This will determine the effect of changing ligament attachment sites which becomes relevant when they vary between groups. A much heavier emphasis will be placed on the assessment of morphological differences and the associated effect on mechanics. Together these two aspects will give an enhanced perspective on knee mechanics for these groups.

While research has been undertaken to determine morphological differences between patients and link those differences to kinematic performance, this is an area where mathematical modeling can be particularly applicable to expand the depth and breadth of the analysis.

8.3 Methods

8.3.1 Testing Ligament Attachment Sites

In order to evaluate the effect of ligament attachment sites on joint mechanics, a sensitivity assessment was performed evaluating the origins and insertions of the LCL, MCL and patella ligament. This was done by moving the attachment sites individually on the femur in the AP, ML, and SI directions and keeping all other parameters consistent (Figure 112). Values of three mm were used, as this is a reasonable deviation expected from morphological differences. This simulates potential variations in femoral attachment sites due to bone morphology. In addition, a second sensitivity was performed where the tibia

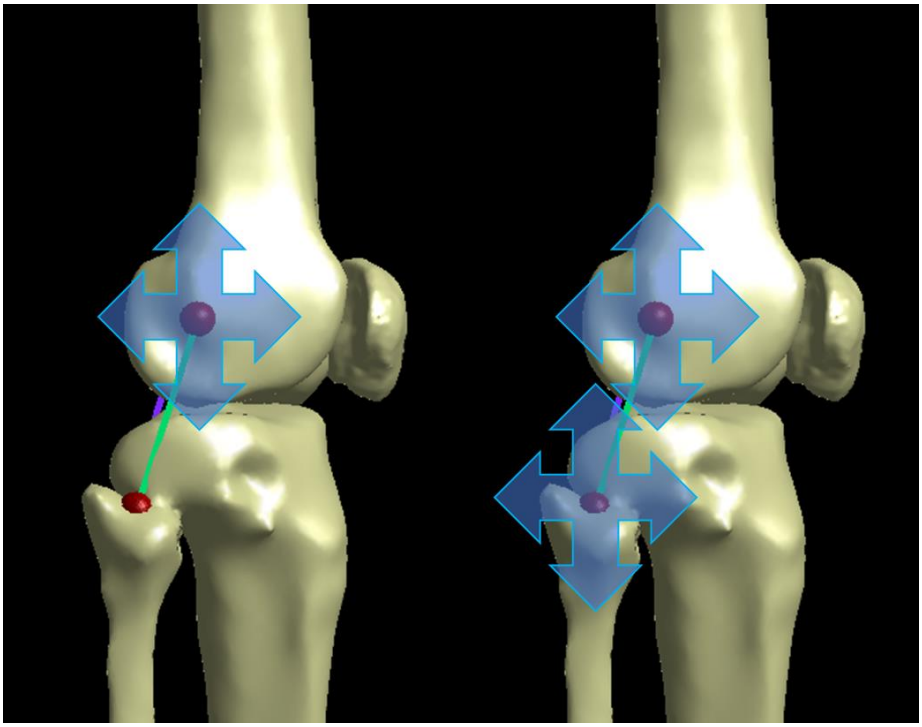


Figure 112: In order to assess the role of soft tissue location regarding kinematics, a sensitivity analysis will be performed both where only origins are shifted and where both origins and insertions are translated.

attachment sites were moved as well to simulate the entire ligament and both attachments being moved. In doing so, this presents several test cases testing ligament site attachment. These simulations were then evaluated for kinematics and compared to better understand the role of constraining soft tissue in the knee.

8.3.2 Testing Articulating Geometries

Using the process described in chapter four for the parameterization of the normal knee, CAD geometries for ten subjects were prepared to be loaded into the mathematical model. In an effort to identify gender and demographic relationships with respect to knee kinematics, these groups were identified as either male or female and Caucasian, African or East Asian (Figure 113). Much like the normal knee model creation, these models were derived from healthy CT scans which were subsequently smoothed and trimmed to improve model integration and stability.

The scope of this particular analysis is to determine the kinematic effect of articular shape, and every attempt has been made to control all other variables. Although it is neither feasible nor practical to account for all individual variations in heathy subjects, one of the factors that needed to be controlled was the size of the imported bone. To achieve this consistently, every model was normalized to an approximate width of 110 mm using a three-directional re-scale (Figure 114). Particular care was taken to use an isotropic scaling technique as the native curve radii and aspect ratio are maintained.

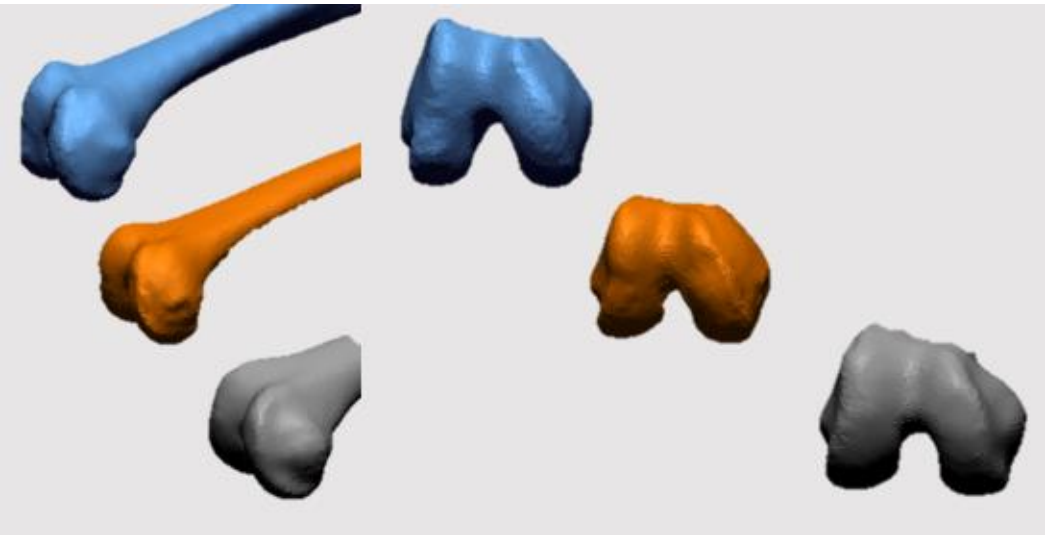


Figure 113: For all African (blue), Asian (orange) and Caucasian (grey) demographics tested, there are unique anatomical features that may contribute to kinematic aberrations.

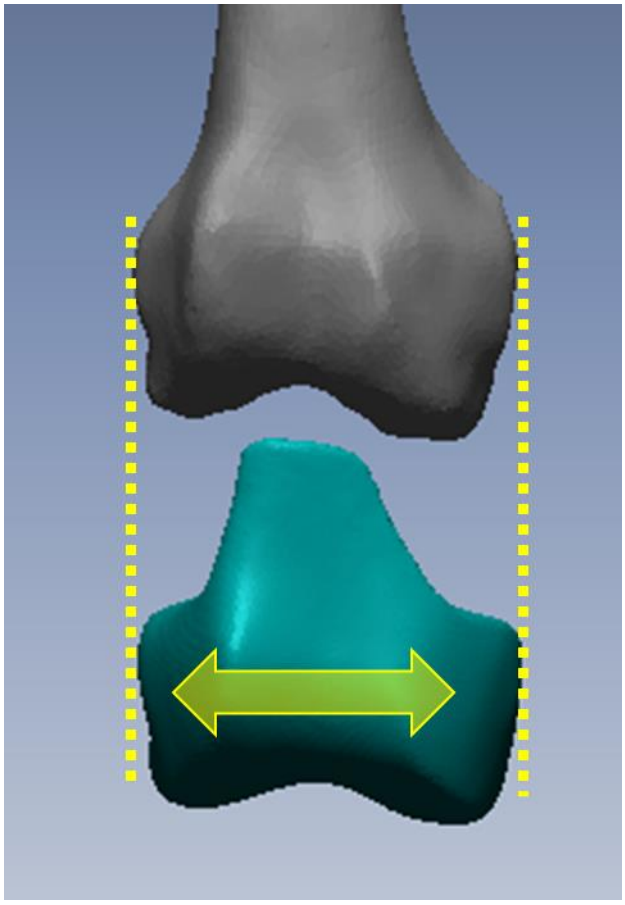


Figure 114: In order to control for bone size, all geometries under evaluation were isotopically scaled to a uniform mediolateral dimension.

Individual geometric parameters can be controlled; however, there is still going to be an influence of individual variations, especially in such a small group tested. While statistics are not feasible for the sample size given, the aim is more to compare these groups and achieve a cursory assessment of the individual variations that exist within these demographics. To achieve this assessment, two subjects from each group were assessed. This makes a total of ten simulations of hypothetical patients where there are two subjects each for five demographic groups.

Using initial conditions that were as similar as possible, all ten theoretical subject geometries were loaded into the model and simulated during an extension from a 90-degree bend of the knee. An extension model was used in lieu of a flexion model because of the ability to solve for equilibrium conditions. It would be expected that individual initial positions would vary respective to subject geometry so the settling component was used to attempt to recreate the stable initial conditions for each subject. Then the kinematics were assessed for each analysis.

8.4 Articular Morphology Results

It has been shown that there are morphological differences between male and female knees, specifically that on average female knees tend to be both more narrow and smaller in size compared to male knees [70]. The fundamental question relates to how these morphological differences relate to function and there is evidence to support that there is a relationship [10].

These gender differences are also consistent across all three of the main demographics tested in the scope of this contribution in addition to the

demographic specific morphology variations. Mahfouz, et al. used a 3D assessment to determine six variations of femur geometries based upon ratios between the dimensions. It is important to note that these morphology differences by definition are independent of scaling, therefore they are size indeterminant which is why the proceeding analysis normalizes to control for size.

8.4.1 Male Theoretical Patients

The two male theoretical subjects experienced knee motion well within the kinematic patterns of the normal knee demonstrated axial rotation and posterior femoral rollback. In total, subject one experienced approximately 19 degrees of femorotibial axial rotation (Figure 115), 12 mm of lateral femoral condyle posterior translation (Figure 116) and 2 mm of anterior medial femoral condyle motion (Figure 117). Subject two experienced greater axial rotation in addition to comparable lateral translation and greater anterior medial femoral translation.

8.4.2 Female Theoretical Patients

Comparing the male subjects to the two female subjects demonstrated greater magnitudes of femoral rotation with a total of approximately 28 degrees for subject one and 22 degrees for subject two with most rotation occurring between 0 and 30 degrees (Figure 118). Most of this rotation is driven by motion of the lateral femoral condyle which likewise concentrates most of its motion in early flexion (Figure 119). Both subjects also experienced highly stable medial condyles with less than 2 mm of motion anteriorly (Figure 120).

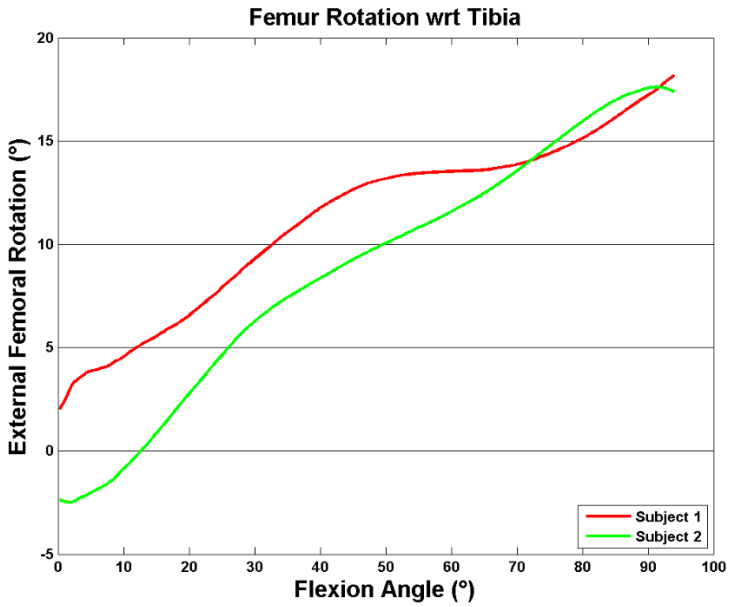


Figure 115: Theoretical subject 2 experienced greater femorotibial axial rotation.

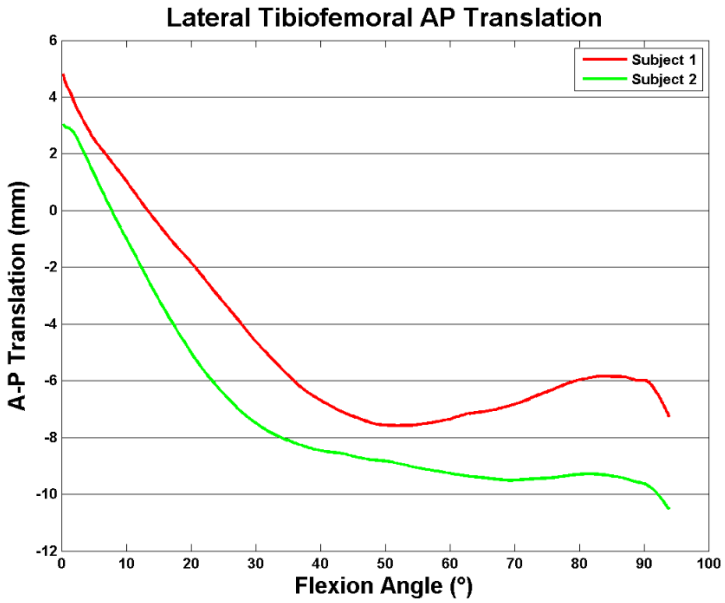


Figure 116: Theoretical subject 2 experienced greater lateral femoral condyle translation.

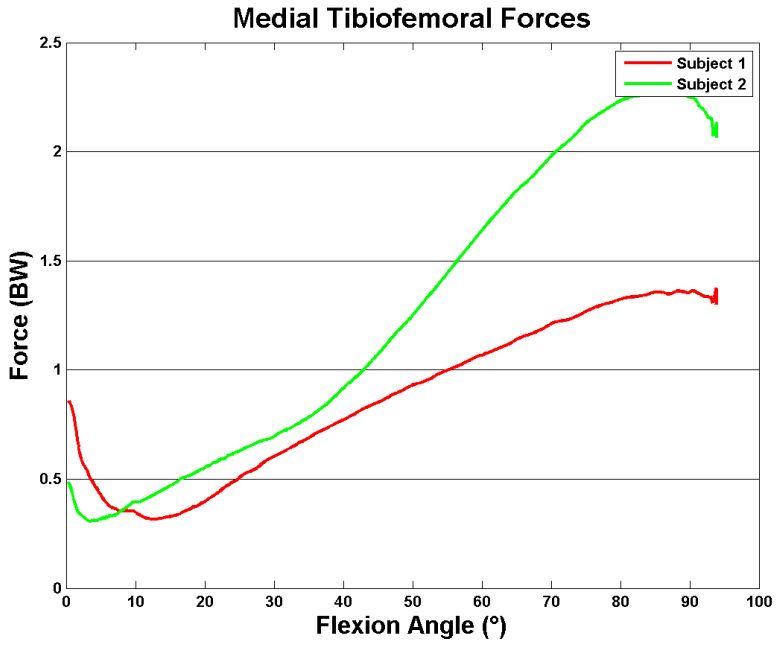


Figure 117: Theoretical subject 2 experienced greater medial femoral condyle translation.

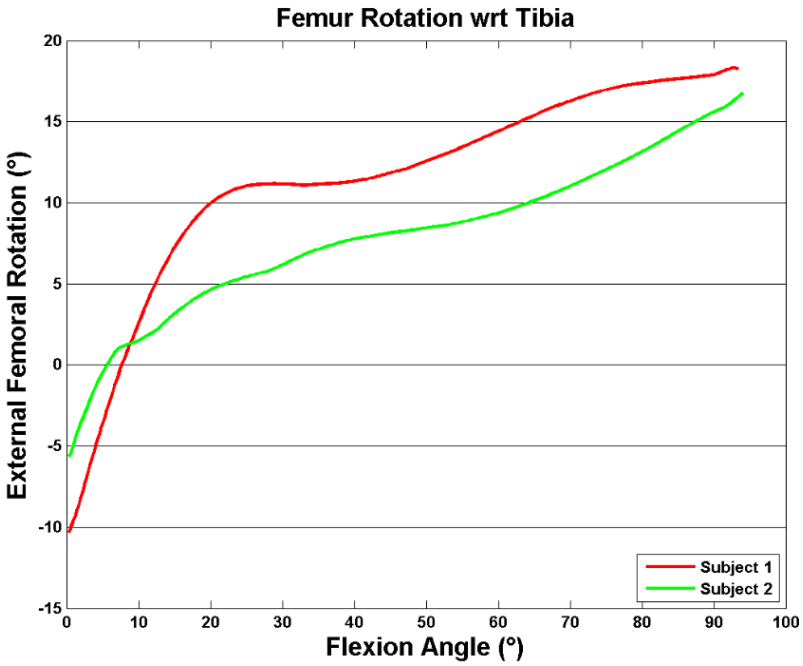


Figure 118: Female femoral tibial rotation for both theoretical subjects.

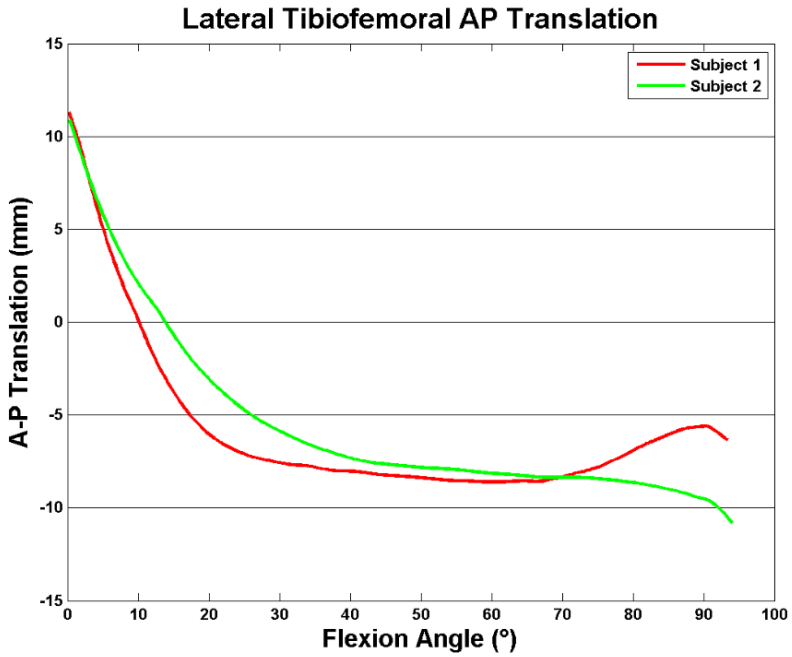


Figure 119: Female lateral femoral condyle translation for both theoretical subjects.

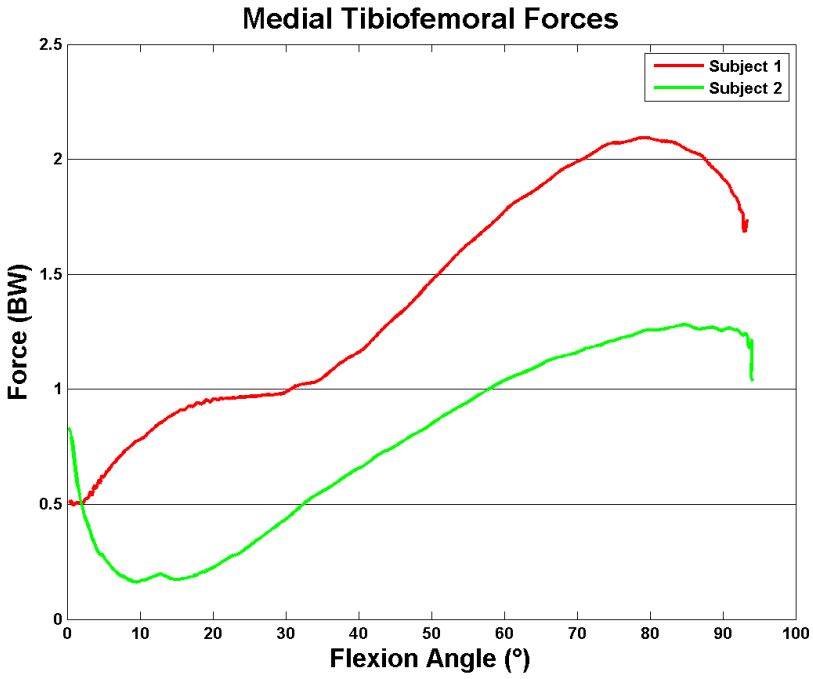


Figure 120: Female medial femoral condyle translation for both theoretical subjects.

8.4.3 Caucasian Theoretical Patients

Both Caucasian subjects overall experienced magnitudes of axial rotation comparable to other normal knee studies. What is interesting, however, about these two theoretical subjects is that the region of flexion from 10 degrees to 25 degrees is exceedingly stationary, especially compared to other subjects that experienced most of the overall motion in early flexion (Figure 121). This pattern appears to be due to a high magnitude of medial posterior rollback counteracting the lateral condyle rollback contributing to a net rotation of zero (Figure 122 & Figure 123). Despite demonstrating paradoxical rotation between the two subjects, the rotation patterns are consistent with normal knee motion except that the medial condyle experiences several millimeters of rollback in early flexion due to anteriorized condyle dwell points. While this is not necessarily a typical pattern for medial contact behavior, this is the nature of working with individual subjects, even under theoretical conditions.

8.4.4 African Theoretical Patients

Varying studies in literature have shown conflicting understandings of morphology differences in African subjects. Some studies have reported larger differences between African and Caucasian morphology with respect to mediolateral and anteroposterior directions [164]. Another study, however, found this not to be the case, and instead, African subjects appeared to have more pronounced gender differences [70]. In general, the African subjects were observed to experience less axial rotation (Figure 124) in addition to medial and lateral motion patterns similar to the Caucasian subject (Figure 125 & Figure 126).

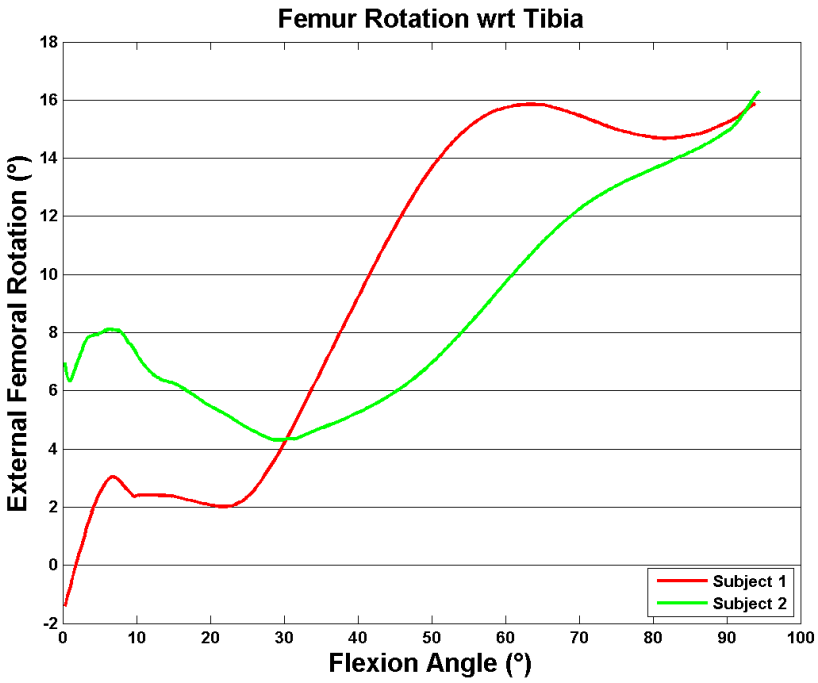


Figure 121: Caucasian femoral tibial rotation for both theoretical subjects.

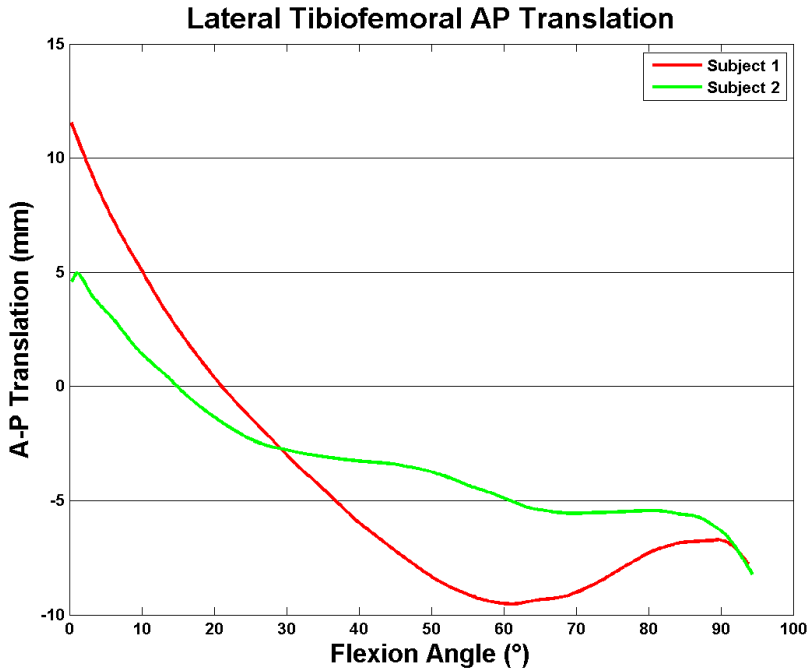


Figure 122: Caucasian lateral femoral condyle translation for both theoretical subjects.

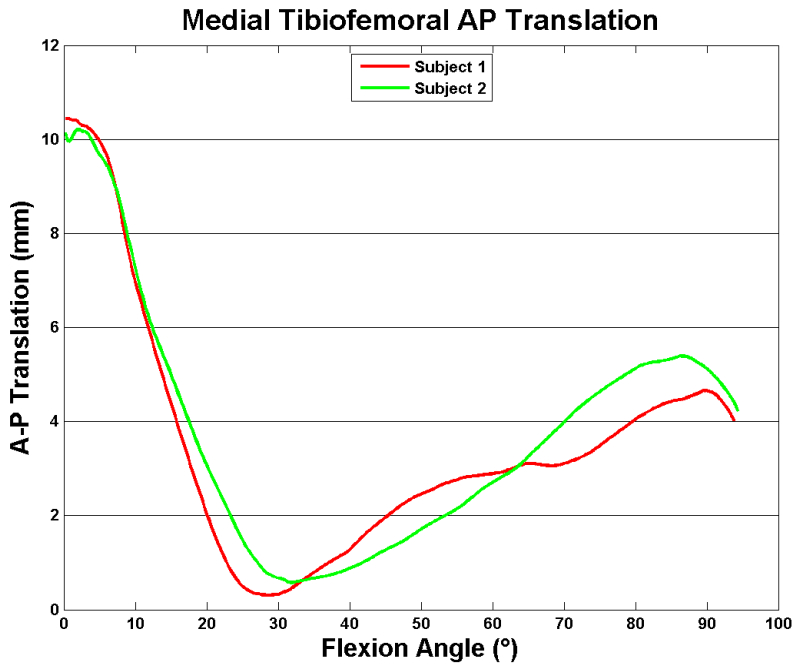


Figure 123: Caucasian medial femoral condyle translation for both theoretical subjects.

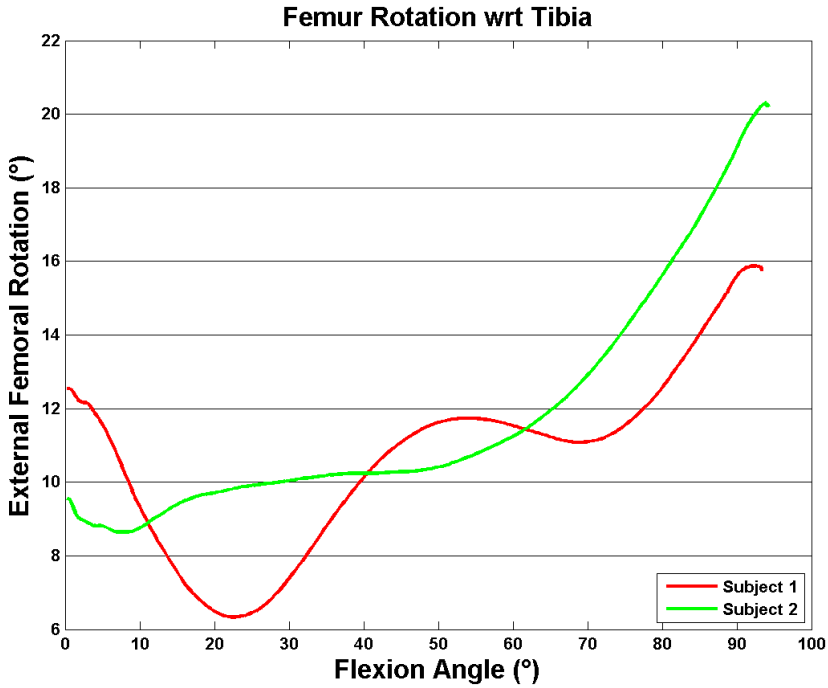


Figure 124: African femoral tibial rotation for both theoretical subjects.

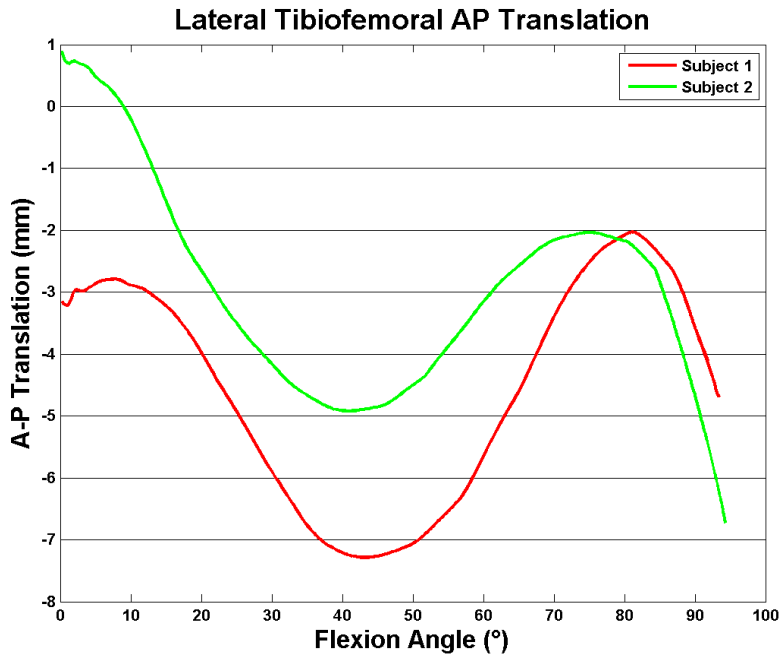


Figure 125: African lateral femoral condyle translation for both theoretical subjects.

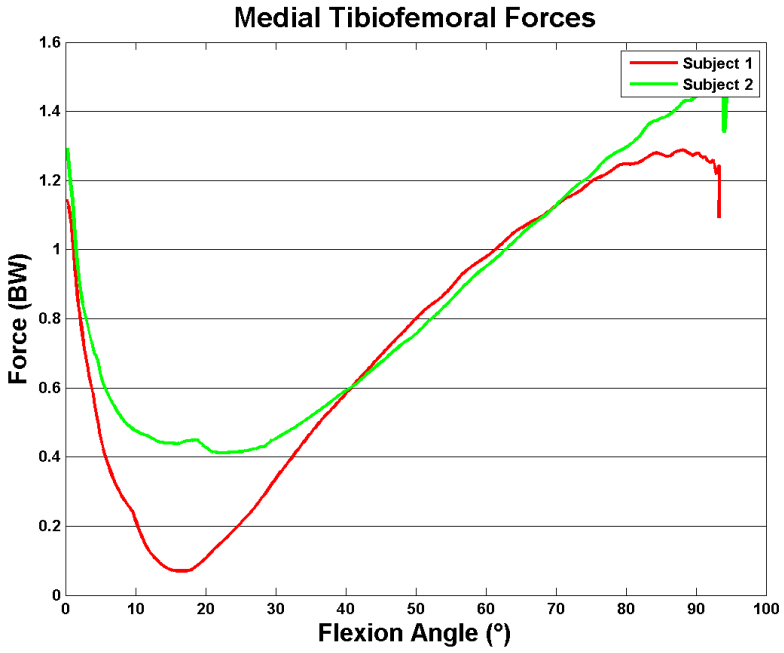


Figure 126: African medial femoral condyle translation for both theoretical subjects.

It is also of note that the lateral translation patterns held oscillatory properties, meaning that the system was potentially having difficulty finding a stable solution to the motions being calculated.

8.4.5 East Asian Theoretical Patients

Compared to Caucasian subjects, Asian subjects tend to have a smaller aspect ratio between mediolateral and anteroposterior directions. Such a geometry contributes to more defined condylar curvature which has been shown to facilitate a larger range of motion [10, 70]. While range of motion is outside the scope of this study, the Asian subjects on average experienced 16 degrees of femorotibial axial rotation (Figure 127) along with 14 mm of lateral condyle translation (Figure 128) and about 1 mm of medial condyle translation (Figure 129).

8.4.6 Comparing Theoretical Patients

Overall, all the theoretical subjects experienced kinematics consistent with previously published subjects having a normal knee [9, 10]. That is, they demonstrated a posterior motion of the lateral femoral condyle, a smaller magnitude translation either anteriorly or posteriorly and the difference between the translation of these two condyles provided axial rotation of the femur relative to the tibia (Figure 130). Even the subjects that experienced less motion between the compared subjects tested still performed better than many of the TKA devices on the market.

With respect to axial rotation, the female subjects experienced the most rotation while the African subjects the least. Again, it is important to note that

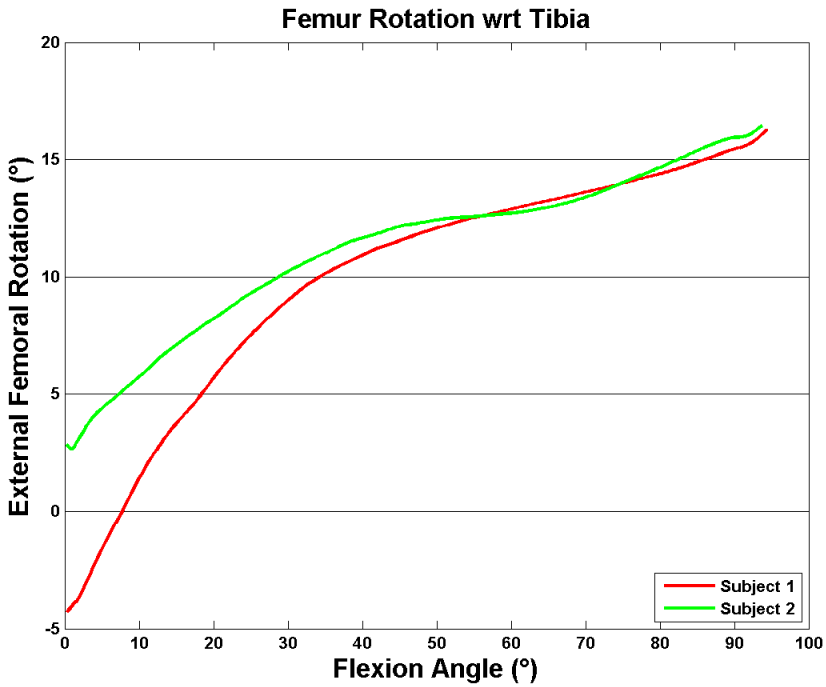


Figure 127: Asian femoral tibial rotation for both theoretical subjects.

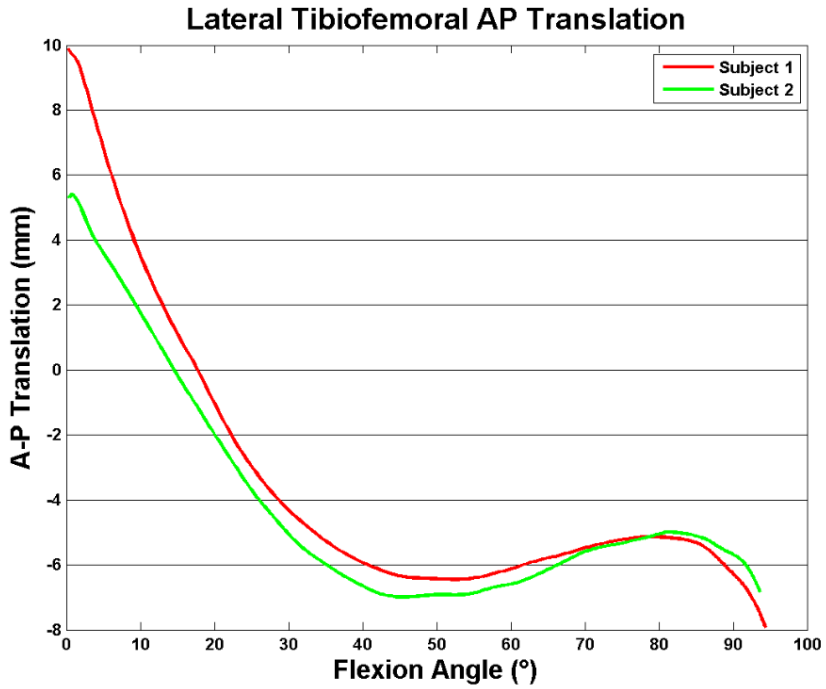


Figure 128: Asian lateral femoral condyle translation for both theoretical subjects.

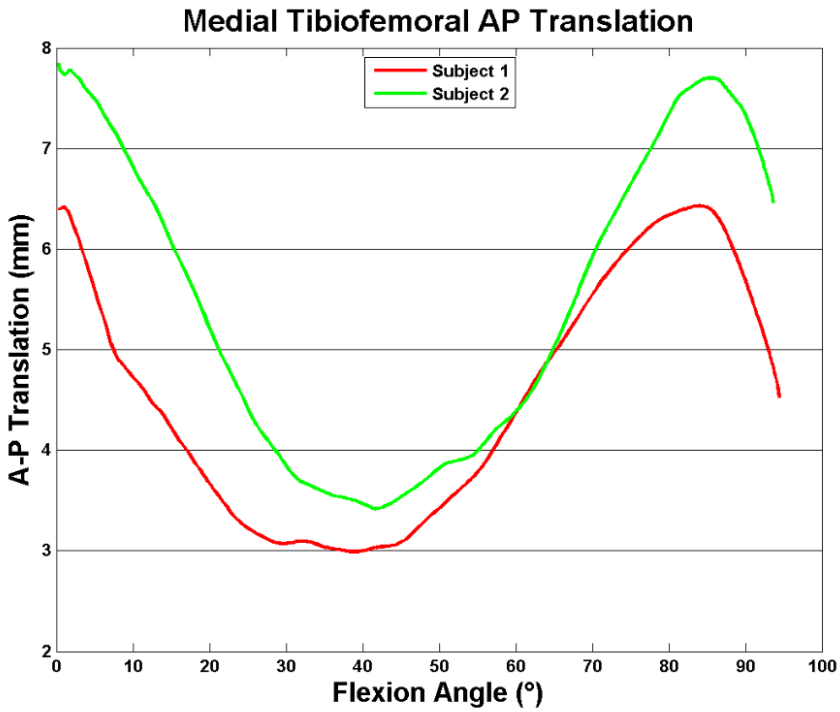


Figure 129: Asian medial femoral condyle translation for both theoretical subjects.

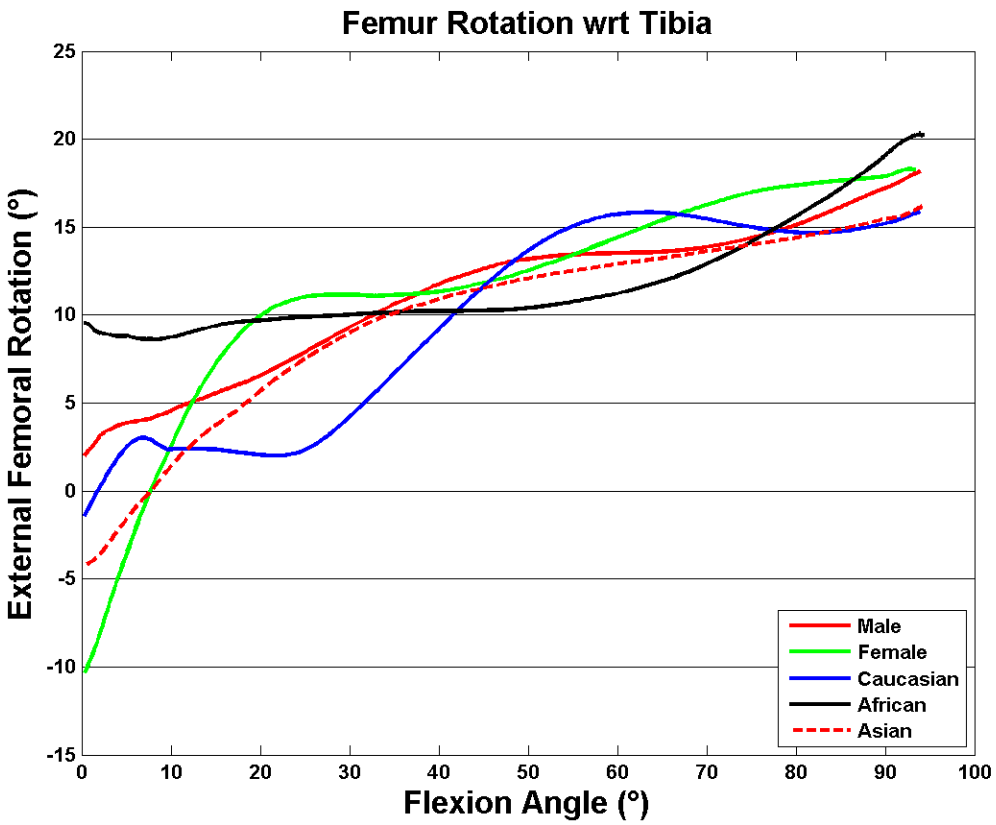


Figure 130: Femoral tibial rotation is compared for a subject from all theoretical groups.

gender and ethnic demographics are not mutually exclusive, so there is a chance that either category may have implicitly affected the other.

The other three groups experienced similar rotation that is comparable in magnitude to both fluoroscopic studies and the atlas model used in Chapter 4. Since these simulations of each theoretical subject featured no other changes beyond articulating geometry, it is believed that these kinematic variations are due to such distinctions between the geometries. This finding is consistent with literature results as female morphology tends to feature enhanced curvature that facilitates both kinematics and range of motion. Conversely since African subjects tend to have a greater mediolateral and anteroposterior resulting in a reduced sagittal curvature compared to the other groups, the condylar motions and thus the rotation would be expected to be less.

The medial and lateral condyle geometries influence knee motions and drive axial rotation, so there would be expected to be a causality between the condyle translations and the previously mentioned axial rotations (Figure 131 & 132). Likewise, these motions are driven respectively by medial and lateral curvatures. Since axial rotation is effectively the angle achieved by the anteroposterior difference between medial and lateral contact points, there are two implicit mechanisms by which axial rotation can occur. The first of these is through posterior translation of the lateral condyle, which is a feature ubiquitous of all of the subject groups. For this reason, the magnitude of posterior lateral translation coupled with the magnitude of medial condyle translation drives rotational differences which are themselves driven by condyle curvature. For example, the

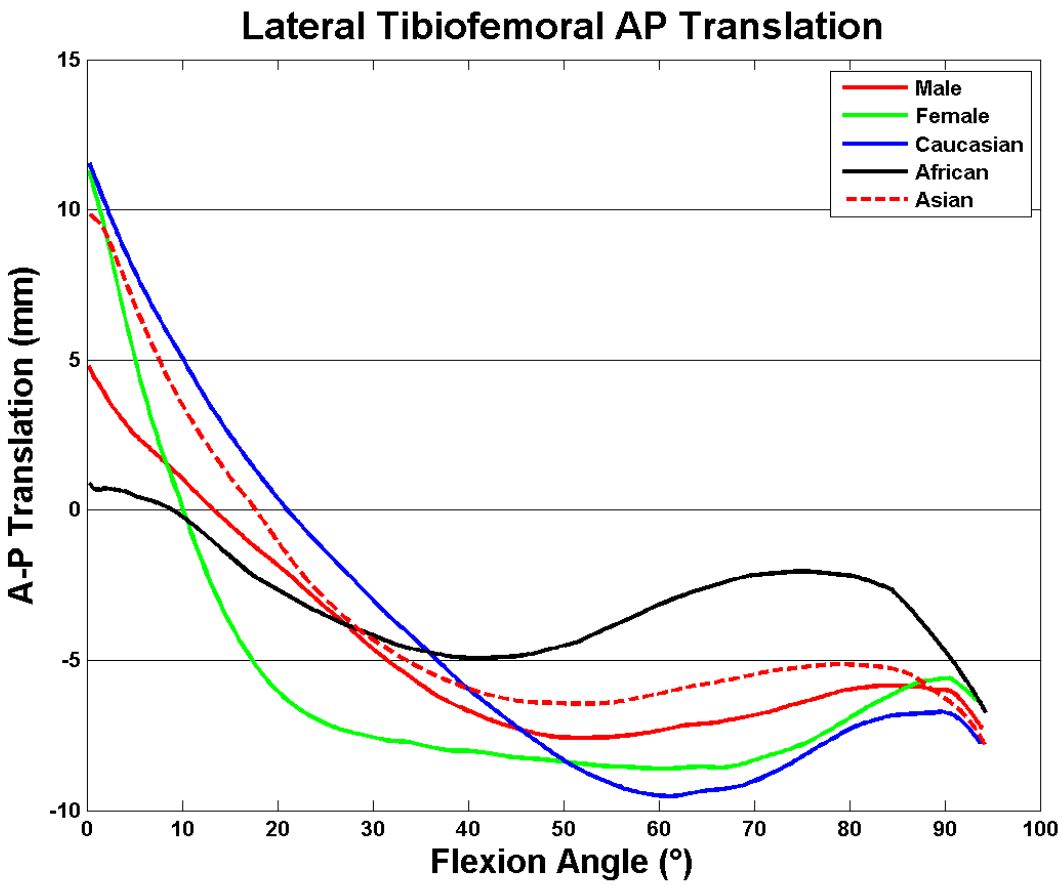


Figure 131: Lateral condyle translation is compared for a subject from all theoretical groups.

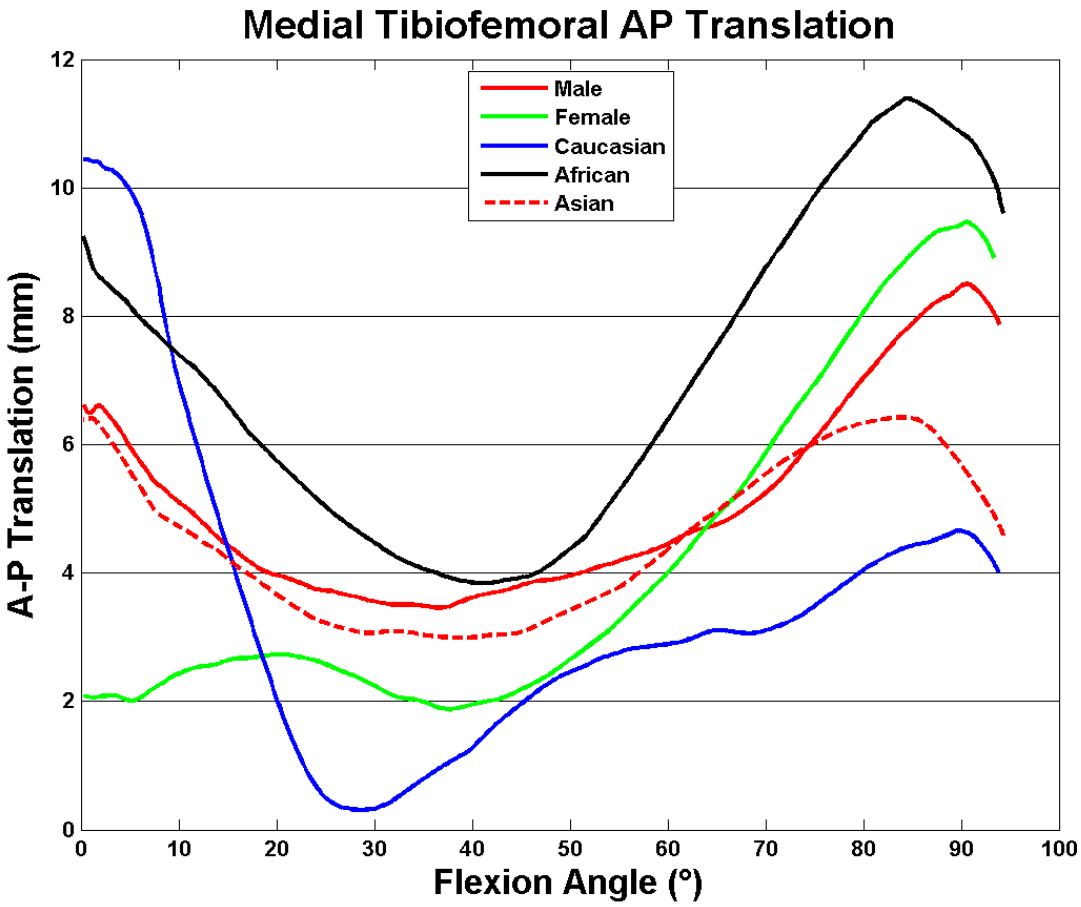


Figure 132: Medial condyle translation is compared for a subject from all theoretical groups.

female subject experienced lateral translations similar to Caucasian and Asian subjects. Because the female subject experienced substantially greater anterior motion of the medial condyle, the difference became much greater, thus contributing to additional rotation compared to the other groups. In a similar manner, the African subjects, because of articulating geometry curvature, experienced less lateral and medial condyle translation and experienced less axial rotation compared to the other groups.

The number of simulations analyzed and the number of subjects tested is not sufficient for statistical analysis. This contribution serves as an important proof of concept that the model is able to evaluate geometric differences and produce kinematic predations consistent with findings elsewhere in literature.

8.5 Soft Tissue Attachment Results

Articulating surface geometry is a very important aspect of normal knee kinematics specific to each particular demographic. While there is clinical relevance in that kinematic patterns are also based on these surface geometries, the total knee arthroplasty process replaces these surfaces entirely diminishing the clinical relevance for variations in geometry. While this is true, many soft tissue attachment sites are based upon bony prominences which can be highly dependent on bone morphology (Figure 133). For this reason, morphological differences can facilitate kinematic motions across subject demographics even outside of the influence of articulating surfaces.

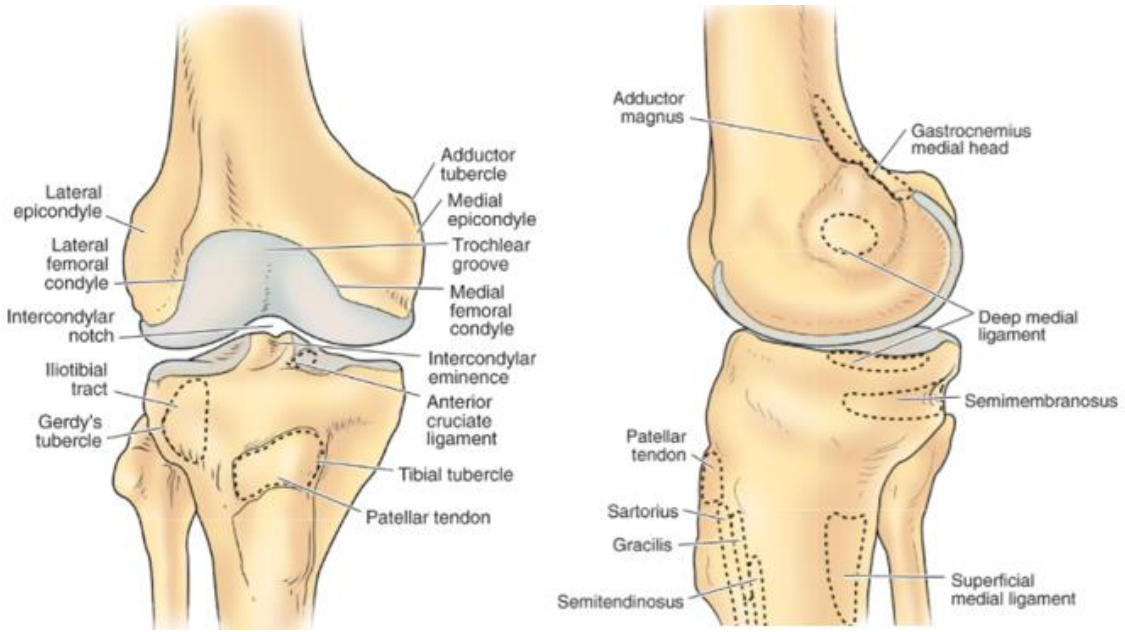


Figure 133: Each soft tissue attachment is defined relative to bony landmarks on the bone architecture. For this reason, it is a reasonable expectation that morphology will shift these bony landmarks and thus shift the attachment sites. Figure modified from [2].

Shifting the LCL origin on the femur independently of the insertion on the tibia does not contribute substantially to variations in kinematics, the only notable difference is a decrease in lateral tibiofemoral AP translation (Figure 134) and a slight deviation in medial condyle translation when the origin is shifted in the proximal direction (Figure 135). This decrease in lateral translation in early flexion also contributes to a decrease of approximately 2 mm in the femorotibial axial rotation (Figure 136). Outside of this proximal shift, no other variations showed sensitivity to kinematics.

Similarly, shifting the origin of the MCL fibers did not contribute to any meaningful differences in kinematics (Figure 137). It does, however, stand to reason that such origins shifts would have substantial effects on the medial compartmental forces which is in fact the case (Figure 138).

When both the origin and insertion sites of the LCL are shifted, effectively translating the LCL, there is neither a kinematic nor kinetic sensitivity in the model (Figure 139). Such a comparison on the MCL demonstrated no discernable sensitivity to ligament translation with the notable exception of a proximal shift, which produced increased lateral femoral translations (Figure 140), as well as decreased medial condyle translations (Figure 141). These differences offset to no net difference in axial rotation (Figure 142). While the kinematics remain relatively unaffected, the most sensitive aspect to MCL translation is that of medial contact forces. These variations, especially in the superior direction, change the ligament location relative to the joint line, and for this reason, during flexion, the constraint forces and point-to-point distance calculations would be expected to change

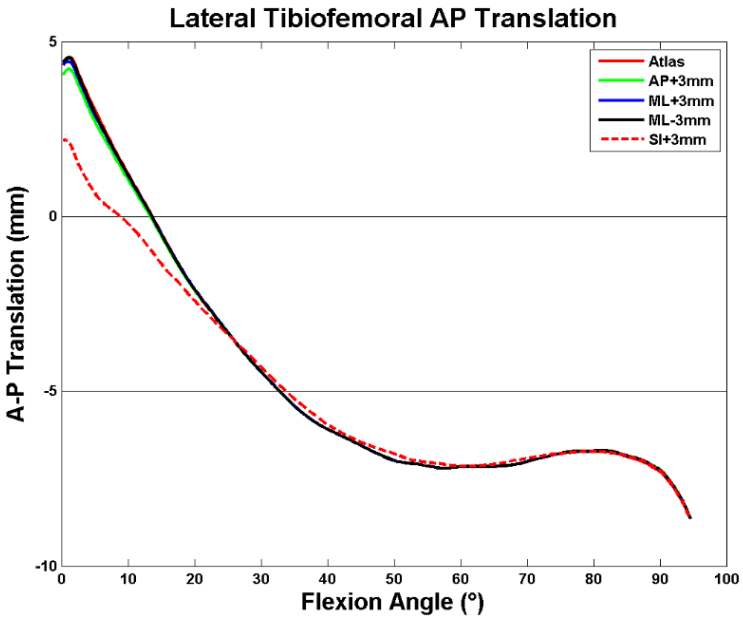


Figure 134: The only LCL origin shift that demonstrated sensitivity to anteroposterior directional translation was a shift in the proximal direction.

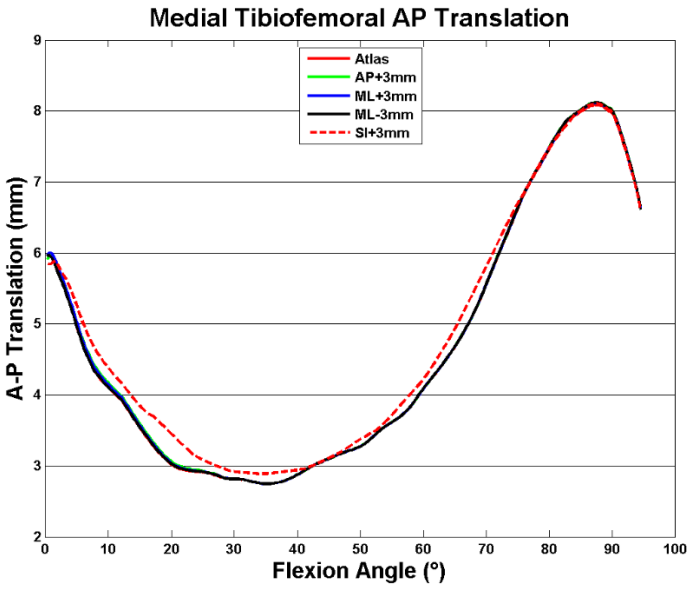


Figure 135: Although a proximal origin shift contributed to a slight deviation from the other analysis, there was not a substantive influence on medial condyle translation.

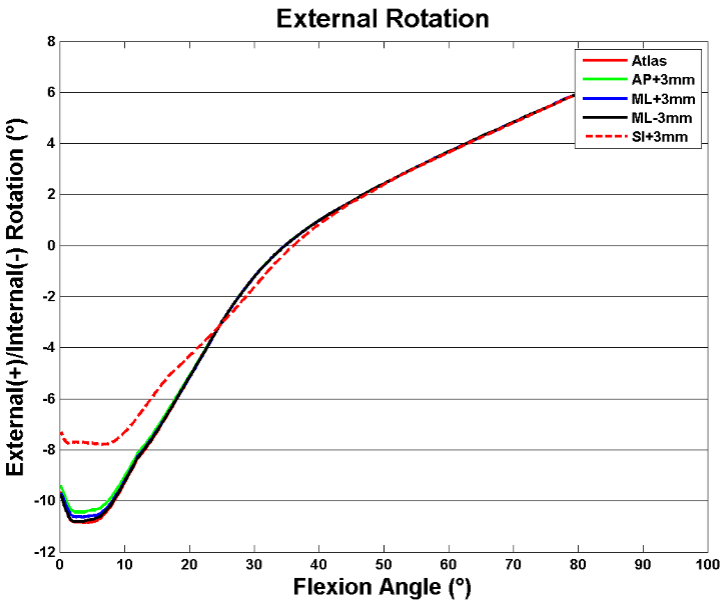


Figure 136: Because of the shift in the lateral condyle translation, the axial rotation also demonstrated a sensitivity to a proximal origin shift.

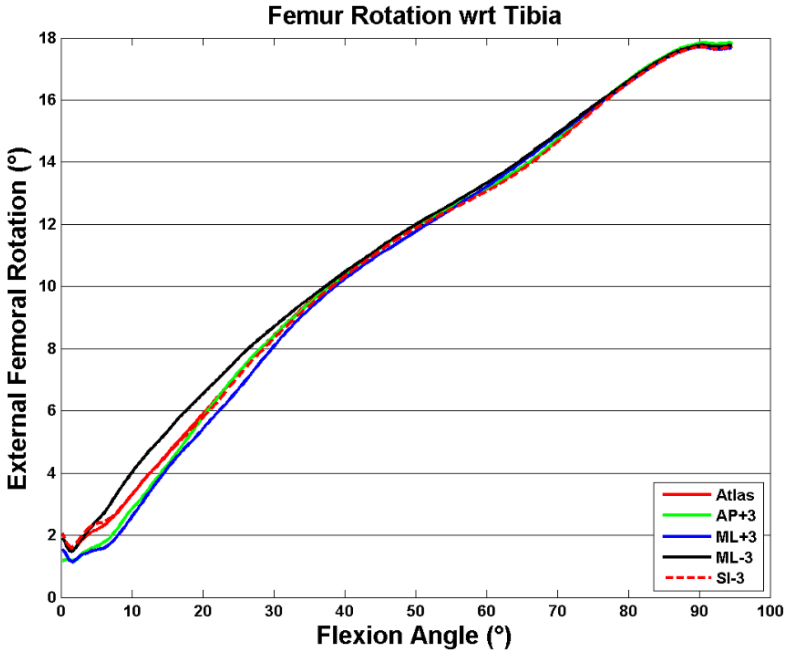


Figure 137: Femoral rotation demonstrated minimal sensitivity to MCL origin shifts.

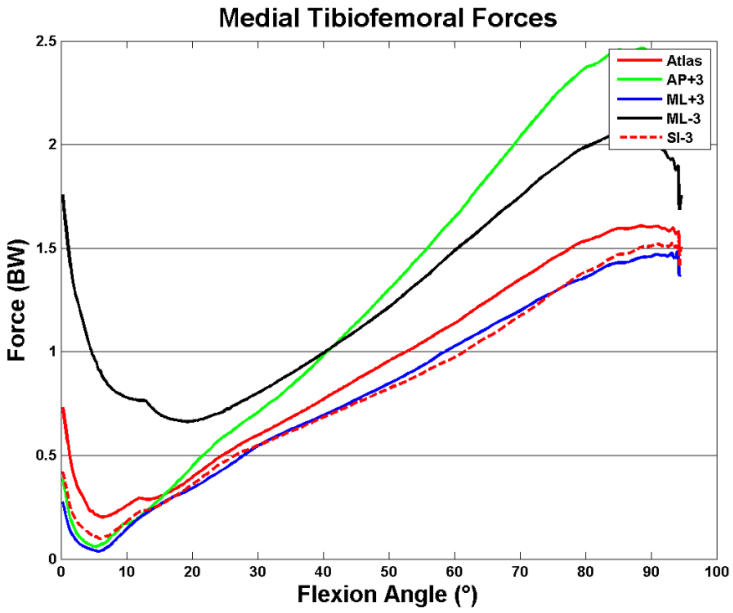


Figure 138: The only analysis to demonstrate sensitivity to MCL origin shifts was the medial compartmental force.

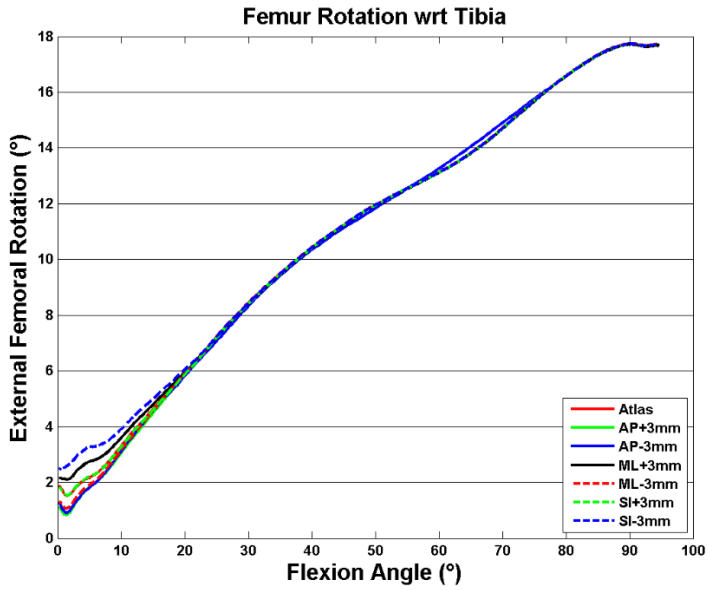


Figure 139: Translating the LCL origin and insertion in various directions does not demonstrate kinematic sensetivity in the model.

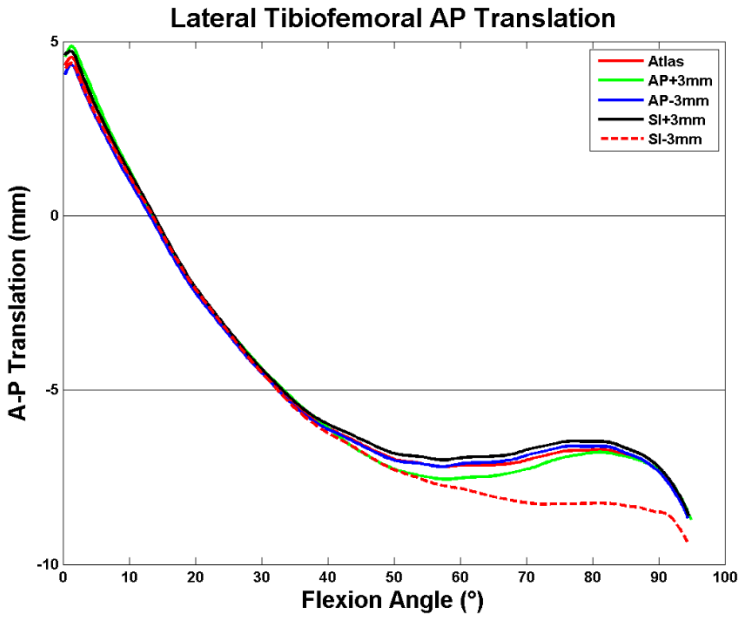


Figure 140: Translation of the MCL contributes to minimal deviations in kinematics except for an increase in posterior femoral translation when shifted proximally.

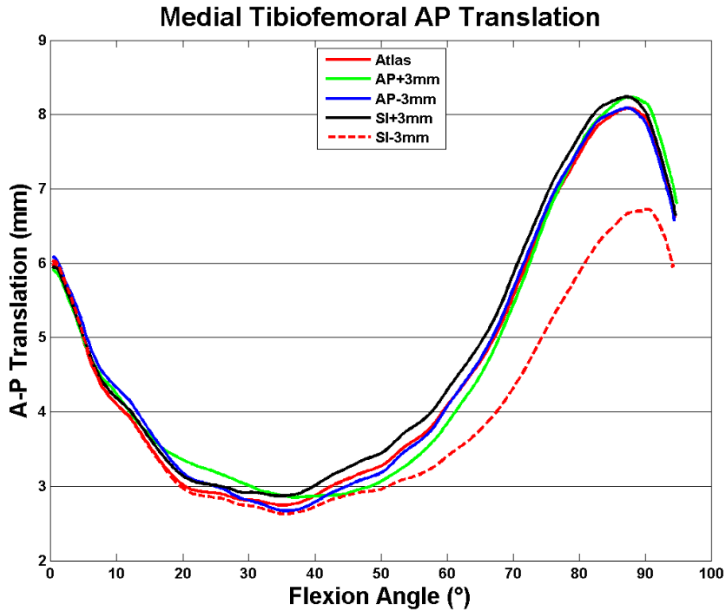


Figure 141: Similarly, compared to the lateral side of the knee, the medial femoral condyle also experienced a posterior shift in medial condyle translation.

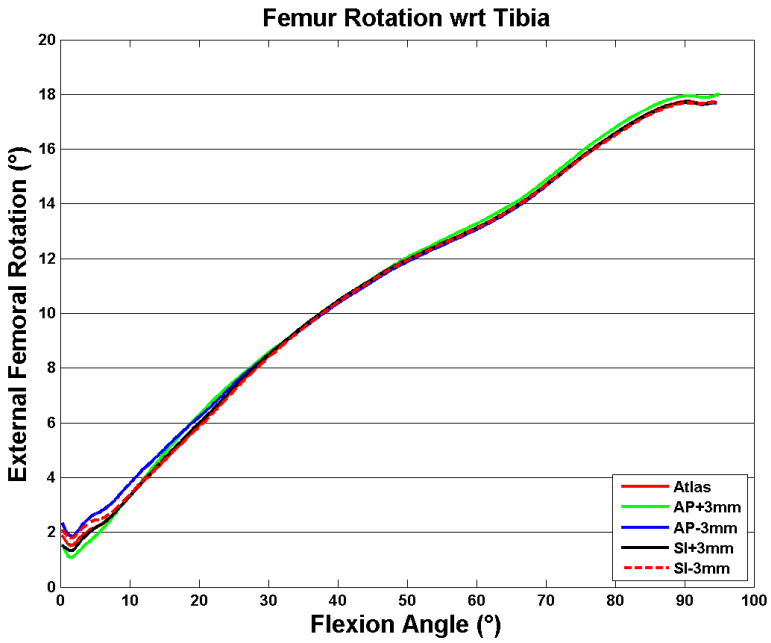


Figure 142: The medial and lateral differences in femoral translation offset to a net consistency when the MCL is shifted, regardless of direction.

drastically. As constraining forces are proportional to soft tissue compliance, deviations in contact and constraining forces would be expected (Figure 143).

The final soft tissue structure to be assessed is the patella tendon which anchors the distal patella to the tibia. Translation of the insertion on the tibia tends to contribute to variations in lateral (Figure 144) and medial (Figure 145) condyle translation which offset to no difference in axial rotation (Figure 146). This sensitivity applies particularly to the anteroposterior translation of the insertion, as anterior shifting tends to contribute to an anterior phase shift in both medial and lateral condyle translations. An anterior shift of the insertion and posterior shift in insertion led to anteriorized and posteriorized motions, respectively. There was no kinetic sensitivity to this analysis.

8.6 Conclusion

Overall, there are two main morphological differences that arise from demographic groups. The first of these is morphology of the bone itself and the second is the soft tissue attachment site location, which is dependent on bony landmarks. Studies had shown that these differences contribute to variations in kinematics between groups, and for this reason, it has been concluded that these morphological variations contribute to kinematic variations.

Using the model with individual theoretical subjects from multiple demographics groups, it agreed with these findings, demonstrating that kinematic (and in some cases kinetic) deviations occur. The most influential factor in this analysis appeared to be the geometry of the articulating surface which featured numerous kinetic and kinematic differences across the analysis, elucidating the

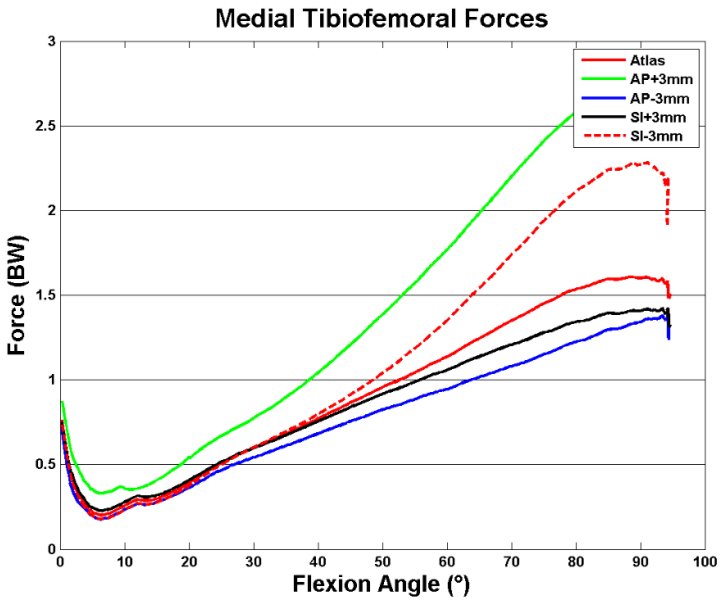


Figure 143: The only factor to be sensitive to MCL translation across all increments is the contact force of the medial femoral condyle.

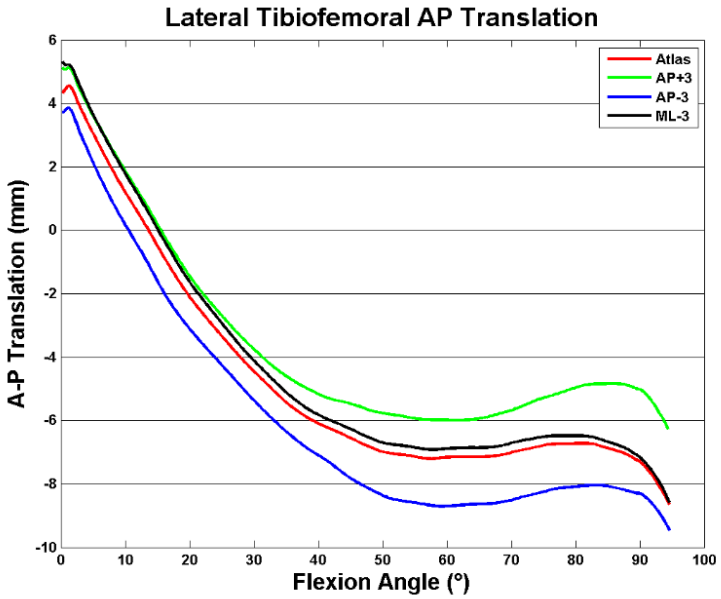


Figure 144: Anterior and posterior shifts to the insertion of the patella tendon tend to contribute to equivalent phase shifts in the translation of the lateral femoral condyle.

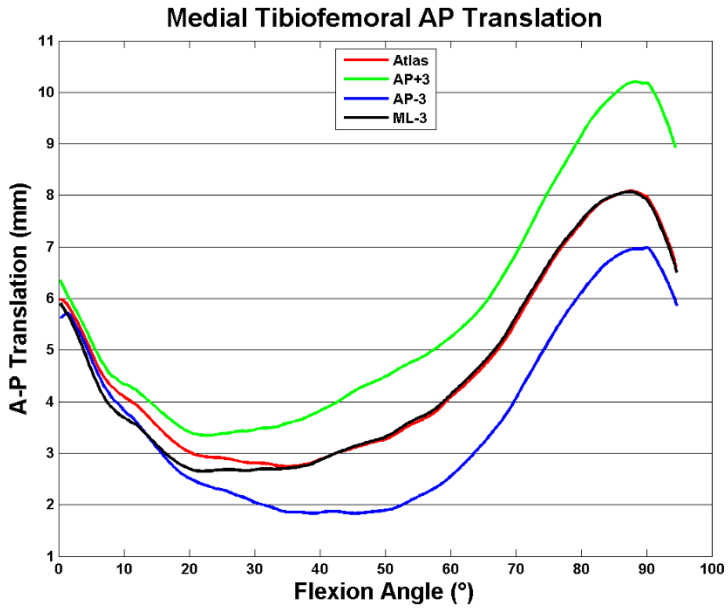


Figure 145: Anterior and posterior shifts to the insertion of the patella tendon also tend to contribute to equivalent phase shifts in the translation of the medial femoral condyle.

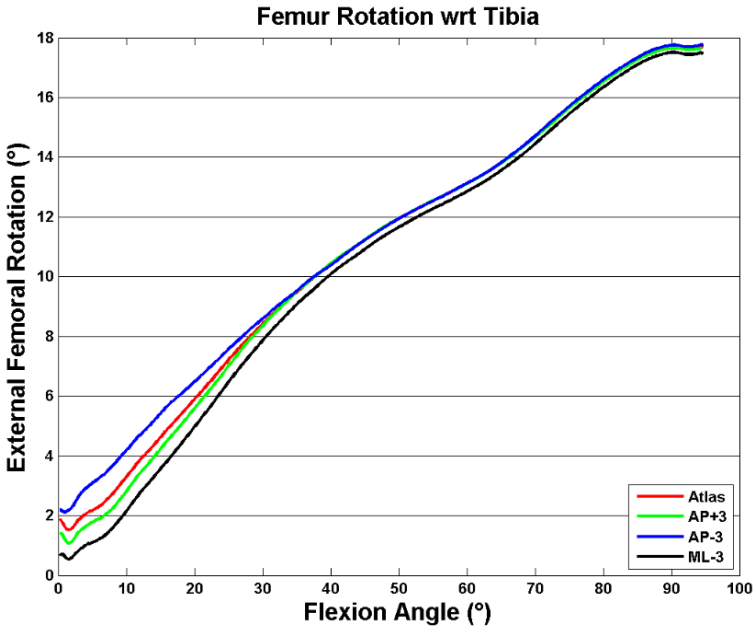


Figure 146: The medial and lateral condyle translational shifts tend to offset constituting to minimal variations in axial rotation.

relationship between articular shape and function. Soft tissue attachment site relocation also contributed to variations in kinematics; however, the clinical significance of this finding is much more ambiguous compared to that of articular geometry. It is specifically worth noting that this analysis featured exaggerated ligament attachment variations, which in turn, produced minimal differences in mechanics. It can therefore be concluded that soft tissue attachment sites and demographically induced spatial differences have an effect on mechanics, although it is a marginal one.

One of the unintended observations of the demographic analysis is the influence of individual variation which appears to be significant. The inclusion of two distinct subjects was specifically intended to evaluate subject-specific kinematic differences, and the results imply that individual variation may be of more consequence than demographic variation. This seems to suggest that a subject-specific model would be advantageous over a demographic-specific model in the future. Unfortunately, such an individually focused model would limit statistical relevance to the evaluation of arthroplasty device design along with extrapolation to larger populations.

The most important finding in this contribution is the confirmation of the viability of the model as a demographic-specific predictor of kinematics. Studies have shown normal knee aberrations specific to morphology and this model likewise reached a similar conclusion. In the broader scope, this emphasis on demographic-specific kinematics emphasizes gender- and ethnicity-specific

kinematics, which is an important consideration in the design of new and improved arthroplasty devices.

CHAPTER NINE: PARAMETERIZING PATHOLOGICAL CONDITIONS

9.1 Purpose

The previous chapter outlined the idea of demographic specific mechanics and applications in TKA design for various subject groups. While much of the motivation for this model revolves around knee arthroplasty design, the model also affords a unique opportunity not possible through other evaluation techniques. That is to evaluate the knee in vivo under healthy and diseased conditions.

While understanding the mechanics of the healthy knee is important, it is possible of greater clinical significance to evaluate knees afflicted by pathological conditions. These conditions include arthritis, compromised cruciate ligaments, and varus and valgus deformities. Since the model affords the opportunity to change conditions and predict mechanics in vivo, there is tremendous potential as a surgical tool to provide surgeons with more information to create more targeted and effective interventional techniques for these conditions.

Using the model, it becomes possible to develop and evaluate theoretical procedures and determine their effectiveness. While this is a future application, the goal of this contribution is to prove the model as a viable tool for the assessment and categorization of various joint pathologies. Evaluating several different pathological conditions, results will be generated and compared to a simulation of a normal healthy knee in order to better understand the role pathologies play in joint mechanics.

9.2 Introduction

Pathological conditions are one of the cornerstones of orthopedics and they are often quantified by aberrations with respect to the normal, healthy knee. One of the most difficult aspects of orthopedic medicine is the complexity of the knee as both a biological and mechanical system. Often these two are implicitly related, however, the mechanisms by which they occur are not always as clear.

While this mathematical model has no intention quantifying biological processes, quantitative assessment is still necessary, especially as it pertains to joint mechanics. There is an understanding of how these factors relate to each other, but the model gives the ability to isolate individual aspects and quantify them on the basis of biological parameters. For example, arthritic subjects typically have substantial cartilage wear and the coefficient of friction for the knee will be much higher. This to simulate an arthritic subject, the tibiofemoral friction can be increased, and as a result, the motion can be assessed. Conversely, if a particular intervention technique is known to quantitatively reduce a coefficient of friction, then the efficacy could be assessed.

Such is the case, as well with soft tissue constraint, which can be a leading cause of poor joint mechanics. Likewise, the model gives the chance to isolate individual structures and in doing so, more information can be provided regarding root causes and solutions can be evaluated.

In addition to interfacial factors and constraining structures, the model can also be used to replicate acquired and congenital deformities. One such example is a varus or valgus deformity where the distal end of the femur is rotated either internally or externally about the anteroposterior axis (Figure 147). Using the

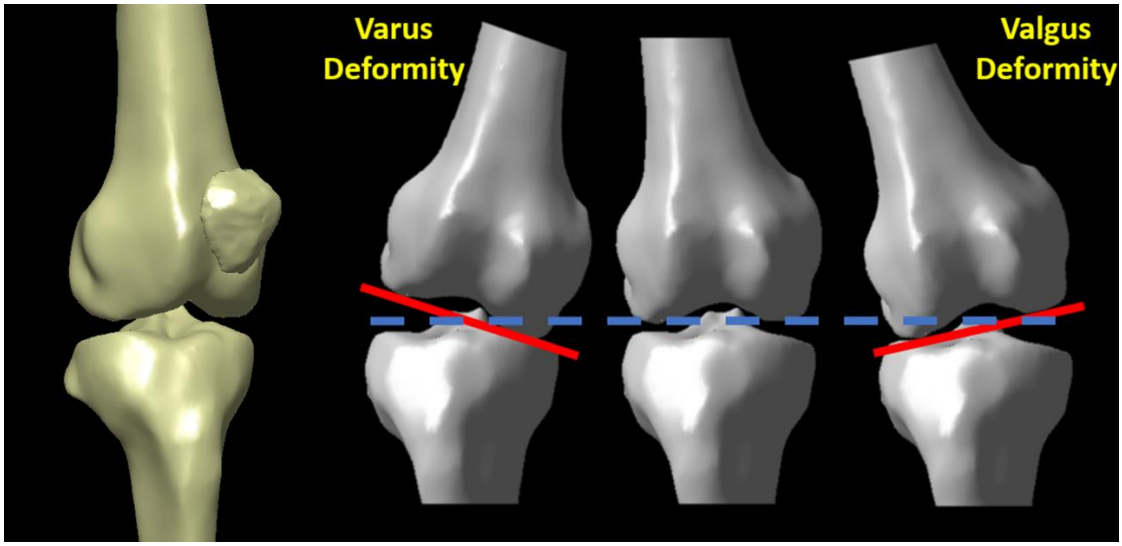


Figure 147: Varus and valgus deformities result from the articulating surface of the femur rotating either internally (varus) or externally (valgus) about the anteroposterior axis compared to the neutral orientation of the femur. While small deformations on an individual basis are common, greater than five degrees of rotation denotes a deformity.

model, a theoretical patient can be configured to demonstrate such deformities, and that same patient can be evaluated through various repair techniques to determine which restores the most optimal function. Once a strategy is developed and tested using the model, a physician can begin the procedure both with more information, as well as an enhanced degree of confidence that the process will work as intended.

While bone deformities are not as common, the model also has additional practical use evaluating pathological conditions to facilitate standard TKA procedures. For instance, one common debate in the orthopedics community is the merit of retaining verses resecting the posterior cruciate ligament. Often this is a decision made qualitatively by the surgeon in the operating room. Using the model, it becomes possible to change a parameter based on empirical measurement and the resulting kinematics can be determined (Figure 148) to assess if the posterior cruciate ligament is mechanically able to provide adequate stability. This is an example where a surgeon can use the information provided to decide as to which device will be best suited to the patient.

Using various anatomical and physiological conditions, the utility of the model and underlying parameters will be assessed under various pathological conditions to better understand their respective roles in joint mechanics. More important than pathological assessment is the prospect of theoretical correction which may become a useful tool to aid the surgical decision-making process. Such a tool is neither possible nor practical without the use of mathematical modeling.

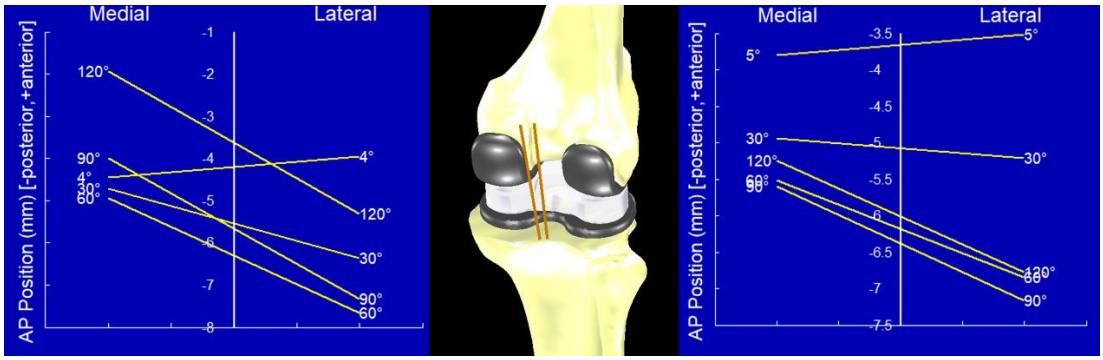


Figure 148: Posterior cruciate retaining total knee devices retain the posterior cruciate ligament (center). While sometimes considered advantageous, if the PCL ligament is compromised, it becomes unable to keep the knee posterior (left) leading to extensor mechanism impingement. A proper PCL maintains the device posteriorly facilitating proper kinematics (right).

9.3 Methods

In total, five theoretical patients will be assessed using the model. One of which is a healthy, normal knee, and the other four have some sort of associated deformity or abnormal condition with respect to pathology. One subject is arthritic, another has a deficient ACL, and the other two are afflicted with either a varus or valgus deformity. Using the parameterized nature of the model, some feature will be assessed to simulate these conditions, and in doing so, the results will be predicted for that particular pathology.

The normal, healthy knee will be used as a control. To create this model, an atlas model was used in which the geometry was based on a collection of anatomical features averaged to a single smoothed geometry. All pathological conditions are derived from this simulation.

To simulate an arthritic patient, it was first assumed that negligible osteophyte formation has occurred. Due to this assumption, the normal geometry can be used and the presenting symptoms can all be reduced to the coefficient to friction at the knee, which is the variable that will be adjusted to simulate arthritic motion parameters. In this particular case, the dynamic coefficient of friction was doubled.

To simulate a knee with a deficient anterior cruciate ligament, the value for the reference strain was increased. This effectively treats the ACL as if it has been loosened, and thus, the amount of constraining force contributed to the mechanics of the knee is drastically decreased. This is the same mechanism by which a degenerative ACL would be limited in the constraining force that is maintained on

the femur. Ligaments over time tend to exhibit viscoelastic behavior progressively, reducing their mechanical effectiveness over time.

To replicate varus and valgus conditions, the femoral articulating surface was rotated relative to the femur bone, and the initial conditions were adjusted to be physiologically feasible. These surfaces were rotated five degrees about the anteroposterior axis, and these rotations were done internally to represent a varus deformity and externally to represent a valgus deformity (Figure 149).

A theoretical patient was set up in the model and evaluated under these conditions and then the results were compared to the otherwise identical normal subjects to assess the effect of the various pathological conditions.

9.4 Results

9.4.1 Arthritic Results

Three scenarios were tested with respect to osteoarthritic patients. The first is a healthy subject with no arthritis, the second is a subject with early stage arthritis and third is a subject with late stage arthritis. To simulate these conditions, the coefficient of friction was set normally for the healthy subject, increased by 50% for an early stage arthritic patient and increased an additional 50% for a late stage arthritic patient. By increasing the coefficient of friction, the interface between articulating surfaces become roughened and less conducive to motion. This is analogous to the mechanism of arthritis as cartilage continues to wear over time.

Compared to the healthy subject, the early and late stage arthritic subjects experienced slightly less tibiofemoral axial rotation in early flexion with otherwise similar kinematics (Figure 150). It is, however, worth noting the increased

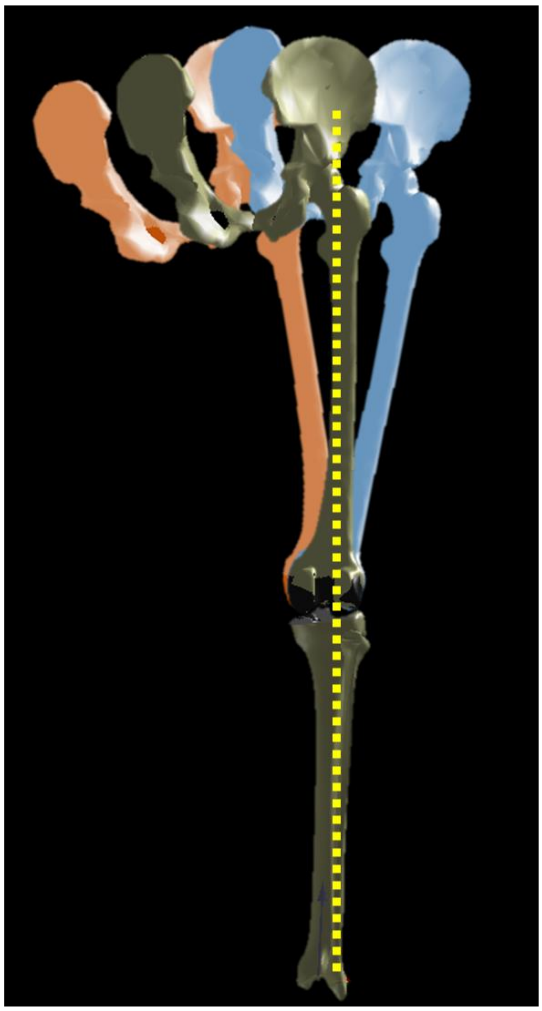


Figure 149: To replicate varus and valgus conditions, the femoral surface was rotated five degrees internally for varus (red) and five degrees externally for valgus (blue).

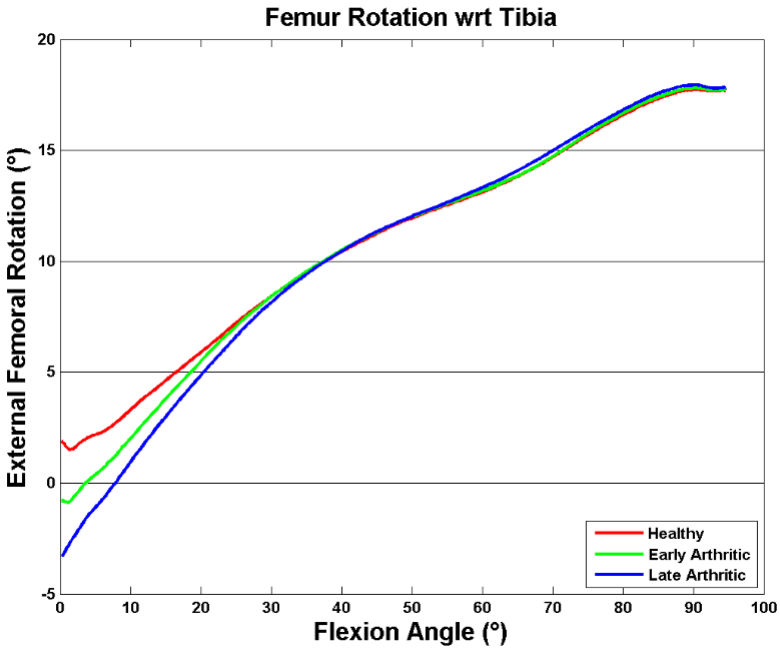


Figure 150: Between the healthy and arthritic subjects, there was minimal kinematic difference outside of early flexion.

coefficient of friction due to osteoarthritis contributed to higher forces in both the quadriceps mechanism, as well as PCL forces (Figure 151 & Figure 152). Greater knee forces overall can be problematic as they may expedite the wear process and exacerbate the problem over time.

Compared to the healthy subject, the early and late stage arthritic subjects experienced slightly less tibiofemoral axial rotation in early flexion with otherwise similar kinematics (Figure 150). It is, however, worth noting the increased coefficient of friction due to osteoarthritis contributed to higher forces in both the quadriceps mechanism, as well as PCL forces (Figure 151 & Figure 152). Greater knee forces overall can be problematic as they may expedite the wear process and exacerbate the problem over time.

9.4.2 ACL Deficient Results

Using a modified version of the healthy knee, three simulations in total were performed. The first was for a healthy knee, the second was for a situation in which the slack length is doubled and third case where the slack length is halved. Lengthening the slack distance for a ligament effectively reduces the amount of stretch that ligament experiences. Since force is a function of the change from an initial length, this effectively reduces the force when the slack length is doubled and increases when the slack length is halved. Another way to look at such a setup is that one theoretical patient has an ACL with double tension and the other has half tension.

As would be expected, increasing the tension in the ACL tends to increase ACL forces as calculated by the model (Figure 153). Because this force is

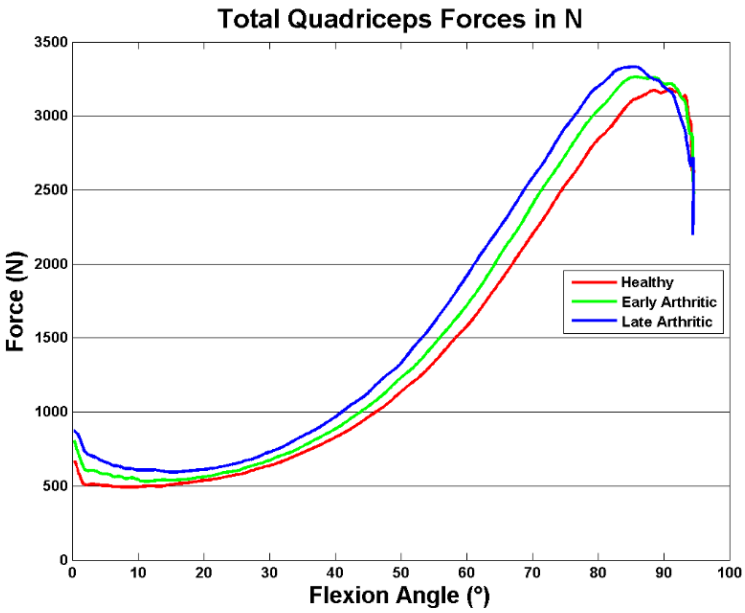


Figure 151: Increased friction in the model produced a need for greater quadriceps force.

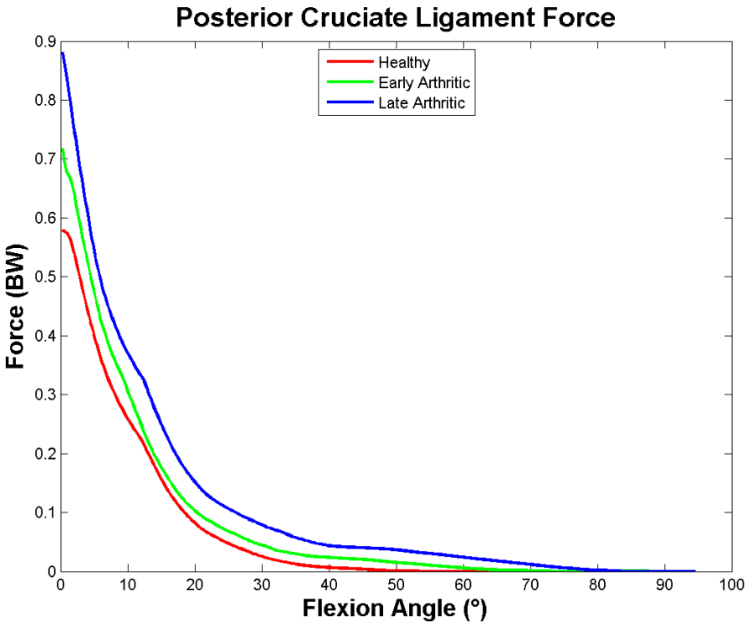


Figure 152: Greater coefficients of friction also contributed to increased PCL forces.

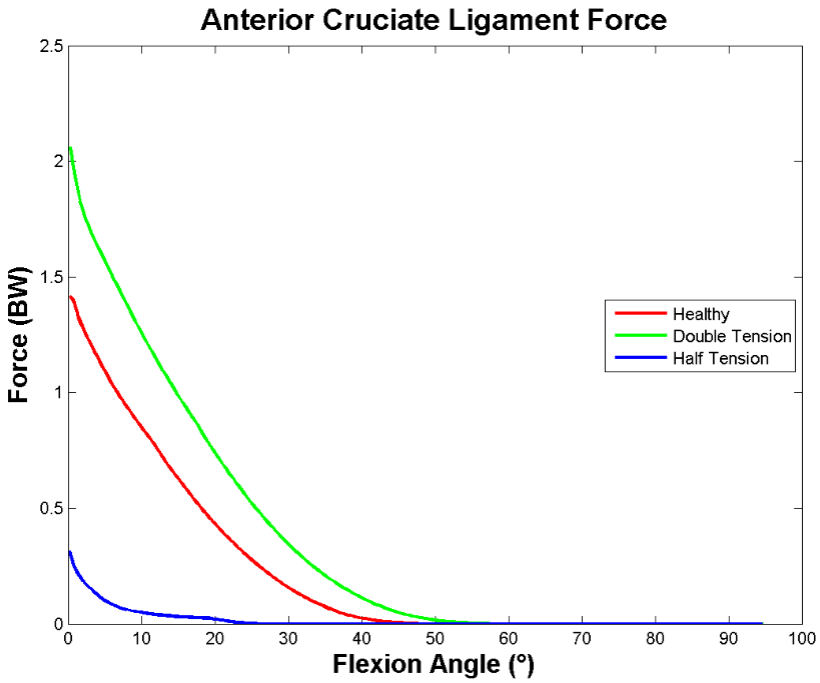


Figure 153: Putting the ACL in tension or in slack directly contributes to the ACL force applied within the model.

diminished, there would be an expected to be significant paradoxical motions when the ACL is deficient.

When the ACL is deficient, the initial position of the lateral femoral condyle is significantly more posterior (Figure 154). For this reason, the overall translation over the course of the activity is diminished, contributing to motions atypical of a healthy knee. This difference is also reflected in the femoral axial rotation where the femoral articulating surface begins four degrees externally rotated compared to the neutral orientation (Figure 155). There does not appear to be a short term adverse effect from an overly tight ACL at least from a kinematics perspective.

9.4.3 Varus Valgus Deformity Results

Three subjects were compared to assess the role of varus and valgus deformities. The first was a subject that had an alignment similar to the healthy knee which is approximately three degrees rotated off the mechanical axis. The other two subjects were evaluated with a 5-degree rotation of the femoral articulating surface in either direction relative to the femur to assess the mechanics with the approximated deformity.

One of the most interesting aspects of varus and valgus deformities is that the kinematics are, for the most part, marginally or not affected at all by the deformity (Figure 156). What is significantly affected, however, are the medial and lateral condyle forces which follow an intuitive pattern. Compared to the healthy subject, the varus deformity exhibited greater medial condyle contact forces and lesser lateral contact forces (Figure 157 & Figure 158). The theoretical subject with the valgus deformity experienced greater lateral contact forces and lesser medial

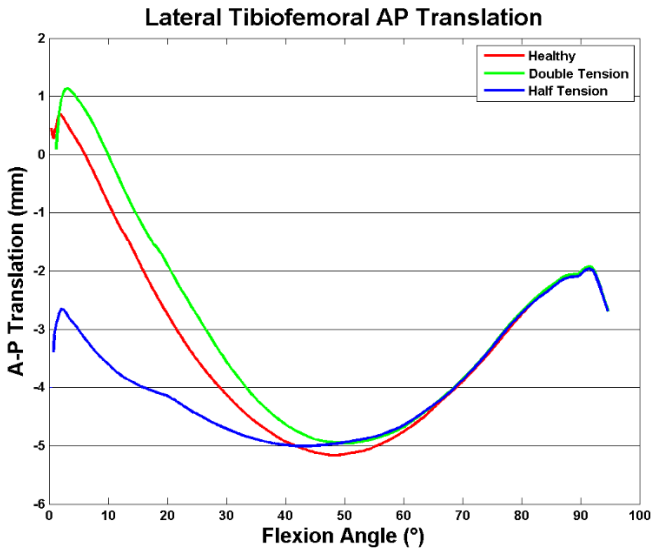


Figure 154: When the ACL is in slack, the initial position of the lateral condyle begins posteriorly compared to a properly tensioned ACL. This initial position contributes to mitigated rotation and adverse kinematics.

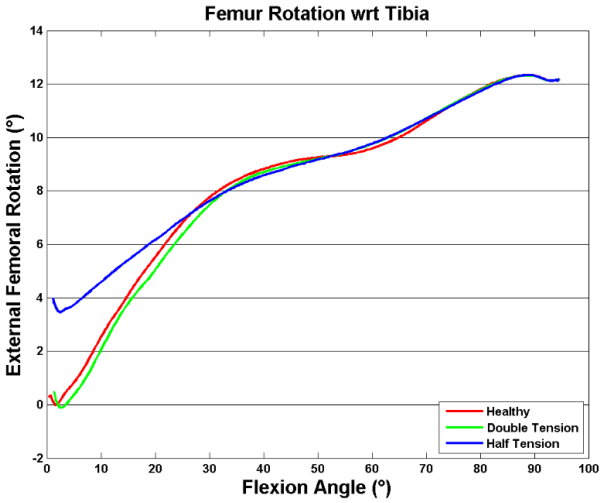


Figure 155: Partially due to the difference in lateral translation, a PCL with half the tension begins four degrees externally rotated. The motion patterns become similar around 25 degrees of flexion.

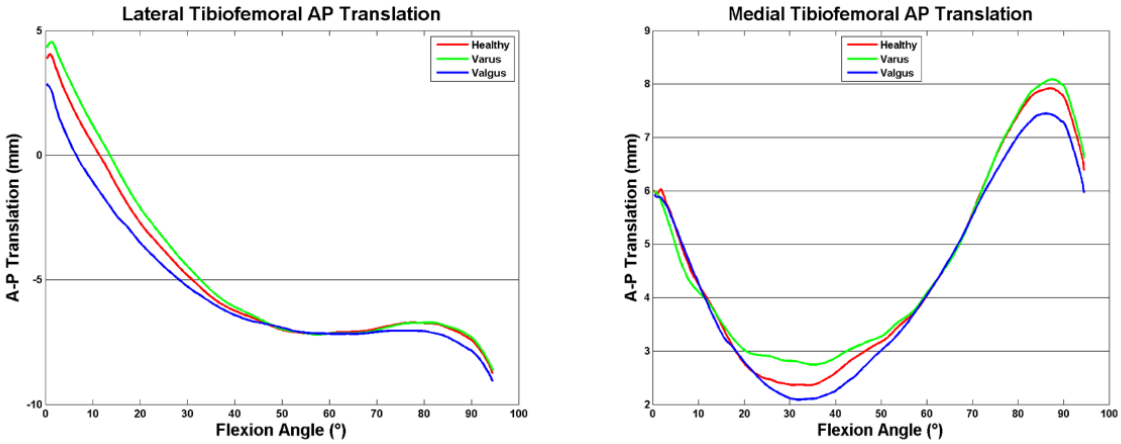


Figure 156: Between healthy and varus or valgus aligned knees, there is not a substantial effect on kinematics due to the deformity.

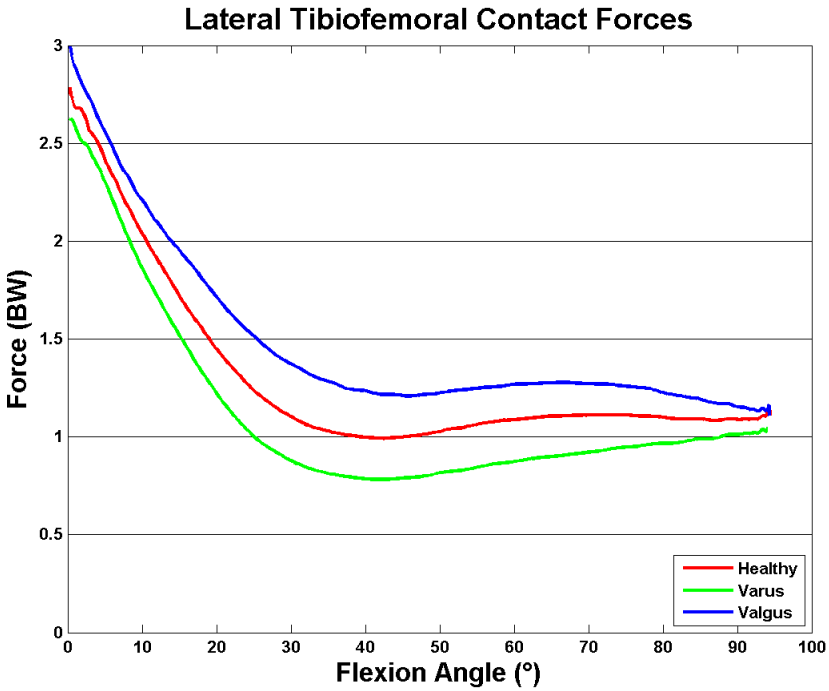


Figure 157: The theoretical subject with the valgus deformity demonstrated lateral contact forces greater than the healthy knee while the varus subject demonstrated lesser medial contact forces.

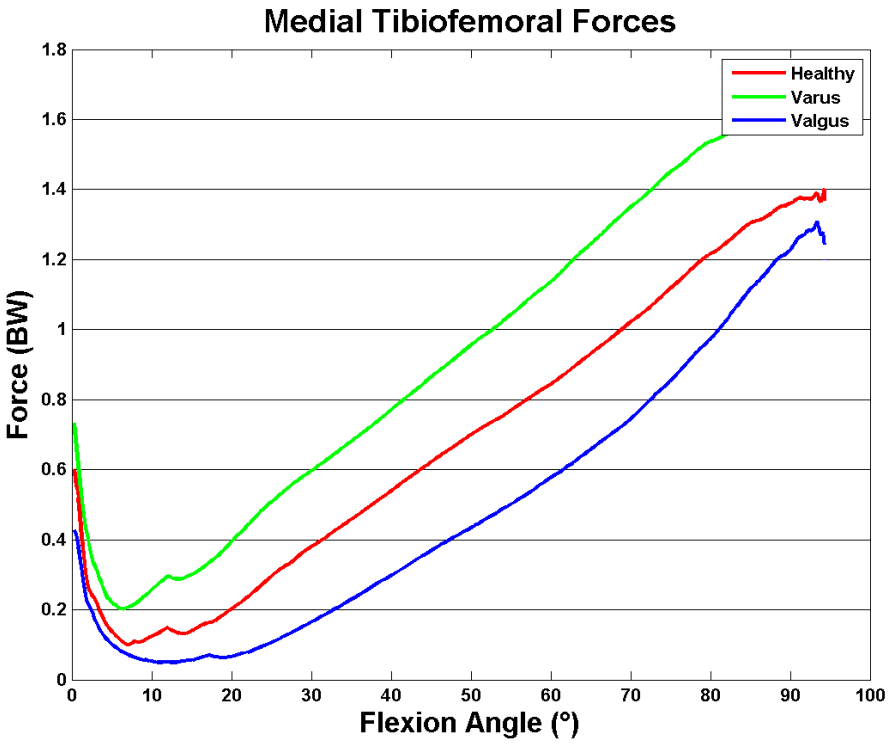


Figure 158: The theoretical subject with the varus deformity demonstrated medial contact forces greater than the healthy knee while the valgus subjects demonstrated lesser medial contact forces.

contact forces. These results are evident as the nature a varus deformity rotated the articulating surface away from the lateral surface and toward the medial condyle surface. The converse is also true for valgus rotations as the initial rotation is from the medial condyle concentrating force on the lateral condyle.

9.5 Conclusion

Under many conditions, either of the four pathologies can contribute to adverse kinematics and kinetics. During the onset of osteoarthritis, the coefficient of friction within the model can increase substantially, leading to greater muscle forces. This also contributed to larger contact forces, which may very well worsen the problem. ACL deficient knees experience poor kinematics due to the inability of the ACL to keep the knee forward on the tibial plateau. This results in posterior components, anterior sliding and bone impingement deep in flexion. With respect to varus and valgus deformities, the model showed minimal kinematic differences; however, the distribution of force between the two condyle tends to favor the lateral and medial compartments for valgus and varus deformities, respectively.

All of these findings successfully show the potential for further problems if not corrected. Overstretched ligaments tend to exhibit fatigue behavior and excessive contact forces tend to expedite cartilage wear compounding the problem. While the model was able to identify these issues, it also has the capability to evaluate healthy knees meaning there is a potential for surgeons to use this process as a tool to determine the best course of action to best correct for the issues that have been evaluated.

CHAPTER TEN: PARAMETERIZING OF GAIT

10.1 Purpose

Thus far much of the focus of this model has focused on the evaluation of flexion based activities. While these are a good measure kinematic performance of the knee, deep flexion activities are not as common compared to basic ambulatory function, such as walking. One of the focuses of the model is the expansion of newer activities that can give additional predictions to knee performance.

The goal of this contribution is to develop an additional activity to the model to simulate gait based activities. While this particular contribution will focus on level ground gait, it is theoretically possible to expand into step and inclined surfaces with later additions and definitions.

10.2 Introduction

Unlike a deep knee bend, the standard gait cycle only reaches 30-50 degrees of flexion and is divided into two separate phases. These are stance and swing phase, and they represent active and passive flexion, respectively. Fundamentally, the muscle control for the knee is nearly identical to that of standing flexion. The fundamental difference is the gait relies heavily on muscle activation from the foot, which is driven primarily by the gastrocnemius muscles [165]. Such a motion pattern allows the foot to move both eccentrically and concentrically to drive flexion during stance phase. Swing phase is fundamentally different as the activity is non-weight bearing.

Gait is significant as an activity for analysis because it is the most common and repeated activity performed by humans. For this very reason, it is important to have a thorough understanding of how the knee moves and what sort of motions provide not only comfortable but also efficient motions. The aim of this contribution is to continue the development of the model to be able to account for a gait cycle and predict associated kinematics.

10.3 Methods

From the perspective of the knee, there is not much different about gait compared to traditional knee flexion. The muscle roles are similar between the quadriceps and the hamstrings. The only difference is with respect to the flexion profile that drives the knee flexion through the PID controller because gait is not a continuous flexion motion, but rather a motion that reverses from flexion to extension and back to flexion. Whereas flexion activities focused exclusively on flexion or extension, this model will feature a revised flexion profile that accounts for flexion and extension.

While gait is similar to other activities at the knee, the ankle is where much of the new activation will occur. Since this is fundamentally a knee model, the motions at the ankle will all be treated as inverse in that muscle control will be omitted with the flexion profiles dictated directly through mathematical functions. This is similar to the process where the foot was added in Chapter 6.

There are, however, two important distinctions that need to be made for gait compared to stationary flexion. The first of these is the addition of the toes which help to drive the forward motion through eccentric contractions from the

gastrocnemius muscle group (Figure 159 & Figure 160) and secondly, a moving contact point will be added that moves from the ankle to the toes as weight transfers during gait (Figure 161). Another important note is that, thus far, most flexion profile functions have been as a function of flexion. While this is sufficient for flexion based activities, gait will require these functions to be as a function of time as each phase is further divided between a flexion and extension phase. Once complete, this model will show a gait cycle through stance phase.

Swing phase is very different, as it is one of the first passive flexion activities to be evaluated through the model. One fundamental difference between swing and stance phase in the difference between open and closed chain or loop systems. Stance phase is a “closed chain” system because it connects the kinematic chain directly to the Newtonian frame which occurs at the point of contact on the ground. For swing phase, such a point does not exist as there is no foot contact with the ground. This makes it an “open chain.” Due to the open chained nature of the model, it requires the definitions of the model to be inverted since the motion is derived exclusively from the torso in place of the ground (Figure 162).

10.4 Results

During stance phase, the foot maintains in constant contact with the ground as the knee drives through tibiofemoral flexion and extension (Figure 163 & Figure 164). Due to the nature of the PID controller function, an approximate maximum flexion of 36 degrees was assumed. This value was derived using average fluoroscopic data over a set of 20 TKA subjects during gait. In order to provide context for kinematics of the gait cycle, the analysis is accompanied by kinematics

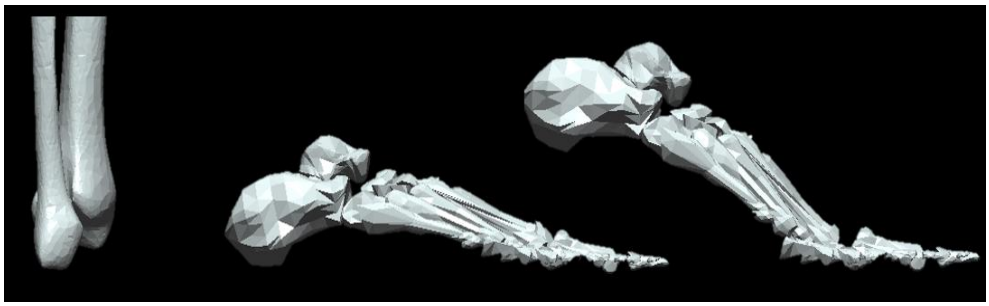


Figure 159: Throughout the development of the model, the ankle definition has gradually added elements from the ankle, to the foot and finally the toes, which are necessary for gait.

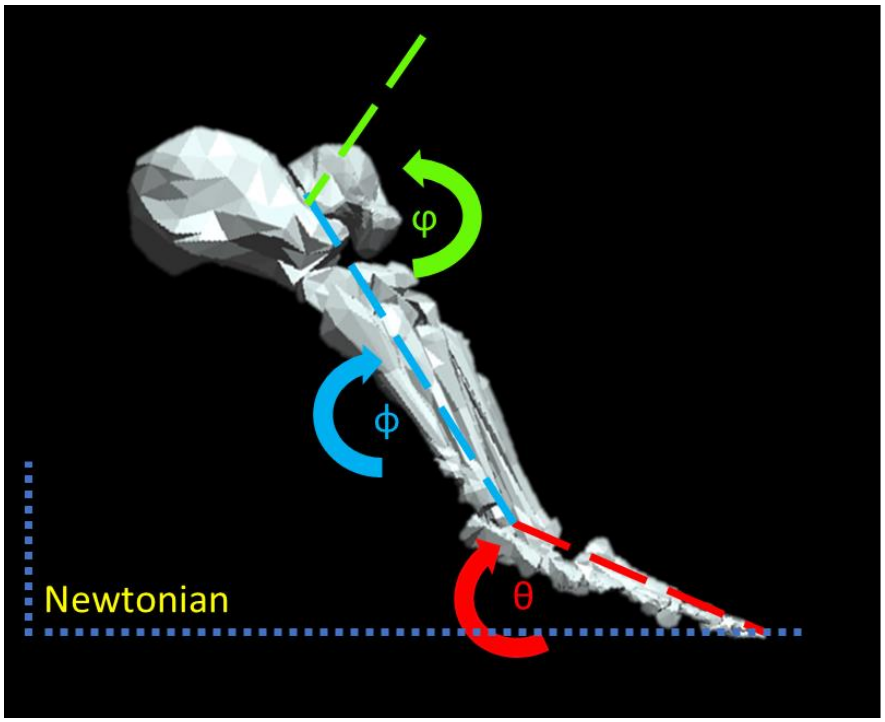


Figure 160: The addition of the toes adds another set of specified angle rotations to the model. The θ angle represents the rotation of the toes with respect to the Newtonian reference frame, the angle ϕ represents the angle between the foot and the toes, and φ represents the angle between the foot and ankle.

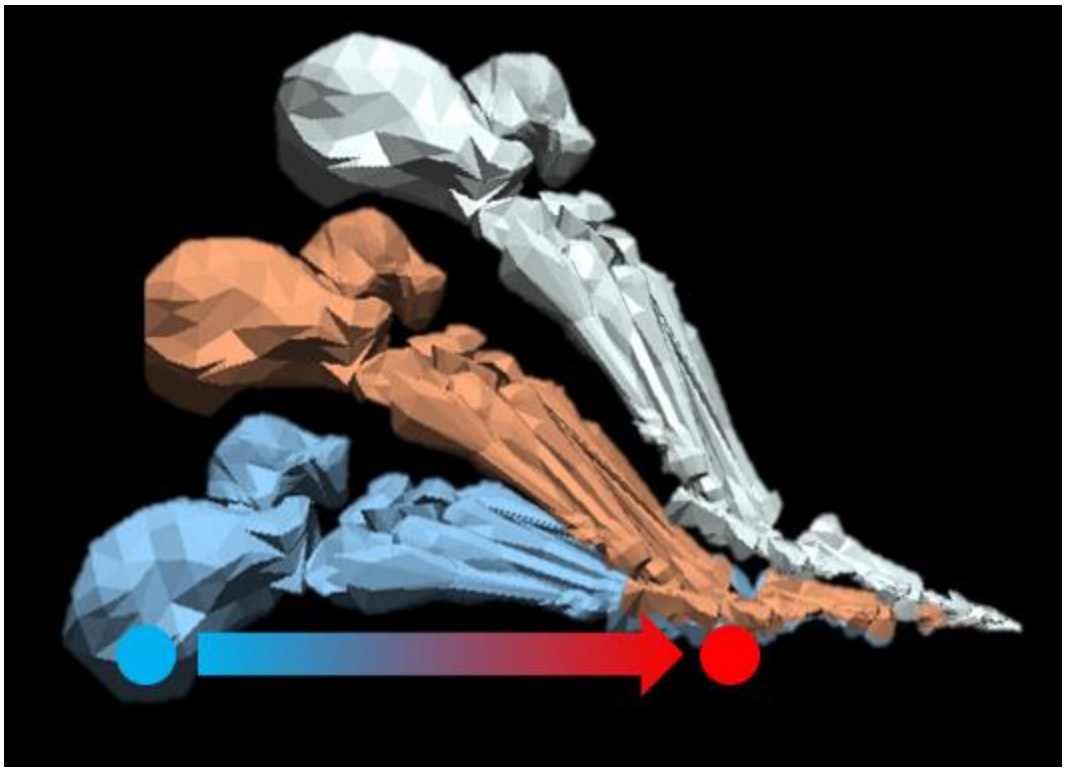


Figure 161: Throughout the gait cycle, the flexion of the foot increases with respect to the Newtonian frame. In addition, the contact point where the forces connect to the Newtonian frame shifts anteriorly to replicate the motion and contact pattern of the foot.

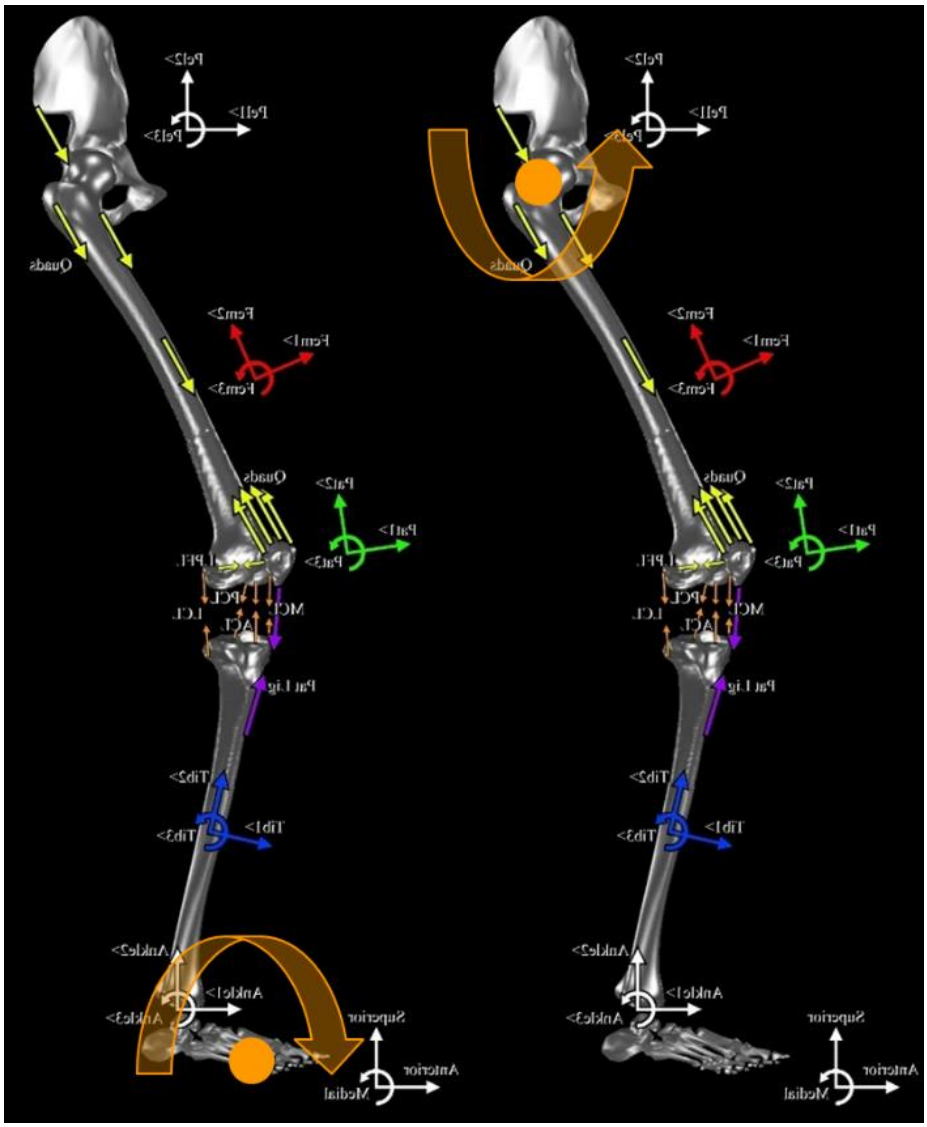


Figure 162: To make the transition from stance phase (left) to swing phase (right) the model must be inverted and center the rotation on the pelvis instead of the foot.

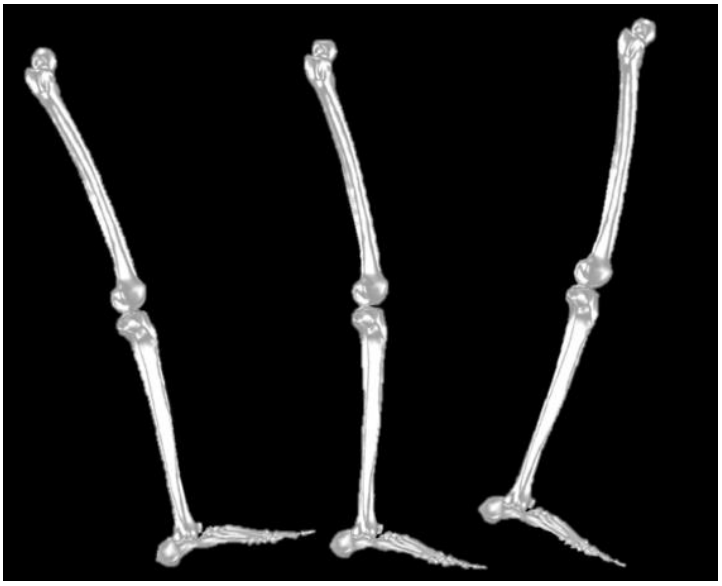


Figure 163: During stance phase the foot maintains constant ground contact while the knee enters a cycle of flexion followed by extension.

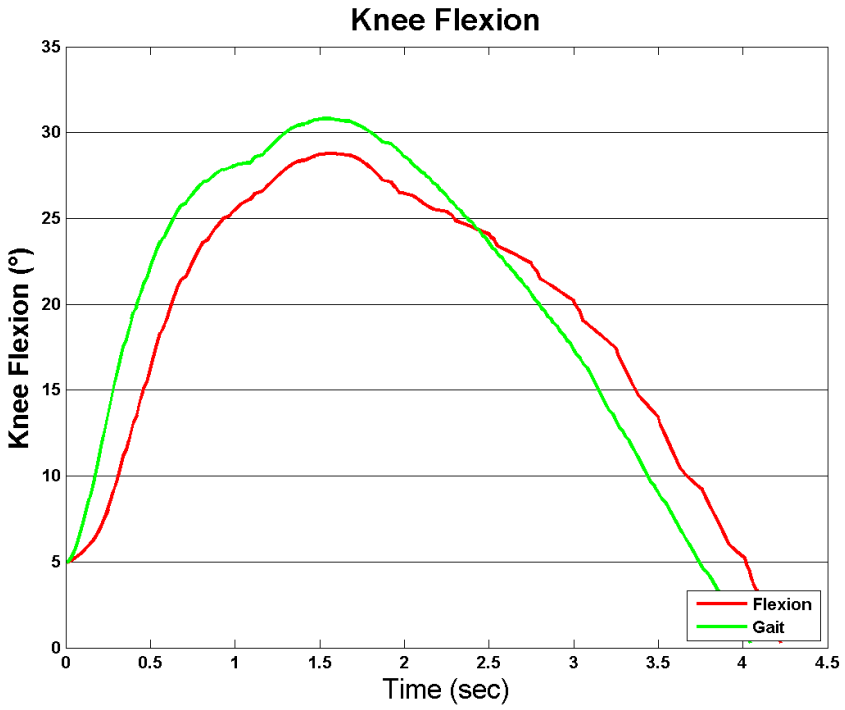


Figure 164: The knee flexion increments have slight differences between stationary flexion and gait where the gait pattern experiences a narrower parabolic pattern with greater flexion.

results of a shallow flexion activity which is roughly equivalent to a gait cycle assuming the foot is to remain stationary. It is proposed herein that the gait cycle is effectively a shallow flexion with the additional motion of the foot and for this reason the results are compared to such a control simulation.

Compared to a standard shallow flexion, the gait cycle in the model tends to demonstrate that the knee experiences equivalent magnitudes of tibiofemoral axial rotation during early and late stance along with lower magnitudes of axial rotation at mid stance (Figure 165). This pattern is very similar for translation of the medial condyle (Figure 166), meaning that medial anterior slide may be the causality for such rotational patterns. Lateral condyle motion appears to be inverted in that the lateral condyle translation is greater during gait than during standing flexion (Figure 167). It is also interesting that the lateral translation pattern is skewed right compared to the equivalent flexion profile. This is noted as the transition from lateral posterior translation (consistent with flexion) and lateral anterior translation (consistent with extension) occurs at 0.75 seconds, whereas the flexion-extension transition occurs at 1.5 seconds.

Unlike stance phase, the foot and ankle collectively do not experience any ground contact during swing phase (Figure 168). Outside of the center of rotation being changed, the rest of the activity is similar to stance phase where the knee experiences flexion then extension, where the maximum flexion value based on empirical data was 36 degrees.

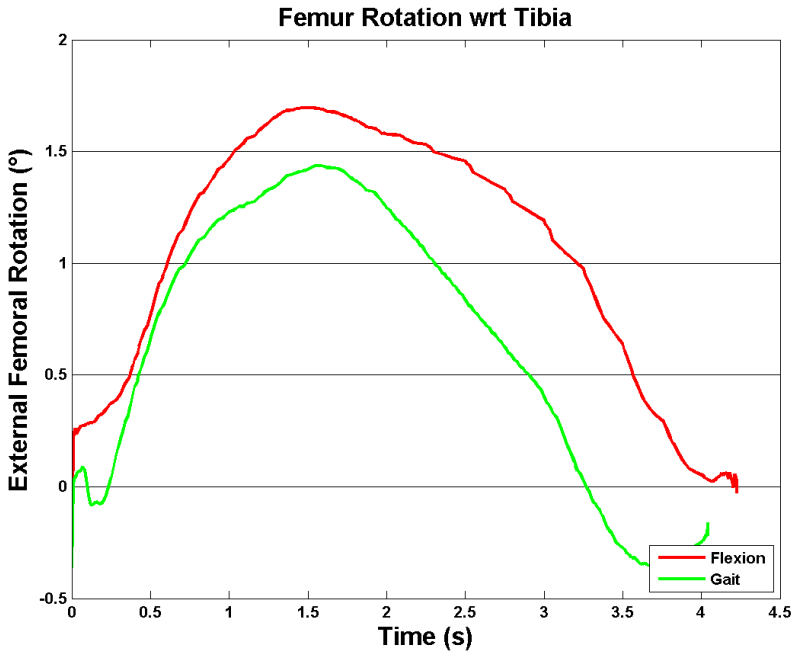


Figure 165: During gait the simulation predicted less tibiofemoral axial rotation compared to stationary flexion.

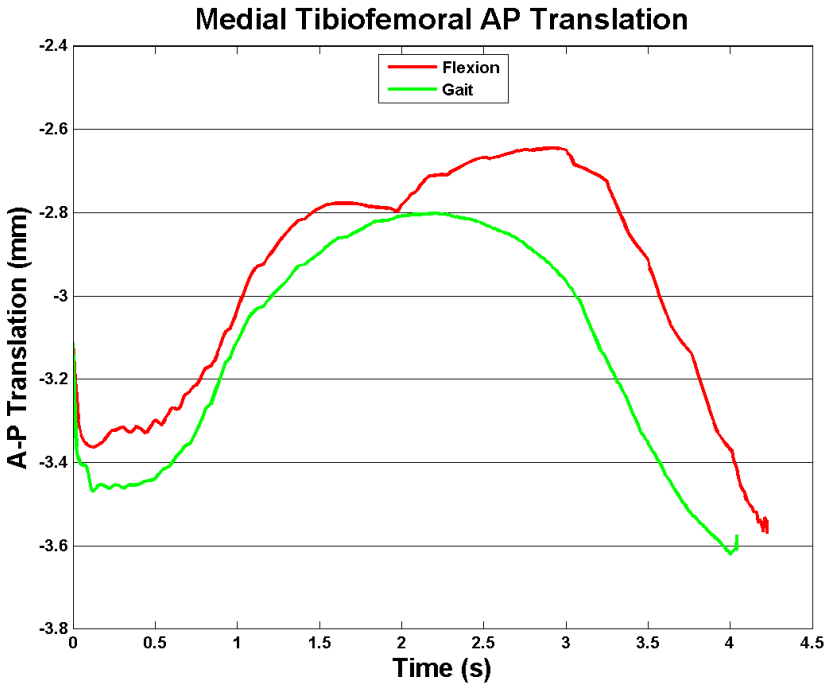


Figure 166: Compared to stationary flexion, the gait pattern produced a similar pattern with smaller magnitudes of medial anteroposterior translation.

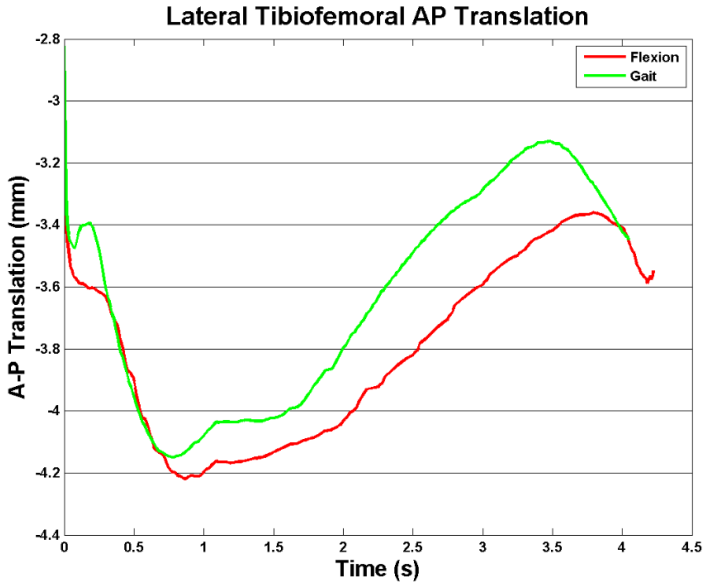


Figure 167: Compared to stationary flexion, the gait model produced a smaller overall magnitude of lateral condyle translation with the posterior to anterior transition occurring prior to the flexion extension transition in the model.

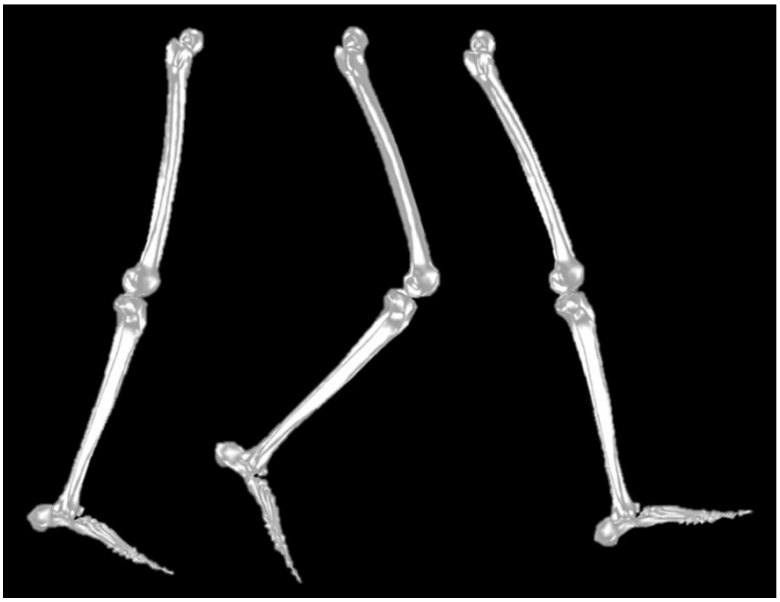


Figure 168: Swing phase occurs immediately following stance phase as the foot leaves the ground. The activity then becomes passive until the foot reestablishes contact with the ground.

Overall the stance and swing phase kinematic patterns during gait are quite similar. The flexion profile experiences a slightly positive phase shift for swing phase compared to stance phase, although the overall magnitudes of flexion are the same (Figure 169). There is not a discernable difference in tibiofemoral axial rotation over the course of swing phase (Figure 170). Likewise, there is not a significant difference between the medial and lateral condyle translations (Figure 171 & Figure 172), although the controller is less stable in passive flexion leading to increased oscillation of the kinematic patterns. It is noteworthy that the lateral condyle maintains a significant posterior translation pattern late in the swing phase motion. Such a pattern is not present in the stance phase comparison.

10.5 Conclusion

Overall the transition between a stationary shallow flexion and extension model to a gait model is relatively simple, where much of the additional motion is introduced through an inverse element on the foot. There are some substantial variations that come from converting a stationary model to a stance phase gait model; however, the swing phase model kinematics show minimal differences. As a passive flexion activity, there is only marginal clinical significance.

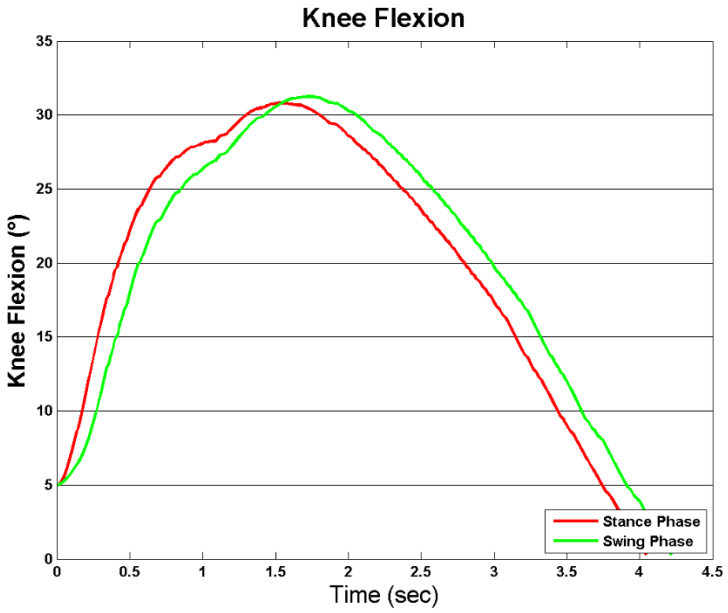


Figure 169: Aside from a slight phase shift in the positive time direction, the two flexion patterns between swing and stance phase are similar.

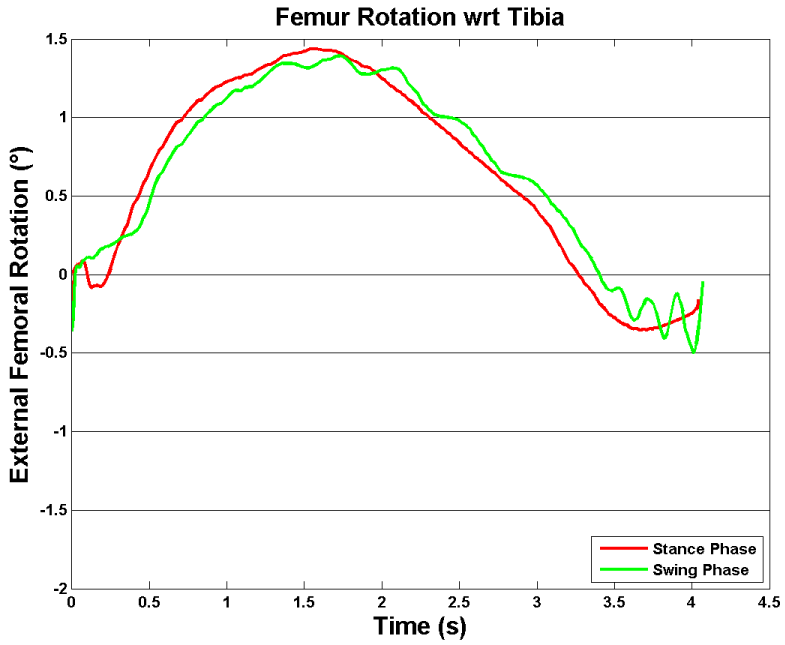


Figure 170: Between swing and stance phase, the femoral rotation patterns are similar.

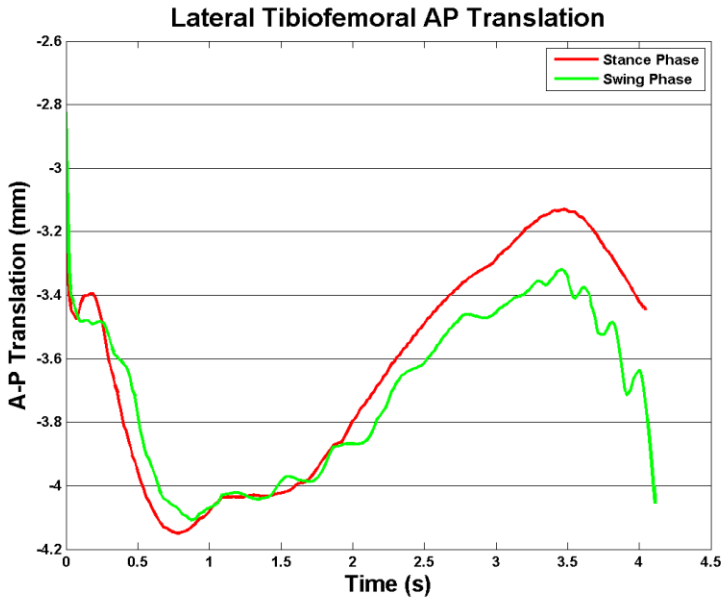


Figure 171: The swing and stance phase motion patterns are similar with the notable exception of the posterior motion occurring as swing phase ends.

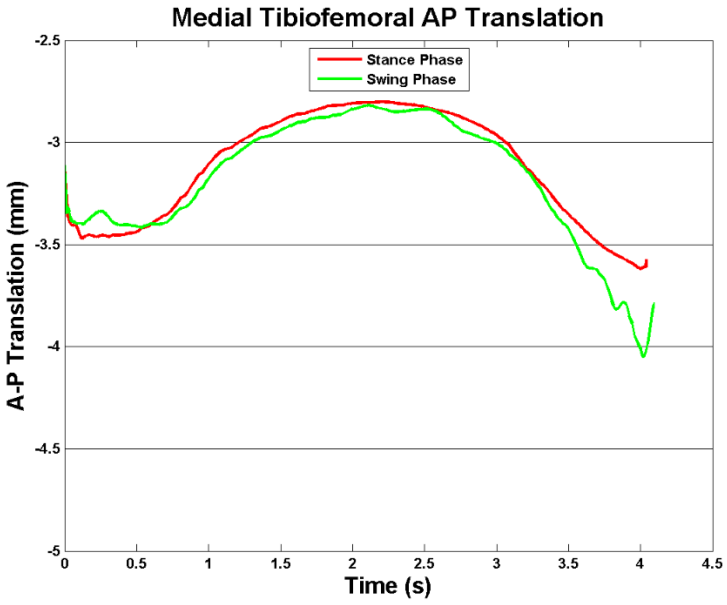


Figure 172: The medial condyle translations are similar between both swing and stance phase.

CHAPTER ELEVEN: VALIDATION

Unfortunately, much of the analysis that has been done is difficult to validate for a number or reasons. Many of the subjects evaluated were evaluated retrospectively, making further data acquisition difficult. The validation processes are also very time and equipment intensive making large scale operations difficult.

Despite these limitations to the validation process, certain aspects of the model can be validated using prior data and these methodologies may be sufficient to provide a broader scope of validation. Therefore, in an order to validate the model as well as possible, three aspects are taken and validated individually. In doing so, this shows the validity of each aspect of the model.

11.1 Validation Using Fluoroscopy

Fluoroscopy is the ideal measurement for the validation of knee kinematics which is an essential element of the forward solution model. The fundamental principle behind validation through fluoroscopy is simple, first a subject is evaluated fluoroscopically. Then those same geometries are put into the model and the results are compared. Ideally, the model results should match the fluoroscopic results.

Such is the method that was used in Chapter 4 with the validation of the normal knee. Ten subjects were assessed fluoroscopically, and during this process, 3D models of bone geometries were made. These same models were smoothed to promote integration into the model and then evaluated for the same activity. Model and fluoroscopic results were then averaged and compared.

Overall, the model and fluoroscopic results compared well. The condyle translations were comparable at their endpoints, and there were some slight deviations in mid flexion. Comparing axial rotation, the overall magnitude over flexion was greater for the model; however, there is a definite oscillatory behavior centered (Figure 173).

The results are very good approximations, meaning that the model was successful in predicting kinematics for this particular patient set. Unless we have the exact location of soft tissue attachment sites and patient-specific geometric and pathological data, it is difficult to conduct an exact match with a particular patient. While this is a process that ideally would be repeated to achieve statistical significance between model and fluoroscopic data, the model shows that at least for small scale studies (ten subjects), the generated kinematic prediction is valid.

In addition to fluoroscopy of these specific subjects, it is also possible to compare to existing published fluoroscopic studies to determine the accuracy of existing models and devices.

11.2 Validating with Telemetry

Fluoroscopy is one of the most accurate measurements for the assessment of in vivo kinematics. However, it is unable to accurately make predictions on device kinetics in vivo. For this reason, the use of a telemetric knee device is the most reliable method of assessing contact forces. A telemetric knee is a device implanted with force sensors, able to transcutaneous transmit force data in vivo (Figure 174). In order to use the technology to validate the model, a retrospective analysis must be done where a patient previously analyzed through fluoroscopy

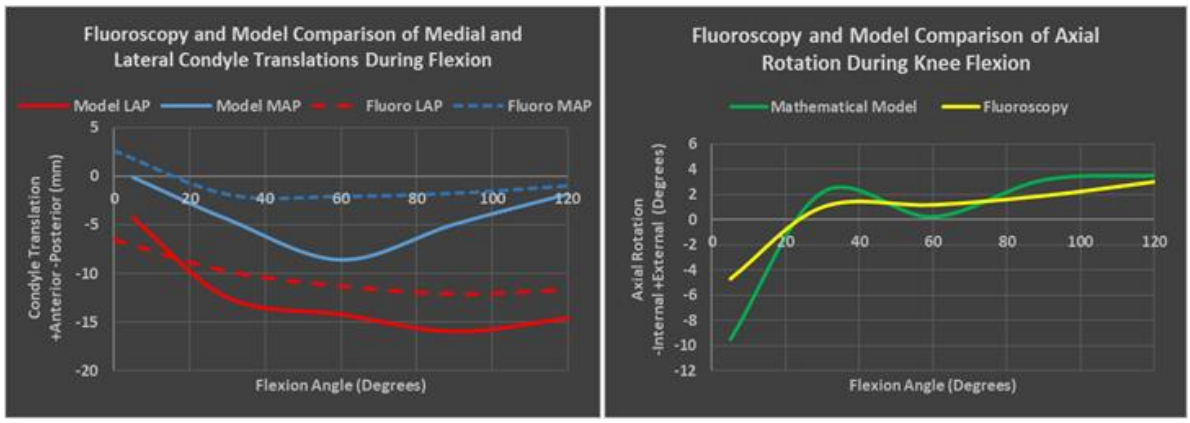


Figure 173: Average kinematic results for ten normal, healthy subjects evaluated both through the model and through fluoroscopy.

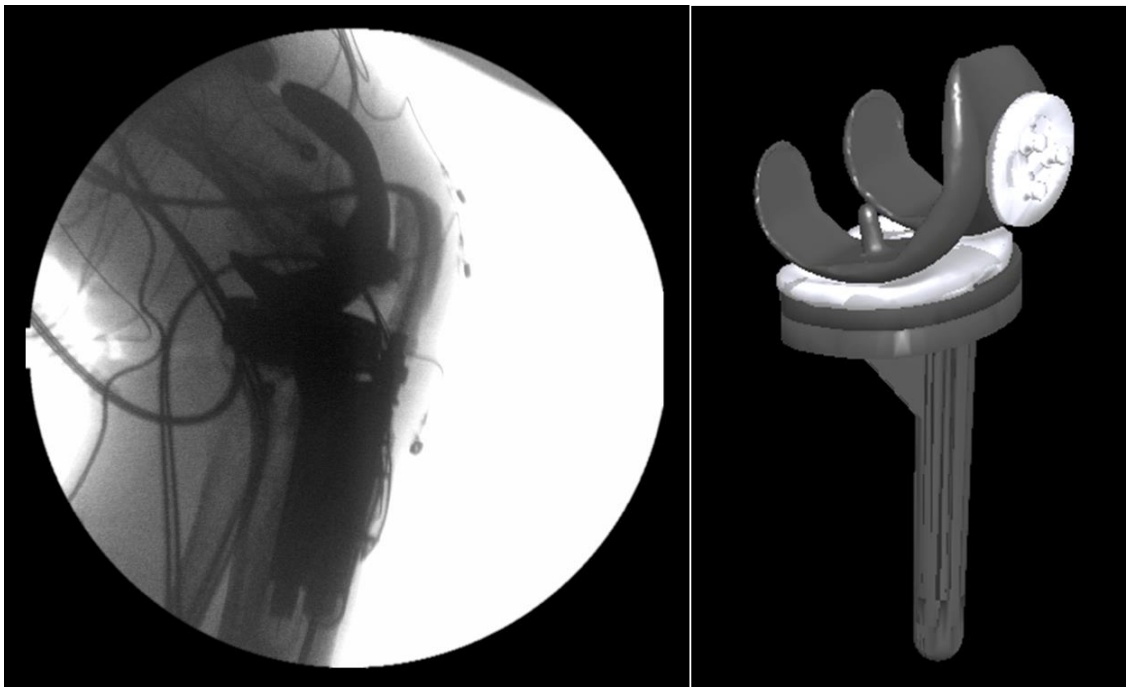


Figure 174: The telemetric device is a modified total knee arthroplasty where the tibia component is equipped with a force sensor that transmits force measurements externally to a data acquisition system.

with contact forces known through the telemetric device. The geometries associated with this particular patient can then be loaded into the model.

Once the geometries of the patient with known contact forces obtained through telemetry are loaded into the model, a simulation can be performed to assess if the contact forces predicted by the model closely match those measured telemetry. There is, however, one important factor to consider: the BW for the actual telemetric patient may vary from the value used in the model which assumes an average weight of 750 N or approximately 168 lbs. Because of this difference, between the two subjects' BWs, the model weight was updated post hoc to match that of the actual fluoroscopic patient.

Upon the completion of this process, the resulting model and measured forces were compared. It was determined that the model generally predicted contact forces to within 15 degrees (Figure 175), which overall is a reasonable value for model prediction. This is an accuracy that can be improved over larger patient populations; however, in this case, it is sufficient accuracy to consider the model valid.

11.3 Validating with Other Models

Fluoroscopy and telemetry are great methods of validating the kinematics and kinetics, respectively, although these are inherently predicated on access to retrospective data. In the case of this dissertation, much of this data was available and it was possible to use the same geometries in both modeling and in vivo testing.

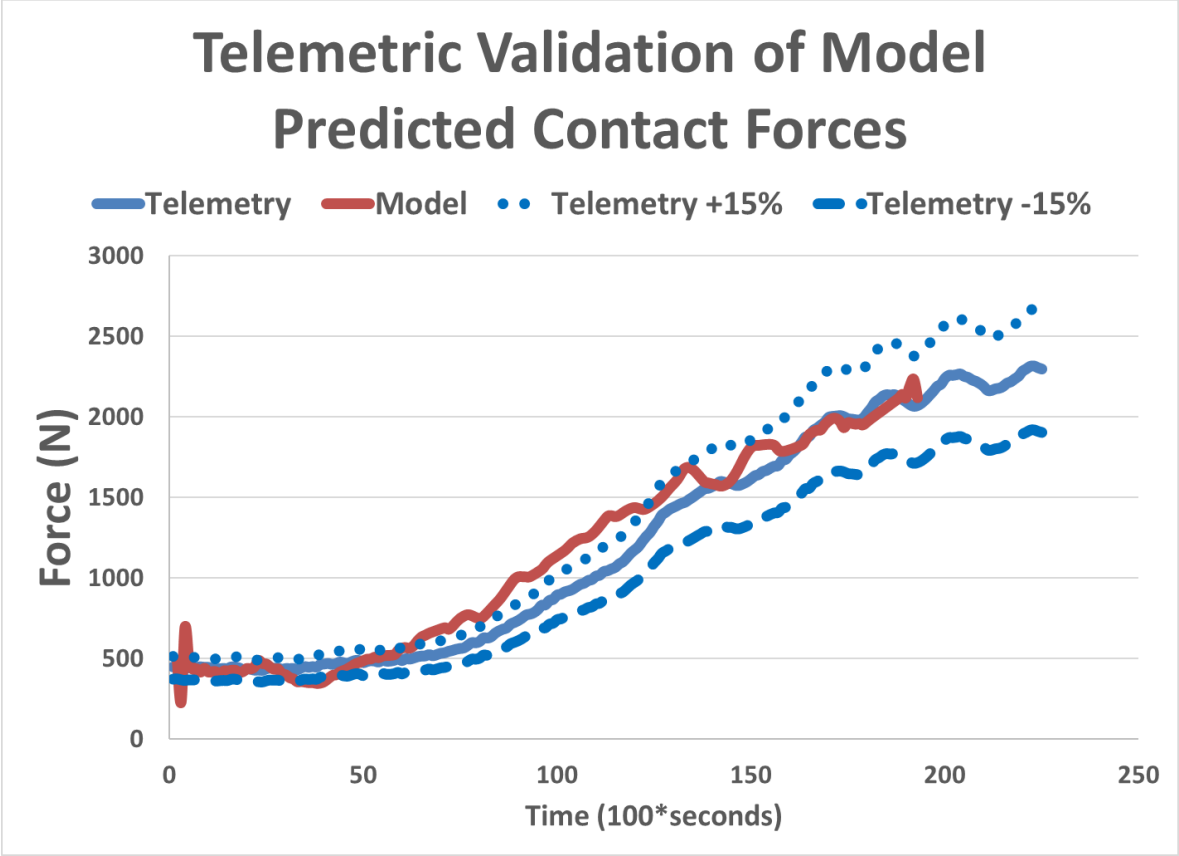


Figure 175: The mathematical model was able to predict contact forces to within 15% of the telemetrically measured values.

Should such a case not be available, another option would be to compare results for a model to other models elsewhere in literature. Of course, this is limited to models of known specific conditions. Therefore, model-to-model comparison is only of significance when comparing to an otherwise validated model.

CHAPTER TWELVE: ASSUMPTIONS LIMITATIONS AND FUTURE DIRECTION

12.1 Assumptions

Many of the initial assumptions utilized in previous iterations of the model are maintained through this iteration as well. Some of the more detailed assumptions are centered around the reduction nature of the model. This includes the assumption that all forces and torques are summed around each degree of freedom and are independent of the individual muscle forces. In other words, most of the joints are evaluated through inverse dynamics. The notable exception to this is the knee, which is calculated through forward dynamics, and it is assumed that the quadriceps forces are the primary muscles driving this motion. These muscles are placed, along with all other attachment sites, using the definitions from Opensim modeling software and it assumed that there is a roughly even distribution between these fibers.

In the normal knee analysis, a significant smoothing function was applied to the native geometries, which likely led to minor variations in the shape of articulating surfaces

In many cases where inverse motion patterns are specified, the fitting functions are often simplified to be of a cubic order or smaller. While analysis was done and curve fitting was done for 5th and 6th order, the inclusion of these functions resulted in inherent instabilities which were resolved using lower order functions. While attempts were made to keep these motions as physiologically

accurate as possible, which was an improvement of this iteration of the model, there are still assumptions included in the motions outside of the knee.

One of the largest assumptions relates to initial conditions for the models. Since geometries and mathematical representations thereof are from subject-to-subject and device-to-device, it is often assumed that models are operating in extension instead of flexion. This is because in the extension models, the knee will fall through its flexion cycle and arrive at the initial position that is most stable considering equilibrium conditions. Initially, the initial positions for a deep flexion maneuver are stabilized and established. Then, the model can run in extension, demonstrating the desired kinematic prediction. Therefore, the initial conditions may be different across the board. This also means that each simulation achieves its ideal initial positioning prior to analysis. The alternative to this would be to set initial conditions individually which would be problematic, as the early conditions may be unstable and inconsistent across each subject. Similarly, it is also assumed that ligament properties were consistent across patients and patient groups.

12.2 Limitations

One general limitation to this dissertation is that the analysis in most cases are intended to be used as proof of concept for use and further analysis. While useful observations have arisen from this analysis, many of these findings are novel in the context of computational modeling. For this very reason, sample sizes are small and much of the data collected for comparison to the computational model was evaluated retrospectively. These sample sizes, unfortunately, are too small to adequately run statistics which would be necessary to draw confident,

meaningful conclusions from the data. The aim here is to show that such analysis is possible and to suggest a number of otherwise preliminary findings for further investigation.

The most evident example of this is with regard to the demographic subjects. While this is one of the first studies to evaluate individual models based on gender, ethnicity and pathology, the process is only conducive to evaluating two patients for each group. Therefore, it is difficult to assess what differences are due to individual variations and what are due to variables being tested.

The nature of the knee also denotes many confounding variables due individual variations, some of which are not quantifiable, including ligament condition and shape of articulating surfaces. While these are factors that can be change in the model, they are often difficult to otherwise measure, making them often relegated to assumptions in the overall model. To attempt to account for this, often similar values were used across subject groups. However, this then raises the question of individual variations which are difficult to account for outside of an individualized model for every subject.

12.3 Future Direction

The first and most intuitive future direction for this model is the addition of multiple activities. While this iteration saw advances such as the addition of the foot and the inclusion of gait as an activity for analysis, there are additional alterations that can be made to assess other activities of daily living, such as inclined gait and stair stepping. These are activities useful in the assessment of

TKA devices, and they are also activities which hinder arthritic patients, making this a logical next step for the development of the model.

One of the inherent weaknesses of the analysis proposed with this model version is the limitation of sample size for the analysis of various demographic simulation sets. Increasing the number of patients evaluated adds statistical power to the analysis, ultimately contributing to more meaningful results that can be applied to wider populations. While the current model proposes a good start, more subjects and simulations are needed for enhanced meaning to these findings.

Another facet of the model that was not addressed in depth in this version of the model was the patella. As the main force transfer site from the extensor mechanism, the patella plays a large role in proper flexion and extension. While kept mostly consistent in this analysis, future work should focus on enhancing the patella interaction and building a better understanding of the role it plays during flexion.

Finally, this is the first forward solution mathematical model to evaluate the role of demographics and pathology to assess knee mechanics. While this is a worthwhile goal that was successfully achieved, it also highlighted the individual variations within each patient group. This leads to the logical conclusion that an individualized model would likely be logical next step to creating a universally useful model.

CHAPTER THIRTEEN: CONCLUSION

Throughout the course of this dissertation, seven novel contributions are proposed to advance the understanding of the human knee through enhanced parameterization of mathematically derived simulations. This includes the development of a model to evaluate the normal knee that successfully matches fluoroscopic results. It also includes a series of enhancements to the extensor mechanism, which allows for substantially increased efficiency of the extensor mechanism. Additionally, empirical data was collected on physiological joint motions which were then reapplied to the model to better simulate human motion. Furthermore, parametrically derived surfaces were designed which could be universally output to CAD software and a subsequent conformity analysis was performed. Moreover, ligament site and geometric differences between gender and ethnic groups were assessed for their respective effects on kinematics in addition to pathological conditions and their respective effects on kinematics. Finally, the model was amended to include gait as an additional activity.

All of these parameterizations aim to increase the applicability of the model to clinical situations. This model was originally intended to be a surgical design tool, and the advances that have been made not only enhance the capabilities but also the applications where it can be useful. The latest iteration of the model can be used as a tool to predict mechanics dependent on demographics and even based on diseases that may be present. The hope is that such a tool can be useful both to design engineers as a fast and efficient design evaluation technique and a tool for surgeons to understand joint diseases and target a better way to treat them.

In accomplishing these tasks, the enhancements of the model seek to create a tool to not only better understand how the knee moves, but also provide a resource that in capable hands, affords the ability to improve the overall function of the knee joint for every patient in every case.

LIST OF REFERENCES

[1] D. Swaminathan, H. Thornburg, J. Mumford, S. Rajko, J. James, T. Ingalls*, et al.*, "A dynamic bayesian approach to computational laban shape quality analysis," *Advances in Human-Computer Interaction,* vol. 2009, p. 2, 2009.
[2] H. D. Clarke, M. J. Krasdorf, C. R. Conley, Henrik Bo Pederson, and W. N. Scott, "Basic Science: Anatomy," in *Insall & Scott Surgery of the knee*. vol. 1, W. N. Scott, Ed., 6th ed Philidelphia PA: El Sevier, 2016, pp. 1-49.
[3] B. D. Ratner, H. Allan S, F. J. Schoen, and J. E. Lemons, "Orthopedic Applications," in *Biomaterials Science: An Introduction to Materials in Medicine*, Second ed: Elsevier Academic Press, 2004, pp. 526-698.
[4] J. D. Humphrey and D. Sherry L, "Biosolid Mechanics," in *An Introduction to Biomechanics*, ed: Springer, 2004, pp. 43-328.
[5] S. Claes, E. Vereecke, M. Maes, J. Victor, P. Verdonk, and J. Bellemans, "Anatomy of the anterolateral ligament of the knee," *Journal of anatomy,* vol. 223, pp. 321-328, 2013.
[6] M. M. Alzahrani, S. Aldebeyan, F. Abduljabbar, and P. A. Martineau, "Hamstring injuries in athletes: diagnosis and treatment," *JBJS reviews,* vol. 3, 2015.
[7] J. N. Insall, G. R. Scuderi, R. D. Komistek, K. Math, D. A. Dennis, and D. T. Anderson, "Correlation between condylar lift-off and femoral component alignment," *Clinical orthopaedics and related research,* vol. 403, pp. 143-152, 2002.
[8] D. Dennis, R. Komistek, S. Walker, E. Cheal, and J. Stiehl, "Femoral condylar lift-off in vivo in total knee arthroplasty," *Journal of Bone & Joint Surgery, British Volume,* vol. 83, pp. 33-39, 2001.
[9] R. D. Komistek, D. A. Dennis, and M. Mahfouz, "In vivo fluoroscopic analysis of the normal human knee," *Clinical orthopaedics and related research,* vol. 410, pp. 69-81, 2003.
[10] F. Leszko, K. R. Hovinga, A. L. Lerner, R. D. Komistek, and M. R. Mahfouz, "In vivo normal knee kinematics: is ethnicity or gender an influencing factor?," *Clinical Orthopaedics and Related Research®,* vol. 469, pp. 95-106, 2011.
[11] T. Fukubayashi, P. Torzilli, M. Sherman, and R. Warren, "An in vitro biomechanical evaluation of anterior-posterior motion of the knee. Tibial displacement, rotation, and torque," *The Journal of bone and joint surgery. American volume,* vol. 64, pp. 258-264, 1982.
[12] D. Foti and J. S. Koketsu, "Activities of daily living," *Pedretti's Occupational Therapy: Practical Skills for Physical Dysfunction,* vol. 7, pp. 157-232, 2013.
[13] H. M. Frost, "Wolff's Law and bone's structural adaptations to mechanical usage: an overview for clinicians," *The Angle Orthodontist,* vol. 64, pp. 175-188, 1994.
[14] H. Frost, "Skeletal structural adaptations to mechanical usage (SATMU): 1. Redefining Wolff's law: the bone modeling problem," *The Anatomical Record,* vol. 226, pp. 403-413, 1990.

[15] T. Hayami, M. Pickarski, G. A. Wesolowski, J. Mclane, A. Bone, J. Destefano*, et al.*, "The role of subchondral bone remodeling in osteoarthritis: reduction of cartilage degeneration and prevention of osteophyte formation by alendronate in the rat anterior cruciate ligament transection model," *Arthritis & Rheumatology,* vol. 50, pp. 1193-1206, 2004.
[16] A. A. o. O. Surgeons. (2014, February). *Arthritis of the Knee*.
[17] H. Behrend, K. Giesinger, J. M. Giesinger, and M. S. Kuster, "The “forgotten joint” as the ultimate goal in joint arthroplasty: validation of a new patient-reported outcome measure," *The Journal of arthroplasty,* vol. 27, pp. 430-436. e1, 2012.
[18] F. Eymard, A. Charles-Nelson, S. Katsahian, X. Chevalier, and M. Bercovy, ""Forgotten knee” after total knee replacement: a pragmatic study from a single-centre cohort," *Joint Bone Spine,* vol. 82, pp. 177-181, 2015.
[19] G. R. Scuderi, R. B. Bourne, P. C. Noble, J. B. Benjamin, J. H. Lonner, and W. Scott, "The new knee society knee scoring system," *Clinical Orthopaedics and Related Research®,* vol. 470, pp. 3-19, 2012.
[20] E. Ghanem, I. Pawasarat, A. Lindsay, L. May, K. Azzam, A. Joshi*, et al.*, "Limitations of the Knee Society Score in evaluating outcomes following revision total knee arthroplasty," *JBJS,* vol. 92, pp. 2445-2451, 2010.
[21] J. N. Insall, L. D. Dorr, R. D. Scott, and W. N. Scott, "Rationale of the Knee Society clinical rating system," *Clin Orthop relat res,* vol. 248, pp. 13-14, 1989.
[22] E. M. Roos, H. P. Roos, L. S. Lohmander, C. Ekdahl, and B. D. Beynnon, "Knee Injury and Osteoarthritis Outcome Score (KOOS)—development of a self-administered outcome measure," *Journal of Orthopaedic & Sports Physical Therapy,* vol. 28, pp. 88-96, 1998.
[23] G. Yildirim, P. S. Walker, and J. Boyer, "Total knees designed for normal kinematics evaluated in an up-and-down crouching machine," *Journal of Orthopaedic Research,* vol. 27, pp. 1022-1027, 2009.
[24] D. A. Dennis, M. R. Mahfouz, R. D. Komistek, and W. Hoff, "In vivo determination of normal and anterior cruciate ligament-deficient knee kinematics," *Journal of biomechanics,* vol. 38, pp. 241-253, 2005.
[25] D. A. Dennis, R. D. Komistek, M. R. Mahfouz, B. D. Haas, and J. B. Stiehl, "Conventry Award Paper: Multicenter Determination of In Vivo Kinematics After Total Knee Arthroplasty," *Clinical orthopaedics and related research,* vol. 416, pp. 37-57, 2003.
[26] J. G. Anderson, R. L. Wixson, D. Tsai, S. D. Stulberg, and R. W. Chang, "Functional outcome and patient satisfaction in total knee patients over the age of 75," *The Journal of arthroplasty,* vol. 11, pp. 831-840, 1996.
[27] P. C. Noble, M. A. Conditt, K. F. Cook, and K. B. Mathis, "The John Insall Award: Patient expectations affect satisfaction with total knee arthroplasty," *Clinical orthopaedics and related research,* vol. 452, pp. 35-43, 2006.

[28] P. Baker, J. Van der Meulen, J. Lewsey, and P. Gregg, "The role of pain and function in determining patient satisfaction after total knee replacement Data from the National Joint Registry for England and Wales," *Journal of Bone & Joint Surgery, British Volume,* vol. 89, pp. 893-900, 2007.
[29] R. B. Bourne, B. M. Chesworth, A. M. Davis, N. N. Mahomed, and K. D. Charron, "Patient satisfaction after total knee arthroplasty: who is satisfied and who is not?," *Clinical Orthopaedics and Related Research®,* vol. 468, pp. 57-63, 2010.
[30] F. Merle-Vincent, C. M. Couris, A.-M. Schott, T. Conrozier, M. Piperno, P. Mathieu*, et al.*, "Factors predicting patient satisfaction 2 years after total knee arthroplasty for osteoarthritis," *Joint Bone Spine,* vol. 78, pp. 383-386, 2011.
[31] N. Clement and R. Burnett, "Patient satisfaction after total knee arthroplasty is affected by their general physical well-being," *Knee Surgery, Sports Traumatology, Arthroscopy,* vol. 21, pp. 2638-2646, 2013.
[32] H. Du, H. Tang, J.-M. Gu, and Y.-X. Zhou, "Patient satisfaction after posterior-stabilized total knee arthroplasty: a functional specific analysis," *The Knee,* vol. 21, pp. 866-870, 2014.
[33] S. A. Banks, G. D. Markovich, and W. A. Hodge, "In vivo kinematics of cruciate-retaining and-substituting knee arthroplasties," *The Journal of arthroplasty,* vol. 12, pp. 297-304, 1997.
[34] S. M. Zingde, F. Leszko, A. Sharma, M. R. Mahfouz, R. D. Komistek, and D. A. Dennis, "In vivo determination of cam-post engagement in fixed and mobile-bearing TKA," *Clinical Orthopaedics and Related Research®,* vol. 472, pp. 254-262, 2014.
[35] D. A. Dennis, R. D. Komistek, J. B. Stiehl, S. A. Walker, and K. N. Dennis, "Range of motion after total knee arthroplasty The effect of implant design and weight-bearing conditions," *The Journal of arthroplasty,* vol. 13, pp. 748-752, 1998.
[36] H. E. Cates, R. D. Komistek, M. R. Mahfouz, M. A. Schmidt, and M. Anderle, "In vivo comparison of knee kinematics for subjects having either a posterior stabilized or cruciate retaining high-flexion total knee arthroplasty," *The Journal of arthroplasty,* vol. 23, pp. 1057-1067, 2008.
[37] N. Arnout, L. Vanlommel, J. Vanlommel, J. Luyckx, L. Labey, B. Innocenti*, et al.*, "Post-cam mechanics and tibiofemoral kinematics: a dynamic in vitro analysis of eight posterior-stabilized total knee designs," *Knee Surgery, Sports Traumatology, Arthroscopy,* vol. 23, pp. 3343-3353, 2015.
[38] I. M. Zeller, A. Sharma, W. B. Kurtz, M. R. Anderle, and R. D. Komistek, "Customized versus Patient-Sized Cruciate-Retaining Total Knee Arthroplasty: An In Vivo Kinematics Study Using Mobile Fluoroscopy," *The Journal of Arthroplasty,* vol. 32, pp. 1344-1350, 2017.
[39] L. Hallen and O. Lindahl, "The “screw-home” movement in the knee-joint," *Acta Orthopaedica Scandinavica,* vol. 37, pp. 97-106, 1966.

[40] K. Moglo and A. Shirazi-Adl, "Cruciate coupling and screw-home mechanism in passive knee joint during extension–flexion," *Journal of biomechanics,* vol. 38, pp. 1075-1083, 2005.
[41] J. B. Stiehl, D. A. Dennis, R. D. Komistek, and H. S. Crane, "In vivo determination of condylar lift-off and screw-home in a mobile-bearing total knee arthroplasty," *The Journal of arthroplasty,* vol. 14, pp. 293-299, 1999.
[42] T. Andriacchi, J. Galante, and R. Fermier, "The influence of total knee-replacement design on walking and stair-climbing," *JBJS,* vol. 64, pp. 1328-1335, 1982.
[43] L. D. Dorr, J. L. Ochsner, J. Gronley, and J. Perry, "Functional Comparison of Posterior Cruciate Retained versus Cruciate-Sacrificed Total Knee Arthroplasty," *Clinical orthopaedics and related research,* vol. 236, pp. 36-43, 1988.
[44] D. A. Dennis, R. D. Komistek, and M. R. Mahfouz, "In vivo fluoroscopic analysis of fixed-bearing total knee replacements," *Clinical orthopaedics and related research,* vol. 410, pp. 114-130, 2003.
[45] S. Nakamura, A. Sharma, K. Nakamura, N. Ikeda, S. M. Zingde, and R. D. Komistek, "Can post-cam function be replaced by addition of a third condyle in PS TKA?," *The Journal of arthroplasty,* vol. 29, pp. 1871-1876, 2014.
[46] F. Orozco and A. Ong, *Posterior Stabilized Total Knee Arthroplasty*: INTECH Open Access Publisher, 2012.
[47] S. A. Wilson, P. D. McCann, R. S. Gotlin, H. Ramakrishnan, M. E. Wootten, and J. N. Insall, "Comprehensive gait analysis in posterior-stabilized knee arthroplasty," *The Journal of arthroplasty,* vol. 11, pp. 359-367, 1996.
[48] A. Sharma, R. D. Komistek, C. S. Ranawat, D. A. Dennis, and M. R. Mahfouz, "In vivo contact pressures in total knee arthroplasty," *The Journal of arthroplasty,* vol. 22, pp. 404-416, 2007.
[49] J. Fisher, H. McEwen, J. Tipper, L. Jennings, R. Farrar, M. Stone*, et al.*, "Wear-simulation analysis of rotating-platform mobile-bearing knees," *Orthopedics,* vol. 29, pp. S36-41, 2006.
[50] J. Fisher, H. M. McEwen, J. L. Tipper, A. L. Galvin, J. Ingram, A. Kamali*, et al.*, "Wear, debris, and biologic activity of cross-linked polyethylene in the knee: benefits and potential concerns," *Clinical orthopaedics and related research,* vol. 428, pp. 114-119, 2004.
[51] Z. D. Post, W. Y. Matar, T. Van De Leur, E. L. Grossman, and M. S. Austin, "Mobile-bearing total knee arthroplasty: better than a fixed-bearing?," *The Journal of arthroplasty,* vol. 25, pp. 998-1003, 2010.
[52] S. Bhan, R. Malhotra, E. K. Kiran, S. Shukla, and M. Bijjawara, "A comparison of fixed-bearing and mobile-bearing total knee arthroplasty at a minimum follow-up of 4.5 years," *J Bone Joint Surg Am,* vol. 87, pp. 2290-2296, 2005.
[53] Y.-H. Kim, S.-H. Yoon, and J.-S. Kim, "The long-term results of simultaneous fixed-bearing and mobile-bearing total knee replacements

performed in the same patient," *Bone & Joint Journal,* vol. 89, pp. 1317-1323, 2007.
[54] A. S. Ranawat, R. Rossi, I. Loreti, V. J. Rasquinha, J. A. Rodriguez, and C. S. Ranawat, "Comparison of the PFC Sigma fixed-bearing and rotating-platform total knee arthroplasty in the same patient: short-term results," *The Journal of arthroplasty,* vol. 19, pp. 35-39, 2004.
[55] M. W. Pagnano, R. T. Trousdale, M. J. Stuart, A. D. Hanssen, and D. J. Jacofsky, "Rotating platform knees did not improve patellar tracking: a prospective, randomized study of 240 primary total knee arthroplasties," *Clinical orthopaedics and related research,* vol. 428, pp. 221-227, 2004.
[56] R. C. Wasielewski, R. D. Komistek, S. M. Zingde, K. C. Sheridan, and M. R. Mahfouz, "Lack of axial rotation in mobile-bearing knee designs," *Clinical orthopaedics and related research,* vol. 466, pp. 2662-2668, 2008.
[57] D. A. Dennis, R. D. Komistek, M. R. Mahfouz, S. A. Walker, and A. Tucker, "A multicenter analysis of axial femorotibial rotation after total knee arthroplasty," *Clinical orthopaedics and related research,* vol. 428, pp. 180-189, 2004.
[58] M. T. LaCour, A. Sharma, C. B. Carr, R. D. Komistek, and D. A. Dennis, "Confirmation of long-term in vivo bearing mobility in eight rotating-platform TKAs," *Clinical Orthopaedics and Related Research®,* vol. 472, pp. 2766-2773, 2014.
[59] K. C. Bertin, R. D. Komistek, D. A. Dennis, W. A. Hoff, D. T. Anderson, and T. Langer, "In vivo determination of posterior femoral rollback for subjects having a NexGen posterior cruciate–retaining total knee arthroplasty," *The Journal of arthroplasty,* vol. 17, pp. 1040-1048, 2002.
[60] J. Bellemans, K. Carpentier, H. Vandenneucker, J. Vanlauwe, and J. Victor, "The John Insall Award: both morphotype and gender influence the shape of the knee in patients undergoing TKA," *Clinical Orthopaedics and Related Research®,* vol. 468, pp. 29-36, 2010.
[61] A. F. Kamath, J. G. Horneff, V. Gaffney, C. L. Israelite, and C. L. Nelson, "Ethnic and gender differences in the functional disparities after primary total knee arthroplasty," *Clinical Orthopaedics and Related Research®,* vol. 468, pp. 3355-3361, 2010.
[62] P. Li, T.-Y. Tsai, J.-S. Li, S. Wang, Y. Zhang, Y.-M. Kwon*, et al.*, "Gender analysis of the anterior femoral condyle geometry of the knee," *The Knee,* vol. 21, pp. 529-533, 2014.
[63] S. Guy, M. Farndon, S. Sidhom, M. Al-Lami, C. Bennett, and N. London, "Gender differences in distal femoral morphology and the role of gender specific implants in total knee replacement: a prospective clinical study," *The Knee,* vol. 19, pp. 28-31, 2012.
[64] J. E. Stoddard, D. J. Deehan, A. M. Bull, A. W. McCaskie, and A. A. Amis, "The kinematics and stability of single-radius versus multi-radius femoral components related to Mid-range instability after TKA," *Journal of Orthopaedic Research,* vol. 31, pp. 53-58, 2013.
[65] T. F. Grieco, A. Sharma, R. D. Komistek, and H. E. Cates, "Single Versus Multiple-Radii Cruciate-Retaining Total Knee Arthroplasty: An In Vivo

Mobile Fluoroscopy Study," *The Journal of arthroplasty,* vol. 31, pp. 694-701, 2016.
[66] D. F. Dalury, "ATTUNE™ KNEE SYSTEM: ATTUNE GRADIUS™ CURVE."
[67] W. J. Hurd and L. Snyder-Mackler, "Knee instability after acute ACL rupture affects movement patterns during the mid-stance phase of gait," *Journal of Orthopaedic Research,* vol. 25, pp. 1369-1377, 2007.
[68] C. W. Clary, C. K. Fitzpatrick, L. P. Maletsky, and P. J. Rullkoetter, "The influence of total knee arthroplasty geometry on mid-flexion stability: an experimental and finite element study," *Journal of biomechanics,* vol. 46, pp. 1351-1357, 2013.
[69] B. S. Parsley, R. Bertolusso, M. Harrington, A. Brekke, and P. C. Noble, "Influence of gender on age of treatment with TKA and functional outcome," *Clinical Orthopaedics and Related Research®,* vol. 468, pp. 1759-1764, 2010.
[70] M. Mahfouz, E. E. A. Fatah, L. S. Bowers, and G. Scuderi, "Three-dimensional morphology of the knee reveals ethnic differences," *Clinical Orthopaedics and Related Research «,* vol. 470, pp. 172-185, 2012.
[71] D. J. van den Heever, C. Scheffer, P. Erasmus, and E. Dillon, "Classification of gender and race in the distal femur using self organising maps," *The Knee,* vol. 19, pp. 488-492, 2012.
[72] I. M. Zeller, A. Sharma, W. B. Kurtz, M. R. Anderle, and R. D. Komistek, "Customized versus Patient-Sized Cruciate-Retaining Total Knee Arthroplasty: An In Vivo Kinematics Study Using Mobile Fluoroscopy," *The Journal of Arthroplasty,* 2016.
[73] S. Yoshiya, N. Matsui, R. D. Komistek, D. A. Dennis, M. Mahfouz, and M. Kurosaka, "In vivo kinematic comparison of posterior cruciate-retaining and posterior stabilized total knee arthroplasties under passive and weight-bearing conditions," *The Journal of arthroplasty,* vol. 20, pp. 777-783, 2005.
[74] M. Tanzer, K. Smith, and S. Burnett, "Posterior-stabilized versus cruciate-retaining total knee arthroplasty: balancing the gap," *The Journal of arthroplasty,* vol. 17, pp. 813-819, 2002.
[75] S. Maruyama, S. Yoshiya, N. Matsui, R. Kuroda, and M. Kurosaka, "Functional comparison of posterior cruciate-retaining versus posterior stabilized total knee arthroplasty," *The Journal of arthroplasty,* vol. 19, pp. 349-353, 2004.
[76] H. Horiuchi, S. Akizuki, T. Tomita, K. Sugamoto, T. Yamazaki, and N. Shimizu, "In vivo kinematic analysis of cruciate-retaining total knee arthroplasty during weight-bearing and non–weight-bearing deep knee bending," *The Journal of arthroplasty,* vol. 27, pp. 1196-1202, 2012.
[77] M. A. Conditt, P. C. Noble, R. Bertolusso, J. Woody, and B. S. Parsley, "The PCL significantly affects the functional outcome of total knee arthroplasty," *The Journal of arthroplasty,* vol. 19, pp. 107-112, 2004.
[78] E. Li and M. A. Ritter, "The case for retention of the posterior cruciate ligament," *The Journal of Arthroplasty,* vol. 10, pp. 560-564, 1995.

[79] B. Yue, K. M. Varadarajan, A. L. Moynihan, F. Liu, H. E. Rubash, and G. Li, "Kinematics of medial osteoarthritic knees before and after posterior cruciate ligament retaining total knee arthroplasty," *Journal of Orthopaedic Research,* vol. 29, pp. 40-46, 2011.
[80] D. E. Font-Rodriguez, G. R. Scuderi, and J. N. Insall, "Survivorship of cemented total knee arthroplasty," *Clinical orthopaedics and related research,* vol. 345, pp. 79-86, 1997.
[81] C. S. Ranawat and O. Boachie-Adjei, "Survivorship analysis and results of total condylar knee arthroplasty: eight-to 11-year follow-up period," *Clinical orthopaedics and related research,* vol. 226, pp. 6-13, 1988.
[82] C. S. Ranawat, W. F. FLYNN JR, S. Saddler, K. K. Hansraj, and M. J. Maynard, "Long-Term Results of the Total Condylar Knee Arthroplasty: A 15-Year Survivorship Study," *Clinical orthopaedics and related research,* vol. 286, pp. 94-102, 1993.
[83] D. M. Zuckerman, P. Brown, and S. E. Nissen, "Medical device recalls and the FDA approval process," *Archives of internal medicine,* vol. 171, pp. 1006-1011, 2011.
[84] J. S. Kirkpatrick and T. Stevens, "The FDA process for the evaluation and approval of orthopaedic devices," *JAAOS-Journal of the American Academy of Orthopaedic Surgeons,* vol. 16, pp. 260-267, 2008.
[85] J. S. Kahan, "Premarket approval versus premarket notification: different routes to the same market," *Food Drug Cosm. LJ,* vol. 39, p. 510, 1984.
[86] C. J. Lavernia, R. J. Sierra, D. S. Hungerford, and K. Krackow, "Activity level and wear in total knee arthroplasty: a study of autopsy retrieved specimens," *The Journal of arthroplasty,* vol. 16, pp. 446-453, 2001.
[87] M. Rohrbach, M. Lüem, and P. E. Ochsner, "Patient and surgery related factors associated with fatigue type polyethylene wear on 49 PCA and DURACON retrievals at autopsy and revision," *Journal of orthopaedic surgery and research,* vol. 3, p. 8, 2008.
[88] J. B. Meding, L. K. Meding, M. A. Ritter, and E. M. Keating, "Pain relief and functional improvement remain 20 years after knee arthroplasty," *Clinical Orthopaedics and Related Research®,* vol. 470, pp. 144-149, 2012.
[89] J. D. DesJardins, P. S. Walker, H. Haider, and J. Perry, "The use of a force-controlled dynamic knee simulator to quantify the mechanical performance of total knee replacement designs during functional activity," *Journal of Biomechanics,* vol. 33, pp. 1231-1242, 2000.
[90] J. H. Currier, M. A. Bill, and M. B. Mayor, "Analysis of wear asymmetry in a series of 94 retrieved polyethylene tibial bearings," *Journal of biomechanics,* vol. 38, pp. 367-375, 2005.
[91] R. C. Wasielewski, N. Parks, I. Williams, H. Surprenant, J. P. Collier, and G. Engh, "Tibial insert undersurface as a contributing source of polyethylene wear debris," *Clinical orthopaedics and related research,* pp. 53-59, 1997.
[92] R. C. Wasielewski, J. O. Galante, R. M. Leighty, R. N. Natarajan, and A. G. Rosenberg, "Wear patterns on retrieved polyethylene tibial inserts and

their relationship to technical considerations during total knee arthroplasty," *Clinical orthopaedics and related research,* pp. 31-43, 1994.
[93] F. W. Werner, D. C. Ayers, L. P. Maletsky, and P. J. Rullkoetter, "The effect of valgus/varus malalignment on load distribution in total knee replacements," *Journal of biomechanics,* vol. 38, pp. 349-355, 2005.
[94] J. P. Halloran, C. W. Clary, L. P. Maletsky, M. Taylor, A. J. Petrella, and P. J. Rullkoetter, "Verification of predicted knee replacement kinematics during simulated gait in the Kansas knee simulator," *Journal of biomechanical engineering,* vol. 132, p. 081010, 2010.
[95] K. M. Varadarajan, R. E. Harry, T. Johnson, and G. Li, "Can in vitro systems capture the characteristic differences between the flexion–extension kinematics of the healthy and TKA knee?," *Medical Engineering and Physics,* vol. 31, pp. 899-906, 2009.
[96] B. D. Stemper, N. Yoganandan, M. R. Stineman, T. A. Gennarelli, J. L. Baisden, and F. A. Pintar, "Mechanics of fresh, refrigerated, and frozen arterial tissue," *Journal of Surgical Research,* vol. 139, pp. 236-242, 2007.
[97] K. M. Varadarajan, A. L. Moynihan, D. D'Lima, C. W. Colwell, and G. Li, "In vivo contact kinematics and contact forces of the knee after total knee arthroplasty during dynamic weight-bearing activities," *Journal of biomechanics,* vol. 41, pp. 2159-2168, 2008.
[98] D. D. D'Lima, N. Steklov, S. Patil, and C. W. Colwell, "The Mark Coventry Award: in vivo knee forces during recreation and exercise after knee arthroplasty," *Clinical orthopaedics and related research,* vol. 466, pp. 2605-2611, 2008.
[99] S. Zingde, "In Vivo Mechanics and Vibrations of the Knee Joint," in *Insall & Scott Surgery of the knee* vol. 1, R. D. Komistek, Ed., Fifth ed Philidelphia: Elseveir, 2012, p. 143.
[100] I. Zeller, "In Vivo Mechanics and Vibrations of the Knee Joint," in *Insall & Scott Surgery of the knee* vol. 1, R. D. Komistek, Ed., Sixth ed Philidelphia: Elseveir, 2016, pp. 338-345.
[101] D. D. D'Lima, S. Patil, N. Steklov, S. Chien, and C. W. Colwell, "In vivo knee moments and shear after total knee arthroplasty," *Journal of Biomechanics,* vol. 40, pp. S11-S17, 2007.
[102] M. R. Mahfouz, W. Hoff, R. D. Komistek, and D. Dennis, "A robust method for registration of three-dimensional knee implant models to two-dimensional fluoroscopy images," *Medical Imaging, IEEE Transactions on,* vol. 22, pp. 1561-1574, 2003.
[103] W. A. Hoff, R. D. Komistek, D. A. Dennis, S. M. Gabriel, and S. A. Walker, "Three-dimensional determination of femoral-tibial contact positions under in vivo conditions using fluoroscopy," *Clinical Biomechanics,* vol. 13, pp. 455-472, 1998.
[104] S. A. Banks and W. A. Hodge, "Accurate measurement of three-dimensional knee replacement kinematics using single-plane fluoroscopy," *Biomedical Engineering, IEEE Transactions on,* vol. 43, pp. 638-649, 1996.

[105] R. Schmidt, R. D. Komistek, J. D. Blaha, B. L. Penenberg, and W. J. Maloney, "Fluoroscopic analyses of cruciate-retaining and medial pivot knee implants," *Clinical orthopaedics and related research,* vol. 410, pp. 139-147, 2003.
[106] J. B. Stiehl, R. D. Komistek, D. A. Dennis, R. D. Paxson, and W. Hoff, "Fluoroscopic analysis of kinematics after posterior-cruciate-retaining knee arthroplasty," *Journal of Bone & Joint Surgery, British Volume,* vol. 77, pp. 884-889, 1995.
[107] D. A. Dennis, R. D. Komistek, W. A. Hoff, and S. M. Gabriel, "In vivo knee kinematics derived using an inverse perspective technique," *Clinical orthopaedics and related research,* vol. 331, pp. 107-117, 1996.
[108] J. P. Holden, J. A. Orsini, K. L. Siegel, T. M. Kepple, L. H. Gerber, and S. J. Stanhope, "Surface movement errors in shank kinematics and knee kinetics during gait," *Gait & Posture,* vol. 5, pp. 217-227, 1997.
[109] J. Fuller, L.-J. Liu, M. Murphy, and R. Mann, "A comparison of lower-extremity skeletal kinematics measured using skin-and pin-mounted markers," *Human movement science,* vol. 16, pp. 219-242, 1997.
[110] C. Reinschmidt, A. Van Den Bogert, B. Nigg, A. Lundberg, and N. Murphy, "Effect of skin movement on the analysis of skeletal knee joint motion during running," *Journal of biomechanics,* vol. 30, pp. 729-732, 1997.
[111] T. Mommersteeg, R. Huiskes, L. Blankevoort, J. Kooloos, and J. Kauer, "An inverse dynamics modeling approach to determine the restraining function of human knee ligament bundles," *Journal of biomechanics,* vol. 30, pp. 139-146, 1997.
[112] G. Li, K. R. Kaufman, E. Chao, and H. Rubash, "Prediction of antagonistic muscle forces using inverse dynamic optimization during flexion/extension of the knee," *Journal of Biomechanical Engineering,* vol. 121, pp. 316-322, 1999.
[113] H. J. Lundberg, K. C. Foucher, and M. A. Wimmer, "A parametric approach to numerical modeling of TKR contact forces," *Journal of biomechanics,* vol. 42, pp. 541-545, 2009.
[114] T. P. Andriacchi and D. E. Hurwitz, "Gait biomechanics and total knee arthroplasty," *The American journal of knee surgery,* vol. 10, pp. 255-260, 1996.
[115] K. B. Shelburne, M. R. Torry, and M. G. Pandy, "Contributions of muscles, ligaments, and the ground-reaction force to tibiofemoral joint loading during normal gait," *Journal of orthopaedic research,* vol. 24, pp. 1983-1990, 2006.
[116] F. Johnson, S. Leitl, and W. Waugh, "The distribution of load across the knee. A comparison of static and dynamic measurements," *Bone & Joint Journal,* vol. 62, pp. 346-349, 1980.
[117] R. W. Hsu, S. Himeno, M. B. Coventry, and E. Y. Chao, "Normal axial alignment of the lower extremity and load-bearing distribution at the knee," *Clinical orthopaedics and related research,* vol. 255, pp. 215-227, 1990.

[118] B. A. Meccia, "Next Generation In-Vivo Forward Solution Physiological Model of the Human Lower Limb to Predict Implanted Knee Mechanics," 2016.
[119] J. K. P. Mueller, "Development of a Rigid Body Forward Solution Physiological Model of the Lower Leg to Predict Non Implanted and Implanted Knee Kinematics and Kinetics," 2011.
[120] R. D. Komistek, J. B. Stiehl, D. A. Dennis, R. D. Paxson, and R. W. Soutas-Little, "Mathematical model of the lower extremity joint reaction forces using Kane's method of dynamics," *Journal of Biomechanics,* vol. 31, pp. 185-189, 1997.
[121] W. R. Taylor, M. O. Heller, G. Bergmann, and G. N. Duda, "Tibio-femoral loading during human gait and stair climbing," *Journal of Orthopaedic Research,* vol. 22, pp. 625-632, 2004.
[122] S. Taylor, P. Walker, J. Perry, S. Cannon, and R. Woledge, "The forces in the distal femur and the knee during walking and other activities measured by telemetry," *The Journal of arthroplasty,* vol. 13, pp. 428-437, 1998.
[123] S. Taylor and P. Walker, "Forces and moments telemetered from two distal femoral replacements during various activities," *Journal of Biomechanics,* vol. 34, pp. 839-848, 2001.
[124] R. D. Crowninshield and R. A. Brand, "A physiologically based criterion of muscle force prediction in locomotion," *Journal of biomechanics,* vol. 14, pp. 793-801, 1981.
[125] R. A. Brand, D. R. Pedersen, and J. A. Friederich, "The sensitivity of muscle force predictions to changes in physiologic cross-sectional area," *Journal of biomechanics,* vol. 19, pp. 589-596, 1986.
[126] G. T. Yamaguchi, D. W. Moran, and J. Si, "A computationally efficient method for solving the redundant problem in biomechanics," *Journal of Biomechanics,* vol. 28, pp. 999-1005, 1995.
[127] A. Sharma, "Development of a Computational Model to Predict the In Vivo Contact Mechanics of Modern Total Knee Arthroplasty," 2008.
[128] A. Sharma, R. D. Komistek, G. R. Scuderi, and H. E. Cates Jr, "High-flexion TKA designs: what are their in vivo contact mechanics?," *Clinical orthopaedics and related research,* vol. 464, pp. 117-126, 2007.
[129] R. D. Komistek, T. R. Kane, M. Mahfouz, J. A. Ochoa, and D. A. Dennis, "Knee mechanics: a review of past and present techniques to determine in vivo loads," *Journal of biomechanics,* vol. 38, pp. 215-228, 2005.
[130] F. Catani, B. Innocenti, C. Belvedere, L. Labey, A. Ensini, and A. Leardini, "The Mark Coventry Award Articular: contact estimation in TKA using in vivo kinematics and finite element analysis," *Clinical Orthopaedics and Related Research®,* vol. 468, pp. 19-28, 2010.
[131] Y. Wang, Y. Fan, and M. Zhang, "Comparison of stress on knee cartilage during kneeling and standing using finite element models," *Medical Engineering and Physics,* vol. 36, pp. 439-447, 2014.
[132] S. L. Delp, F. C. Anderson, A. S. Arnold, P. Loan, A. Habib, C. T. John*, et al.*, "OpenSim: open-source software to create and analyze dynamic

simulations of movement," *IEEE transactions on biomedical engineering,* vol. 54, pp. 1940-1950, 2007.
[133] D. G. Thelen and F. C. Anderson, "Using computed muscle control to generate forward dynamic simulations of human walking from experimental data," *Journal of biomechanics,* vol. 39, pp. 1107-1115, 2006.
[134] E. M. Arnold, S. R. Ward, R. L. Lieber, and S. L. Delp, "A model of the lower limb for analysis of human movement," *Annals of biomedical engineering,* vol. 38, pp. 269-279, 2010.
[135] M. Damsgaard, J. Rasmussen, S. T. Christensen, E. Surma, and M. De Zee, "Analysis of musculoskeletal systems in the AnyBody Modeling System," *Simulation Modelling Practice and Theory,* vol. 14, pp. 1100-1111, 2006.
[136] M. A. Marra, V. Vanheule, R. Fluit, B. H. Koopman, J. Rasmussen, N. Verdonschot*, et al.*, "A subject-specific musculoskeletal modeling framework to predict in vivo mechanics of total knee arthroplasty," *Journal of biomechanical engineering,* vol. 137, p. 020904, 2015.
[137] B. Innocenti, S. Pianigiani, L. Labey, J. Victor, and J. Bellemans, "Contact forces in several TKA designs during squatting: a numerical sensitivity analysis," *Journal of biomechanics,* vol. 44, pp. 1573-1581, 2011.
[138] A. Veloso, G. Esteves, S. Silva, C. Ferreira, and F. Brandão, "Biomechanics modeling of human musculoskeletal system using Adams multibody dynamics package," in *Proceedings of the 24th IASTED International Conference on Biomedical Engineering, Innsbruck*, 2006, pp. 401-407.
[139] K. H. Bloemker, T. M. Guess, L. Maletsky, and K. Dodd, "Computational knee ligament modeling using experimentally determined zero-load lengths," *The open biomedical engineering journal,* vol. 6, p. 33, 2012.
[140] Y. Bei and B. J. Fregly, "Multibody dynamic simulation of knee contact mechanics," *Medical Engineering and Physics,* vol. 26, pp. 777-789, 2004.
[141] R. Huston, "Multibody dynamics—modeling and analysis methods," *Applied Mechanics Reviews,* vol. 44, pp. 109-117, 1991.
[142] T. R. Kane and D. A. Levinson, *Dynamics, theory and applications*: McGraw Hill, 1985.
[143] M. W. Spong, S. Hutchinson, and M. Vidyasagar, *Robot modeling and control* vol. 3: Wiley New York, 2006.
[144] A. F. Mannion, S. Kämpfen, U. Munzinger, and I. Kramers-de Quervain, "The role of patient expectations in predicting outcome after total knee arthroplasty," *Arthritis Res Ther,* vol. 11, p. R139, 2009.
[145] C. Baumann, A.-C. Rat, D. Mainard, C. Cuny, and F. Guillemin, "Importance of patient satisfaction with care in predicting osteoarthritis-specific health-related quality of life one year after total joint arthroplasty," *Quality of Life Research,* vol. 20, pp. 1581-1588, 2011.
[146] R. B. Bourne, R. W. McCalden, S. J. MacDonald, L. Mokete, and J. Guerin, "Influence of patient factors on TKA outcomes at 5 to 11 years

followup," *Clinical orthopaedics and related research,* vol. 464, pp. 27-31, 2007.
[147] D. A. Heck, C. A. Melfi, L. A. Mamlin, B. P. Katz, D. S. Arthur, R. S. Dittus*, et al.*, "Revision rates after knee replacement in the United States," *Medical care,* vol. 36, pp. 661-669, 1998.
[148] G. Bergmann, G. Deuretzbacher, M. Heller, F. Graichen, A. Rohlmann, J. Strauss*, et al.*, "Hip contact forces and gait patterns from routine activities," *Journal of biomechanics,* vol. 34, pp. 859-871, 2001.
[149] I. Kutzner, B. Heinlein, F. Graichen, A. Bender, A. Rohlmann, A. Halder*, et al.*, "Loading of the knee joint during activities of daily living measured< i> in vivo</i> in five subjects," *Journal of biomechanics,* vol. 43, pp. 2164-2173, 2010.
[150] A. Seireg and R. Arvikar, "The prediction of muscular load sharing and joint forces in the lower extremities during walking," *Journal of biomechanics,* vol. 8, pp. 89-102, 1975.
[151] A. Seireg and R. Arvikar, "A mathematical model for evaluation of forces in lower extremeties of the musculo-skeletal system," *Journal of biomechanics,* vol. 6, pp. 313IN19323-322IN20326, 1973.
[152] M. R. Mahfouz, W. A. Hoff, R. D. Komistek, and D. A. Dennis, "A robust method for registration of three-dimensional knee implant models to two-dimensional fluoroscopy images," *Medical Imaging, IEEE Transactions on,* vol. 22, pp. 1561-1574, 2003.
[153] T. R. Kane and D. A. Levinson, "The use of Kane's dynamical equations in robotics," *The International Journal of Robotics Research,* vol. 2, pp. 3-21, 1983.
[154] M. D. Lewek, T. G. Hornby, Y. Y. Dhaher, and B. D. Schmit, "Prolonged quadriceps activity following imposed hip extension: a neurophysiological mechanism for stiff-knee gait?," *Journal of neurophysiology,* vol. 98, pp. 3153-3162, 2007.
[155] D. T. Reilly and M. Martens, "Experimental analysis of the quadriceps muscle force and patello-femoral joint reaction force for various activities," *Acta Orthopaedica Scandinavica,* vol. 43, pp. 126-137, 1972.
[156] S. Hagood, M. Solomonow, R. Baratta, B. Zhou, and R. D'ambrosia, "The effect of joint velocity on the contribution of the antagonist musculature to knee stiffness and laxity," *The American journal of sports medicine,* vol. 18, pp. 182-187, 1990.
[157] C. A. Jacobs and C. P. Christensen, "Factors influencing patient satisfaction two to five years after primary total knee arthroplasty," *The Journal of arthroplasty,* vol. 29, pp. 1189-1191, 2014.
[158] B. N. Devers, M. A. Conditt, M. L. Jamieson, M. D. Driscoll, P. C. Noble, and B. S. Parsley, "Does greater knee flexion increase patient function and satisfaction after total knee arthroplasty?," *The Journal of arthroplasty,* vol. 26, pp. 178-186, 2011.
[159] J. E. Stevens, R. L. Mizner, and L. Snyder-Mackler, "Quadriceps strength and volitional activation before and after total knee arthroplasty for

osteoarthritis," *Journal of Orthopaedic Research,* vol. 21, pp. 775-779, 2003.
[160] R. L. Mizner, S. C. Petterson, J. E. Stevens, K. Vandenborne, and L. Snyder-Mackler, "Early quadriceps strength loss after total knee arthroplasty: the contributions of muscle atrophy and failure of voluntary muscle activation," *The Journal of bone and joint surgery. American volume,* vol. 87, p. 1047, 2005.
[161] D. B. Schaechter, D. A. Levinson, and T. R. Kane, *Autolev user's manual*: Online Dynamics, 1988.
[162] J. Skinner, J. N. Weinstein, S. M. Sporer, and J. E. Wennberg, "Racial, ethnic, and geographic disparities in rates of knee arthroplasty among Medicare patients," *New England Journal of Medicine,* vol. 349, pp. 1350-1359, 2003.
[163] S. V. Vaidya, C. S. Ranawat, A. Aroojis, and N. Laud, "Anthropometric measurements to design total knee prostheses for the Indian population," *The Journal of arthroplasty,* vol. 15, pp. 79-85, 2000.
[164] R. Gillespie, A. Levine, S. Fitzgerald, J. Kolaczko, M. DeMaio, R. Marcus*, et al.*, "Gender differences in the anatomy of the distal femur," *J Bone Joint Surg Br,* vol. 93, pp. 357-363, 2011.
[165] S. Simon, R. Mann, J. Hagy, and L. Larsen, "Role of the posterior calf muscles in normal gait," *The Journal of bone and joint surgery. American volume,* vol. 60, pp. 465-472, 1978.

VITA

Ian Michael Zeller was born September 26th, 1988, just outside of Cleveland Ohio. Over the next 18 years, he would live in St. Charles MO, St. Bonifacious MN, Grand Haven MI and finally Powell OH where he graduated from Olentangy Liberty High School. Growing up he developed a fascination with science and understanding how the world around him, especially chemistry and physics. That eventually lead him to attend Clemson University to study Chemical Engineering. Eventually he would transition to studying materials engineering as it was a combination of chemistry and physics.

While at Clemson Ian became involved in research and would eventually complete projects in surface modification and integral transformations while also working as a ceramic engineer and a research chemist in South Carolina. As a Senior, Ian became interested in medical applications of materials and started taking biomechanics courses which lead to a passion for the human aspect of engineering, ultimately leading him to pursue a graduate degree in biomechanics at the University of Tennessee.

In his free time Ian enjoys the outdoors, particularly swimming, biking hiking and especially running. He is has completed five marathons and plans to continue running at half distance (to preserve his knees). Ian's favorite places are the North Carolina mountains and the Florida beach, especially with his wife Jennifer and dogs Ruby and Maxwell. Following his PhD. Ian plans to continue his career in Biomechanics as a forensic engineer to better understand and prevent injuries.